

DETERMINATION AND INFLUENCE OF SHEAR  
STRENGTH PARAMETERS OF MATERIAL INTERFACES  
ASSOCIATED WITH GROUND SUPPORT SYSTEMS

DÉTERMINATION ET INFLUENCE DES PARAMÈTRES DE  
RÉSISTANCE AU CISAILLEMENT AUX INTERFACES DE  
MATÉRIAUX ASSOCIÉES AUX ANCRAGES DANS LES  
SOLS

A Thesis Submitted to the Division of Graduate Studies of the Royal Military  
College of Canada by

Stephen William Holt,  
Captain

In Partial Fulfillment of the Requirements for the Degree of  
Masters of Applied Science

Jan, 2017

© This thesis may be used within the Department of National Defence but  
copyright for open publication remains the property of the author.

## **Dedication**

Ad Majorem Dei Gloriam

## Acknowledgements

I must begin by thanking my supervisor, Dr. Nicholas Vlachopoulos, who was a constant source of knowledge, guidance and encouragement from day one to the last thesis deadline. I would also like to thank Mr. Dexter Gaskin for his dedication and positive attitude when resurrecting the old direct shear machine and preparing it for testing. I would like to express my gratitude to the entire Civil Engineering Department at Royal Military College of Canada for all of their support during my master's degree program.

I must thank my peers Brad Forbes and Ioannis Vazaios for their guidance and support with course work, conferences and hospitality at Queen's University.

I also wish to thank Mr. Mat Mirza from Durham Instruments for all his assistance in learning how to use the data acquisition and assisting with trouble shooting multiple instrumentation problems. I also want to thank Ms. Roxanna Gholami for her assistance organizing my test data.

Lastly, but definitely not least, I must thank my family. To my wife Christina thank you for your love, patience and support during these past few months, I know this was tough on you and Benjamin. I must also thank my parents for their love throughout my life and continued support to this day.

## **Abstract**

Ground support and reinforcement techniques are commonly used in a diverse array of geotechnical engineering works. Reinforcement and support elements may be found in the form of pile foundations, rock bolts, soil nails, spiles, and forepoles, among other devices. There is currently limited knowledge on the mechanisms involved with how, specifically, the surface of the support element interacts with the ground and (if present) the adhesive medium (e.g. grout or resin epoxy) which often fills an annulus between the support element and ground. Consequently there also exists a limited database in literature that contains specific support parameters for the diverse material interface scenarios (i.e. grout-ground, grout-support, support-ground) involved in support and reinforcement systems. These parameters are fundamental for design purposes, including input parameters for numerical modelling programs.

In order to provide the scientific community with accurate and relevant interaction reference values for the shear interaction behaviour of relevant support system over 190 modified ASTM 3080 constant strain rate direct shear tests were conducted. The experimental results provided the Mohr-Coulomb shear strength envelope and stiffness of the diverse interfaces between different geo-materials and support system materials. This collected data was utilized within numerical simulations that were created based on a constant strain rate direct shearbox test within the 2 dimensional (2D) numerical software package Phase 2 (Rocscience Inc. 2014). From these numerical simulations, the shear stress versus displacement behaviour was compared to the laboratory shear stress versus displacement curves. The thesis report summarizes the results from the physical testing program as well as the numerical analyses that were conducted as part of this line of research.

## Résumé

Les techniques de soutènement au sol et d'armature sont couramment utilisées dans un large éventail de travaux d'ingénierie géotechnique. Les éléments de renfort et de support peuvent se trouver sous la forme de fondations de pieux, de boulons de roche, de clous de sol, de chalumeaux et «forepoles», entre autres dispositifs. On connaît actuellement peu les mécanismes impliqués dans la manière dont la surface de l'élément de support interagit avec le sol et (le cas échéant) le milieu adhésif (par exemple coulis ou résine époxy) qui remplit souvent un espace annulaire entre l'élément de support et le sol. Par conséquent, il existe également une base de données limitée dans la littérature qui contient des paramètres de support spécifiques pour les différents scénarios d'interface de matériau impliqués dans des systèmes de support et de renforcement (par exemple, coulis-sol, coulis-support, support-sol). Ces paramètres sont fondamentaux à des fins de conception, y compris les paramètres d'entrée pour les programmes de modélisation numérique.

Afin de fournir à la communauté scientifique des valeurs de référence d'interaction précises et pertinentes pour le comportement d'interaction de cisaillement du système de support pertinent, on a effectué plus de 190 essais de cisaillement direct à vitesse de déformation constante ASTM 3080 modifiée. Les résultats expérimentaux ont fourni l'enveloppe de résistance au cisaillement de Mohr-Coulomb et la rigidité des différentes interfaces entre différents géomatériaux et matériaux du système de support. Ces données collectées ont été utilisées dans le cadre de simulations numériques qui ont été créées sur la base d'un test de cisaillement direct à vitesse de déformation constante dans le logiciel numérique 2D (2D) Phase 2 (Rocscience Inc. 2014). A partir de ces simulations numériques, le comportement de contrainte de cisaillement versus déplacement a été comparé à la courbe de cisaillement en laboratoire par rapport aux courbes de déplacement. Le rapport de thèse résume les résultats du programme de tests physiques ainsi que les analyses numériques qui ont été menées dans le cadre de cette ligne de recherche.

## Table of Contents

Dedication.....	ii
Acknowledgements.....	iii
Abstract.....	iv
Résumé.....	v
Table of Contents.....	vi
List of Tables .....	ix
List of Figures.....	x
List of Symbols, Abbreviations, & Acronyms.....	xxii
1 Introduction.....	1
1.1 Topic .....	2
1.2 Methodology.....	3
1.3 Organization.....	5
1.4 Objectives .....	7
2 Background.....	9
2.1 Excavations.....	10
2.2 Ground Support.....	12
2.3 Interaction .....	17
2.4 Knowledge Gaps.....	20
2.5 Plan to fill Knowledge Gaps .....	22
2.6 Shear Testing .....	22
2.7 Modelling.....	28
2.8 Summary .....	29
3 Materials .....	31
3.1 Field Construction Methods.....	32
3.2 Ground - Rock .....	33
3.3 Ground - Soil .....	34
3.4 Steel .....	39
3.5 Grout.....	40

3.6	Concrete .....	41
3.7	Summary .....	42
4	Testing and Instrumentation .....	44
4.1	Overview .....	45
4.2	Direct Shear Testing .....	45
4.3	Wykeham Farrance 2500 Shearbox Machine .....	47
4.4	Wykeham Farrance 25403 – Shearbox Machine .....	49
4.5	Instrumentation Utilized in Conjunction with Shearbox Machines .....	49
4.5.1	Shear Force .....	50
4.5.2	Displacement Transducers .....	51
4.6	Calibration .....	54
4.7	Data Acquisition .....	57
4.8	Testing .....	59
4.9	Test Procedure .....	61
4.10	Validation of WF 2500 Machine .....	64
4.11	Summary .....	67
5	Laboratory Results and Discussion.....	69
5.1	Properties of Interest .....	70
5.2	Shear Strength of Brighton Sand .....	70
5.3	Shear Stiffness of Brighton Sand.....	72
5.4	Shear Strength of Brighton Sand and Steel.....	76
5.5	Shear Stiffness of Sand and Steel .....	77
5.6	Shear Strength of Brighton Sand and Grout .....	81
5.7	Shear Stiffness of Brighton sand and Grout.....	81
5.8	Shear Strength of Coburg Limestone and Steel .....	85
5.9	Shear Stiffness of Coburg Limestone and Steel.....	86
5.10	Shear Strength of Coburg Limestone and Grout.....	91
5.11	Shear Stiffness of Coburg Limestone and Grout .....	91
5.12	Shear Strength of Grout and Steel .....	97
5.13	Shear Stiffness of Grout and Steel .....	97
5.14	Shear Strength of Concrete and Grout .....	101

5.15	Shear Stiffness of Concrete and Grout.....	101
5.16	Summary of Results.....	105
6	Numerical Analysis Results and Discussion.....	110
6.1	Introduction.....	111
6.2	Software Selection .....	111
6.3	Phase 2 Software.....	113
6.4	Direct Shearbox Simulation Preparation and Calibration of Numerical Model	115
6.4.1	Initial Model Design .....	115
6.4.2	Model Calibration .....	116
6.4.3	Final Model Design and Run .....	123
6.5	Brighton Beach Sand .....	124
6.6	Brighton Beach Sand and Grout .....	127
6.7	Brighton Beach Sand and Steel.....	129
6.8	Coburg Limestone and Grout.....	132
6.9	Coburg Limestone and Steel.....	134
6.10	Grout and Steel .....	137
6.11	Grout and Concrete.....	139
6.12	Discussion.....	142
6.13	Summary .....	147
7	Conclusions and Recommendations .....	149
7.1	Conclusion .....	150
7.2	Contributions .....	151
7.3	Recommendations.....	151
	References.....	153
	APPENDIX A.....	160
	APPENDIX B .....	215
	APPENDIX C .....	223

## List of Tables

<b>Table 2-1</b> List of examples of support and reinforcement systems and their applications .....	14
<b>Table 2-2</b> Anchorage coefficients ( $\alpha_g$ ) for cohesionless soils (CFEM, 2007) .....	16
<b>Table 3-1</b> Strength and elastic properties of Coburg limestone (Ghazvinian et al., 2015) .....	34
<b>Table 3-2</b> Results as obtained from the sieve analysis tests .....	36
<b>Table 3-3</b> Properties of non-shrink grout *(King Packaged Materials Company, 2016) .....	41
<b>Table 3-4</b> Properties of concrete sample *(EngineeringToolBox, 2016) .....	42
<b>Table 3-5</b> Material strength and elastic parameters <sup>1</sup> (Geotechdata, 2013) <sup>2</sup> (King Packaged Materials Company, 2016) <sup>3</sup> (Ghazvinian et al., 2015) <sup>4</sup> (EngineeringToolBox, 2016) .....	43
<b>Table 4-1</b> Type, normal stress, and number of interface tests .....	60
<b>Table 4-2</b> Procedure for tests with SP soil .....	62
<b>Table 4-3</b> Procedure for tests involving rock or monolithic samples .....	63
<b>Table 5-1</b> Laboratory results for $\Phi$ , $k_s$ , and $R^2$ .....	105
<b>Table 5-2</b> Maximum and minimum vertical displacements relative to starting position .....	108
<b>Table 6-1</b> Material strength and elastic parameters <sup>1</sup> (MatWeb, 2016) <sup>2</sup> (Geotechdata, 2013) <sup>3</sup> (King Packaged Materials Company, 2016) <sup>4</sup> (Ghazvinian et al., 2015) <sup>5</sup> (EngineeringToolBox, 2016) .....	124
<b>Table 6-2</b> Summary of model and laboratory peak and residual shear strengths. ....	143
<b>Table A-1</b> Test Index .....	161
<b>Table B-1</b> Vertical displacements from laboratory results .....	216
<b>Table C-1</b> Index by interface test type .....	224

## List of Figures

<b>Figure 1-1</b> Generic cross section of grouted support member .....	4
<b>Figure 1-2</b> Cross section of direct shear test of interface between two different materials.....	4
<b>Figure 1-3</b> Diagram Outlining Thesis Contents.....	7
<b>Figure 2-1</b> (A) Stress conditions pre-excavation, (B) stresses at moment of excavation, (C) tunnel without support deforming under stress, and (D) excavation with support applied stresses controlling displacement of tunnel.....	11
<b>Figure 2-2</b> (A) Stress condition pre-excavation, (B) stresses at moment of excavation, (C) excavation collapse due to stress redistribution, and (D) excavation supported resisting earth pressures .....	11
<b>Figure 2-3</b> Diagram of complete support systems and placement modified from (Grasso et al., 2003; Oke et al., 2012a).....	13
<b>Figure 2-4</b> Schematic of earth pressures in an anchor reinforced excavation wall (CFEM, 2007).....	15
<b>Figure 2-5</b> Vector diagram of forces from anchor wall in <b>Figure 2-4</b> (CFEM, 2007).....	16
<b>Figure 2-6</b> Adhesion factors with respect to undrained shear strength of cohesive soils (CFEM, 2007).....	17
<b>Figure 2-7</b> An example of interface scenarios found in a common tunnel support cross section.....	18
<b>Figure 2-8</b> Generic shearbox cross section .....	19
<b>Figure 2-9</b> Stress transfer across interfaces in a generic fully grouted cable bolt cross-section loaded axially from a block failure .....	19
<b>Figure 2-10</b> Cross-section showing forces acting on a sample during direct shear testing.....	20
<b>Figure 2-11</b> (A) Free body diagram of support element in FLAC 3D model, (B) Global image of element position in model, (C) Details of interaction between nodes of the support and the ground material (Itasca Consulting Group Inc., 2009) .....	21
<b>Figure 2-12</b> Shear failure of grout-concrete interface for axial testing of steel rebar rock-bolt. Note: Concrete simulates rock in these tests. (Cruz et al., 2016).....	22
<b>Figure 2-13</b> Generic plot of a Mohr-Coulomb failure envelope ( $C$ = cohesion constant, $\phi$ = Friction angle, $\tau$ = shear stress, $\sigma_n$ = normal stress, $\sigma_{1,3}$ = principle stresses).....	23
<b>Figure 2-14</b> Summary of shear strength results for poorly graded sand, poorly graded sand with concrete, and poorly graded sand with steel (Potyondy, 1961) ..	24
<b>Figure 2-15</b> Results from direct shear tests of pressurized grout-CDG interfaces, with direct shear results of pure CDG for reference (Hossain and Yin, 2014).....	25
<b>Figure 2-16</b> Shear strength versus grouting pressure plot for direct shear tests of CDG - grout interfaces (Hossain and Yin, 2014).....	26

<b>Figure 2-17</b> Demonstration of secant friction angle determination from direct shear tests 0007-0009 for Brighton Beach Sand .....	27
<b>Figure 2-18</b> Presentation of secant friction angle results for Brighton Beach Sand .....	27
<b>Figure 2-19</b> (A) 2D model of tunnel cross section modelled by homogeneous region (B) 2D cross section of tunnel modelled by individual forepoles (Oke et al., 2012a) .....	28
<b>Figure 3-1</b> Schematic of generic grouted tunnel support member highlighting the different interface scenarios .....	32
<b>Figure 3-2</b> Schematic of generic un-grouted tunnel support and relevant interface scenarios.....	33
<b>Figure 3-3</b> First Coburg Limestone sample .....	34
<b>Figure 3-4</b> Poorly graded Brighton Beach Sand .....	35
<b>Figure 3-5</b> Sieve analysis results of 2 separate samples of Brighton sand (ASTM D2487, 2011; ASTM D6913, 2004) .....	36
<b>Figure 3-6</b> Compaction curve of Brighton Beach Sand by Vlachopoulos N. (2000) .....	37
<b>Figure 3-7</b> Tests of pure SP on WF 2500 direct shear machine, $\sigma_n$ 25 – 100 kPa .	38
<b>Figure 3-8</b> Tests of pure SP on WF 25403 direct shear machine, $\sigma_n$ 25 – 100 kPa	38
<b>Figure 3-9</b> Steel Sample Used for the Direct Shear Tests.....	39
<b>Figure 3-10</b> Grout samples for both shear and compressive strength testing .....	40
<b>Figure 3-11</b> Type 10 Portland cement based non-shrink grout.....	41
<b>Figure 3-12</b> Concrete Sample used for the Direct Shear Tests .....	42
<b>Figure 4-1</b> Cross section of direct shearbox and parameters related to testing .....	46
<b>Figure 4-2</b> Generic Mohr-Coulomb strength envelope [Shear Stress ( $\tau$ ), Normal Stress at failure ( $\sigma_n$ ), Principal Stresses ( $\sigma_1$ , $\sigma_3$ ), Cohesion (C), Friction Angle ( $\phi$ )] .....	46
<b>Figure 4-3</b> Generic direct shear test set-up for rock.....	47
<b>Figure 4-4</b> WF 2500 constant rate of strain direct shear machine .....	48
<b>Figure 4-5</b> Image of modified parts on WF 2500 .....	48
<b>Figure 4-6</b> WF 25403 Constant Rate of Strain Direct Shear Machine.....	49
<b>Figure 4-7</b> Example of Wheatstone bridge circuit (National Instruments, 2016)..	50
<b>Figure 4-8</b> AL-JP 1000lb high-output load cell .....	51
<b>Figure 4-9</b> Cross section of LVDT (Marco Sensors, 2014) .....	52
<b>Figure 4-10</b> Signal changes with respect to core position (Data Track Pi, 2014)..	52
<b>Figure 4-11</b> Corrected LVDT output (Macro Sensors, 2014).....	53
<b>Figure 4-12</b> RDP D2/200A DCDT used for vertical displacement .....	54
<b>Figure 4-13</b> Circuit diagram of D2/200A DCDT (RDP Group, 2014b) .....	54
<b>Figure 4-14</b> SE Labs DCDT used for horizontal displacement .....	54
<b>Figure 4-15</b> Calibration data for AL-JP load cell.....	55
<b>Figure 4-16</b> Pedestal micrometer calibration set-up .....	56
<b>Figure 4-17</b> Calibration data for horizontal DCDT.....	56
<b>Figure 4-18</b> Calibration data for vertical DCDT .....	57

<b>Figure 4-19</b> Quantum X MX440A DAQ .....	58
<b>Figure 4-20</b> 15-Pin serial connector .....	58
<b>Figure 4-21</b> MGC Plus DAQ used for testing .....	59
<b>Figure 4-22</b> Shear tests of rock and steel with varied displacement rates, $\sigma_n = 100$ kPa (*Sample cracked part way through this test, believed to have caused the lower shear strength) .....	64
<b>Figure 4-23</b> Test of fine grained fused quartz on WF2500 .....	65
<b>Figure 4-24</b> Direct shear tests of SP on WF 2500 .....	66
<b>Figure 4-25</b> Direct shear tests of SP on WF25403 .....	67
<b>Figure 5-1</b> General layout of shear stress versus displacement plots .....	71
<b>Figure 5-2</b> Example of chord method shear stiffness calculation for one plot .....	73
<b>Figure 5-3</b> Test 0008 Brighton sand sample, $\tau$ versus displacement $\sigma_n$ 25 to 100kPa .....	73
<b>Figure 5-4</b> Test 0022 Brighton sand sample, $\tau$ versus displacement $\sigma_n$ 425 to 500kPa .....	74
<b>Figure 5-5</b> Test 0008 Brighton sand sample, vertical versus horizontal displacement, $\sigma_n$ 25 to 100kPa .....	74
<b>Figure 5-6</b> Test 0022 Brighton sand sample, vertical versus horizontal displacement, $\sigma_n$ 425 to 500kPa .....	75
<b>Figure 5-7</b> Test 0007-0009 Mohr-Coulomb peak and residual shear strength envelope, $\sigma_n$ 25 to 100kPa .....	75
<b>Figure 5-8</b> Test 0021-0023 Mohr-Coulomb peak and residual shear strength envelope, $\sigma_n$ 425 to 500kPa .....	76
<b>Figure 5-9</b> Test 0019 SP soil – steel sample, $\tau$ versus horizontal displacement, $\sigma_n$ 25 to 100kPa .....	78
<b>Figure 5-10</b> Test 0029 SP soil – steel sample, $\tau$ versus horizontal displacement, $\sigma_n$ 425 to 500kPa .....	78
<b>Figure 5-11</b> Test 0019 SP soil – steel sample, vertical versus horizontal displacement, $\sigma_n$ 25 to 100kPa .....	79
<b>Figure 5-12</b> Test 0029 SP soil – steel sample, vertical versus horizontal displacement, $\sigma_n$ 425 to 500kPa .....	79
<b>Figure 5-13</b> Test 0018-0020 Mohr-Coulomb peak and residual shear strength envelope, $\sigma_n$ 25 to 100kPa .....	80
<b>Figure 5-14</b> Test 0027-0029 Mohr-Coulomb peak and residual shear strength envelope, $\sigma_n$ 425 to 500kPa .....	80
<b>Figure 5-15</b> Test 0017 SP soil – grout sample, $\tau$ versus horizontal displacement, $\sigma_n$ 25 to 100kPa .....	82
<b>Figure 5-16</b> Test 0026 SP soil – grout sample, $\tau$ versus horizontal displacement, $\sigma_n$ 425 to 500kPa .....	83
<b>Figure 5-17</b> Test 0017 SP soil – grout sample, vertical versus horizontal displacement, $\sigma_n$ 25 to 100kPa .....	83
<b>Figure 5-18</b> Test 0026 SP soil – grout sample, vertical versus horizontal displacement, $\sigma_n$ 425 to 500kPa .....	84

<b>Figure 5-19</b> Test 0015-0017 Mohr-Coulomb peak and residual shear strength envelope, $\sigma_n$ 25 to 100kPa.....	84
<b>Figure 5-20</b> Test 0024-0026 Mohr-Coulomb peak and residual shear strength envelope, $\sigma_n$ 425 to 500kPa.....	85
<b>Figure 5-21</b> Rock and steel sample after Test 0031 .....	87
<b>Figure 5-22</b> First rock sample after damage in Test 0040 at 475 kPa.....	87
<b>Figure 5-23</b> Test 0032 limestone – steel sample, $\tau$ versus horizontal displacement, $\sigma_n$ 25 to 100kPa.....	88
<b>Figure 5-24</b> Test 0041 limestone – steel sample, $\tau$ versus horizontal displacement, $\sigma_n$ 425 to 500kPa.....	88
<b>Figure 5-25</b> Test 0032 limestone – steel sample, vertical versus horizontal displacement, $\sigma_n$ 25 to 100kPa.....	89
<b>Figure 5-26</b> Test 0041 limestone – steel sample, vertical versus horizontal displacement, $\sigma_n$ 425 to 500kPa.....	89
<b>Figure 5-27</b> Test 0031-0033 Mohr-Coulomb peak and residual shear strength envelope, $\sigma_n$ 25 to 100kPa.....	90
<b>Figure 5-28</b> Test 0040-0042 Mohr-Coulomb peak and residual shear strength envelope, $\sigma_n$ 425 to 500kPa.....	90
<b>Figure 5-29</b> First rock sample after Test 0039 at 475 kPa .....	92
<b>Figure 5-30</b> Test 0035 limestone – grout sample, $\tau$ versus horizontal displacement, $\sigma_n$ 25 to 100kPa.....	93
<b>Figure 5-31</b> Test 0038 limestone – grout sample, $\tau$ versus horizontal displacement, $\sigma_n$ 425 to 500kPa.....	93
<b>Figure 5-32</b> Test 0039 limestone – grout sample, $\tau$ versus horizontal displacement, $\sigma_n$ 425 to 500kPa.....	94
<b>Figure 5-33</b> Test 0035 limestone – grout sample, vertical versus horizontal displacement, $\sigma_n$ 25 to 100kPa.....	94
<b>Figure 5-34</b> Test 0038 limestone – grout sample, vertical versus horizontal displacement, $\sigma_n$ 425 to 500kPa.....	95
<b>Figure 5-35</b> Test 0039 limestone – grout sample, vertical versus horizontal displacement, $\sigma_n$ 425 to 500kPa.....	95
<b>Figure 5-36</b> Test 0034-0036 Mohr-Coulomb peak and residual shear strength envelope, $\sigma_n$ 25 to 100kPa.....	96
<b>Figure 5-37</b> Test 0037-0039 Mohr-Coulomb peak and residual shear strength envelope, $\sigma_n$ 425 to 500kPa.....	96
<b>Figure 5-38</b> Test 0044 grout - steel sample, $\tau$ versus horizontal displacement, $\sigma_n$ 25 to 100kPa .....	98
<b>Figure 5-39</b> Test 0047 Grout - steel sample, $\tau$ versus horizontal displacement, $\sigma_n$ 425 to 500kPa .....	98
<b>Figure 5-40</b> Test 0044 Grout - steel sample, vertical versus horizontal displacement, $\sigma_n$ 25 to 100kPa.....	99
<b>Figure 5-41</b> Test 0047 Grout - steel sample, vertical versus horizontal displacement, $\sigma_n$ 425 to 500kPa.....	99

<b>Figure 5-42</b> Test 0043-0045 Mohr-Coulomb peak and residual shear strength envelope, $\sigma_n$ 25 to 100kPa.....	100
<b>Figure 5-43</b> Test 0046-0048 Mohr-Coulomb peak and residual shear strength envelope, $\sigma_n$ 425 to 500kPa.....	100
<b>Figure 5-44</b> Test 0049 Grout - concrete sample, $\tau$ versus horizontal displacement, $\sigma_n$ 25 to 100kPa.....	102
<b>Figure 5-45</b> Test 0052 Grout - concrete sample, $\tau$ versus horizontal displacement, $\sigma_n$ 425 to 500kPa.....	102
<b>Figure 5-46</b> Test 0049 Grout - steel sample, vertical versus horizontal displacement, $\sigma_n$ 25 to 100kPa.....	103
<b>Figure 5-47</b> Test 0052 Grout - steel sample, vertical versus horizontal displacement, $\sigma_n$ 425 to 500kPa.....	103
<b>Figure 5-48</b> Test 0049-0051 Mohr-Coulomb peak and residual shear strength envelope, $\sigma_n$ 25 to 100kPa.....	104
<b>Figure 5-49</b> Test 0052-0054 Mohr-Coulomb peak and residual shear strength envelope, $\sigma_n$ 425 to 500kPa.....	104
<b>Figure 5-50</b> Comparison of shear strength envelope results for pure sand samples and sand-steel samples between the author and (Potyondy, 1961).....	107
<b>Figure 6-1</b> Rheological model of joint boundary using a Mohr-Coulomb constitutive model based off description by Rocscience, 2014 ( $k_s$ = shear stiffness, $k_n$ = normal stiffness $\phi$ = friction angle, $c$ = cohesion factor, and $\sigma_t$ = tensile strength).....	115
<b>Figure 6-2</b> Boundary conditions used in model of direct shearbox .....	116
<b>Figure 6-3</b> First assessment of the direct shear test model using Brighton beach sand at 25 kPa normal stress and boundaries (circled in red) between the box and sand set as material boundaries.....	117
<b>Figure 6-4</b> Interpret results for $\sigma_1$ principle stress within the model from <b>Figure 6-3</b> at 4mm displacement.....	118
<b>Figure 6-5</b> 25 kPa laboratory test results (0007-01) compared with model average shear stress versus displacement varying shearbox and sample boundary type between material and joint types.....	118
<b>Figure 6-6</b> Two part shearbox with same dimensions (wall thickness 17mm)....	119
<b>Figure 6-7</b> Two part shearbox with thicker walls (20mm thick).....	120
<b>Figure 6-8</b> Two part shearbox thicker top and bottom (walls 17mm thick) (top and bottom 20mm thick).....	120
<b>Figure 6-9</b> Laboratory test of sand at 25 KPa normal stress (0007-01) compared to model results of the two part shearbox, and changes to shearbox dimensions .....	121
<b>Figure 6-10</b> Model for shear test normal stiffness at the joint (circled in red) set to $3 \times 10^6$ kPa/m.....	122
<b>Figure 6-11</b> Laboratory test at 25 kPa normal stress (0007-01) compared with model results at different normal stiffnesses for the joint between the two shearbox halves .....	122
<b>Figure 6-12</b> Diagram of boundary types in model.....	123

<b>Figure 6-13</b> Model of Brighton sand test at 100 kPa normal stress and 5mm displacement .....	125
<b>Figure 6-14</b> Contoured results for $\sigma_1$ principle stress of model from <b>Figure 6-13</b> at 5mm displacement .....	125
<b>Figure 6-15</b> Select laboratory results for direct shear Brighton sand at 25 kPa to 100 kPa compared to model results .....	126
<b>Figure 6-16</b> Select laboratory results for direct shear of Brighton sand 425 kPa to 500 kPa compared to model results .....	126
<b>Figure 6-17</b> Model of Brighton sand and grout test at 100 kPa normal stress and 5mm displacement .....	127
<b>Figure 6-18</b> Contoured results for $\sigma_1$ principle stress of model from <b>Figure 6-17</b> at 5mm displacement .....	128
<b>Figure 6-19</b> Select laboratory results for direct shear Brighton sand and grout at 25 kPa to 100 kPa compared to model results .....	128
<b>Figure 6-20</b> Select laboratory results for direct shear Brighton sand and grout at 425 kPa to 500 kPa compared to model results .....	129
<b>Figure 6-21</b> Model of Brighton sand and steel test at 100 kPa normal stress and 5mm displacement .....	130
<b>Figure 6-22</b> Contoured results for $\sigma_1$ principle stress of model from <b>Figure 6-21</b> at 5mm displacement .....	130
<b>Figure 6-23</b> Select laboratory results for direct shear Brighton sand and steel at 25 kPa to 100 kPa compared to model results .....	131
<b>Figure 6-24</b> Select laboratory results for direct shear Brighton sand and steel at 425 kPa to 500 kPa compared to model results .....	131
<b>Figure 6-25</b> Model of Coburg limestone and grout test at 100 kPa normal stress and 5mm displacement .....	132
<b>Figure 6-26</b> Contoured results for $\sigma_1$ principle stress of model from <b>Figure 6-25</b> at 5mm displacement .....	133
<b>Figure 6-27</b> Select laboratory results for direct shear Coburg limestone and grout at 25 kPa to 100 kPa compared to model results .....	133
<b>Figure 6-28</b> Select laboratory results for direct shear Coburg limestone and grout at 425 kPa to 500 kPa compared to model results .....	134
<b>Figure 6-29</b> Model of Coburg limestone and steel test at 100 kPa normal stress and 5mm displacement .....	135
<b>Figure 6-30</b> Contoured results for $\sigma_1$ principle stress of model from <b>Figure 6-29</b> at 5mm displacement .....	135
<b>Figure 6-31</b> Select laboratory results for direct shear Coburg limestone and steel at 25 kPa to 100 kPa compared to model results .....	136
<b>Figure 6-32</b> Select laboratory results for direct shear Coburg limestone and steel at 425 kPa to 500 kPa compared to model results .....	136
<b>Figure 6-33</b> Model of grout and steel test at 100 kPa normal stress and 5mm displacement .....	137

<b>Figure 6-34</b> Contoured results for $\sigma_1$ principle stress of model from <b>Figure 6-33</b> at 5mm displacement .....	138
<b>Figure 6-35</b> Select laboratory results for direct shear tests of grout and steel at 25 kPa to 100 kPa compared to model results .....	138
<b>Figure 6-36</b> Select laboratory results for direct shear tests of grout and steel at 425 kPa to 500 kPa compared to model results .....	139
<b>Figure 6-37</b> Model of grout and concrete test at 100 kPa normal stress and 5mm displacement .....	140
<b>Figure 6-38</b> Contoured results for $\sigma_1$ principle stress of model from <b>Figure 6-37</b> at 5mm displacement .....	140
<b>Figure 6-39</b> Select laboratory results for direct shear tests of grout and concrete at 25 kPa to 100 kPa compared to model results .....	141
<b>Figure 6-40</b> Select laboratory results for direct shear tests of grout and concrete at 425 kPa to 500 kPa compared to model results .....	141
<b>Figure A-1</b> Test 0007 sand 25-100kPa shear stress versus horizontal displacement .....	162
<b>Figure A-2</b> Test 0007 sand 25-100 kPa vertical versus horizontal displacement	162
<b>Figure A-3</b> Test 0008 sand 25-100kPa shear stress versus horizontal displacement .....	163
<b>Figure A-4</b> Test 0008 sand 25-100 kPa vertical versus horizontal displacement	163
<b>Figure A-5</b> Test 0009 sand 25-100kPa shear stress versus horizontal displacement .....	164
<b>Figure A-6</b> Test 0009 sand 25-100 kPa vertical versus horizontal displacement	164
<b>Figure A-7</b> Mohr-Coulomb shear strength 25-100 kPa Brighton Sand WF 2500	165
<b>Figure A-8</b> Test 0010 sand 25-100kPa shear stress versus horizontal displacement .....	165
<b>Figure A-9</b> Test 0010 sand 25-100 kPa vertical versus horizontal displacement	166
<b>Figure A-10</b> Test 0011 sand 25-100kPa shear stress versus horizontal displacement .....	166
<b>Figure A-11</b> Test 0011 sand 25-100 kPa vertical versus horizontal displacement .....	167
<b>Figure A-12</b> Test 0012 sand 25-100kPa shear stress versus horizontal displacement .....	167
<b>Figure A-13</b> Test 0012 sand 25-100 kPa vertical versus horizontal displacement .....	168
<b>Figure A-14</b> Mohr-Coulomb shear strength 25-100 kPa Brighton Sand WF 25403 .....	168
<b>Figure A-15</b> Test 0015 sand-grout 25-100kPa shear stress versus horizontal displacement .....	169
<b>Figure A-16</b> Test 0015 sand-grout 25-100 kPa vertical versus horizontal displacement .....	169
<b>Figure A-17</b> Test 0016 sand-grout 25-100kPa shear stress versus horizontal displacement .....	170

<b>Figure A-18</b>	Test 0016 sand-grout 25-100 kPa vertical versus horizontal displacement .....	170
<b>Figure A-19</b>	Test 0017 sand-grout 25-100kPa shear stress versus horizontal displacement .....	171
<b>Figure A-20</b>	Test 0017 sand-grout 25-100 kPa vertical versus horizontal displacement .....	171
<b>Figure A-21</b>	Mohr-Coulomb shear strength 25-100 kPa sand and grout.....	172
<b>Figure A-22</b>	Test 0018 sand-steel 25-100kPa shear stress versus horizontal displacement .....	172
<b>Figure A-23</b>	Test 0018 sand-steel 25-100 kPa vertical versus horizontal displacement .....	173
<b>Figure A-24</b>	Test 0019 sand-steel 25-100kPa shear stress versus horizontal displacement .....	173
<b>Figure A-25</b>	Test 0019 sand-steel 25-100 kPa vertical versus horizontal displacement .....	174
<b>Figure A-26</b>	Test 0020 sand-steel 25-100kPa shear stress versus horizontal displacement .....	174
<b>Figure A-27</b>	Test 0020 sand-steel 25-100 kPa vertical versus horizontal displacement .....	175
<b>Figure A-28</b>	Mohr-Coulomb shear strength 25-100 kPa sand and steel .....	175
<b>Figure A-29</b>	Test 0021 sand 425-500kPa shear stress versus horizontal displacement .....	176
<b>Figure A-30</b>	Test 0021 sand 425-500 kPa vertical versus horizontal displacement .....	176
<b>Figure A-31</b>	Test 0022 sand 425-500kPa shear stress versus horizontal displacement .....	177
<b>Figure A-32</b>	Test 0022 sand 425-500 kPa vertical versus horizontal displacement .....	177
<b>Figure A-33</b>	Test 0023 sand 425-500kPa shear stress versus horizontal displacement .....	178
<b>Figure A-34</b>	Test 0023 sand 425-500 kPa vertical versus horizontal displacement .....	178
<b>Figure A-35</b>	Mohr-Coulomb shear strength 425-500 kPa Brighton sand.....	179
<b>Figure A-36</b>	Test 0024 sand-grout 425-500kPa shear stress versus horizontal displacement .....	179
<b>Figure A-37</b>	Test 0024 sand-grout 425-500 kPa vertical versus horizontal displacement .....	180
<b>Figure A-38</b>	Test 0025 sand-grout 425-500kPa shear stress versus horizontal displacement .....	180
<b>Figure A-39</b>	Test 0025 sand-grout 425-500 kPa vertical versus horizontal displacement .....	181
<b>Figure A-40</b>	Test 0026 sand-grout 425-500kPa shear stress versus horizontal displacement .....	181

<b>Figure A-41</b> Test 0026 sand-grout 425-500 kPa vertical versus horizontal displacement .....	182
<b>Figure A-42</b> Mohr-Coulomb shear strength 425-500 kPa sand and grout.....	182
<b>Figure A-43</b> Test 0027 sand-steel 425-500kPa shear stress versus horizontal displacement .....	183
<b>Figure A-44</b> Test 0027 sand-steel 425-500 kPa vertical versus horizontal displacement .....	183
<b>Figure A-45</b> Test 0028 sand-steel 425-500kPa shear stress versus horizontal displacement .....	184
<b>Figure A-46</b> Test 0028 sand-steel 425-500 kPa vertical versus horizontal displacement .....	184
<b>Figure A-47</b> Test 0029 sand-steel 425-500kPa shear stress versus horizontal displacement .....	185
<b>Figure A-48</b> Test 0029 sand-steel 425-500 kPa vertical versus horizontal displacement .....	185
<b>Figure A-49</b> Mohr-Coulomb shear strength 425-500 kPa sand and steel.....	186
<b>Figure A-50</b> Test 0031 rock-steel 25-100 kPa shear stress versus horizontal displacement .....	186
<b>Figure A-51</b> Test 0031 rock-steel 25-100 kPa vertical versus horizontal displacement .....	187
<b>Figure A-52</b> Test 0032 rock-steel 25-100 kPa shear stress versus horizontal displacement .....	187
<b>Figure A-53</b> Test 0032 rock-steel 25-100 kPa vertical versus horizontal displacement .....	188
<b>Figure A-54</b> Test 0033 rock-steel 25-100 kPa shear stress versus horizontal displacement .....	188
<b>Figure A-55</b> Test 0033 rock-steel 25-100 kPa vertical versus horizontal displacement .....	189
<b>Figure A-56</b> Mohr-Coulomb shear strength 25-100 kPa rock and steel .....	189
<b>Figure A-57</b> Test 0034 rock-grout 25-100 kPa shear stress versus horizontal displacement .....	190
<b>Figure A-58</b> Test 0034 rock-grout 25-100 kPa vertical versus horizontal displacement .....	190
<b>Figure A-59</b> Test 0035 rock-grout 25-100 kPa shear stress versus horizontal displacement .....	191
<b>Figure A-60</b> Test 0035 rock-grout 25-100 kPa vertical versus horizontal displacement .....	191
<b>Figure A-61</b> Test 0036 rock-grout 25-100 kPa shear stress versus horizontal displacement .....	192
<b>Figure A-62</b> Test 0036 rock-grout 25-100 kPa vertical versus horizontal displacement .....	192
<b>Figure A-63</b> Mohr-Coulomb shear strength 25-100 kPa rock and grout .....	193

<b>Figure A-64</b> Test 0037 rock-grout 425-500 kPa shear stress versus horizontal displacement .....	193
<b>Figure A-65</b> Test 0037 rock-grout 425-500 kPa vertical versus horizontal displacement .....	194
<b>Figure A-66</b> Test 0038 rock-grout 425-500 kPa shear stress versus horizontal displacement .....	194
<b>Figure A-67</b> Test 0038 rock-grout 425-500 kPa vertical versus horizontal displacement .....	195
<b>Figure A-68</b> Test 0039 rock-grout 425-500 kPa shear stress versus horizontal displacement .....	195
<b>Figure A-69</b> Test 0039 rock-grout 425-500 kPa vertical versus horizontal displacement .....	196
<b>Figure A-70</b> Mohr-Coulomb shear strength 425-500 kPa rock and grout .....	196
<b>Figure A-71</b> Test 0040 rock-steel 425-500 kPa shear stress versus horizontal displacement .....	197
<b>Figure A-72</b> Test 0040 rock-steel 425-500 kPa vertical versus horizontal displacement .....	197
<b>Figure A-73</b> Test 0041 rock-steel 425-500 kPa shear stress versus horizontal displacement .....	198
<b>Figure A-74</b> Test 0041 rock-steel 425-500 kPa vertical versus horizontal displacement .....	198
<b>Figure A-75</b> Test 0042 rock-steel 425-500 kPa shear stress versus horizontal displacement .....	199
<b>Figure A-76</b> Test 0042 rock-steel 425-500 kPa vertical versus horizontal displacement .....	199
<b>Figure A-77</b> Mohr-Coulomb shear strength 425-500 kPa rock and steel .....	200
<b>Figure A-78</b> Test 0043 grout-steel 25-100 kPa shear stress versus horizontal displacement .....	200
<b>Figure A-79</b> Test 0043 grout-steel 25-100 kPa vertical versus horizontal displacement .....	201
<b>Figure A-80</b> Test 0044 grout-steel 25-100 kPa shear stress versus horizontal displacement .....	201
<b>Figure A-81</b> Test 0044 grout-steel 25-100 kPa vertical versus horizontal displacement .....	202
<b>Figure A-82</b> Test 0045 grout-steel 25-100 kPa shear stress versus horizontal displacement .....	202
<b>Figure A-83</b> Test 0045 grout-steel 25-100 kPa vertical versus horizontal displacement .....	203
<b>Figure A-84</b> Mohr-Coulomb shear strength 25-100 kPa grout and steel .....	203
<b>Figure A-85</b> Test 0046 grout-steel 425-500 kPa shear stress versus horizontal displacement .....	204
<b>Figure A-86</b> Test 0046 grout-steel 425-500 kPa vertical versus horizontal displacement .....	204

<b>Figure A-87</b> Test 0047 grout-steel 425-500 kPa shear stress versus horizontal displacement .....	205
<b>Figure A-88</b> Test 0047 grout-steel 425-500 kPa vertical versus horizontal displacement .....	205
<b>Figure A-89</b> Test 0048 grout-steel 425-500 kPa shear stress versus horizontal displacement .....	206
<b>Figure A-90</b> Test 0048 grout-steel 425-500 kPa vertical versus horizontal displacement .....	206
<b>Figure A-91</b> Mohr-Coulomb shear strength 425-500 kPa grout and steel.....	207
<b>Figure A-92</b> Test 0049 grout-concrete 25-100 kPa shear stress versus horizontal displacement .....	207
<b>Figure A-93</b> Test 0049 grout-concrete 25-100 kPa vertical versus horizontal displacement .....	208
<b>Figure A-94</b> Test 0050 grout-concrete 25-100 kPa shear stress versus horizontal displacement .....	208
<b>Figure A-95</b> Test 0050 grout-concrete 25-100 kPa vertical versus horizontal displacement .....	209
<b>Figure A-96</b> Test 0051 grout-concrete 25-100 kPa shear stress versus horizontal displacement .....	209
<b>Figure A-97</b> Test 0051 grout-concrete 25-100 kPa vertical versus horizontal displacement .....	210
<b>Figure A-98</b> Mohr-Coulomb shear strength 25-100 kPa grout and concrete.....	210
<b>Figure A-99</b> Test 0052 grout-concrete 425-500 kPa shear stress versus horizontal displacement .....	211
<b>Figure A-100</b> Test 0052 grout-concrete 425-500 kPa vertical versus horizontal displacement .....	211
<b>Figure A-101</b> Test 0053 grout-concrete 425-500 kPa shear stress versus horizontal displacement .....	212
<b>Figure A-102</b> Test 0053 grout-concrete 425-500 kPa vertical versus horizontal displacement .....	212
<b>Figure A-103</b> Test 0054 grout-concrete 425-500 kPa shear stress versus horizontal displacement .....	213
<b>Figure A-104</b> Test 0054 grout-concrete 425-500 kPa vertical versus horizontal displacement .....	213
<b>Figure A-105</b> Mohr-Coulomb shear strength 425-500 kPa grout and concrete...	214
<b>Figure C-1</b> Sand sample model versus test 0007 .....	225
<b>Figure C-2</b> Sand sample model versus test 0008 .....	225
<b>Figure C-3</b> Sand sample model versus test 0009 .....	226
<b>Figure C-4</b> Sand sample model versus test 0021 .....	226
<b>Figure C-5</b> Sand sample model versus test 0022 .....	227
<b>Figure C-6</b> Sand sample model versus test 0023 .....	227
<b>Figure C-7</b> Sand-grout sample, model versus test 0015 .....	228
<b>Figure C-8</b> Sand-grout sample, model versus test 0016 .....	228

<b>Figure C-9</b> Sand-grout sample, model versus test 0017 .....	229
<b>Figure C-10</b> Sand-grout sample, model versus test 0024 .....	229
<b>Figure C-11</b> Sand-grout sample, model versus test 0025 .....	230
<b>Figure C-12</b> Sand-grout sample, model versus test 0026 .....	230
<b>Figure C-13</b> Sand-steel sample, model versus test 0018 .....	231
<b>Figure C-14</b> Sand-steel sample, model versus test 0019 .....	231
<b>Figure C-15</b> Sand-steel sample, model versus test 0020 .....	232
<b>Figure C-16</b> Sand-steel sample, model versus test 0027 .....	232
<b>Figure C-17</b> Sand-steel sample, model versus test 0028 .....	233
<b>Figure C-18</b> Sand-steel sample, model versus test 0029 .....	233
<b>Figure C-19</b> Rock-grout sample, model versus test 0034.....	234
<b>Figure C-20</b> Rock-grout sample, model versus test 0035.....	234
<b>Figure C-21</b> Rock-grout sample, model versus test 0036.....	235
<b>Figure C-22</b> Rock-grout sample, model versus test 0037.....	235
<b>Figure C-23</b> Rock-grout sample, model versus test 0038.....	236
<b>Figure C-24</b> Rock-grout sample, model versus test 0039.....	236
<b>Figure C-25</b> Rock-steel sample, model versus test 0031.....	237
<b>Figure C-26</b> Rock-steel sample, model versus test 0032.....	237
<b>Figure C-27</b> Rock-steel sample, model versus test 0033.....	238
<b>Figure C-28</b> Rock-steel sample, model versus test 0040.....	238
<b>Figure C-29</b> Rock-steel sample, model versus test 0041.....	239
<b>Figure C-30</b> Rock-steel sample, model versus test 0042.....	239
<b>Figure C-31</b> Grout-steel sample, model versus test 0043.....	240
<b>Figure C-32</b> Grout-steel sample, model versus test 0044.....	240
<b>Figure C-33</b> Grout-steel sample, model versus test 0045.....	241
<b>Figure C-34</b> Grout-steel sample, model versus test 0046.....	241
<b>Figure C-35</b> Grout-steel sample, model versus test 0047.....	242
<b>Figure C-36</b> Grout-steel sample, model versus test 0048.....	242
<b>Figure C-37</b> Grout-concrete sample, model versus test 0049.....	243
<b>Figure C-38</b> Grout-concrete sample, model versus test 0050.....	243
<b>Figure C-39</b> Grout-concrete sample, model versus test 0051.....	244
<b>Figure C-40</b> Grout-concrete sample, model versus test 0052.....	244
<b>Figure C-41</b> Grout-concrete sample, model versus test 0053.....	245
<b>Figure C-42</b> Grout-concrete sample, model versus test 0054.....	245
<b>Figure C-43</b> Calibration of shearbox-sample boundary conditions at 25kPa normal stress with pure sand.....	246
<b>Figure C-44</b> Calibration of shearbox dimensions at 25 kPa normal stress with pure sand.....	246
<b>Figure C-45</b> Calibration of horizontal stiffness of shear joint at 25kPa normal stress with pure sand.....	247

## List of Symbols, Abbreviations, & Acronyms

$\tau$  = Shear Stress

$\tau_p$  = Peak Shear Stress

$\tau_r$  = Residual Shear Stress

$\sigma$  = Normal Stress

$\sigma$  = Principle Stress

$\delta$  = Displacement

$\phi$  = Friction Angle

$\phi_p$  = Peak Friction Angle

$\phi_r$  = Residual Friction Angle

C = Cohesion Value

$k_s$  = Shear Stiffness

$k_n$  = Normal Stiffness

E = Young's Modulus

$\nu$  = Poisson's Ratio

DAQ = Data Acquisition System

UCS = Uniaxial Compressive Strength

RMC = Royal Military College of Canada

WF = Wykeham Farrance

ASTM = American Society for Testing and Materials

LVDT = Linear Variable Displacement Transducer

# **1 Introduction**

## 1.1 Topic

The field of Geotechnical and Geological Engineering has experienced many technological advances in recent history. As the natural strength of materials is exceeded by the infrastructure requirements of ever-larger tunnels in weaker ground, the development of new support and reinforcement technology is necessary. These developments are also present in surface excavations where larger projects have been made possible by similar support and reinforcement advances. These advances not only allow for new, bolder designs but they also must ensure that the tunnels and excavations are safer for the workers present.

One of the common support systems used in modern excavations and tunnels is the rock bolt. Initially, the behaviour of these support elements was poorly understood, however, considerable research and lessons learned from practical applications has provided input in to producing better designs, installation methods, and improved performance of rock-bolts and other support systems (Brady and Brown, 1993; Doucet and Voyzelle, 2012; Forbes, 2015; Gervais, 2003; Oke, Vlachopoulos, and Marinos, 2013). Despite such advances, a significant knowledge gap exists in the research of these support systems. Though the behaviour of support systems as a whole are better understood, as are the geological conditions (Hoek, 2014; Marinos and Hoek, 2001; Terzaghi et al., 1996), there has been limited cited literature to date with respect to the determination of interaction strength parameters at the interfaces where the support, grout, and ground material interact (Oke et al., 2012b). Understanding implicitly the micro-mechanisms and strength/interaction parameters associated at these peripheries, both before and after peak strengths of the materials have been reached, is critical not only for effective design of such support (individually and within support arrangements) but also for numerical modelling and analysis purposes. Current support modelling techniques associated with industry-standard modelling software packages have their limitations. There is limited information available associated with the shear strength and stiffness at the support interfaces (including interfaces between rock bolts and the ground as well as with the grout, for example). Common industrial practice is to use engineering judgement with respect to these input parameters which provide a 'reasonable' model response (Oke et al., 2012b), however, this does not constitute a best practice. These concepts and gaps in the current literature are further explained in Chapter 2.

In order to address such gaps in scientific knowledge, it is necessary to conduct field and/or laboratory testing with a view to developing a comprehensive database for these interface shear parameters; which, in turn, could be used for numerical model calibration or validation. These in-situ or laboratory-obtained parameters will add value with respect to engineering analysis and design decisions. As well, such interaction parameters will also provide valid input parameters in order to help improve numerical models used to predict ground behaviour which include support systems. This thesis includes a combination of

laboratory tests in order to obtain such interaction parameters as well as computer models which assess the software package's ability to accept or include such parameters.

## 1.2 Methodology

The test methodology applied in this research investigation was non-trivial. To the best of the author's knowledge through a comprehensive literature review, there is no specific apparatus or test standard which focuses on the direct shear testing of interfaces between these dissimilar materials. Accordingly, it was decided to utilize a modified ASTM D3080 constant rate of strain direct shear test. The chosen testing apparatus was relatively simple as shear testing of materials is common and has been used for similar interface testing of geo-synthetics (O'Rourke et al. 1990, Goodhue et al. 2001, T. Krahn et al. 2007), skin friction of pile foundations (Potyondy 1961), and pressurized grout and soil tests (Hossain and Yin 2014).

These previous works demonstrated that direct shear testing could effectively be used for testing of the interface shear behaviour between two materials, provided the boundary between the materials was aligned with the shear plane of the shearbox. These material interfaces are commonly seen in ground support systems in tunnels and other excavations. **Figure 1-1** demonstrates a common tunnel profile displaying a typical profile of ground support member. When examining the individual profile of a support member two distinct interface scenarios are seen for the grouted support member: one between the support member and the grout, and another between the grout and the surrounding ground. As the surrounding ground mass moves in towards the excavation (and coaxial with the support member) shear stresses develop along the interfaces between the support element, grout (if present), and ground. If these interfaces, highlighted in **Figure 1-1**, are examined more closely in cross section, they resemble in appearance and in stress condition the sample placed in the direct shearbox in **Figure 1-2**.

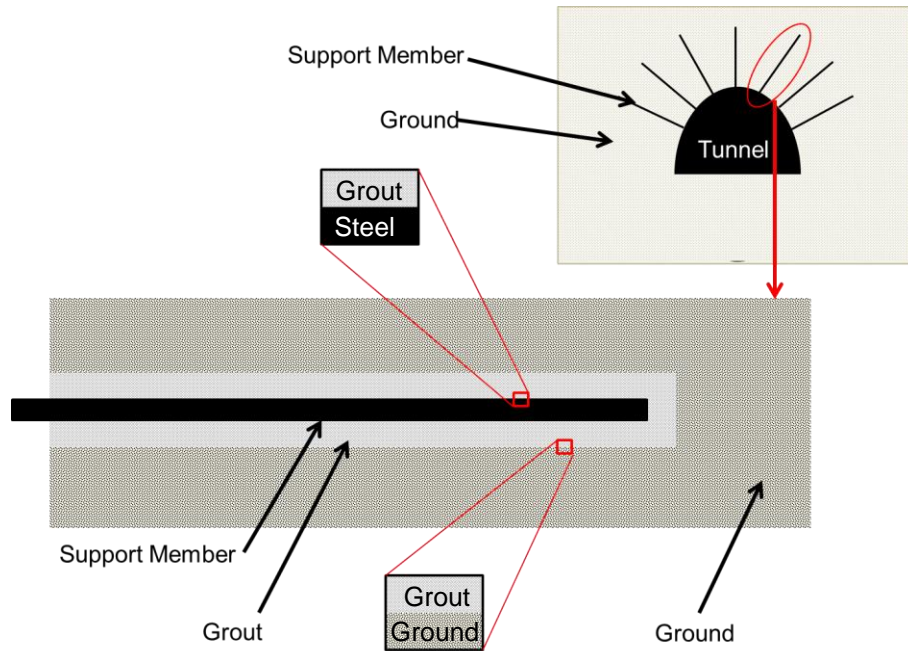


**Figure 1-1** Generic cross section of grouted support member

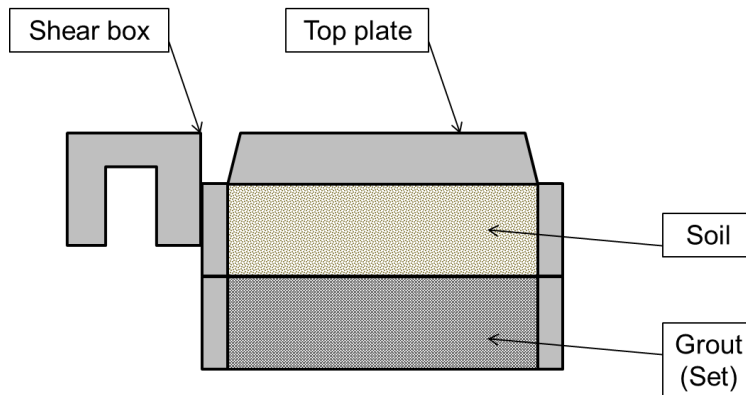


**Figure 1-2** Cross section of direct shear test of interface between two different materials

Since direct shear was the desirable test method for these material interfaces, a direct shear test apparatus was selected from the soils laboratory at RMC. The direct shear machine was validated by two means in order to confirm their normal function. The first method was to use a geo-material of known shear strength recorded in literature and compare the results with those from a WF2500

shear machine. Agreement of the results between the shear machines would confirm that the rebuilt WF2500 machine was providing accurate output. The second validation method considered the testing of the Brighton sand material and a comparison test on another direct shear machine. After both machines yielded comparable values it was confirmed that the main test apparatus was functioning adequately. Further details of the validation are elaborated upon in Chapter 4.

After validation, the shear tests of the following different interfaces were conducted:

- a. Pure sand sample;
- b. sand and grout;
- c. sand and steel;
- d. rock and grout;
- e. rock and steel;
- f. grout and steel; and,
- g. grout and concrete.

From the test data for all the above interface scenarios, the Mohr-Coulomb shear strength envelope as well as the shear stiffness associated with the material interfaces was determined. With this information, it was possible to create a 2D numerical simulation of the direct shear test. This model was created in a manner that the average of the shear stress along the interface was taken at each stage of displacement. From this, the shear stress versus displacement was plotted alongside the laboratory direct shear tests. Further details and results of the testing program are presented in Chapter 5 and APPENDIX A.

The data was then used to reach the second objective of this research. This was to validate if the numerical simulations would correctly predict the shear behaviour of interfaces when given the experimentally determined parameters. A numerical simulation of a direct shearbox was produced which mimicked the conditions of the laboratory test apparatus and used the parameters determined from the experimental testing. Theoretically, the shear stress across the shear plane of the simulated shearbox at different displacements should yield the same shear strength versus displacement plots as the laboratory tests. Further details and results are summarized in Chapter 6 and APPENDIX C.

### **1.3 Organization**

This Thesis is organized into 7 chapters and follows the thesis writing guidelines for the Royal Military College of Canada. A diagram of the contents, methodology and components of the thesis is provided in **Figure 1-3** to demonstrate how different chapters and ideas connect to one another. The chapters and their contents are listed below:

**Chapter 1 Introduction:** This chapter introduces the main objectives of the research and the methodology that was used.

**Chapter 2 Background:** This chapter briefly discusses the background of tunnelling, tunnel support design and function. It also discusses knowledge gaps on support systems and how this research aims to address current gaps in scientific knowledge.

**Chapter 3 Materials:** This chapter includes the types of materials that were used in testing. The chapter summarizes the properties of the materials used for comparison and numerical modelling.

**Chapter 4 Testing and Instrumentation:** This chapter provides details associated with the test methodology, preparation of the direct shear apparatus, and limitations and validation of the direct shear machine. This chapter also discusses the selection and calibration of instrumentation, data acquisition, and software. The details of the testing program and the steps of the testing procedure are additionally summarized.

**Chapter 5 Laboratory Results and Discussion:** This chapter summarizes and discusses the results associated with the testing that was conducted as part of this research. It incorporates the major findings, overall trends, limitations, and discussion points with respect to the interface shear behaviour of the arrangements that were tested.

**Chapter 6 Numerical Analysis - Results and Discussion:** This chapter describes the modelling software, technique, development, and the evaluation of the numerical model that was created for this research. It also discusses the differences between the results of the numerical models and the results determined experimentally.

**Chapter 7 Conclusion:** This chapter summarizes the results of all tests detailing how the research contributes to the understanding of shear behaviour of ground support systems and associated modelling. It also provides direction and recommendations for the next steps of research within this domain as well as implications to ground support design.

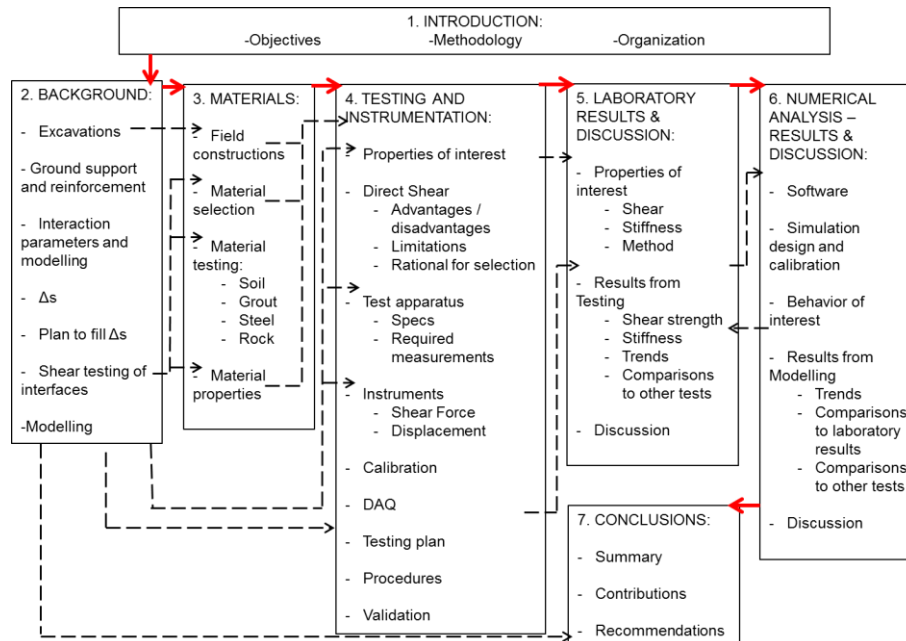


**Figure 1-3** Diagram Outlining Thesis Contents

## 1.4 Objectives

The two primary objectives of this research are to:

- I. Obtain, document and provide interface shear behaviour parameters for various support materials and geo-materials. These include:
  - a. Soil-Soil;
  - b. Soil-Steel (i.e. interaction between in-situ soil and rebar/rock bolt);
  - c. Soil-Grout (i.e. interaction between in-situ soil and grout utilized in ground support);
  - d. Rock-Steel (i.e. interaction between in-situ rock and rebar/rock bolt);
  - e. Rock-Grout (i.e. interaction between in-situ rock and grout utilized in ground support);
  - f. Grout-Steel (i.e. interaction between grout and rebar/rockbolt); and,
  - g. Grout-Concrete (related ongoing research);

- II. Assess the performance of numerical models using the shear parameters determined from laboratory tests with a view to determine the suitability or relevance of:
  - a. The default input interaction parameters that are utilized within industry-standard numerical modelling programs; and,
  - b. The ability for the numerical software to incorporate experimental values of laboratory-determined input parameters.

Ultimately, the accomplishment of both these objectives provides the scientific community with an improved database of interaction parameters and initiates future investigative research into the shear behaviour of the interfaces between ground support and geo-materials.

## **2 Background**

## 2.1 Excavations

Excavations are associated with some of the oldest engineering works in the world. As time passed, and human tools and engineering knowledge developed, the scope of these works also grew. Eventually, the excavations began to exceed the natural strength of the ground and resulted in collapses. Humans recognized the need to reinforce the ground using artificial means. Over time, this knowledge has greatly improved human capacity to construct earth works including tunnelling, mining and surface excavations.

Tunnelling has been a challenging task due to the unpredictability of the material being tunnelled through and the mass of the earth being supported. For centuries, efforts were made to better understand geology and this has aided tremendously in our ability to determine if the ground is stable enough for construction. This determination is further complicated because by excavating, the equilibrium of the ground is disturbed. This results in a change of the stress regime within the ground. Typically, the ground deforms to reach a new point of equilibrium. This is a problem, since tunnels must typically maintain specific dimensions in order to fulfill their function and maintain their design specifications. As well, fractures throughout a rock mass or unstable soil could cause a cave-in when stresses which used to confine the material are released. Though these risks initially limited the excavation of tunnels, builders developed methods of reinforcement and support that aided to control the movement of the ground and stress redistribution within the materials as illustrated in **Figure 2-1**.

Surface excavations have presented some unique problems, but they are related to tunnelling in that the ground is disturbed by excavation and stresses are redistributed to reach a new equilibrium within the ground. Often, this has resulted in collapses of the excavation creating danger to workers and equipment. Over time, to prevent this, support systems were developed to control both stresses and displacements as seen in **Figure 2-2**.

As excavations have continued to go deeper and further and into more complex geology, support and reinforcement has become a significant focus for research by geotechnical engineers and practitioners.

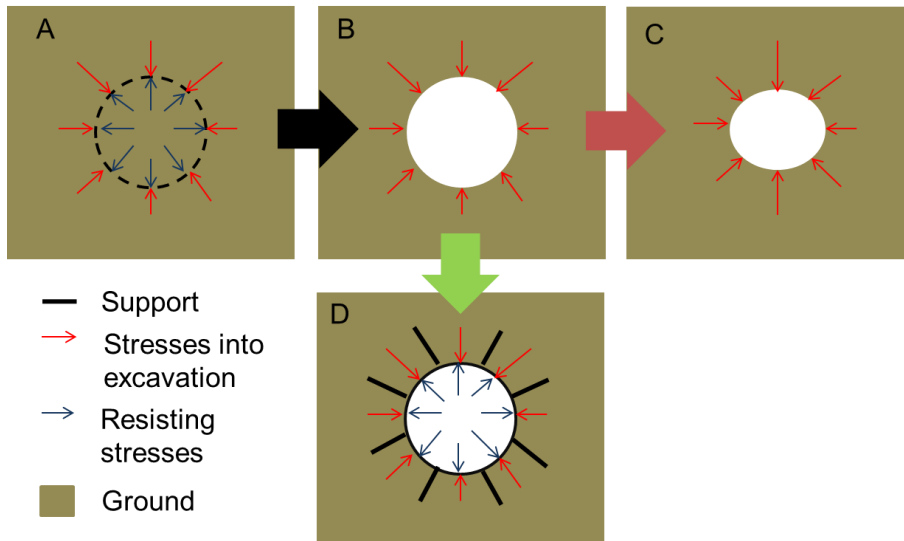


**Figure 2-1** (A) Stress conditions pre-excitation, (B) stresses at moment of excavation, (C) tunnel without support deforming under stress, and (D) excavation with support applied stresses controlling displacement of tunnel

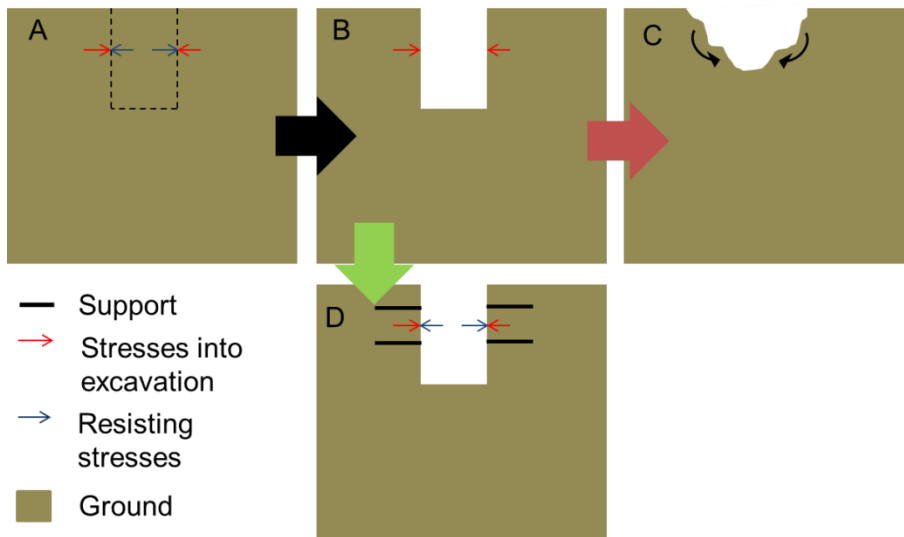


**Figure 2-2** (A) Stress condition pre-excitation, (B) stresses at moment of excavation, (C) excavation collapse due to stress redistribution, and (D) excavation supported resisting earth pressures

## 2.2 Ground Support

Ground support has been around for centuries from the simple use of wooden boards by sappers in the middle-ages supporting tunnels while undermining castle walls, to supporting the hanging wall in mines and infrastructure tunnels. Now modern resin bonded steel supports, umbrella arch systems, and various other means are used to provide this support and control the movement of the ground around an excavation (Brady and Brown, 1993; Gervais, 2003; Hudson and Harrison, 1997).

Ground support comes in diverse forms and has different applications depending on the design purpose and life of the excavation. It can also depend on whether it is pre-excavation support, installed during excavation, or support installed after excavation. Spiles and forepoles are a type of pre-support commonly used and installed ahead of the tunnel face in what is commonly called an umbrella arch. This helps to stabilize the roof of the next section of tunnel giving protection to workers and equipment in weak rock while further support is installed after the excavation (Oke et al., 2013).

There are a wide variety of these support systems and the naming of these supports has historically differed from continent to continent however, recent efforts have been made to standardise naming conventions for different types and methods of ground support (Oke, Vlachopoulos, and Marinos, 2013). Spiles are commonly solid steel rods, similar to rebar, employed in regions where geological structure could result in local failures. To protect against local failures such as spalling or ravelling they are typically installed less than 30cm apart. The length of installation is typically shorter (less than the Height of the excavation) and is done at angles between  $5^{\circ}$  and  $40^{\circ}$  to control the structural behaviour of the rock mass.

Forepoles are another type of support. They are commonly hollow sectional pipes used in umbrella arches. Typically, these are meant for areas with varying geology and fracture orientations anticipated ahead of the face. Forepoles have length greater than the height of the excavation and can extend up to 30m ahead of the face. These are longitudinal support members that are inserted parallel to the direction of excavation. Depending on the forepole diameter, and the desired confinement of rock between the forepoles, spacing is between 30cm and 60cm. The angle of the support installation is between  $3^{\circ}$  and  $8^{\circ}$  allowing for support to extend beyond the plastic region ahead of the tunnel face (Oke et al., 2014).

The next stages of support typically involve the installation of rock bolts and anchors in both the crown and invert of the tunnel's cross section. **Figure 2-3** demonstrates a generalized installation pattern for these umbrella arch and rock bolt systems. As well, steel sets (typically composed of W-sections) can be installed depending on design considerations. These steel supports act as ribs to control the deformation of the rock into the excavation in concert with the other support measures. They are typically spaced between 1m and 2m apart (Hudson and Harrison, 1997; Oke et al., 2013).

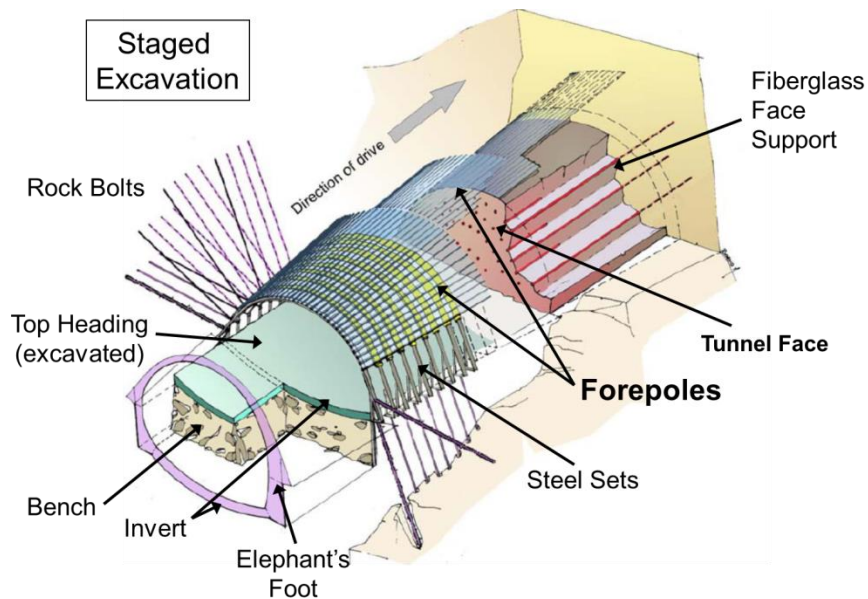


**Figure 2-3** Diagram of complete support systems and placement modified from (Grasso et al., 2003; Oke et al., 2012a)

Over time, it has become necessary to better understand the ground material and how it behaves in conjunction with the support in order to optimise such support for cost and safety reasons. Literature values for parameters regarding interaction between the support and ground materials are extremely limited. This is a serious knowledge gap as it is critical component for a full understanding of the behaviour and performance of supported excavations, and for numerical modelling of the support systems and tunnels. Thus far, research has focused on geology and how geo-materials, whether rock or soil, behave (Hoek, 2014; Marinos and Hoek, 2001; Terzaghi et al., 1996). This has been critical because if stresses and deformation of the ground are not understood and predicted then appropriate support cannot be employed (Brady and Brown, 1993).

Support design and selection is also critical for tunnelling and is something that has undergone tremendous changes over recent decades (Oke et al., 2013). Initially, support was employed in a very subjective manner using previous experience and engineering judgment. Though the support usually worked, it was not necessarily efficient or well designed. Gradually, the behaviour of the supports themselves was better understood with respect to strength and how the loading of the supports occurred. The understanding of support behaviour continues to improve with the use of new instrumentation techniques to continuously monitor the behaviour and performance of support in demanding environments (Forbes, 2015; Oke et al., 2013).

Though the term support and reinforcement have been used interchangeably by some, an accepted technical difference in meaning exists between ground “support” and ground “reinforcement”. Support refers to a method of controlling a tunnel or excavation’s deformation by applying external loads (eg. shoring, gravity walls, or steel sets). In these cases as the ground deforms into an excavation the support systems begin to apply a resistive stress to control the movement of the ground into the excavations (Hudson and Harrison, 1997). Reinforcement refers to materials installed in the ground to improve the ability of the material to support itself. Commonly, these reinforced ground masses behave similarly to steel-reinforced concrete or other such composite materials whereby the materials provide strength in bending or tension. Examples of reinforcement include forepoles, spiles, soil nails, or geo-grid (Hudson and Harrison, 1997). For the purposes of this research, support and reinforcement were used interchangeably as these shear interaction parameters can apply to both, depending on the mechanism of interaction between the ground and the element(s) within.

As mentioned above, there are a wide range of different support and reinforcement systems. Each system has its own attributes, nuances and design considerations. A comprehensive summary of these design methods would be a large undertaking and therefore, for the purposes of this research it was considered reasonable to use one example from the many different types of support and reinforcement in order to provide a general idea of what is involved in support design and behaviour. In **Table 2-1** a list of several different types of support and reinforcement systems and their application is shown.

**Table 2-1** List of examples of support and reinforcement systems and their applications

Support Type	Application
Forepoles	Tunnel
Spiles	Tunnel
Rock Bolts	Excavation/Tunnel
Dowels	Tunnel/Excavations
Anchors	Tunnel/Excavations
Piles	Excavations

A good example of support from the above list is grouted anchors. They are commonly used in both surface excavations and tunnelling and cover general design considerations of both reinforcement and support systems.

Calculations for the installation of support have now been well established. The Canadian Foundation Engineering Manual 4<sup>th</sup> Edition (2007) describes how the failure of these systems can occur in retaining wall structures. The method proposed to solve these problems was to use earth pressure theory in order to determine the stresses acting on the wall. From this, the various force vectors were

solved for using statics. This allows for the appropriate anchor strength and direction to be determined (Figure 2-4).

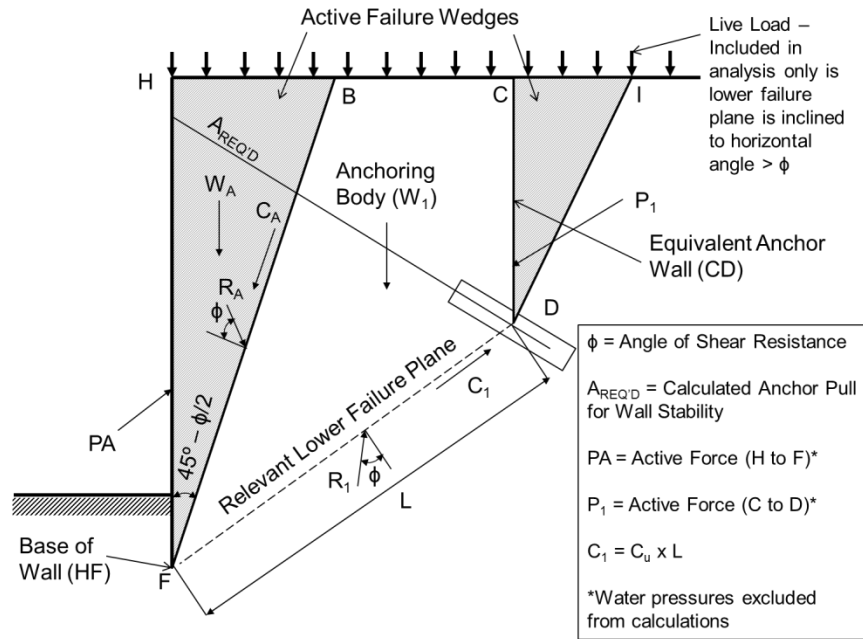
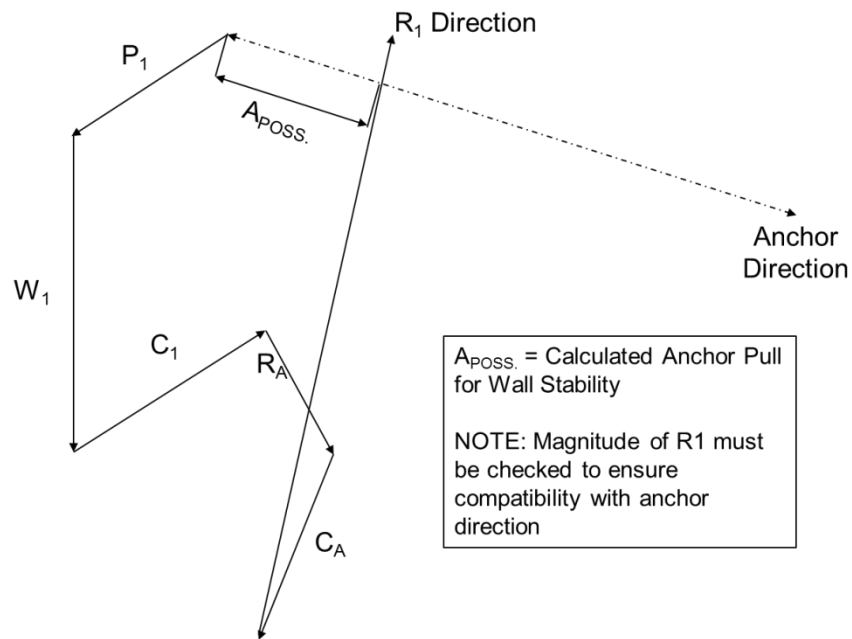


Figure 2-4 Schematic of earth pressures in an anchor reinforced excavation wall (CFEM, 2007)



**Figure 2-5** Vector diagram of forces from anchor wall in **Figure 2-4** (CFEM, 2007)

Guidance in the Canadian Foundation Engineering Manual provides equations for different ground conditions to calculate the pull-out strength of the anchors. It also states that these equations are not substitutes for field testing during the construction phase. For grouted-anchors installed in cohesionless soils, **Equation 2-1** is used, where the effective vertical stress ( $\sigma'_z$ ) applied to the surface area ( $A_s$  = effective unit surface area of bonded grout and  $L_s$  = effective length of bonded grout) of the anchor is related to the axial pull-out resistance ( $P_{ar}$ ) by an anchorage coefficient ( $\alpha_g$ ) taken from **Table 2-2** (CFEM, 2007). No reference was available for these anchorage co-efficients, or how they were determined, but it would be reasonable to assume they were produced from the aggregate anchor performance data of various pull-out tests or failures at different engineering sites or laboratories.

$$P_{ar} = \sigma'_z A_s L_s \alpha_g \quad \text{Equation 2-1}$$

**Table 2-2** Anchorage coefficients ( $\alpha_g$ ) for cohesionless soils (CFEM, 2007)

Soil Type	Different Relative Density		
	Loose	Compact	Dense
Silt	0.1	0.4	1.0
Fine sand	0.2	0.6	1.5

Soil Type	Different Relative Density		
	Loose	Compact	Dense
Medium sand	0.5	1.2	2.0
Coarse sand, gravel	1.0	2.0	3.0

For grouted-anchors installed in stiff clays the pullout resistance is determined using **Equation 2-2**, where the average undrained shear strength of the clay over the anchor length ( $s_u$ ) is multiplied by the effective anchorage area and an adhesion factor ( $\alpha_c$ ). This factor is determined from a chart related to the undrained shear strength of the soil (**Figure 2-6**) (CFEM, 2007). These coefficients also lacked a source or description of their derivation and it was not clear how the shear strength for the stiff clay soil was determined at the point where the anchor was grouted.

$$P_{ar} = \alpha_c A_s L_s s_u \quad \text{Equation 2-2}$$

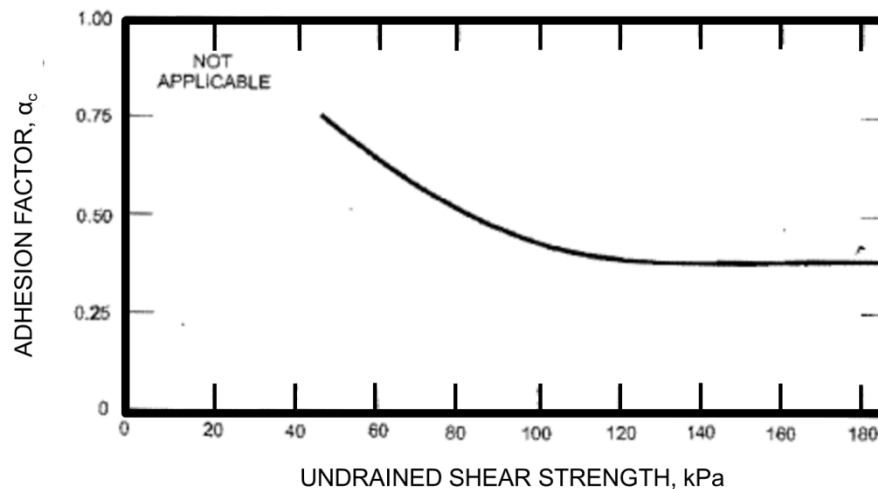


**Figure 2-6** Adhesion factors with respect to undrained shear strength of cohesive soils (CFEM, 2007)

The adhesion and anchorage coefficients for these design formulas have worked well in the past for design and construction. Despite past performance, uncertainty has remained about the underlying shear behaviour between the anchor and ground materials where they meet and interact during loading.

### 2.3 Interaction

With these advancements in understanding how ground behaves, and how ground support and reinforcement behave, the next step is assessing how these

materials interact with one another at the boundary between the two materials. Interaction refers to the physical and mechanical behaviour of a finite element at the boundary between two materials. Looking at **Figure 2-7**, which is a cross section of tunnel and generic support, there are a variety of different points where different materials form interfaces. These regions are the area of focus for this research.

One thing to note when looking closely at these interfaces is how similar a small region across the interface is with respect to a direct shear sample (**Figure 2-8**). This similarity makes use of ASTM D3080 direct shear a preferable option for determining these parameters.

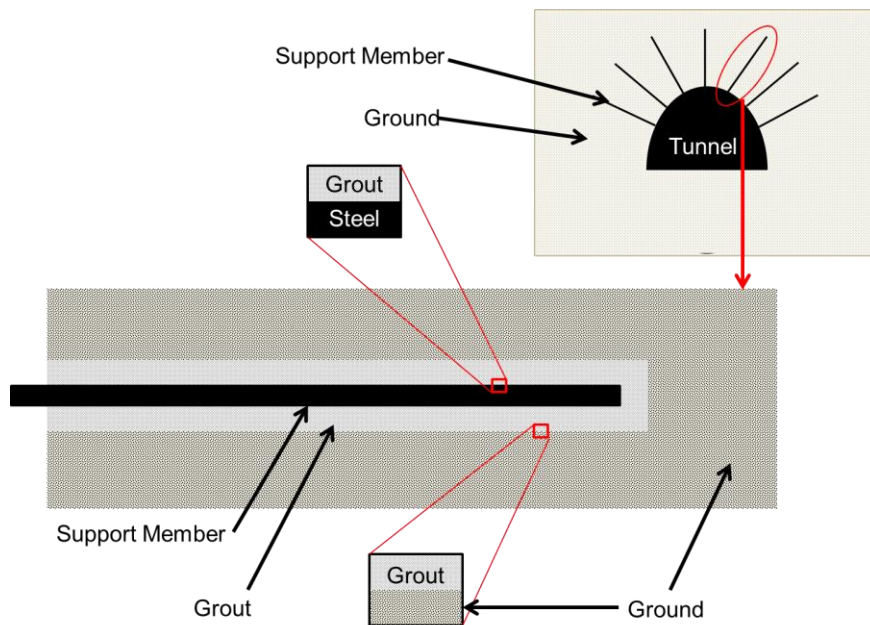


**Figure 2-7** An example of interface scenarios found in a common tunnel support cross section

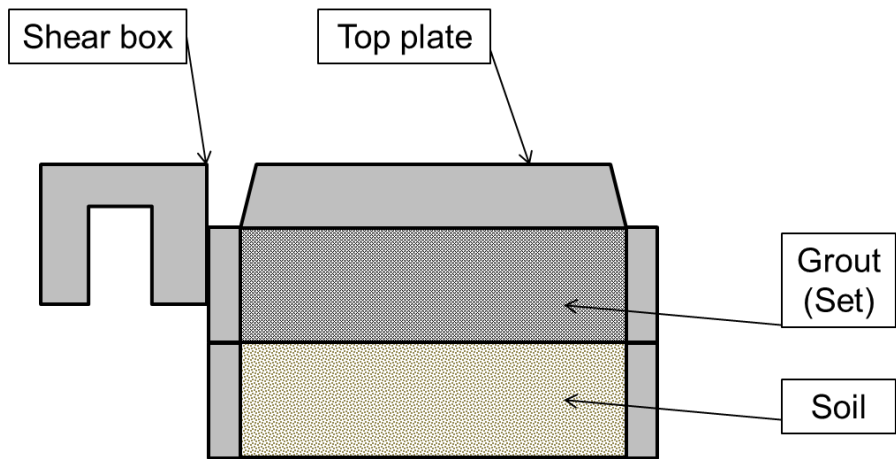


**Figure 2-8** Generic shearbox cross section

It is common for these support and reinforcement members to fail axially due to shearing at the interfaces. This shear failure fits well with the direct shear tests; Specifically, if the examples from above are taken and loading is applied, it is clear how the direct shear test is able to replicate the small scale interaction between the materials as seen in **Figure 2-9** and **Figure 2-10** below.

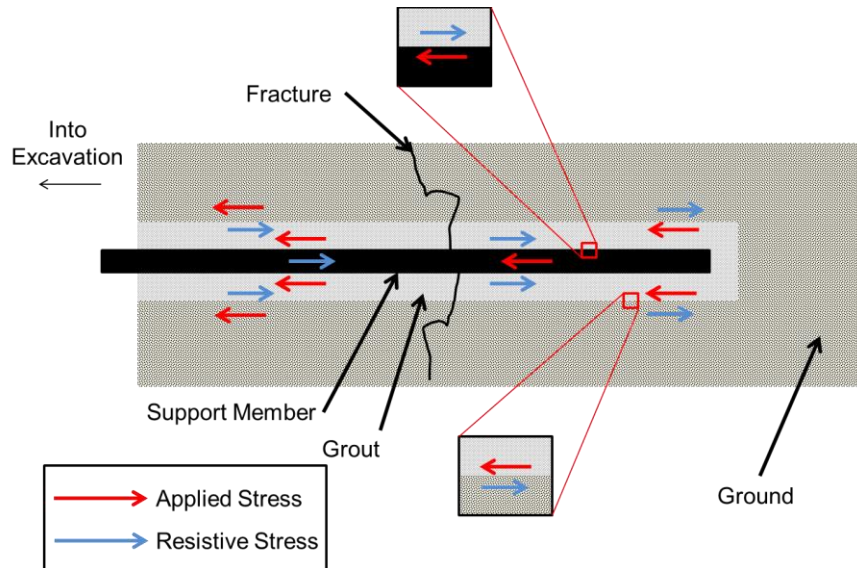


**Figure 2-9** Stress transfer across interfaces in a generic fully grouted cable bolt cross-section loaded axially from a block failure

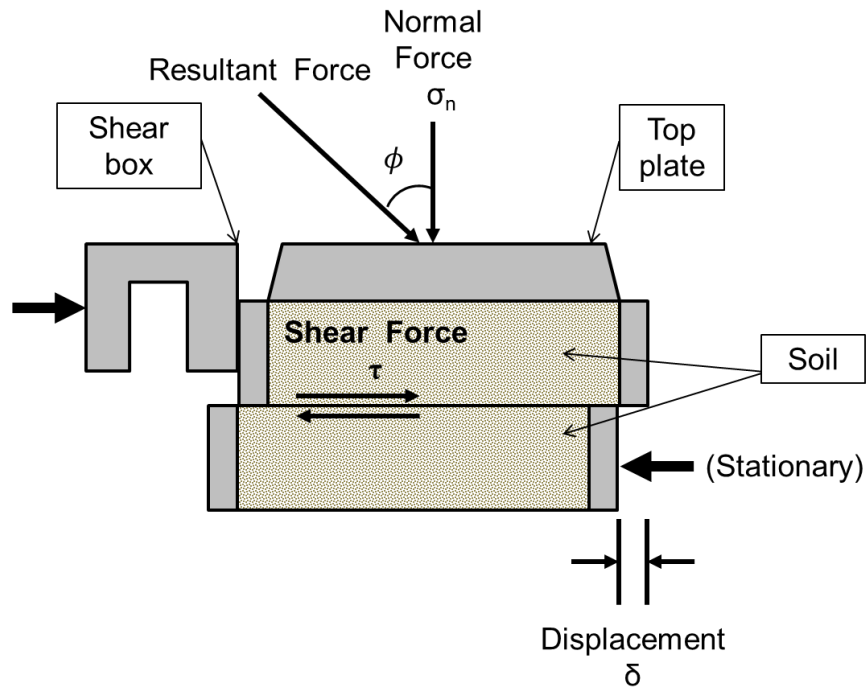


**Figure 2-10** Cross-section showing forces acting on a sample during direct shear testing

Interface scenarios are not limited to rock bolts but are present as previously seen with grouted anchors, forepoles, dowels, and various other reinforcement and support systems. These interfaces are critical to design as they must be capable of withstanding stresses applied to them even at the construction stage in order to prevent failure which could result in death, injury, or destruction of equipment.

## 2.4 Knowledge Gaps

The use of support and reinforcement members in tunnelling and surface excavations has necessitated a substantial ongoing effort to understand the behaviour of the individual supports, as well as the ground in which the materials are placed. The members do not act alone, but they act in concert with the ground. The general behaviour of forepole and pile supports in tunnels indicates a longitudinal load transfer which applies a shear force parallel to the individual members (Oke et al., 2012a). Empirical data on these interactions has been very limited making design challenging. This empirical data is also essential to properly model the mechanistic behaviour of support members both individually and globally. Parameters of specific interest are values of shear strength and stiffness of the interfaces between support elements, any adhesive materials used for

installation, and the surrounding ground (Oke et al., 2012a; Oke et al., 2012b). Selected numerical analysis programs, such as FLAC 3D (Itasca, 2009), allow for inputs to be made using the Mohr-Coulomb failure criterion (for example). These input parameters set the properties of springs and sliders between nodes of the ground and the support elements (**Figure 2-11**). The springs and sliders are representative of the stiffness and shear strength respectively (Oke et al., 2012a). The input parameters for such interaction arrangements are not specifically known and/or available in literature. As well, the default values used within the numerical programs can vary between programs.

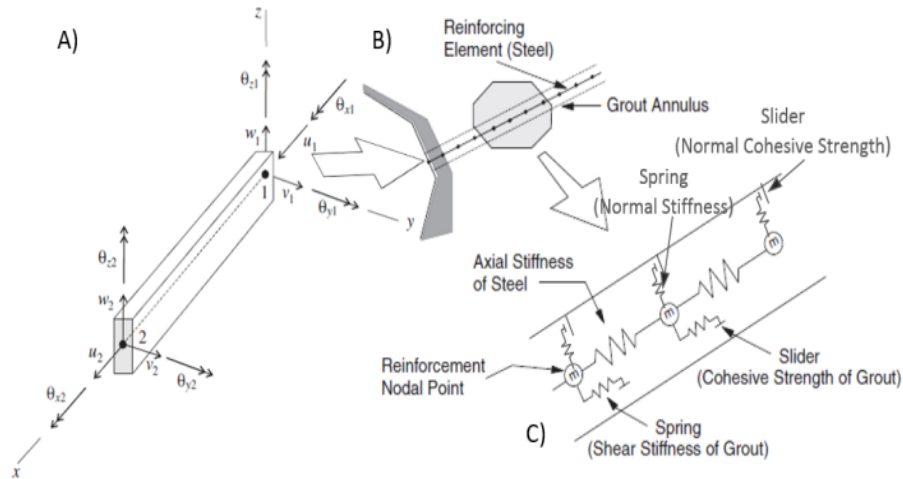


**Figure 2-11** (A) Free body diagram of support element in FLAC 3D model, (B) Global image of element position in model, (C) Details of interaction between nodes of the support and the ground material (Itasca Consulting Group Inc., 2009)

**Figure 2-11** is a simple rheological model for the shear interfaces but it was a logical means of representing the mechanisms / behaviour that is anticipated in reality. Phase 2 (a 2 Dimensional modelling software (Rocscience Inc., 2014)) employs similar rheological models for modelling joint interfaces. Though joints in Phase 2 can have their shear parameters modified, when using the support design tool within Phase 2, the simulation does not account for the shear behaviour of the support-ground interface (Rocscience Inc., 2014). This simplification of support could be dangerous as shear failure commonly occurs at the interface between support and the ground or support and the grout (Brady and Brown, 1993).

This failure at interfaces between materials has been seen in laboratory testing of support systems by Cruz et al. in 2016. While conducting laboratory tests on steel rebar type rock bolts in simulated boreholes it was noticed that shear failure was occurring at the interface between the grout, around the anchor, and the concrete used to simulate the rock mass (**Figure 2-12**). These tests were focused on utilizing optical fibre as a means of measuring strain on the steel member;

however, they have provided an example of the importance of understanding the shear behaviour and mechanisms associated with these interfaces (Cruz et al., 2016).

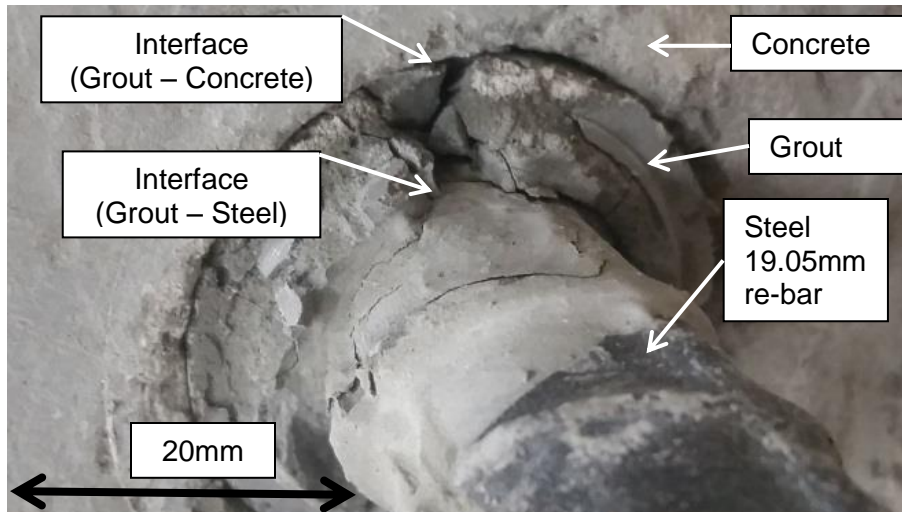


**Figure 2-12** Shear failure of grout-concrete interface for axial testing of steel rebar rock-bolt. Note: Concrete simulates rock in these tests. (Cruz et al., 2016)

## 2.5 Plan to fill Knowledge Gaps

It is important to fill in the above-mentioned knowledge gaps to utilize correct interaction parameters for such support elements as well as to utilize realistic input parameters for numerical models for design purposes. Since current models have used the Mohr-Coulomb failure criterion for their design of interfaces of discontinuities, it is logical to begin the investigation by assessing the Mohr-Coulomb shear strength of the interfaces between the different materials involved in support system to ground interfaces. One of the most used and trusted methods for this measurement is ASTM D3080 direct shear testing which will be discussed in the next section.

## 2.6 Shear Testing

Direct shear testing dates back to the late 18<sup>th</sup> century and early methods of shear testing (not unlike the modern ones) were used by Coulomb, C. in his Essay on Statics in 1774 (Heyman et al., 1972). This work eventually led to the development of the Mohr-Coulomb strength envelope by Mohr, C. in 1882 (**Figure 2-13**). The development allowed for a way to relate normal stress, shear stress, and principle stresses at failure for a finite element within a material. **Equation 2-3** gives the general form of the failure envelope (Heyman et al., 1972).

Ultimately, the ubiquitous use of the Mohr-Coulomb shear strength envelope for numerical modelling made it a preferable method for displaying the direct shear results. The Mohr-Coulomb shear strength envelope is also commonly used within other research related to shear strength (i.e. in soils and rocks). However, relevant research has been limited on the subject of interaction parameters (specifically) the two most relevant works are by Potyondy in 1961, and Hossain and Yin in 2014.

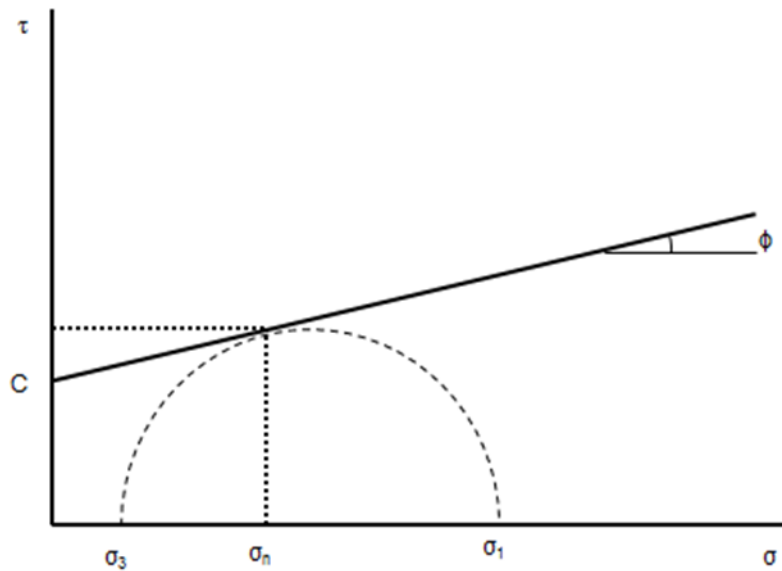


**Figure 2-13** Generic plot of a Mohr-Coulomb failure envelope ( $C$  = cohesion constant,  $\phi$  = Friction angle,  $\tau$  = shear stress,  $\sigma_n$  = normal stress,  $\sigma_{1,3}$  = principle stresses)

$$\tau = \sigma_n \tan \phi + c \quad \text{Equation 2-3}$$

Potyondy's paper was focused on the direct shear testing of diverse interface scenarios common to pile foundations. The results gave a guide to what the expected behaviour of the interfaces between these materials and soil were depending on the material's surface condition and type of soil. For construction materials, steel, concrete, and wood were used. The geo-materials he used were poorly graded sand, clay, cohesive granular soil, and rock-flour (silt) (Potyondy, 1961). With the construction materials, he also considered the surface condition and prepared rough and smooth samples of the concrete and steel for comparison. For the wood, he considered whether the direction of shear was normal to or in-line with the wood grain.

Though Potyondy considered many materials, his results were based on a limited number of direct shear tests. He conducted two tests for each interface condition, one at a normal stress of 50kPa (1000 lbf/sqft) and one at a normal stress of 150kPa (3000 lbf/sqft). These two data points from each interface scenario were then used to determine the friction angle and cohesion values for the interfaces, a selection of which can be seen in **Figure 2-14**. This was a sound starting point for interface shear behaviour, however, it lacked the fidelity and quantity of data necessary to begin creating a real database of interface shear behaviour for a variety of soil types. As well, the focus was on pile foundations and does not cover materials common in tunnelling such as rock and grout.

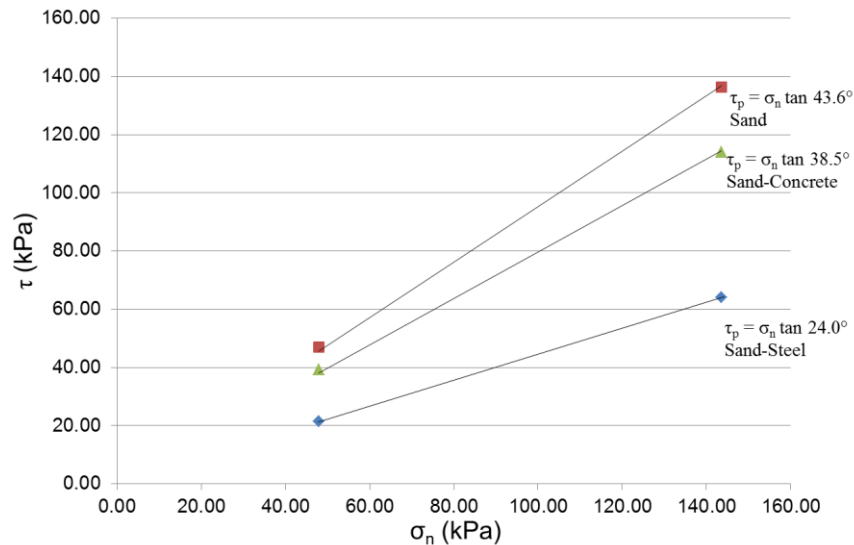


**Figure 2-14** Summary of shear strength results for poorly graded sand, poorly graded sand with concrete, and poorly graded sand with steel (Potyondy, 1961)

Research focused on reinforcement in tunnelling was done recently by Hossain in 2014. A common type of reinforcement used in tunnelling is pressure grouted rock anchors. These reinforcements have typically consisted of steel members where grout is pumped under pressure into the space between the support and the ground. This pressure can vary depending on the grout-water mix ratio and porosity of the soil. This means that grout pressure is typically difficult to determine accurately. As well, surface conditions can vary along the length of the reinforcement complicating interfaces (Hossain and Yin, 2014).

In order to test the influence of grout pressure on the shear strength of soils, Hossain (2014) had the direct shear samples created and then placed in a pressure vessel where a known atmospheric pressure was applied to the samples simulating the pressure grouting of the interface for 30 minutes. After that time,

pressure was slowly relieved and then the sample was left to cure for five days. Following this the sample was removed and installed into a direct shear apparatus to conduct a modified ASTM D3080 direct shear test. This test was repeated at different atmospheric pressures to assess the influence of grout pressure on the shear strength and the results were plotted relative to one another (Hossain and Yin, 2014).

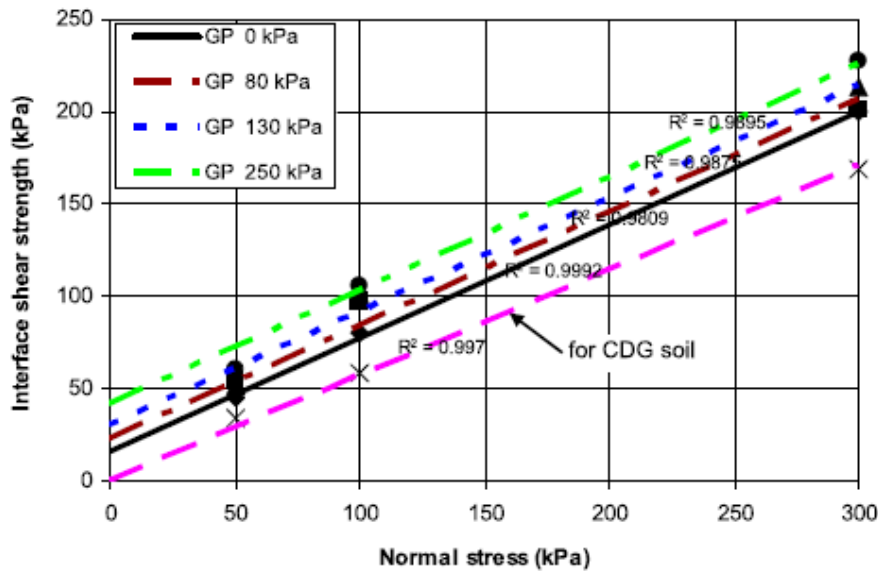


**Figure 2-15** Results from direct shear tests of pressurized grout-CDG interfaces, with direct shear results of pure CDG for reference (Hossain and Yin, 2014)

The common trend observed was that pressure grouting did not change the friction angle of the interface; it only influenced the effective cohesion. This increase was accounted for by adding an independent term to the Mohr-Coulomb shear strength envelope (**Equation 2-4**) (Hossain and Yin, 2014). It included the grout pressure ( $p_g$ ) and a declivity angle ( $\delta^g$ ). This declivity angle provided a means to relate the grout pressure to the increase in the shear strength determined from **Figure 2-16**. These results determined that the declivity angle was independent of the applied normal stress.

$$\tau = \sigma_n \tan \phi + c + p_g \tan \delta^g \quad \text{Equation 2-4}$$

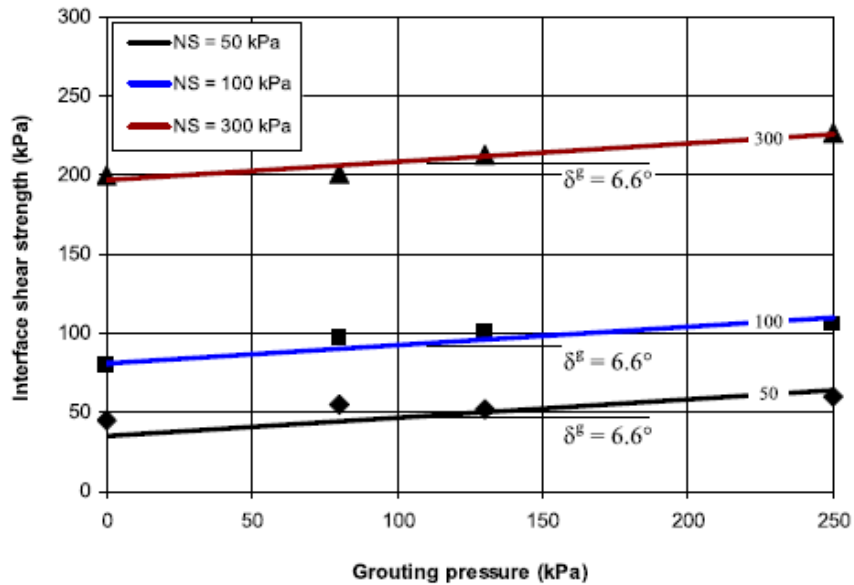


**Figure 2-16** Shear strength versus grouting pressure plot for direct shear tests of CDG - grout interfaces (Hossain and Yin, 2014)

Though Hossain and Yin's work confirmed that grout pressure has an influence on the shear strength, a common challenge has been certainty about the grout pressure and the actual adhesion of the grout to the ground. In rock reinforcement, grout losses have occurred when the pressurized grout flows into discontinuities during the installation process (Archibald, 2012). This uncertainty is also present in soil as there can be different materials of different porosity and water content at different points on the length of a reinforcement member (Hossain and Yin, 2014). This unpredictability has raised some concerns about how reliable design can be when considering these adhesion factors.

The Mohr-Coulomb shear strength envelope discussed above has been used prominently in the geotechnical field; However, there are other methods of displaying the shear behaviour of materials. One such method is the secant friction angle method. This method calculates a friction angle at different normal stresses from a secant between the origin and a data point. The measurement is repeated for each data point and then summarized on a friction angle versus normal stress plot. An example of the determination and presentation of the secant friction angle method can be seen in **Figure 2-17** and **Figure 2-18** respectively.

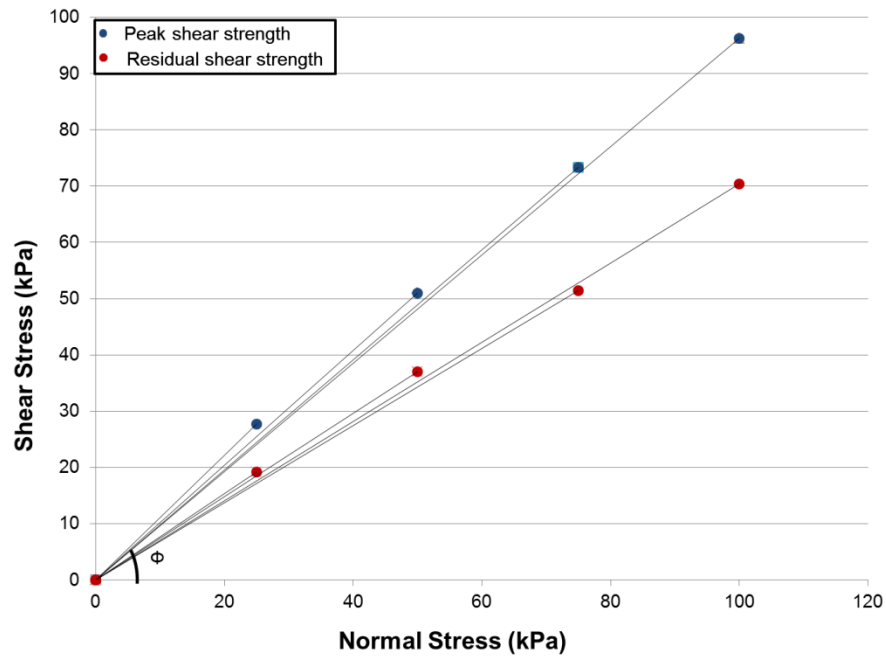


**Figure 2-17** Demonstration of secant friction angle determination from direct shear tests 0007-0009 for Brighton Beach Sand

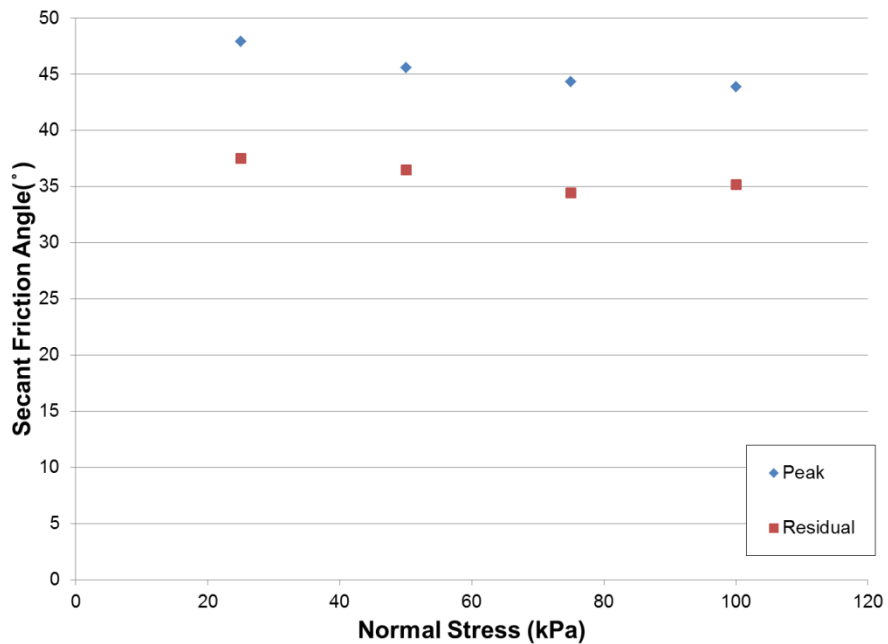


**Figure 2-18** Presentation of secant friction angle results for Brighton Beach Sand

This method has been used for direct shear testing with soil and geosynthetics (Thiel, 2009; Vlachopoulos, 2000); however, the Mohr-Coulomb shear strength envelope has commonly been used for numerical simulations of the interfaces, and was therefore a more practical method for this research.

## 2.7 Modelling

Using similar tests to those used by Potyondy 1961 and Hossain 2014 it would be possible to collect shear strength and stiffness parameters on the soils being used. This data would be useful for design equations as presented in Section 2.2, however, it also has applications within other design tools such as numerical simulations for tunnelling. These tools are relatively new and therefore, efforts continue to refine and improve the ability of the tools to accurately predict the behaviour of excavations and support in the real world as well as the micro-mechanics associated with interfaces. As such, improvement to the numerical tools require empirical data for calibration and validation purposes.

Numerical simulations have been used for several decades to improve the ability to design and predict excavation behaviour. Despite advancements in computer technology, many idealizations have been used for the purposes of modelling tunnels and excavations, especially when support is involved. One example of this is the practice of assuming that the support creates a continuum around the tunnel with unique behaviour compared to the surrounding ground. A typical example can be seen in **Figure 2-19** from work done by Oke et al. 2012.

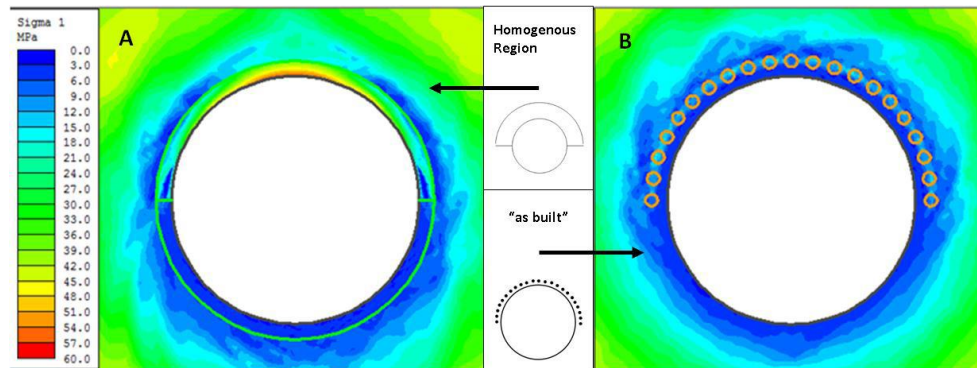


**Figure 2-19** (A) 2D model of tunnel cross section modelled by homogeneous region (B) 2D cross section of tunnel modelled by individual forepoles (Oke et al., 2012a)

Homogeneous region modelling showed two predominant problems. The first was the homogeneous region cannot accurately model stresses and displacements of the whole tunnel as displacements at the invert (bottom of tunnel)

and sides are overestimated. The other issue was that modelling as a homogeneous region ignores the mechanistic behaviour of the forepole elements. It was also noted that 2D models cannot properly account for the mechanistic behaviour of the forepoles which are longitudinal members that are arranged out of plane to the 2D simulations. It was concluded that in order to effectively model tunnels which use support, a 3D numerical simulation must be conducted (Oke et al., 2012a; Oke et al., 2012b).

The use of 3D models and the modelling of each support element individually provided more accurate results for this mechanistic behaviour. This was because it accounted for bending and deflection over the length of the support element and avoided the idealizations of the homogeneous region approach (Oke et al., 2012b). Though the results were much more accurate in the 3D model with individual support elements, no data was available to input for the shear interfaces of these support elements. This missing information made it necessary to assume values for shear strength and stiffness and calibrate the model accordingly (Oke et al., 2012b). Though this practice is common, it is not a rigorous means of designing these numerical simulations.

These design tools do not operate in isolation; they require information from both the laboratory and field in order to confirm their predictions. To further refine and improve the ability of engineers to use these design tools it is essential to determine the interface shear values as it is not reasonable to expect efficient designs when assuming values for how these interfaces will behave in shear.

## **2.8 Summary**

As geotechnical engineers attempt to excavate deeper or further into the ground it has become necessary to use artificial materials to reinforce and improve the natural ground materials or to use support to control the deformation of these materials. These support and reinforcement systems have taken a variety of forms and serve diverse purposes. They have been used in diverse geological conditions to control the behaviour of the ground, reducing risks to personnel and equipment. Significant work has been done to better understand the behaviour of the ground (Hoek and Marinos, 2007; Marinos and Hoek, 2001; Terzaghi et al., 1996), and the behaviour, employment, and efficiency of support systems (Forbes, 2015; Oke et al., 2012a; Vlachopoulos et al., 2014). This has led to significant improvements in the design and installation practices of these ground reinforcement and support devices, and in the modelling of the ground and supports. Unfortunately, significant gaps remain with respect to understanding how these elements interact with the ground material, specifically the interface shear behaviour. These values remain unknown and have a significant influence in numerical simulations which need them to produce accurate results (Oke et al., 2012a; Oke et al., 2012b). Though minimal historical data has been collected on the shear behaviour of these interfaces for ground support, selected, limited related work on similar interfaces

has been conducted successfully through the use of a modified ASTM D3080 direct shear machine (Hossain and Yin, 2014; Potyondy, 1961).

By using a similar test method, and collecting more comprehensive data, the results from these tests can produce a database of relevant interface shear parameters. These parameters will be of importance in terms of more accurate design, and numerical simulation of support systems in excavations. This could be accomplished by comparing the behaviour of numerical models using the laboratory test results as input parameters and comparing the results of these numerical simulations to the results of laboratory tests. From this, the simulations could be calibrated and redesigned to more accurately mimic real world behaviour of these ground support systems.

### **3 Materials**

### 3.1 Field Construction Methods

A wide variety of tunnel support system types and configurations are used as cited in Chapter 2. Designers have a plethora of different products for support design and these depend on the geology, groundwater, stress conditions, availability, logistics, finances as well as other, site-specific considerations. Despite the overall variety, tunnel support systems can generally be distinguished into two main techniques: grouted support, and un-grouted support.

Considering grouted support, there are varieties of grout types that can be used. The most common types of grout are made of a Portland cement base. Cement based grouts have been used for decades and are generally less expensive. Polymer resin grouts are a modern development. They provide different bonding characteristics. Grout can be installed by means such as pressure injected grout, or cartridges which are activated by spinning of the support. Despite the variety of types, once installed the cross section is commonly of the form presented in **Figure 3-1** below.

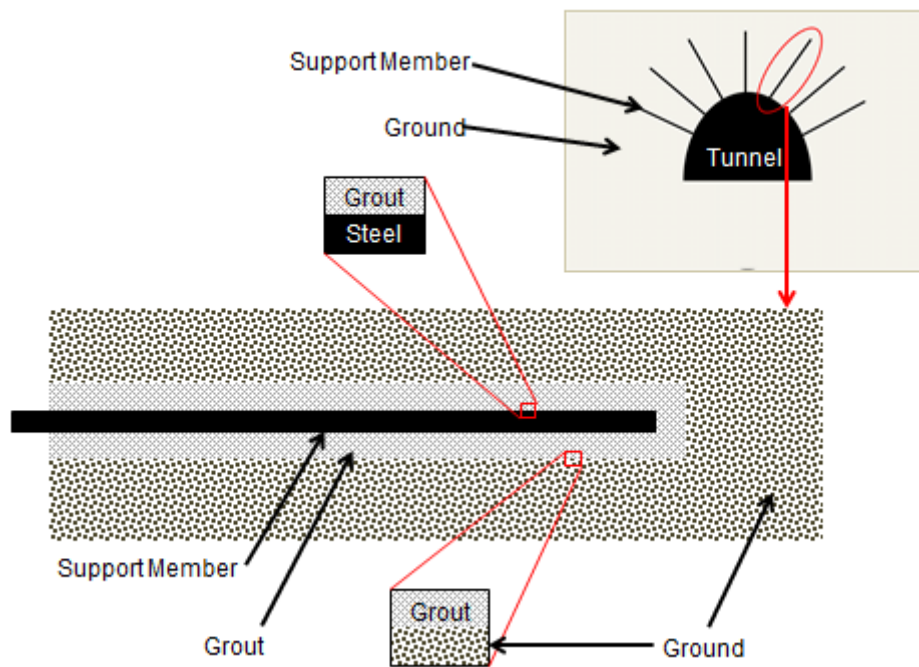


**Figure 3-1** Schematic of generic grouted tunnel support member highlighting the different interface scenarios

Another common form for support to take is the un-grouted scenario. In this case, the support is either driven into the ground, or expanded, by mechanical or hydraulic means, after installation into the hole. This expansion generates a confining stress normal to the circumference of the member. Regardless of the mechanism of installation, the common, general form of these supports after installation is as in **Figure 3-2** below.

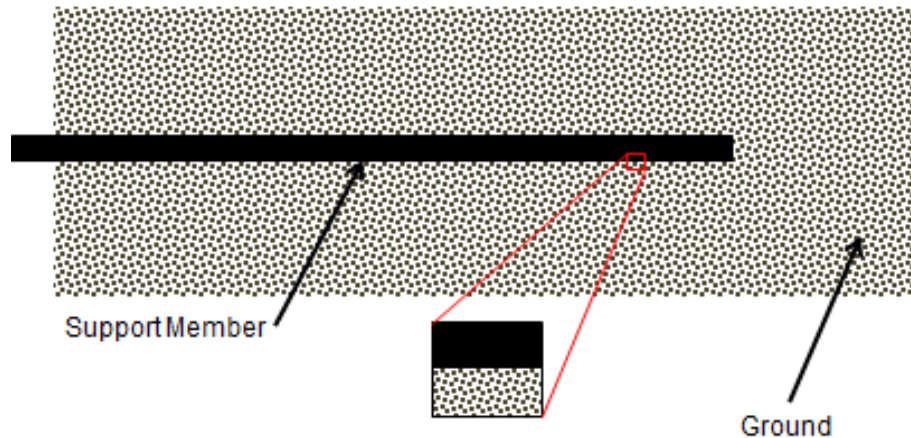


**Figure 3-2** Schematic of generic un-grouted tunnel support and relevant interface scenarios

These two common arrangements were determined as the interface scenarios that were most common for tunnel support systems. As such, the materials for testing were determined by the interface scenarios that exist for this type of common ground support. The interface scenarios that exist are:

- a. Ground – Support;
- b. Ground - Grout; and,
- c. Support - Grout.

In this way, each material was defined and tested independently (i.e. grout), ground (i.e. rock, soil), support (i.e. steel). These are the materials that were examined and included in this chapter. The permutations of interaction scenarios tested are included in Chapter 4 of this thesis.

### **3.2 Ground - Rock**

The rock sample (**Figure 3-3**) selected for use in the test was an agrillaceous Limestone from the Coburg formation, which is a geological

formation found in Eastern and South-central Ontario. The rock contained darker grey bedding layer of argillaceous Limestone with some lighter bands of fossiliferous Limestone. Its homogeneous nature, relative ease of cutting, and availability made it ideal for creating samples for testing. Two samples were cut from an Unconfined Compressive Strength (UCS) test cylinder. One of the samples can be seen in Figure 3 below. The UCS, Young's modulus (E) and Poisson's ratio ( $\nu$ ) was taken from the tests by Ghazvinian et al. (2015). These results are summarized in Table 1 below.



**Figure 3-3** First Coburg Limestone sample

**Table 3-1** Strength and elastic properties of Coburg limestone (Ghazvinian et al., 2015)

Properties	Average Values
UCS	72.5 MPa
E	37GPa
$\nu$	0.18

### 3.3 Ground - Soil

The soil used within this research program was a poorly graded, medium grained, and angular beach sand from Brighton, Ontario (**Figure 3-4**). This sand was chosen due to its availability, relative ease of sample preparation, and having a fines content of <1%. The latter allows it to drain freely and thus minimizes the development of pore water pressure. This soil has been used extensively at RMC

due to these properties (Bathurst et al., 2003; Bathurst et al., 2006; Vlachopoulos, 2000).

The grain size distribution was determined in accordance with ASTM D6913. Test results are shown in **Figure 3-5**. The results also allowed for the diameter at which 10%, 30%, and 60% of the mass of the samples pass the sieve ( $D_{10}$ ,  $D_{30}$ , and  $D_{60}$ ) to be determined. Further, the results in Figure 5 allowed for the coefficient of curvature ( $C_c$ ) and coefficient of uniformity ( $C_u$ ) to be determined. These are summarized in **Table 3-2**



**Figure 3-4** Poorly graded Brighton Beach Sand

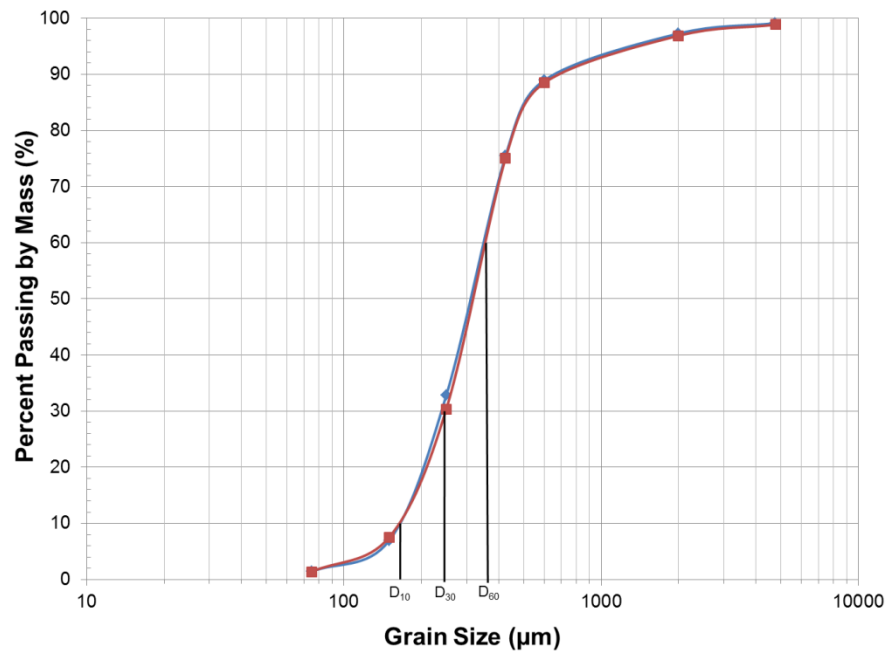


**Figure 3-5** Sieve analysis results of 2 separate samples of Brighton sand (ASTM D2487, 2011; ASTM D6913, 2004)

**Table 3-2** Results as obtained from the sieve analysis tests

Parameter	Values	Units
D <sub>10</sub>	0.16	mm
D <sub>30</sub>	0.23	mm
D <sub>60</sub>	0.35	mm
C <sub>u</sub>	2.2	
C <sub>c</sub>	0.9	

Under the USCS this material was classified as a poorly graded sand (SP) (ASTM D2487, 2011). The sand grains were also found to be highly angular.

The compaction behaviour of the sand was determined from previous soil mechanics research conducted at RMC by Vlachopoulos in 2000. The test was ASTM D698-91 Standard Test Method for Laboratory Compaction of Soil Standard Effort results are presented in **Figure 3-6**. This is the “Standard Proctor” test for determining the relative compaction effort needed to obtain certain dry densities. These test results were a useful reference to validate test preparation by confirming that densities were reasonable values. This information was also included for future research on interface shear to ensure comparable materials are used. These reveal a flat compaction curve, and therefore, moisture content has little influence on compacted dry density (Vlachopoulos, 2000).

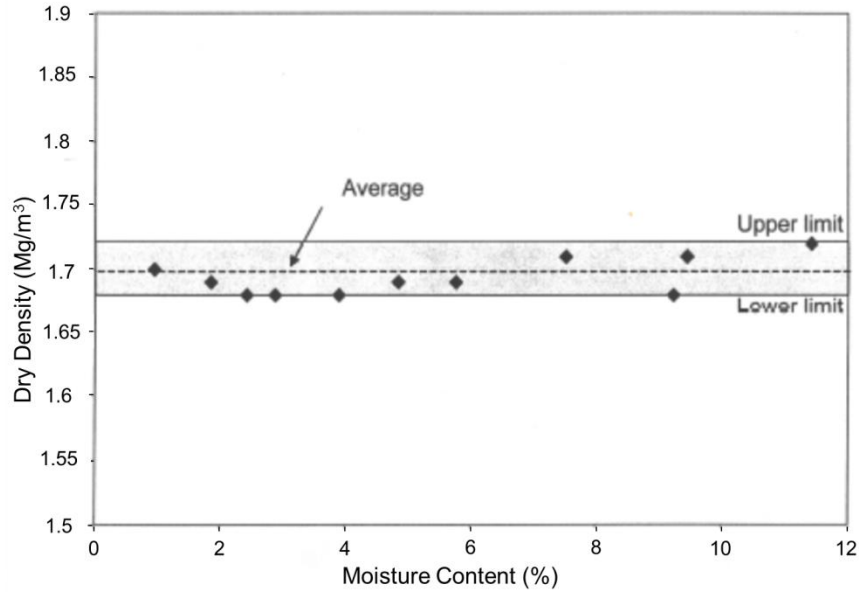


**Figure 3-6** Compaction curve of Brighton Beach Sand by (Vlachopoulos N., 2000)

The shear strength of the soil was determined using ASTM D3080 in order to establish baseline data for the interface interaction tests and also for validation purposes of the direct shear test apparatus. 24 tests were conducted on both the WF 2500 and WF 25403 (details of which are found in Chapter 4) constant rate of strain direct shear test machines / apparatuses. Shearing was conducted at a displacement rate of 0.12 mm/min due to the mechanical limitations of the WF 2500 and the requirements of ASTM D3080. The normal stresses applied were 25, 50, 75, and 100 kPa and 3 test were conducted at each normal stress level on both machines. The results are presented in **Figure 3-7** and **Figure 3-8**. Regressions for the data were conducted assuming cohesion (C) of 0 kPa which is the normal assumption for dry sand materials. As noted by Vlachopoulos (2000), the Brighton sand proved to be free draining when utilized within a full-scale retaining wall test.

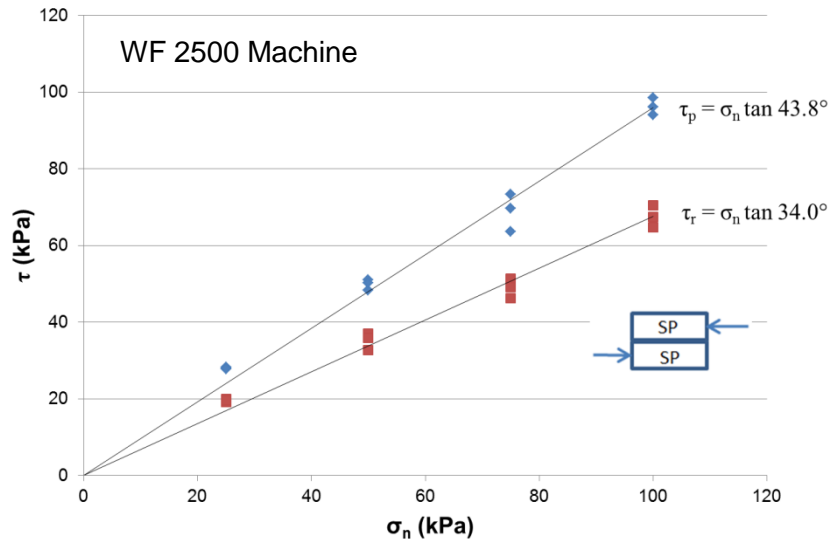


**Figure 3-7** Tests of pure SP on WF 2500 direct shear machine,  $\sigma_n$  25 – 100 kPa

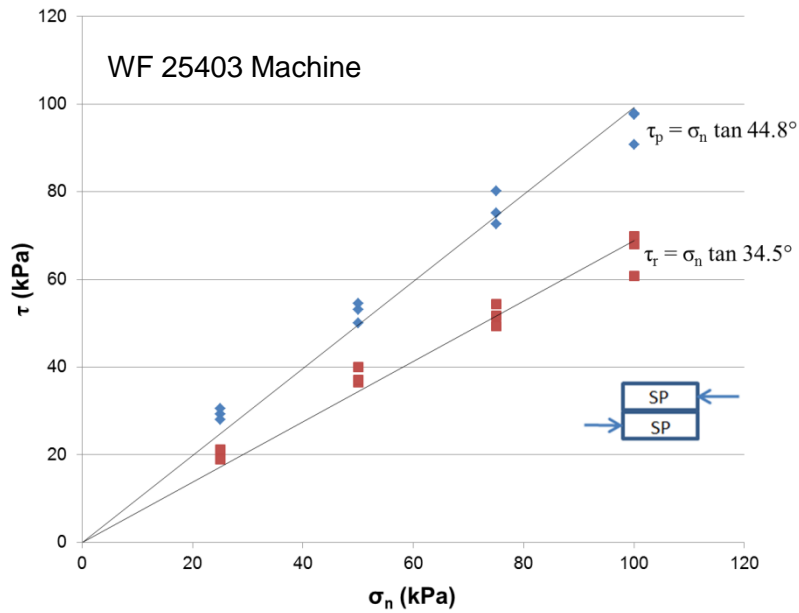


**Figure 3-8** Tests of pure SP on WF 25403 direct shear machine,  $\sigma_n$  25 – 100 kPa

These results obtained from the two separate machines provided very similar peak and residual results. This increased confidence in the direct shear strength values determined from the testing and confirmed the normal function of

the re-built WF 2500 machine; however, shear strength was not the only property of interest for this research.

In order to fully define the material and obtain values to be used as input parameters for numerical models, it was also necessary to determine the Young's modulus and Poisson's ratio. This is difficult to determine for soils through physical testing as it necessitates tri-axial tests of undisturbed samples. However, typically values in literature for such poorly graded sand materials stipulate a Modulus of Elasticity of  $E = 65 \text{ MPa}$  and a Poisson's Ratio of  $\nu = 0.3$  (geomat, 2015).

### 3.4 Steel

Steel used in ground support systems can vary depending on the design, size and purpose of the supports. Typically, 350 MPa yield strength steel is used for forepoles, spiles and anchors; however, yield strengths can be up to 600 MPa (Doucet and Voyzelle, 2012).

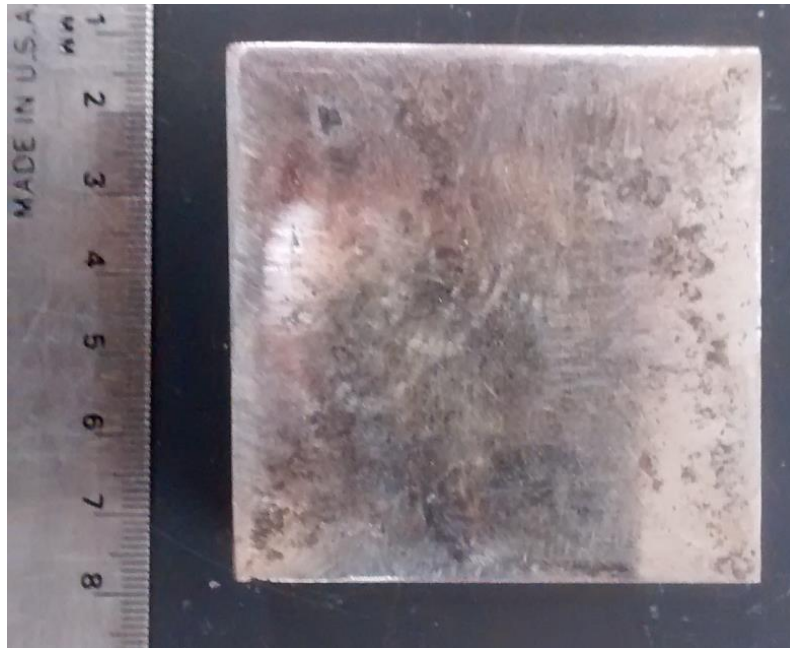


**Figure 3-9** Steel Sample Used for the Direct Shear Tests

The steel sample (**Figure 3-9**) was made from a piece of steel machined to 60mm x 60 mm x 25mm.

The piece of steel used to make the direct shear samples was too small to machine a second specimen for tensile strength testing. There was also no receipt for the steel so it was not possible to determine its precise strength. The strength and type of the steel should have relatively little influence on the shear behaviour though, as the physical interactions are occurring at the grain size level. Differences between the types of steel are at the molecular level. Since lower strength steels are more common, values for 350MPa yield strength steel were used for modelling in Chapter 6.

### 3.5 Grout

Grout for ground support elements can come in a variety of forms ranging from the common cement grouts to modern fast curing resin grouts. Due to complimentary research work in which grout has been utilized (Vlachopoulos et al., 2014) it was decided to use a commercially available grout: King® non-shrink grout with a type 10 Portland cement base. Several samples were cast as well as three 75 mm test cylinders in order to obtain the compressive strength. The mix was made so that the grout was poured in a fluid consistency for ease of handling the water to cement ratio was 4.6 kg : 25 kg.



**Figure 3-10** Grout samples for both shear and compressive strength testing

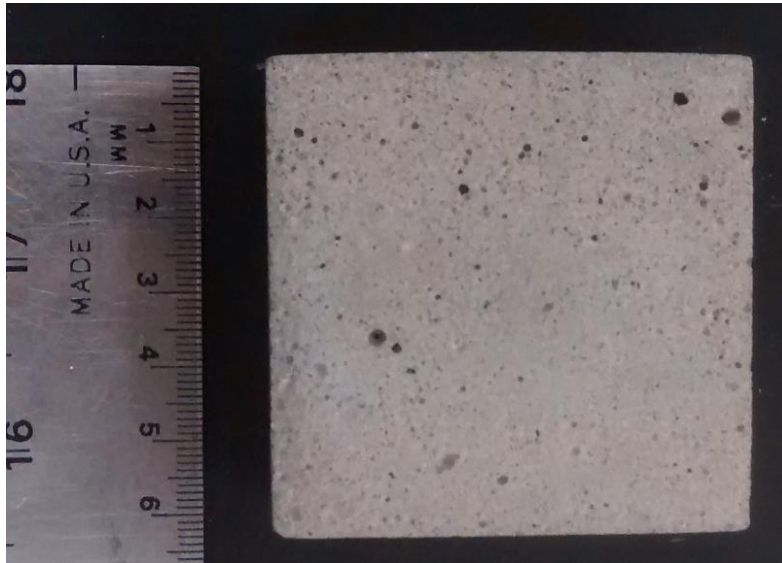


**Figure 3-11** Type 10 Portland cement based non-shrink grout

The UCS, E, and  $\nu$  of the materials are provided in **Table 3-3**. The compressive strength was determined in the RMC structures laboratory from the three 75 mm diameter test cylinders. The test was conducted in accordance with ASTM C39 at a rate of 1mm/min. The Young's modulus and Poisson's ratio were given by the manufacturer.

**Table 3-3** Properties of non-shrink grout \*(King Packaged Materials Company, 2016)

Parameter	Value
Compressive strength	48 MPa
E	24.5 GPa *
$\nu$	0.14 *

### 3.6 Concrete

Complimentary research conducted at RMC is using concrete samples in order to simulate rock for testing of support elements. To assist with the research and provide good laboratory data, it was necessary to conduct direct shear testing of concrete's interface shear behaviour with grout. Therefore, a sample was made for the direct shear machine from the same concrete batch used for this related research. It was also necessary to take samples for compression testing as the concrete properties needed to be quantified for reference and the computer simulations in Chapter 6. Poisson's ratio and the modulus of elasticity were not

determined due to an error during the compression testing, therefore, common values for high strength concrete were used.

**Table 3-4** Properties of concrete sample \*(EngineeringToolBox, 2016)

Parameter	Value
Compressive Strength	46.8 MPa
E	30 GPa *
v	0.2 *

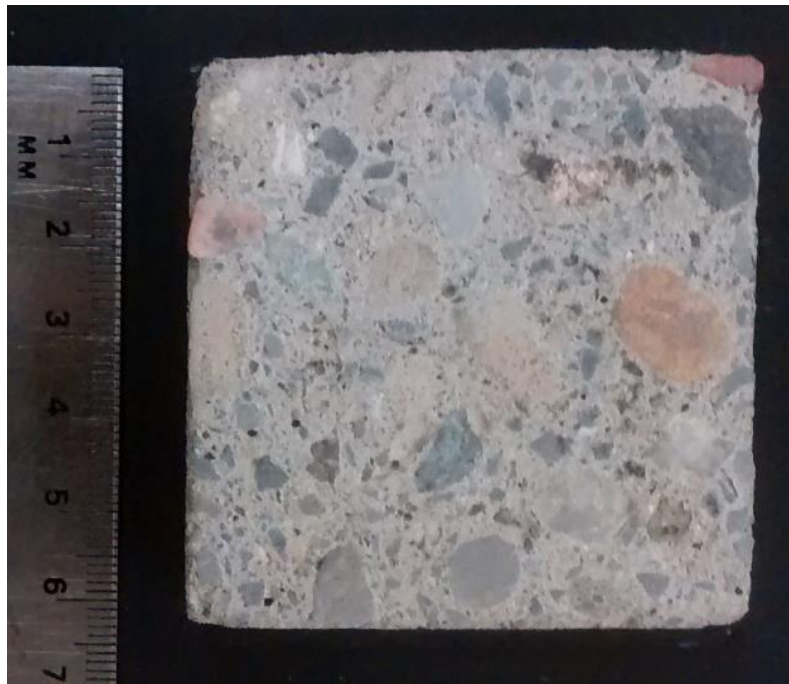


**Figure 3-12** Concrete Sample used for the Direct Shear Tests

### 3.7 Summary

This chapter summarized the significant material properties of the materials used for this research. The five materials were:

- a. Brighton Sand;
- b. Coburg Limestone;
- c. Steel;
- d. Non-Shrink Cement-based Grout; and,
- e. Concrete.

It was critical to both the direct shear testing and modelling to have these materials defined, as these properties were necessary for determining precise details for the conduct of the direct shear tests and appropriate construction of the numerical simulations. A summary of these properties is presented in **Table 3-5**.

**Table 3-5** Material strength and elastic parameters <sup>1</sup>(Geotechdata, 2013) <sup>2</sup>(King Packaged Materials Company, 2016) <sup>3</sup>(Ghazvinian et al., 2015) <sup>4</sup>(EngineeringToolBox, 2016)

Material	Parameter	Value
Brighton Beach Sand	Peak [Residual] Friction Angle (°)	43.8 [34]
	Cohesion (kPa)	0
	E (kPa) <sup>1</sup>	$6.5 \times 10^4$
	$\nu$ <sup>1</sup>	0.3
Grout	UCS (kPa)	$4.8 \times 10^4$
	E (kPa) <sup>2</sup>	$2.45 \times 10^7$
	$\nu$ <sup>2</sup>	0.14
Steel	UCS (kPa) <sup>4</sup>	$1.86 \times 10^5$
	E (kPa) <sup>4</sup>	$2 \times 10^8$
	$\nu$ <sup>4</sup>	0.3
Coburg Limestone	UCS (kPa) <sup>3</sup>	$7.246 \times 10^4$
	E (kPa) <sup>3</sup>	$3.7 \times 10^7$
	$\nu$ <sup>3</sup>	0.18
Concrete	UCS (kPa)	$4.68 \times 10^4$
	E (kPa) <sup>4</sup>	$3 \times 10^7$
	$\nu$ <sup>4</sup>	0.18

With the material parameters summarized, it was possible to proceed with setting up the testing and instrumentation as well as prepare the numerical model. This was a critical step to accomplishing the two objectives of this research. Defining these material properties will also allow for future research to expand on the database of shear parameters as well as ensure within this research that the models are properly designed to mimic the laboratory results improving confidence in the models and the ability to refine the modelling tools.

## **4 Testing and Instrumentation**

## 4.1 Overview

The primary objective of this research was to collect a reliable data set for shear interface parameters (shear strength and stiffness) of common materials used in ground support. The limited previous research, though not sufficient to provide a comprehensive dataset, provided limited guidance on using constant rate of strain direct shear apparatus for measuring interface shear parameters. The ubiquitous nature of the constant rate of strain direct shear test as well as its simplicity made it ideal for the interface shear tests. There were several factors which had to be considered before testing could begin.

This chapter details the work necessary for preparation of the direct shear test apparatus for the conduct of over 192 direct shear tests of the interaction between materials commonly related to ground support and reinforcement. The first step was to select the appropriate test apparatus, transducers, and DAQ systems. The transducers then had to be calibrated to ensure accurate measurement. With calibrated sensors the direct shear test apparatus could then be validated following repair work on the test frame. This was done by two separate methods. It was then possible to obtain accurate and reliable test results for the materials so the testing method and testing program were finalized based on a modified ASTM D3080 test standard.

## 4.2 Direct Shear Testing

Direct shear testing is one of the most common strength tests used in soil and rock mechanics. It is also one of the oldest tests dating back to the late 18<sup>th</sup> century (Heyman et al., 1972; Holtz and Kovacs, 2011). Therefore, it is a proven method with a substantial database of values that can be used for citations and comparative purposes. The direct shear test is simple in its set-up and execution. The test consists of measuring the load required to cause a shear failure within a material sample while a known normal load is applied to the failure plane. The material sample is placed in the shearbox, which is made of an upper and lower half (**Figure 4-1**). The box and sample is then placed inside a carrier onto a test frame where a known normal load is applied via a platen and hanger. During shearing, one half is held stationary while the other half is displaced at a constant rate of strain (ASTM D3080, 2011; Wykeham Farrance Engineering Limited, 1968). With the normal load known, the area of the shear plane known, and the shear load measured, the shear stress and normal stress can be measured. If these are plotted they provide the Mohr-Coulomb shear strength envelope (**Figure 4-2**). This determination allows for reasonable predictions about the shear behaviour of a given material.

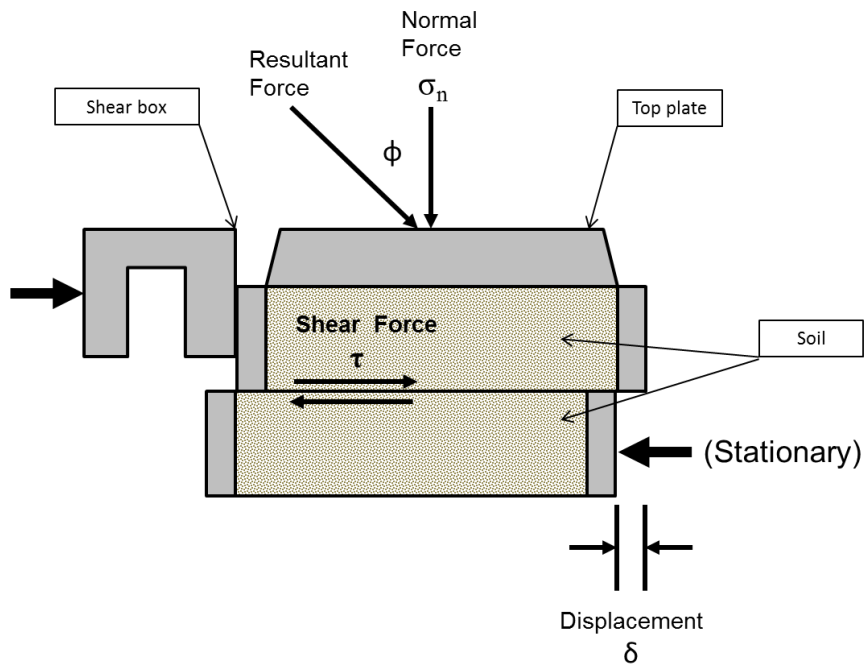


**Figure 4-1** Cross section of direct shearbox and parameters related to testing

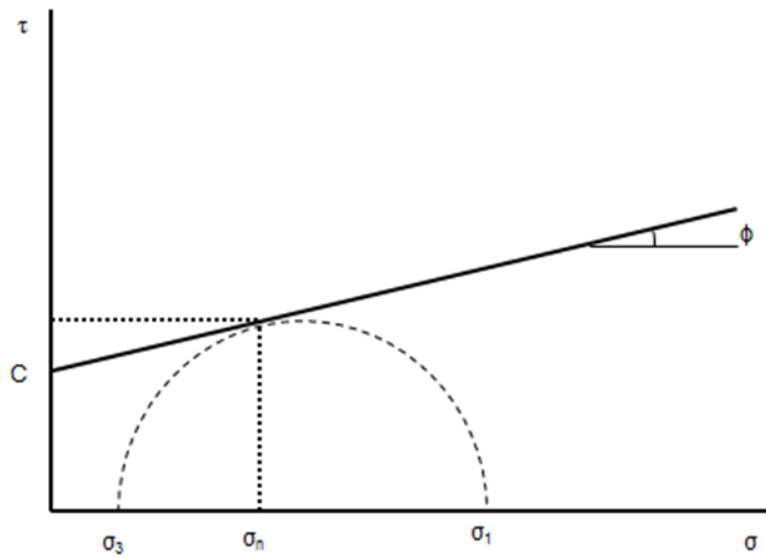


**Figure 4-2** Generic Mohr-Coulomb strength envelope [Shear Stress ( $\tau$ ), Normal Stress at failure ( $\sigma_n$ ), Principal Stresses ( $\sigma_1$ ,  $\sigma_3$ ), Cohesion ( $C$ ), Friction Angle ( $\phi$ )]

The principles for the direct shear testing of rock are similar. The two differences are normal stress range and sample mounting. Typically, the stress is in the MPa range for rock rather than kPa due to higher stresses which generally exist at depth. The samples for direct shear tests in rock are generally cylindrical samples which are held in the two halves of the shearbox by an encapsulating medium (ASTM D5607, 2008). This means that tests require more preparation. In addition, sample preparation requires greater accuracy and effort to square the desired failure plane within the shearbox.

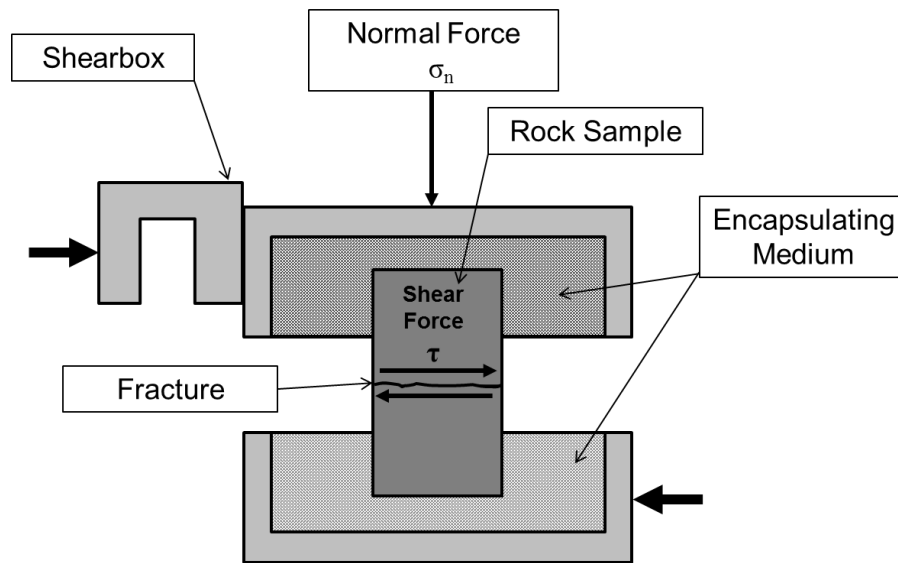


**Figure 4-3** Generic direct shear test set-up for rock

For the purpose of these tests, it was decided to attempt to use the soil direct shear machine for all tests due to its relative simplicity, and its availability at RMC. As well, RMC does not have a rock shear testing apparatus at this time. It was also decided that the lower stress ranges would be acceptable as shallow tunnelling operations, such as undergrounds/metro systems, occur in rock and soil at lower stresses making it unnecessary to reach the higher normal stress of the direct shear test machine for rock.

### 4.3 Wykeham Farrance 2500 Shearbox Machine

The machine used for the majority of tests was a Wykeham Farrance 2500 constant rate of strain direct shear machine (**Figure 4-4**). The box is a square with interior dimensions of 60mm x 60mm x 41mm. It is powered by an electric motor and the rate of strain is adjusted by manually removing and installing different

gears and selecting a different speed on the transfer case. This allows it to have a displacement rate that can be varied from 1.22 mm/min to 0.00488 mm/min.

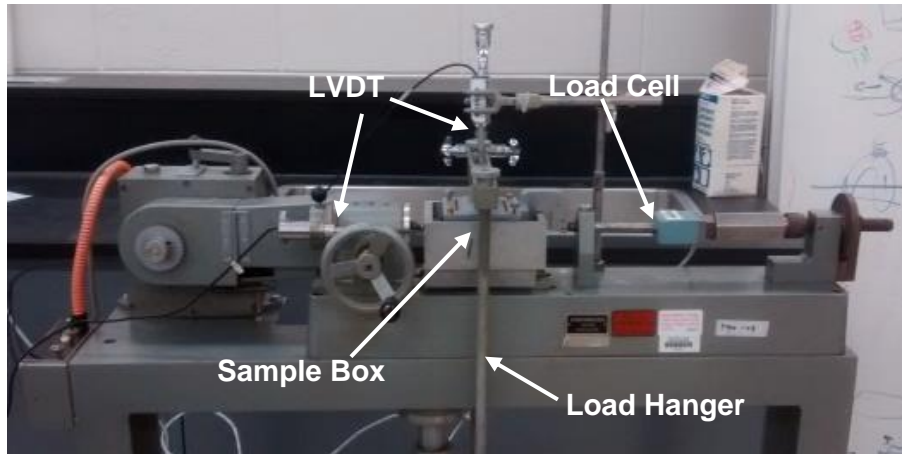


**Figure 4-4** WF 2500 constant rate of strain direct shear machine

The machine was purchased in 1968 and over that time had lost several parts. This necessitated the machining of replacement parts (by the author) for the apparatus such as the load arm and load arm support (**Figure 4-5**).

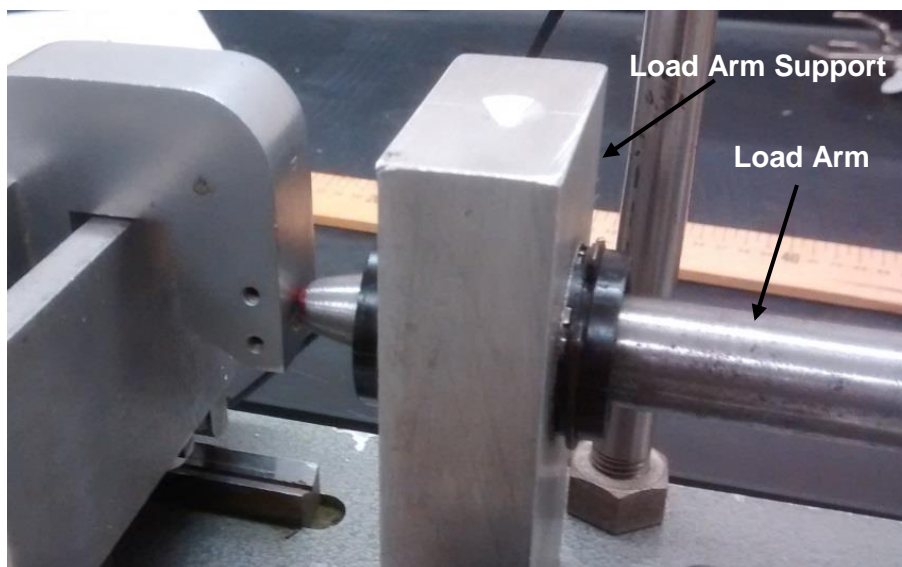


**Figure 4-5** Image of modified parts on WF 2500

#### 4.4 Wykeham Farrance 25403 – Shearbox Machine

The Wykeham Farrance 25403 constant rate of strain direct shear machine (Figure 4-6) was used in order to validate the performance of the Wykeham Farrance 2500 machine after its repairs. It was provided to RMC on an indeterminate loan from 1 Engineer Support Unit (a DND engineering organization that also resides in Kingston, Ontario). This was a newer shearbox configuration which could incorporate the use of a 100mm x 100mm or 60mm x 60mm shearbox. The displacement rate could also be controlled electrically, removing the need to physically change gears in order to adjust the rate of displacement.

The one issue was the lack of adapters for the load cells. This was resolved by machining adapters from bolts. These were drilled and tapped to fit the threads on the load arm.

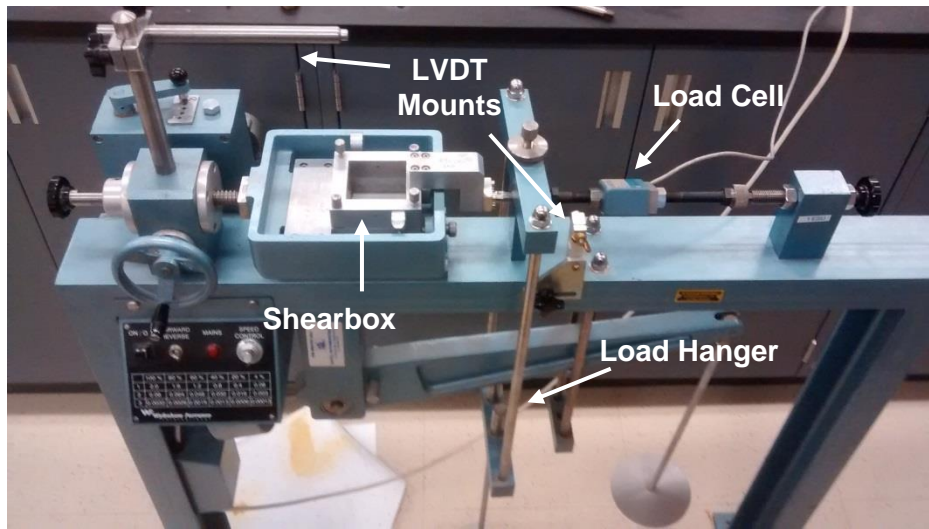


Figure 4-6 WF 25403 Constant Rate of Strain Direct Shear Machine

#### 4.5 Instrumentation Utilized in Conjunction with Shearbox Machines

The direct shear test requires three measurements in order to assess the shear strength and stiffness of the soil:

- a. Shear Force;
- b. Horizontal Displacement; and,
- c. Vertical Displacement.

There were several options for how to measure these parameters. The lowest tech method was to use analog dial gauges for displacement and a load ring for the load, however, the number of tests and lower fidelity data rendered this impractical. For this testing a data acquisition system (DAQ) and electrical transducers were used. These are described in detail in the following sub-sections.

#### 4.5.1 Shear Force

Load cells are transducers which allow for measuring the forces applied to an object or system. These transducers can take many forms whether mechanical, hydraulic, photo-elastic, or electrical (Dunnicliff and Green, 1988).

One of the most common load cell configurations is to use electrical resistance strain gauges arranged in a set geometry on a continuum material such as steel. Since the properties of the steel and the strain behaviour are known at different loads on the material, the strain gauges can be calibrated and the load can be calculated from the change in resistance of the strain gauges. The strain gauges can take various forms whether wire, foil, or crystal semi-conductor strain gauges. For load cells, foil or semi-conductor strain gauges are most common as they are better for smaller scale application (Dunnicliff and Green, 1988).

Strain gauges used in load cells are usually arranged in a full Wheatstone bridge circuit as seen in **Figure 4-7**. The Wheatstone bridge is used because the precision from the direct reading of individual strain gauges is limited. The Wheatstone bridge allows for greater sensitivity to changes in resistance of each strain gauge because any changes to resistance result in a current flow between the legs. The full bridge also reduces temperature effects on the strain gauges and lead wires to negligible amounts (Hoffman, 1986).

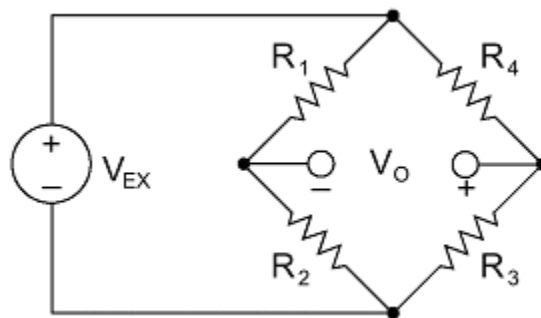


**Figure 4-7** Example of Wheatstone bridge circuit (National Instruments, 2016)

The load cell used was a Honeywell AL-JP high-output load cell (**Figure 4-8**). It is rated to 4.448kN (1000lbf), and uses a full Wheatstone bridge circuit.

The strain gauges are semi-conductor crystals (Honeywell, 2009). The excitation voltage was 10V and it was calibrated by the process described in Section 4.6.

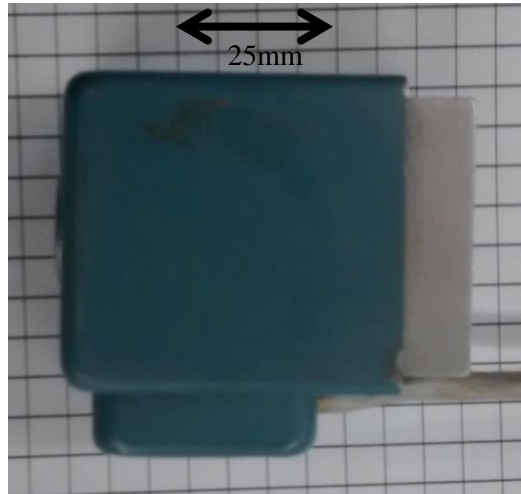


**Figure 4-8** AL-JP 1000lb high-output load cell

#### 4.5.2 Displacement Transducers

There are several different types of displacement transducers which can be used for direct shear testing. For the purposes of this research, Linear Variable Displacement Transducers (LVDTs) were used.

LVDTs are types of transducers which convert linear displacements into electrical signals which can be detected and recorded by computer software. The transducer is composed of a transformer with two coils and a moveable magnetic core attached to an arm (see **Figure 4-9**). The first coil is at the center of the transducer body and receives an AC excitation voltage. The second coil is divided into two halves which are at the ends of the body of the LVDT. The first coil induces an electrical current in the second coil. The signal from this is then amplified, demodulated and sent to the data acquisition system. As the magnetic core is displaced inside the body, it influences the signal in the secondary coil. A null point typically exists at the center of the LVDT where the signals in each half of the secondary coil cancel one another. However, as the core moves left or right of the null point the signal grows in amplitude and this is related to displacement (see **Figure 4-10**) (Kopczynski, 1992; RDP Group, 2014a).

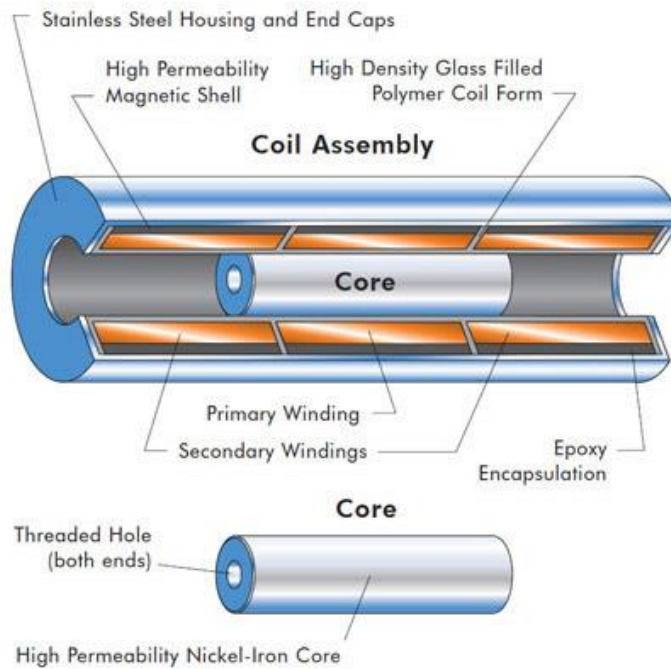


**Figure 4-9** Cross section of LVDT (Marco Sensors, 2014)

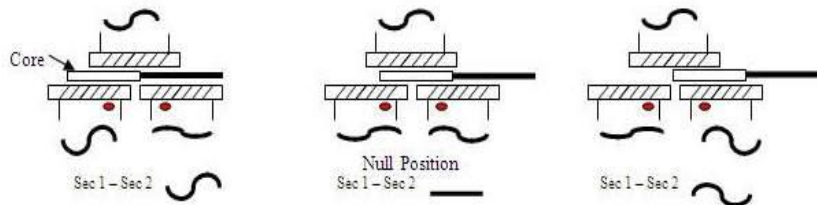


**Figure 4-10** Signal changes with respect to core position (Data Track Pi, 2014)

As mentioned before, this signal is in AC which does not permit for a difference in reading between the core moving forward or backward. As such the signal needs to be amplified and demodulated as seen in **Figure 4-11**. It should also be noted that the linear relationship between displacement and output signal does not hold true at the extremes of the LVDT's range of motion (Dunnicliff and Green, 1988).

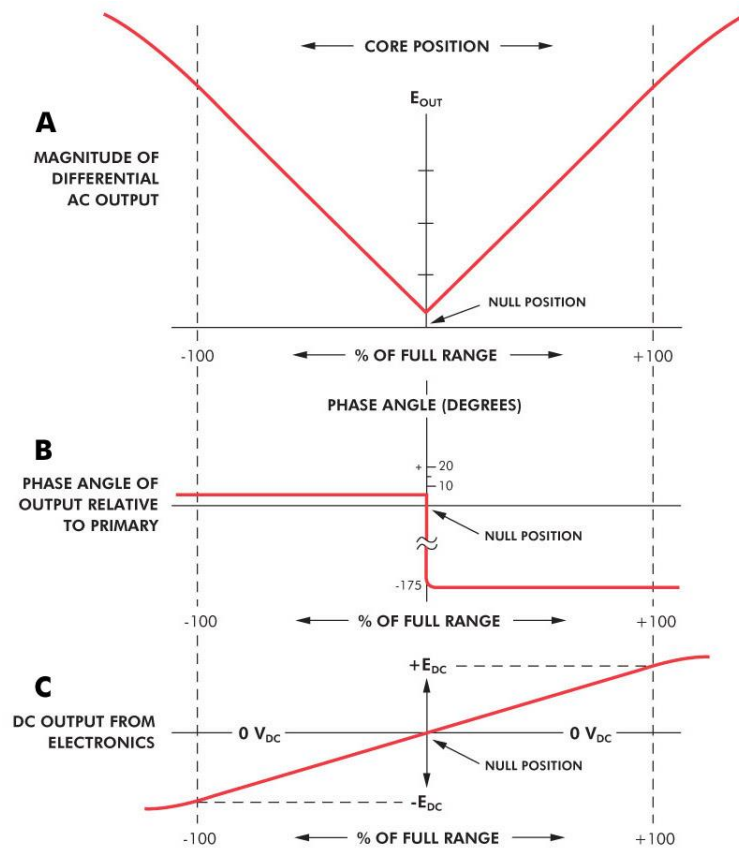


**Figure 4-11** Corrected LVDT output (Macro Sensors, 2014)

The past several decades has seen technological improvements in the miniaturization of electronics which allow for Direct Current Differential Transformers (DCDTs). These are LVDTs which have the amplifier and demodulator as internal components. This means separate systems are not necessary for processing the transducer's signal (Dunnicliff and Green, 1988).

The DCDT used in the vertical direction was made by RDP and was a model D2/200A (See **Figure 4-12**). This was a spring loaded DCDT with a stroke of  $\pm 5$ mm. This DCDT also had an internal filtering circuit (See **Figure 4-13**) which could be included or bypassed by using different output wires (RDP Group, 2014b), but for the purpose of these tests it was not bypassed. Calibration of the DCDT is important and was done as described in Section 4.6



**Figure 4-12** RDP D2/200A DCDT used for vertical displacement

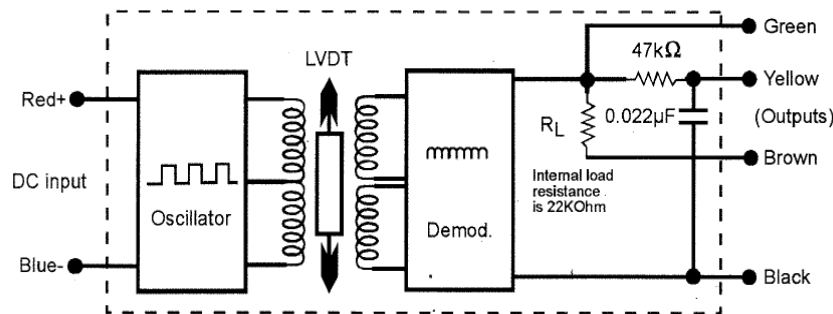


**Figure 4-13** Circuit diagram of D2/200A DCDT (RDP Group, 2014b)

In the horizontal direction, the test frame has an LVDT manufactured by SE Labs (See **Figure 4-14**). No data is available on this LVDT as no documentation can be found in the RMC labs. Observations show that it has a stroke of  $\pm 5$ mm, and based on reading from the DAQ it also has an internal demodulator making it a DCDT. It was also calibrated at 10V with a sensitivity of  $-0.6$ V/mm.



**Figure 4-14** SE Labs DCDT used for horizontal displacement

#### 4.6 Calibration

Calibration was conducted for the load cells by placing the load hanger on the transducer and measuring the voltage output at each load level between 8.9N (2lb) and 444.8N (100lb). This resulted in a very linear calibration plot (**Figure 4-15**) having a sensitivity of  $6.74 \times 10^{-5}$  V/N (0.0003 V/lb) with a coefficient of determination of 1.00. These data points were then input into the calibration table for the load cell within Catman AP®.

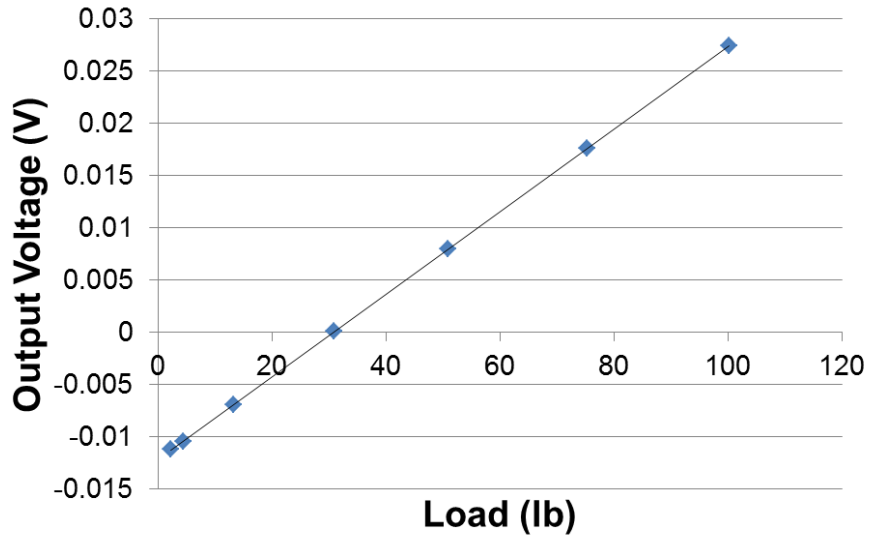


**Figure 4-15** Calibration data for AL-JP load cell

The horizontal DCDT was also calibrated by reading the direct voltage output of the sensor as it was displaced by a pedestal micrometer (**Figure 4-16**). The null point of the DCDT was determined and then displaced to 14 points between 1.5mm and -1.5mm at intervals of  $\pm 0.1\text{mm}$  or  $\pm 0.5\text{mm}$ . The voltage output was measured at each displacement interval and plotted relative to the displacement (**Figure 4-17**). This calibration was done at 10V and yielded a sensitivity of  $-0.6\text{ V/mm}$  with a coefficient of determination of 1.00.



**Figure 4-16** Pedestal micrometer calibration set-up

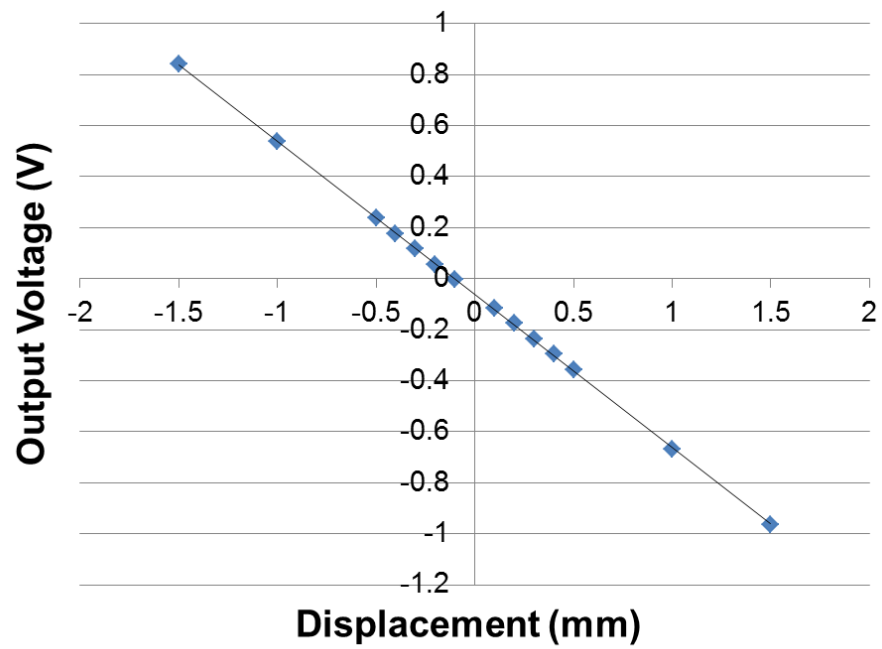


**Figure 4-17** Calibration data for horizontal DCDT

The vertical DCDT was calibrated in the same manner as the horizontal DCDT. The calibration was conducted at 10V and the output voltage plotted in **Figure 4-18**. The sensitivity was determined to be 0.226 V/mm, with a coefficient of determination of 1.00.

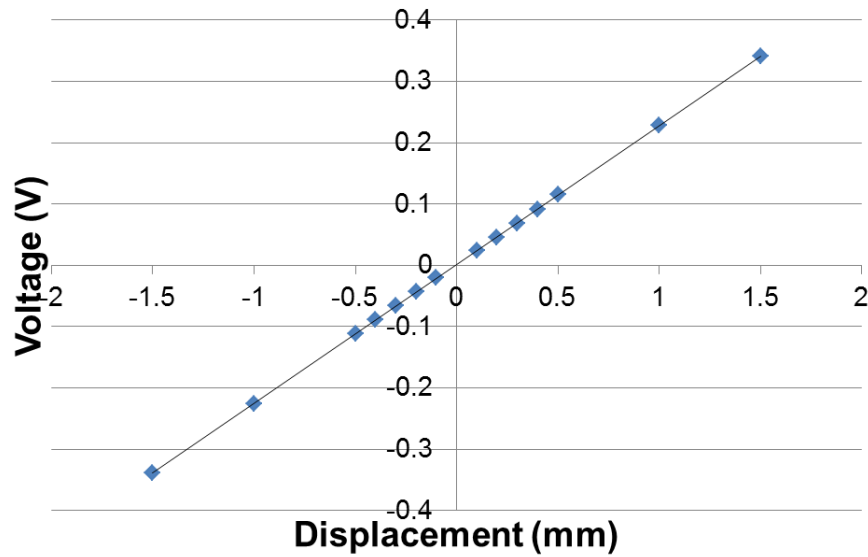


**Figure 4-18** Calibration data for vertical DCDT

#### 4.7 Data Acquisition

The sensors were only one part of the instrumentation system. To connect the sensors to the computer a DAQ and related software was necessary. Two systems, and associated software, were considered for a DAQ. Both were made by Hottinger Baldwin Messtechnik GmbH.

The first one considered was a Quantum X MX440A (**Figure 4-19**). This was a simpler, less powerful, DAQ. It used 15-pin serial connectors (**Figure 4-20**) to communicate with sensors (Durham Instruments, 2014). Wiring was different for various types of sensor inputs whether it was voltage, current, frequency, or resistance. The associated software was Catman® Easy which was designed to be a user friendly (though less powerful) data acquisition software. It had several functions for live data analysis and some ability to post process data but required purchase of separate software modules to gain the same noise cancelation and post processing features as Catman® AP (HBM GmbH, 2015; Durham Instruments, 2015). Due to communication issues with the software and the QuatumX, it was decided to use another DAQ.



**Figure 4-19** Quantum X MX440A DAQ

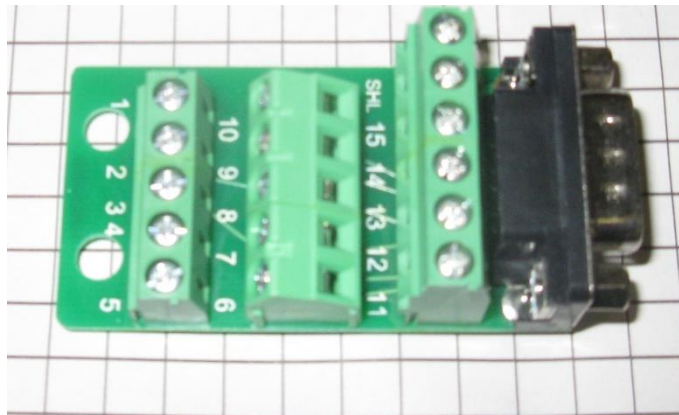


**Figure 4-20** 15-Pin serial connector

The second option was an MGC Plus DAQ which was a more powerful system (**Figure 4-21**) (Hottinger Baldwin Messtechnik GmbH, 2015). The DAQ used different electronic cards which allowed for diverse connectors to be used and different types of signals and parameters to be measured. For the purposes of these tests, voltage needed to be read from the different sensors, and as such, an AP 801 card which could read up to 8 voltage channels was installed into the MGC Plus and the 3 sensors and the supply voltage were connected. The software used for the MGC Plus DAQ was Catman® AP which is a more powerful data acquisition software than Catman® EASY allowing for greater control of graphical displays, data manipulation, sensor calibration, and set-up (HBM GmbH, 2015). Since the system performed well with the first installation process, it was decided that this was a suitable system to use as a DAQ. This was confirmed by the reasonable results given for the shear strength of the materials during the test validation.

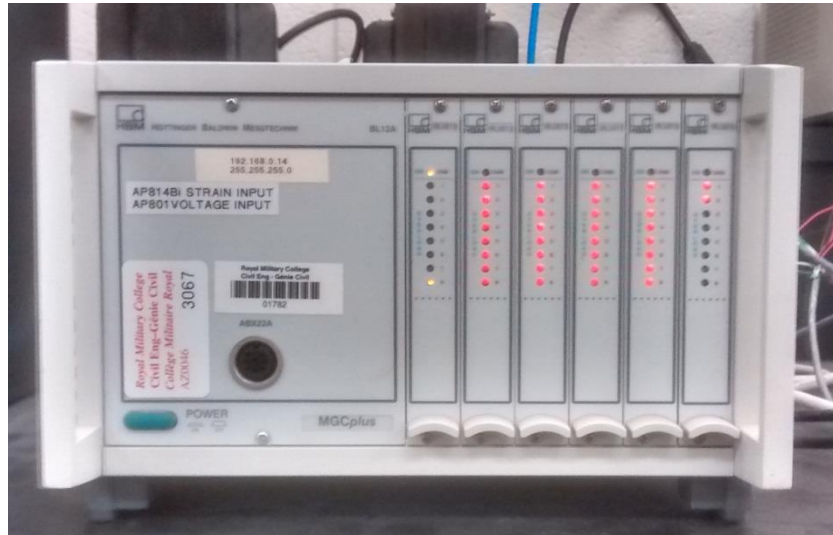


**Figure 4-21** MGC Plus DAQ used for testing

#### **4.8 Testing**

The WF 2500 Direct shear machine needed to be validated before testing could progress. Once the validation was conducted the testing program started by determining the shear strength of the pure Brighton sand. With this baseline information, testing then progressed to the various interface scenarios between sand-steel and sand-grout. Having completed the tests for interface scenarios involving SP soil, the tests of interface scenarios involving rock were begun. Testing the rock-steel and rock-grout interfaces was then followed by testing the grout-steel interface, and the grout-concrete interface. All of the above tests were done at eight normal stress levels and the tests repeated three times at each normal stress level. In total over 192 shearbox tests were completed, excluding selected early validation tests or tests where sensors were not properly set beforehand.

The normal stress ranges selected were at two intervals. The first interval tests were conducted at 25, 50, 75, and 100 kPa. The next sets of tests were conducted at intervals of 425, 450, 475, and 500 kPa. The reason 500 kPa was chosen as the maximum normal stress was that it was the maximum normal stress specified for the WF 2500. This would be representative of relatively shallow excavations such as is the case for metro systems in urban settings. Assuming a bulk density of  $\sim 1800\text{kg/m}^3$  the normal stress of 500 kPa simulates the earth pressure at a depth of approximately 28m. This may be shallow for some tunnels through mountain ranges, but much tunnelling is done near surface where this stress range would be within working stresses, such as undergrounds or utility corridors (Yasitli, 2012). In addition, these tests were the beginning of exploring the shear behaviour of these interfaces as part of a larger testing program. Future

testing will look at higher normal stresses representative of greater depths. With the normal stresses and interface scenarios mentioned above, the series of tests listed in **Table 4-1** were conducted. Typically, sample preparation for the Samples with the Brighton sand required 15 minutes to prepare for testing requiring cleaning and weighing of the empty shear box, tamping of the sample in 3 lifts, weighing, and then instrumentation set-up on the apparatus after sample installation. The test itself would then take 58 minutes to displace the 7mm because of the rate of displacement used which was calculated below. Tests conducted using two monolithic samples (i.e. Limestone – Grout, Grout – Steel) were faster because of there being no noticeable change in density or volume of the solid samples. This meant sample preparation was 7 minutes and the test conduct itself took 17 min due to the selected rate of displacement.

**Table 4-1** Type, normal stress, and number of interface tests

Interface Materials	Normal Stress (kPa)	Repetitions
SP – SP (25-100 kPa: Tests 0007 thru 0009) (425-500 kPa: Tests 0021 thru 0023)	25	3
	50	3
	75	3
	100	3
	425	3
	450	3
	475	3
	500	3
SP - Steel (25-100 kPa: Tests 0018 thru 0020) (425-500 kPa: Tests 0027 thru 0029)	25	3
	50	3
	75	3
	100	3
	425	3
	450	3
	475	3
	500	3
SP – Grout (25-100 kPa: Tests 0015 thru 0017) (425-500 kPa: Tests 0024 thru 0026)	25	3
	50	3
	75	3
	100	3
	425	3
	450	3
	475	3
	500	3

Interface Materials	Normal Stress (kPa)	Repetitions
Coburg Limestone – Steel (100kPa: Test 0030) (25-100 kPa: Tests 0031 thru 0033) (425-500 kPa: Tests 0040 thru 0042)	25	3
	50	3
	75	3
	100	3
	425	3
	450	3
	475	3
	500	3
Coburg Limestone – Grout (25-100 kPa: Tests 0034 thru 0036) (425-500 kPa: Tests 0037 thru 0039)	25	3
	50	3
	75	3
	100	3
	425	3
	450	3
	475	3
	500	3
Grout – Steel (25-100 kPa: Tests 0043 thru 0045) (425-500 kPa: Tests 0046 thru 0048)	25	3
	50	3
	75	3
	100	3
	425	3
	450	3
	475	3
	500	3
Grout – Concrete (25-100 kPa: Tests 0049 thru 0051) (425-500 kPa: Tests 0052 thru 0054)	25	3
	50	3
	75	3
	100	3
	425	3
	450	3
	475	3
	500	3

#### 4.9 Test Procedure

The test procedure used was similar to that outlined in ASTM 3080. For the tests involving the sand, the procedure outlined in **Table 4-2** was used. Tests were conducted at a shear displacement rate of 0.12 mm/min. This was determined by **Equation 4-1**. The displacement at failure ( $d_f$ ) and the time to failure ( $t_f$ ) are

1.5mm and 10min respectively (ASTM D3080, 2011). The resulting rate of displacement ( $R_d$ ) was 0.15mm/min. However, due to the discrete gears of the WF 2500 to control the rate of displacement it was necessary to select the nearest gearing slower than the calculated rate (Wykeham Farrance Engineering Limited, 1968).

$$R_d = \frac{d_f}{t_f} \quad \text{Equation 4-1}$$

**Table 4-2** Procedure for tests with SP soil

Step	Procedure / Action
1	Assemble shearbox
2	Weigh shearbox empty
3	Pour in 1/3 sand
4	Tamp
5	Pour in 1/3 of sand
6	Tamp
7	Pour in 1/3 of sand to bottom of openings
8	Tamp
9	Weigh shearbox with sand
10	Place shearbox on chassis
11	Tighten load arm
12	Tighten horizontal DCDT
13	Place hanger on shearbox
14	Place Vertical DCDT over hanger
15	Place normal load on hanger
16	Measure rise of platen above shearbox
17	Remove retaining screws
18	Gap shearbox
19	Zero sensors in CATMAN
20	Open measurement wizard
21	Clear database channels
22	Start readings
23	Turn on motor
24	Stop measurement wizard
25	Turn off shear machine
26	Save data
27	Remove vertical DCDT
28	Remove normal load & hanger
29	Remove load arm
30	Remove horizontal DCDT

Step	Procedure / Action
31	Disengage clutch
32	Retract load screw
33	Engage clutch
34	Clean shearbox

For tests involving the Coburg limestone samples, the procedure was modified to that shown in **Table 4-3**. Since it was no longer necessary to tamp the sample, or conduct mass and volume measurements sample preparation between shear tests was expedited. The rate of displacement was also changed as the considerations associated with granular materials for rate of displacement did not apply for the limestone (ASTM D3080, 2011).

Due to this difference, and because there was no guidance within ASTM D3080 on rock, it was necessary to conduct a series of tests in order to determine the influence of the rate of displacement was on shear behaviour. Therefore, a series of shear tests (Test number 0030 serials 01-06) were conducted at 100 kPa for a Coburg Limestone to Steel interface. After six tests varying only the rate of displacement (**Figure 4-22**), it was determined there was no correlation between the rate of displacement and the shear behaviour. Therefore, a constant rate of 0.41mm/min was selected for the tests associated with the rock and the other monolithic samples allowing for more expedient testing and for being within the mid-range testing rate of the machine.

**Table 4-3** Procedure for tests involving rock or monolithic samples

Step	Procedure / Action
1	Assemble shearbox
2	Insert sample
3	Place shearbox on chassis
4	Tighten load arm
5	Tighten horizontal DCDT
6	Place hanger on shearbox
7	Place Vertical DCDT over hanger
8	Place normal load on hanger
9	Remove retaining screws
10	Gap shearbox
11	Zero sensors in CATMAN
12	Open measurement wizard
13	Clear database channels
14	Start readings
15	Turn on motor
16	Stop measurement wizard
17	Turn off shear machine

Step	Procedure / Action
18	Save data
19	Remove vertical DCDT
20	Remove normal load & hanger
21	Remove load arm
22	Remove horizontal DCDT
23	Disengage clutch
24	Retract load screw
25	Engage clutch

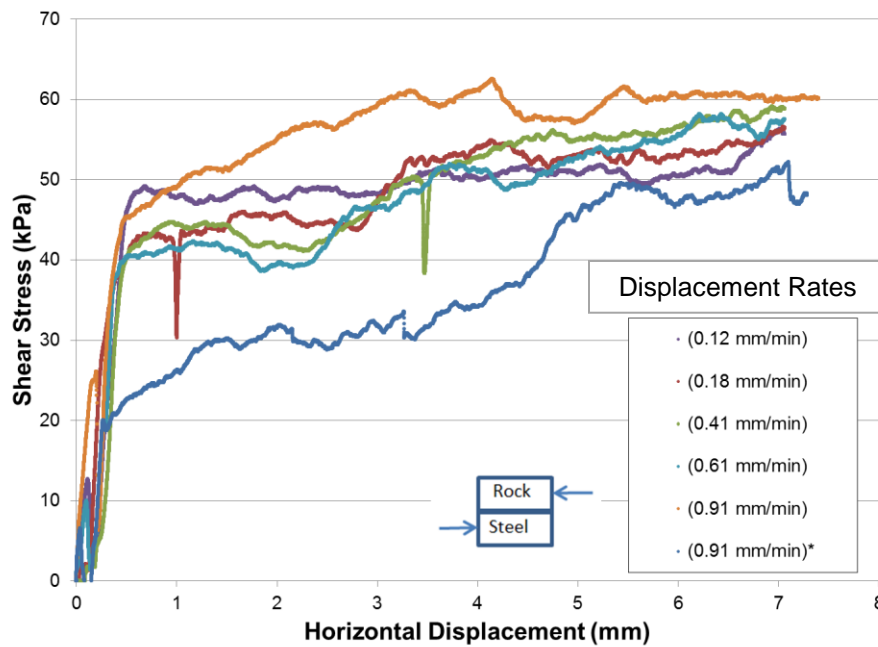


**Figure 4-22** Shear tests of rock and steel with varied displacement rates,  $\sigma_n = 100$  kPa (\*Sample cracked part way through this test, believed to have caused the lower shear strength)

#### 4.10 Validation of WF 2500 Machine

The modifications and instrumentation were functional; however, because of the changes it was necessary to validate the performance of the machine. There were two methods used for validation. The first was to take a material with known direct shear behaviour and test it in the WF 2500. The second validation consisted of testing the shear strength of the Brighton sand and comparing direct shear test

results between the WF 2500 and another direct shear machine which had not undergone the modifications.

The first validation plan used a fine grained fused quartz material used as part of the transparent soil material for testing at RMC. Direct shear testing done on the dry fused quartz by Ezzein and Bathurst in 2011 determined that the peak ( $\Phi_p$ ) and residual ( $\Phi_r$ ) friction angles were  $42^\circ$  and  $37^\circ$  respectively. The tests were conducted at normal stresses of 25, 50, 75, and 100 kPa. The rate of displacement used was 1mm/min rate of displacement. The regression of the test data was forced through the origin setting the cohesion (C) to 0 kPa (Ezzein and Bathurst, 2011). These conditions were replicated for the tests on the WF 2500 apparatus. The results of the tests were summarized in **Figure 4-23** and resulted in a  $\Phi_p$  of  $46.3^\circ$  and  $\Phi_r$  of  $38.3^\circ$ .

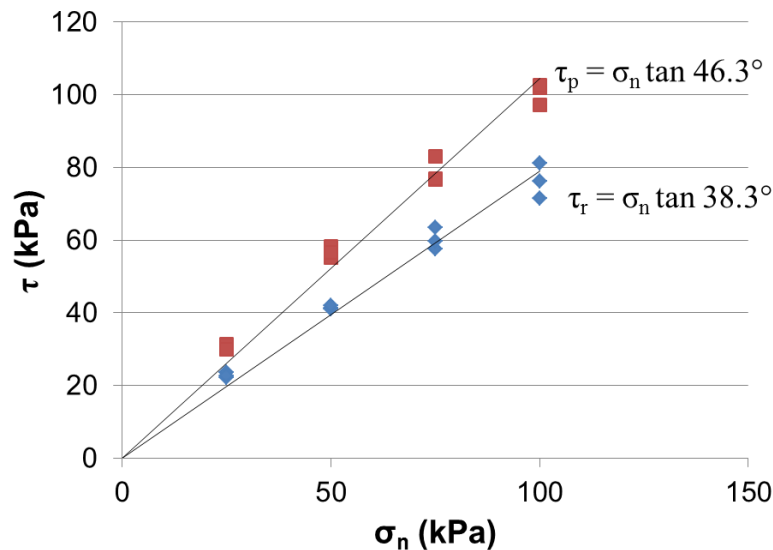


**Figure 4-23** Test of fine grained fused quartz on WF2500

There was a noticeable difference in the peak friction angle between the WF2500 and Ezzein and Bathurst 2011. This is likely due to minor differences in compaction effort. This is reaffirmed by the fact the residual friction angles have only a difference of  $1.3^\circ$ . This indicated that the WF 2500 was in good working order, however, it was also prudent to proceed with the second validation method for certainty.

The second validation was accomplished by conducting three tests at 25, 50, 75 and 100 kPa normal stress with samples of the Brighton sand on both the WF 2500 and the WF 25403. The peak and residual shear strength results from the machines were then plotted relative to the normal stress on separate plots. A linear regression of the 12 peak and 12 residual data points from each machine was

conducted forcing  $C = 0\text{kPa}$ . These regressions resulted in near identical shear strength envelopes when comparing **Figure 4-24** and **Figure 4-25**. This confirmed that the WF 2500 was functional and provided the baseline data for the material properties of the sand.

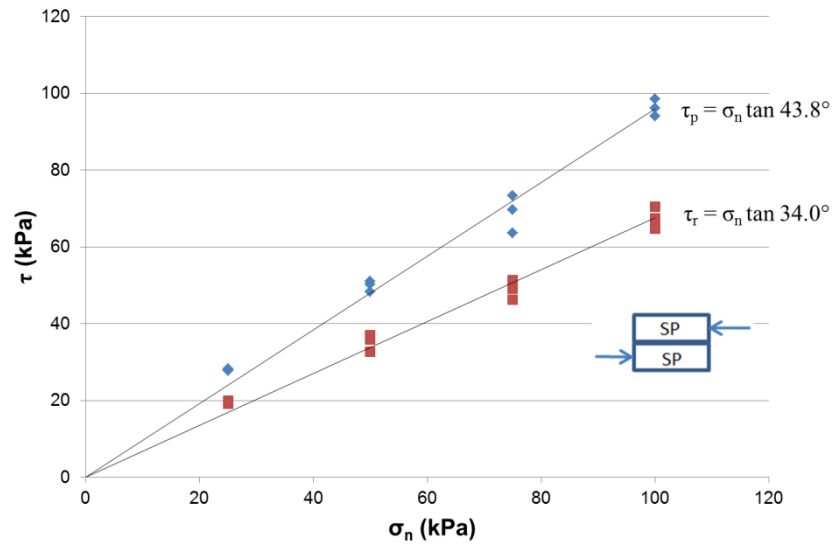


**Figure 4-24** Direct shear tests of SP on WF 2500

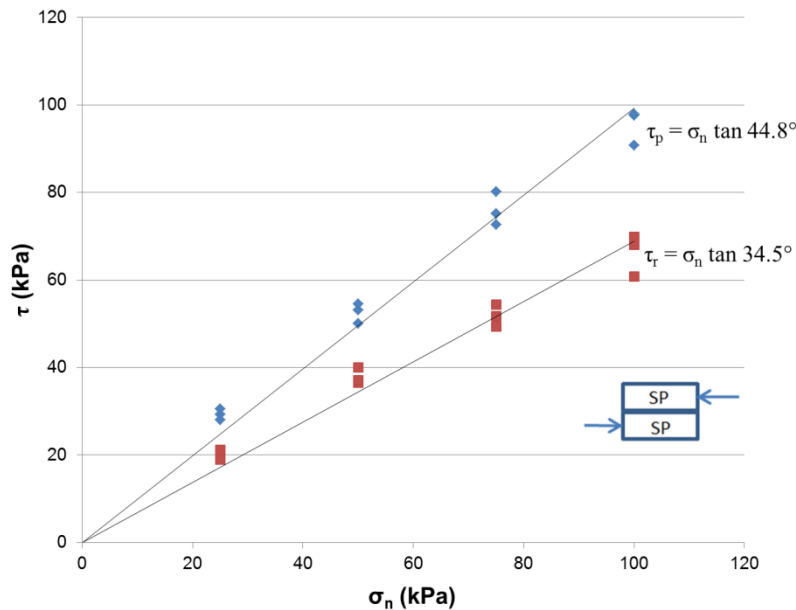


**Figure 4-25** Direct shear tests of SP on WF25403

#### 4.11 Summary

The testing and instrumentation selection was critical to the objective of creating a robust data set for the shear interaction parameters. In order to accomplish this it was necessary to obtain not only quality data, but also a sufficient quantity to be significant. Optimizing both of these was a challenge. It required careful calibration of the instruments, validation of the direct shear testing apparatus, and consistent sample preparation. All of this work took a considerable amount of time to ensure that the over 192 direct shear tests, conducted with diverse materials, would be conducted efficiently, reliably, and accurately. These considerations also included the need for an appropriate DAQ and software.

This chapter outlined the process of selecting the test apparatus, calibrating the transducers, validating the test apparatus' function by two separate methods, and organizing the test program and the procedure. All of this preparation allowed for tests to be conducted in a reliable and expedient manner for the following interface scenarios at two different normal stress ranges:

- a. Sand;
- b. Sand-Steel;
- c. Sand-Grout;
- d. Rock-Steel;
- e. Rock-Grout;

- f. Grout-Steel; and
- g. Grout-Concrete.

With the test apparatus and instrumentation prepared, it was then possible to collect the data from the tests. This data was necessary to accomplish the first objective of this research in building a database for the direct shear behaviour of various material interfaces related to ground support and reinforcement.

## **5 Laboratory Results and Discussion**

## 5.1 Properties of Interest

The properties of specific interest for this investigation were the shear strength and shear stiffness of the ground support-related interfaces. The ultimate goal of this research (as stated in Chapter 1) was to obtain these parameters with a view to: a. providing the scientific community with such parameters which are elusive at the current time, and b. creating a database of such interaction parameters for use within numerical modelling software packages in order to assess their accuracy in representing the real world shear behaviour of the interfaces.

This chapter covers the results of the more than 192 direct shear tests conducted by the author to determine the shear behaviour of the different interface scenarios and materials as outlined in Chapters 3 and 4. Once the tests were completed, an analysis of the data was conducted to determine the peak shear strength ( $\tau_p$ ), residual shear strength ( $\tau_r$ ), and shear stiffness ( $k_s$ ) of each test arrangement / sample.

## 5.2 Shear Strength of Brighton Sand

The shear strength behaviour of pure Brighton sand samples can vary due to the particulars associated with sample preparation. As such, for the shear-box standardized (ASTM D3080) tests containing Brighton sand, both peak shear stress ( $\tau_p$ ) and residual shear stress ( $\tau_r$ ) were determined from the results in APPENDIX A. An example of the plot and layout can be found in **Figure 5-1**. A selection of the results for Brighton sand can be found in **Figure 5-3** through **Figure 5-6**. These results were compared to the work done by Potyondy in 1961 (See Chapter 2) and provided comparable results. The soil is also within the expected range of shear strength for poorly graded, dense sand with angular grains (Holtz and Kovacs, 2011).

The peak and residual shear stress were determined from the first order data. The peak was taken from the maximum shear stress of each shear stress versus displacement curve. The residual shear stress was determined from the shear stress versus displacement curves at 7mm displacement. This was selected as the point at which the residual was taken because at that displacement the entire shear plane was mobilized and had reached a relatively steady state (See **Figure 5-1**). The residual would have been taken at a greater displacement but was limited because the maximum displacement of the direct shear test apparatus was 8mm.

There was one anomaly in the vertical versus horizontal displacement plot for the 450 kPa serial in **Figure 5-6**. The maximum vertical displacement of 0.47mm in test 0022 was distinctly higher than the other results at 450kPa which were 0.347mm and 0.374mm (as per APPENDIX B). This is believed to be attributed to the variation in the sample, perhaps a grain which exceeded 4.75mm diameter (See **Figure 3-5**) which happened to be placed across the shear plane

causing greater dilation and higher peak shear stress. There were otherwise no anomalies within the soil behaviour or properties.

All these data points for peak and residual shear strength were plotted with respect to the applied normal stress. A linear regression was done in MS Excel (Microsoft, 2010) to create the linear Mohr-Coulomb shear strength envelope (Figure 5-7 Test 0007-0009 Mohr-Coulomb peak and residual shear strength envelope,  $\sigma_n$  25 to 100kPa and Figure 5-8) for both peak and residual shear under the 25-100 kPa normal stress range and the 425-500 kPa normal stress range. The peak and residual shear strength envelope for the 25-100 kPa tests was determined to be  $\tau_p = \sigma_n \tan 43.8^\circ$  ( $r^2 = 0.997$ ) and  $\tau_r = \sigma_n \tan 34.0^\circ$  ( $r^2 = 0.997$ ) respectively. The peak and residual for the tests at 425-500 kPa normal stress were  $\tau_p = \sigma_n \tan 41.6^\circ$  ( $r^2 = 0.998$ ) and  $\tau_r = \sigma_n \tan 33.7^\circ$  ( $r^2 = 0.990$ ) respectively.

The shear strength of the soil was predicted with relative consistency. Selected anomalies within the data occurred during the last series of tests at 425-500 kPa. The decrease seemed to be from test 0023 which had mostly lower values for residual shear stress than tests 0021 and 0022 (See Figure A-29, Figure A-31, and Figure A-33 in APPENDIX A). This is not an extreme change; however, it was likely a maximum in the variability of the material.

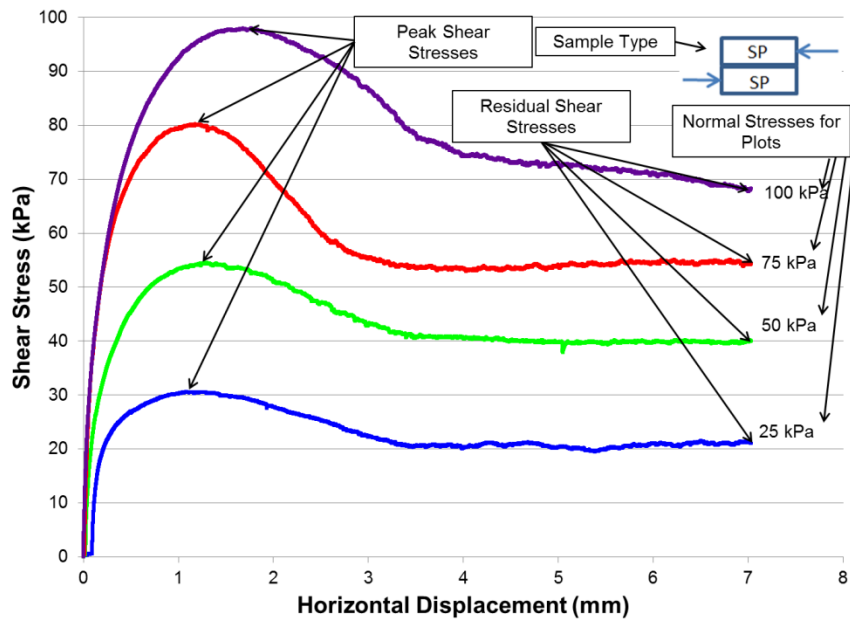


Figure 5-1 General layout of shear stress versus displacement plots

### 5.3 Shear Stiffness of Brighton Sand

The shear stiffness ( $k_s$ ) of the Brighton sand also had to be determined as it was a critical input for modelling in Chapter 6. The shear stiffnesses varied based on the normal stress. As such, values had to be determined separately for each interface test.

The chord method was used (**Figure 5-2**) to approximate the stiffness behaviour of the materials for each shear stress versus horizontal displacement curve (Holtz and Kovacs, 2011). This yielded results which were later applied to numerical models (Chapter 6). The shear stiffnesses for each test serial were calculated and an average was taken for the three tests for sand at each given normal stress interval. These results are summarized in **Table 5-1**.

For the 25-100 kPa stress range, there was a correlation between the normal stress and the average shear stiffness. Generally, as the normal stress increased, the shear stiffness increased (38000 to 98000 kPa/m). For the 425 kPa to 500 kPa range, the shear stiffness was estimated and averaged in a similar fashion. The results had relatively little variation (maximum difference of 35000 kPa/m with an average value of 243000 kPa/m) in the shear stiffness values as normal stress was increased. This is likely due to the grains reaching a critical confinement stress where void spaces are minimized between grains. This would also explain why the 425 kPa to 500 kPa vertical versus horizontal displacement curves all followed very similar trajectories to one another despite the changes in normal stress. A suitable baseline was established using the shear strength and shear stiffness values determined from testing. This allowed the creation, and calibration, of numerical simulations and the conduct of a parametric study on the various interface scenarios that the Brighton sand was subjected to within this study.

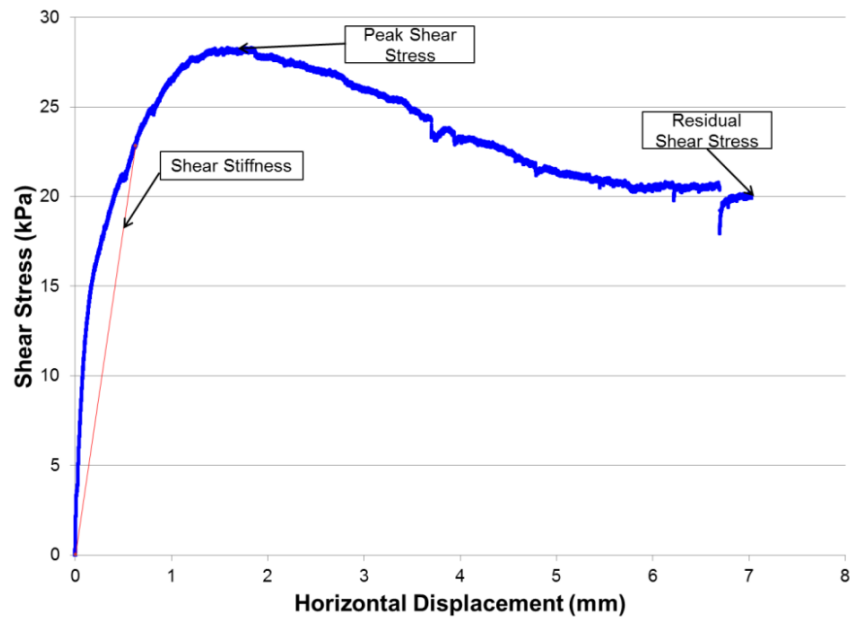


**Figure 5-2** Example of chord method shear stiffness calculation for one plot

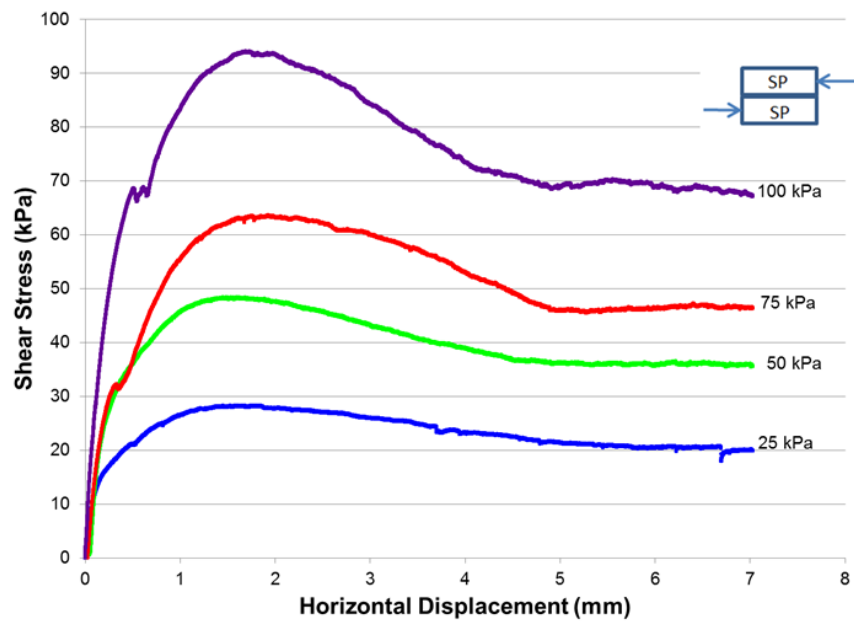


**Figure 5-3** Test 0008 Brighton sand sample,  $\tau$  versus displacement  $\sigma_n$  25 to 100kPa

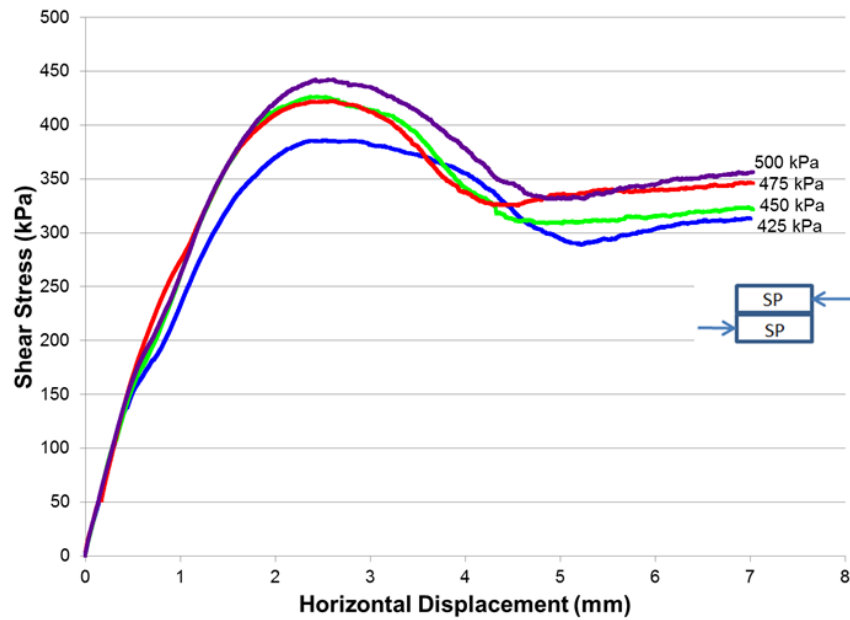


Figure 5-4 Test 0022 Brighton sand sample,  $\tau$  versus displacement  $\sigma_n$  425 to 500kPa

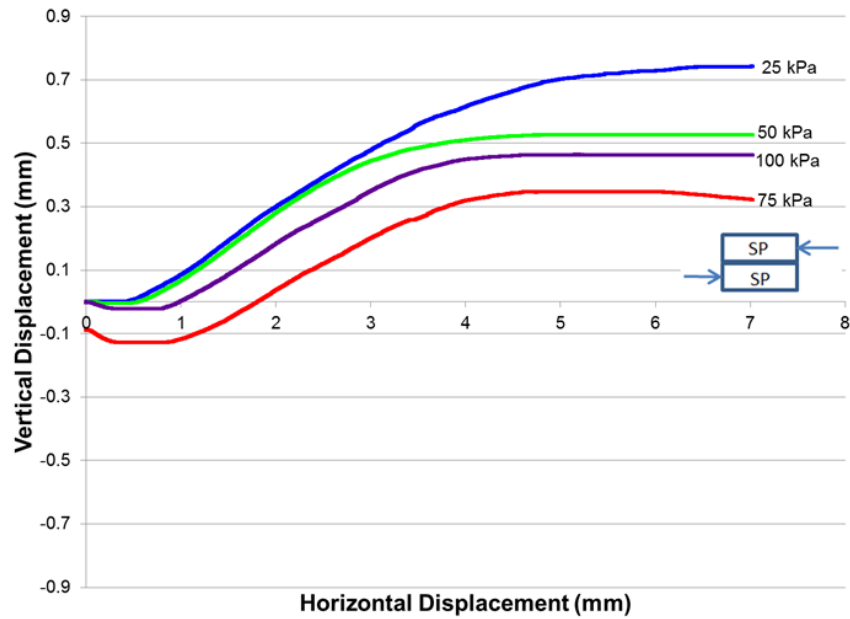
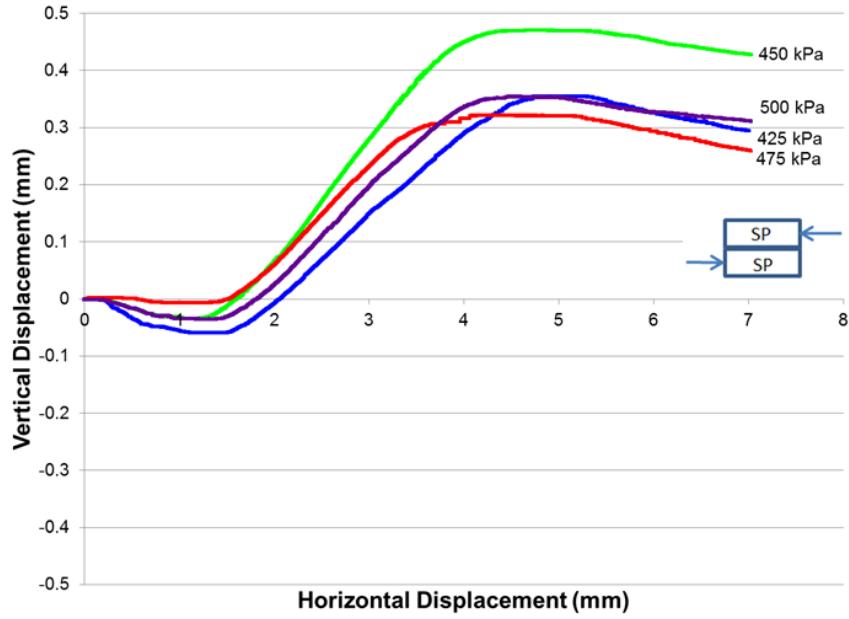
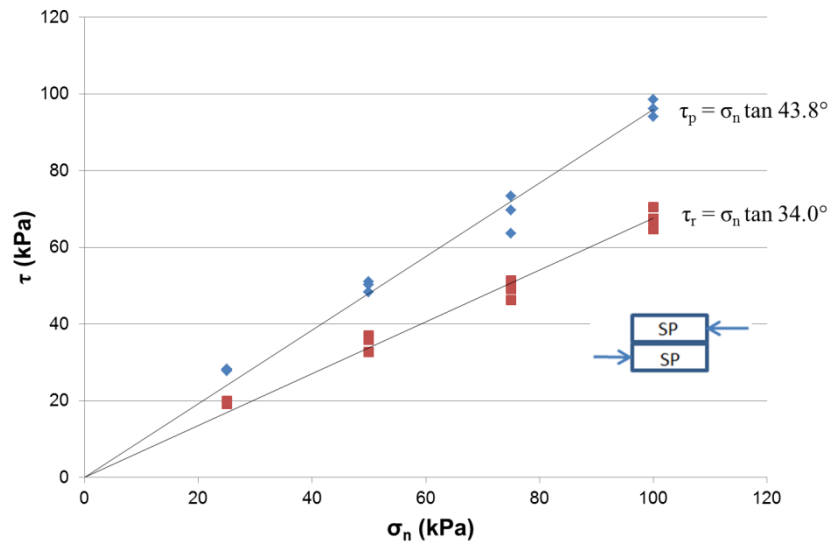


Figure 5-5 Test 0008 Brighton sand sample, vertical versus horizontal displacement,  $\sigma_n$  25 to 100kPa



**Figure 5-6** Test 0022 Brighton sand sample, vertical versus horizontal displacement,  $\sigma_n$  425 to 500kPa



**Figure 5-7** Test 0007-0009 Mohr-Coulomb peak and residual shear strength envelope,  $\sigma_n$  25 to 100kPa

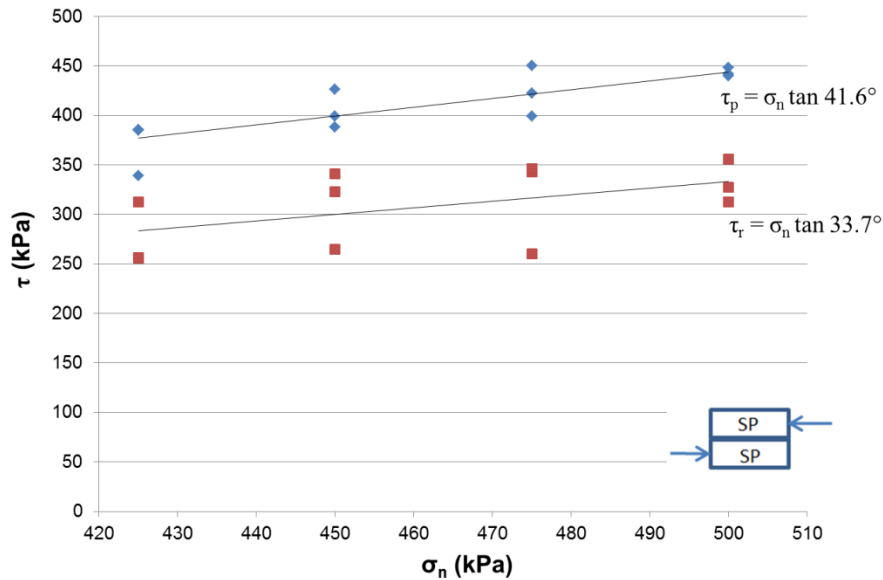


Figure 5-8 Test 0021-0023 Mohr-Coulomb peak and residual shear strength envelope,  $\sigma_n$  425 to 500kPa

#### 5.4 Shear Strength of Brighton Sand and Steel

This section presents the results of modified ASTM D3080 tests associated with the testing of the interface between the Brighton sand and steel. The same methodology as demonstrated in the section above was used in order to obtain both the peak and residual values from **Figure 5-9** and **Figure 5-10**, and plot the results in **Figure 5-13** and **Figure 5-14**. The Mohr-Coulomb shear strength envelope was determined by conducting a linear regression of the peak and residual shear data. This analysis returned a peak and residual shear strength envelope for 25-100 kPa tests of  $\tau_p = \sigma_n \tan 21.6^\circ$  ( $r^2 = 0.969$ ) and  $\tau_r = \sigma_n \tan 19.0^\circ$  ( $r^2 = 0.988$ ) respectively. The peak and residual for the tests at 425-500 kPa normal stress were  $\tau_p = \sigma_n \tan 21.9^\circ$  ( $r^2 = 0.997$ ) and  $\tau_r = \sigma_n \tan 20.0^\circ$  ( $r^2 = 0.995$ ) respectively.

The shear stress versus displacement curves showed different behaviour for the sand-steel interface from those observed for the pure Brighton sand sample. The drop from peak to residual shear strength was less pronounced, but sharper. The failure, rather than being a gradual decrease from peak, was a sudden drop in shear resistance across the failure plane indicating that mobilization happened more or less instantaneously across the entire shear plane. This was also coupled with the limitations associated with forcing a failure plane at this periphery as per the modified ASTM D3080. The minimal difference between peak and residual

shear was likely a result of the relatively hard and smooth steel surface at the interface. Unlike in other samples of sand or grout (discussed in Section 5.6 below), the steel had few asperities for stresses to concentrate on and be redistributed to. Since the stresses could not build up along the soil-steel interface, the grains slid across the surface with minimal rearrangement. The rearrangement was minimal since the Brighton sand and steel interface tests had some of the smallest vertical displacements of all the tests within this investigation (largest vertical displacement was 0.027mm). Most of the displacement occurred in the beginning stages.

Ultimately, the strength of the Brighton sand-steel interface was expected to be one of the weaker interface scenarios due to the smooth, hard surface and the ease with which the sand could mobilize and deform along the surface of the steel. This was confirmed as seen within the Mohr-Coulomb failure envelopes **Figure 5-13** and **Figure 5-14** under both normal stress ranges being the lowest of all the interface tests.

## **5.5 Shear Stiffness of Sand and Steel**

Shear stiffness was also an essential parameter for modelling the sand-steel interface. It was determined by the chord method from the shear stress versus displacement curves and summarized in **Error! Reference source not found.**

The shear stiffness for the interface behaved more or less as expected based on the Brighton sand samples tested before. The shear stiffness increased significantly in the 25 and 100 kPa range (59000 to 177000 kPa/m) but then had minimal variation at the higher normal stress range of 425 kPa to 500 kPa (varied between 292000 and 310000kPa/m).

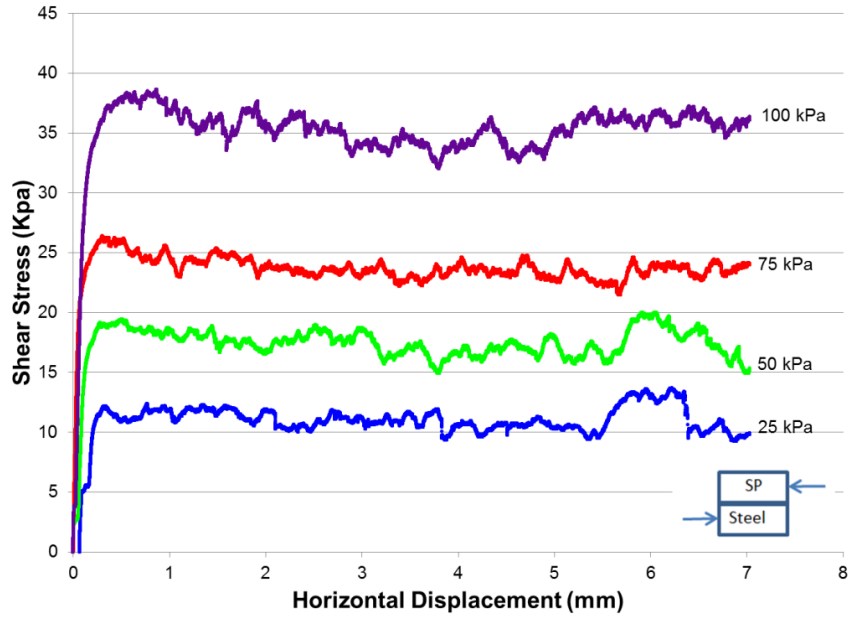


**Figure 5-9** Test 0019 SP soil – steel sample,  $\tau$  versus horizontal displacement,  $\sigma_n$  25 to 100kPa

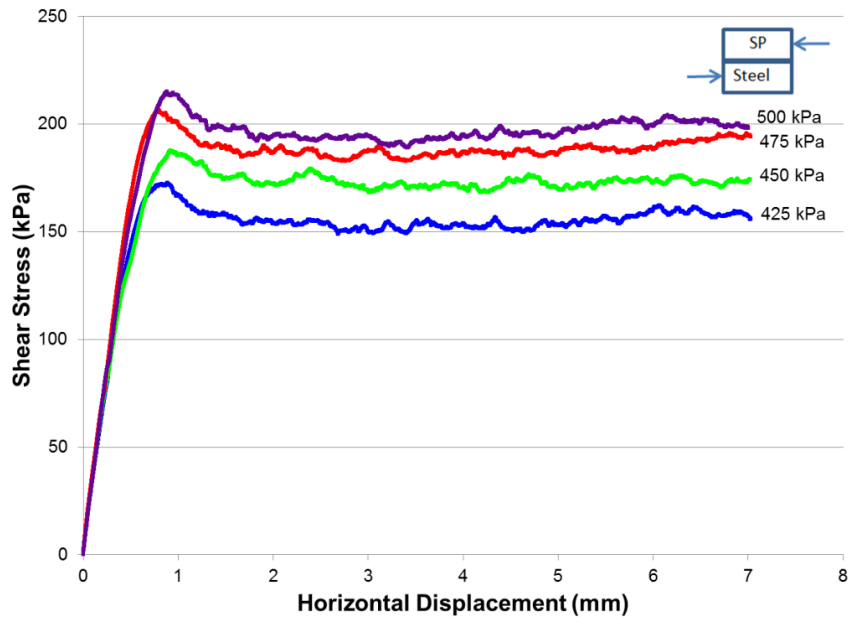


**Figure 5-10** Test 0029 SP soil – steel sample,  $\tau$  versus horizontal displacement,  $\sigma_n$  425 to 500kPa

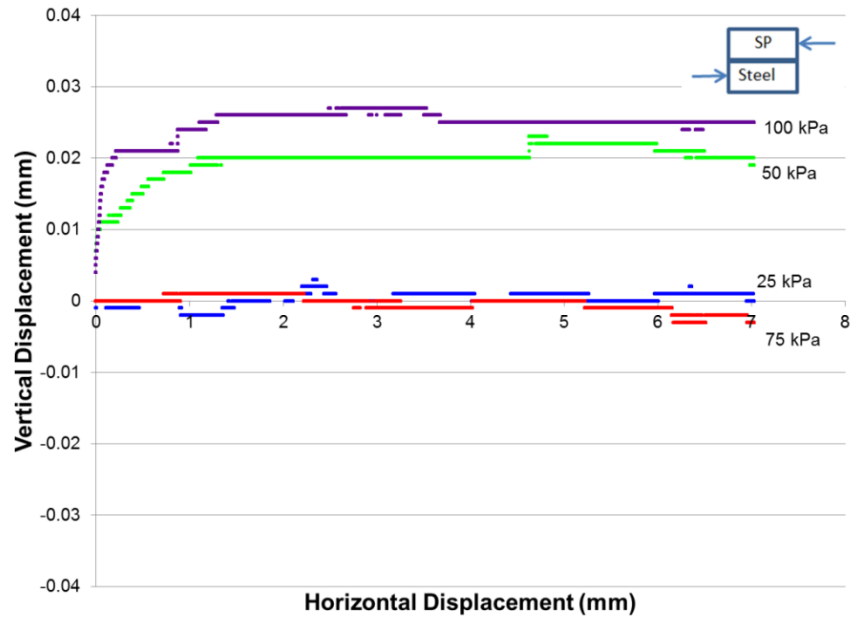


**Figure 5-11** Test 0019 SP soil – steel sample, vertical versus horizontal displacement,  $\sigma_n$  25 to 100kPa

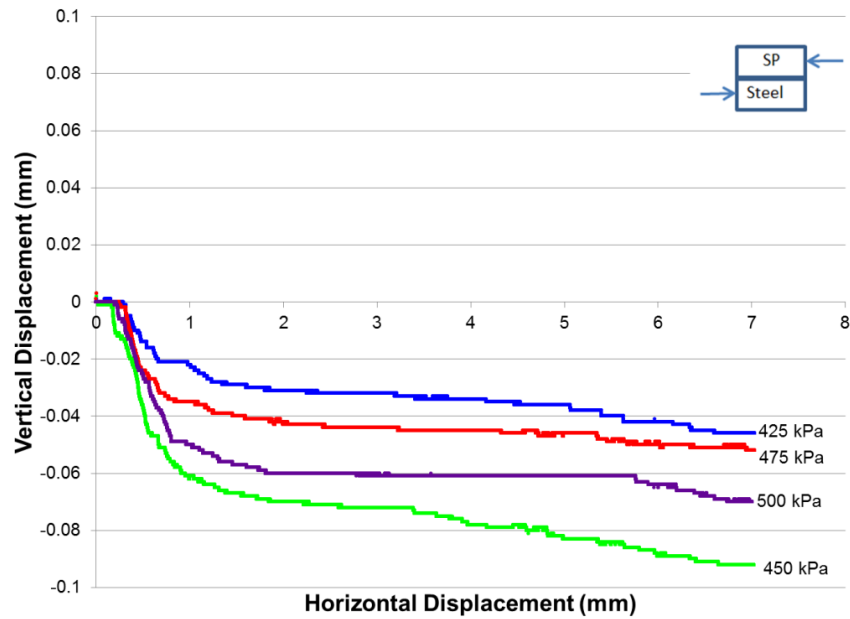


**Figure 5-12** Test 0029 SP soil – steel sample, vertical versus horizontal displacement,  $\sigma_n$  425 to 500kPa

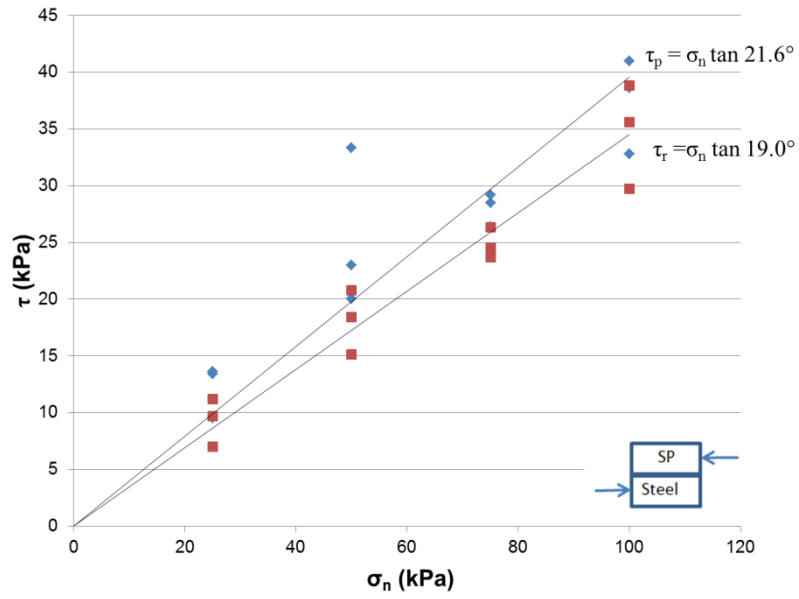


**Figure 5-13** Test 0018-0020 Mohr-Coulomb peak and residual shear strength envelope,  $\sigma_n$  25 to 100kPa

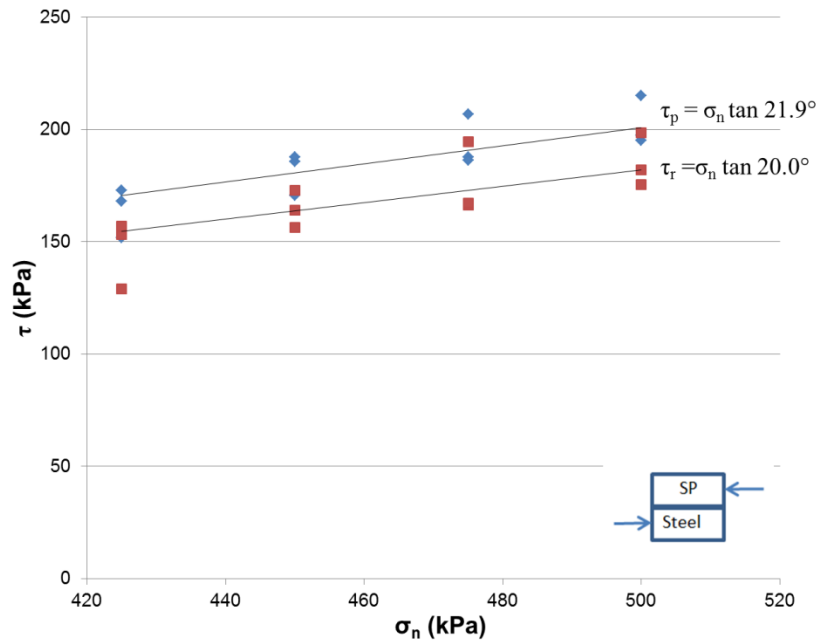


**Figure 5-14** Test 0027-0029 Mohr-Coulomb peak and residual shear strength envelope,  $\sigma_n$  425 to 500kPa

## 5.6 Shear Strength of Brighton Sand and Grout

The Brighton sand and grout interface scenario also required the determination of both peak and residual shear strength due to the variations in the sample preparation of the soil. The peak and residual values were determined from the shear stress versus horizontal displacement curves (**Figure 5-15** and **Figure 5-16**), in the same way as for the previous tests. The Mohr-Coulomb shear strength envelopes (**Figure 5-19** and **Figure 5-20**) from the aggregate test results provided a peak and residual shear strength, for the 25-100 kPa range, of  $\tau_p = \sigma_n \tan 34.5^\circ$  ( $r^2 = 0.992$ ) and  $\tau_r = \sigma_n \tan 26.6^\circ$  ( $r^2 = 0.996$ ) respectively. The peak and residual for the tests at 425-500 kPa normal stress were  $\tau_p = \sigma_n \tan 34.0^\circ$  ( $r^2 = 0.999$ ) and  $\tau_r = \sigma_n \tan 30.8^\circ$  ( $r^2 = 0.998$ ) respectively.

The shear stress versus displacement curves were different from both the pure soil samples and the Brighton sand-steel interface. The peak and residual had a significant difference though not as drastic as that of the pure Brighton sand sample. The drop of the curve to the residual shear strength was also sharper than in the pure Brighton sand sample but more gradual than the Brighton sand and steel shear stress versus displacement curves. This was likely because the grout introduces a preferential failure plane and forms a relatively hard smooth surface for the soil to slide across. However the grout surface is not as hard and smooth as the Brighton sand and steel interface. These conditions resulted in a more sudden drop in strength than was measured in the direct shear tests on pure Brighton sand. This was because the displacement and rearrangement of particles is restricted with the grout interface. However, the results were a more gradual drop than the Brighton sand-steel interface as the grout had more asperities which allowed for concentration of stresses and mechanically provided more strength.

These asperities meant particles had to move around one another for failure to occur. This was seen in the vertical versus horizontal displacement curves (**Figure 5-17** and **Figure 5-18**) where the vertical displacement was an order of magnitude greater for the Brighton sand and grout interface compared to the Brighton sand and steel interface (max vertical displacement of 0.177mm versus 0.027mm at the 25-100 kPa range).

The Mohr-Coulomb failure envelope for Brighton sand and grout was also between that of the pure Brighton sand sample and the Brighton sand-steel interface. This was anticipated due to the difference between the surfaces of the steel and grout sample as well as the weakening of the shear strength by creation of a preferential failure plane where soil and the grout meet.

## 5.7 Shear Stiffness of Brighton sand and Grout

Shear stiffness was an essential parameter for the modelling of the Brighton sand and grout interface. The shear stiffness was determined from the shear stress versus horizontal displacement curves using the chord method.

The shear stiffnesses had a noticeable positive trend for the lower normal stress level of 25 to 100 kPa (74000 to 166000kPa/m) though had no trend and varied relatively little over the 425 to 500 kPa range (259000 to 274000kPa/m). This was similar to the Brighton sand and the sand-steel samples.

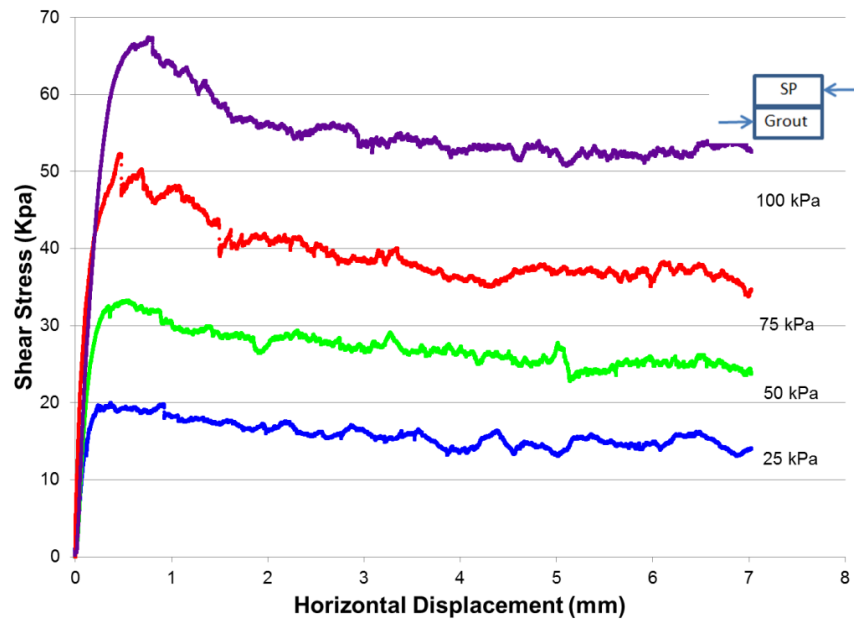


**Figure 5-15** Test 0017 SP soil – grout sample,  $\tau$  versus horizontal displacement,  $\sigma_n$  25 to 100kPa

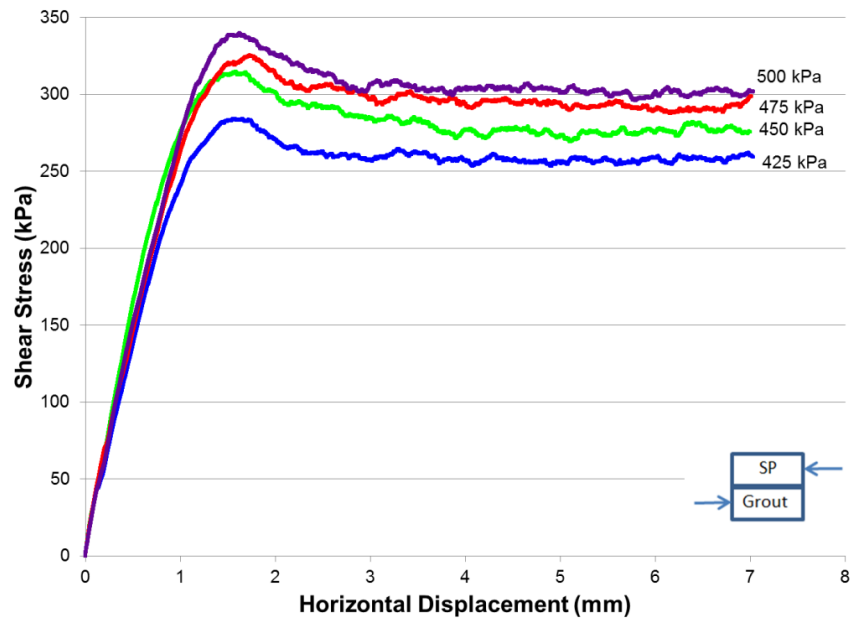


**Figure 5-16** Test 0026 SP soil – grout sample,  $\tau$  versus horizontal displacement,  $\sigma_n$  425 to 500kPa

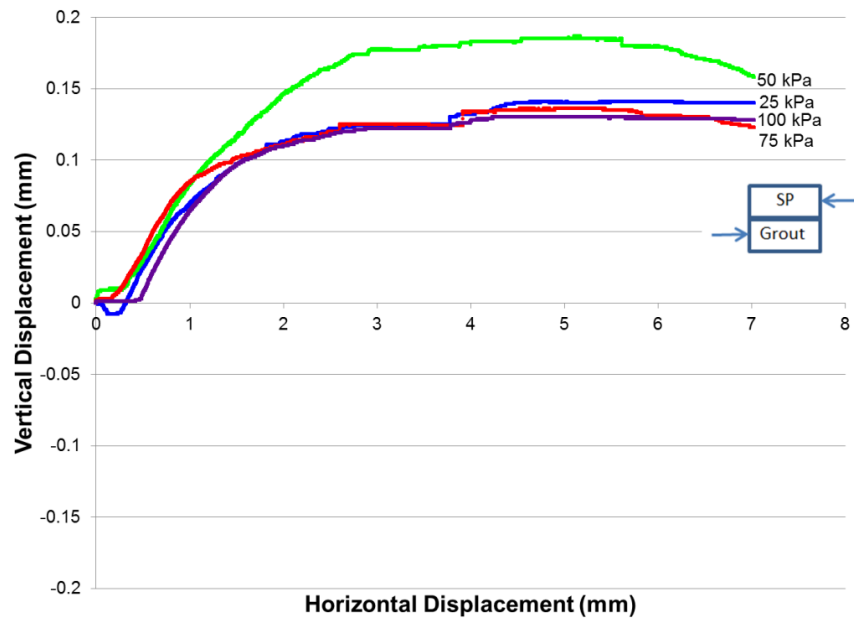


**Figure 5-17** Test 0017 SP soil – grout sample, vertical versus horizontal displacement,  $\sigma_n$  25 to 100kPa

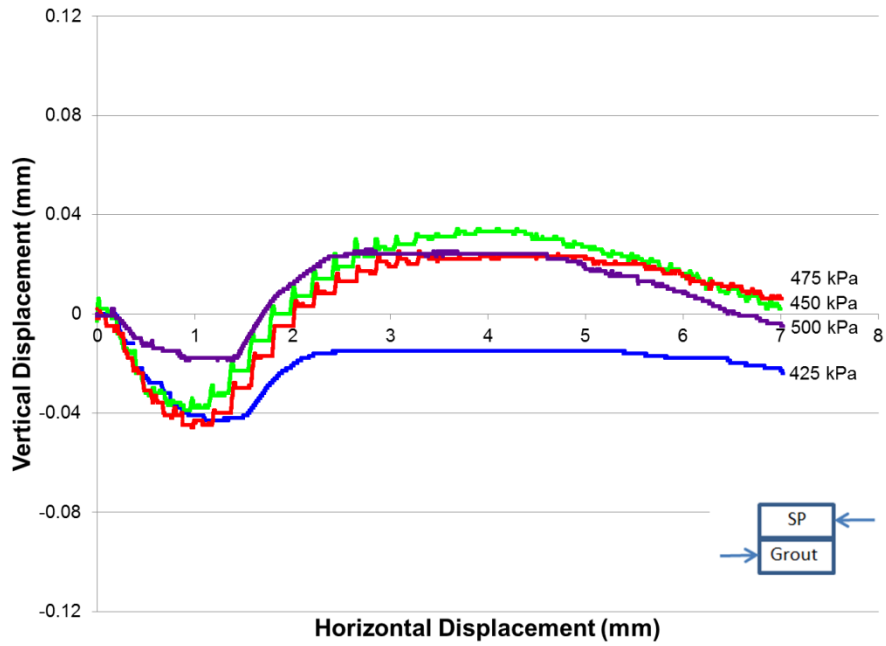


**Figure 5-18** Test 0026 SP soil – grout sample, vertical versus horizontal displacement,  $\sigma_n$  425 to 500kPa

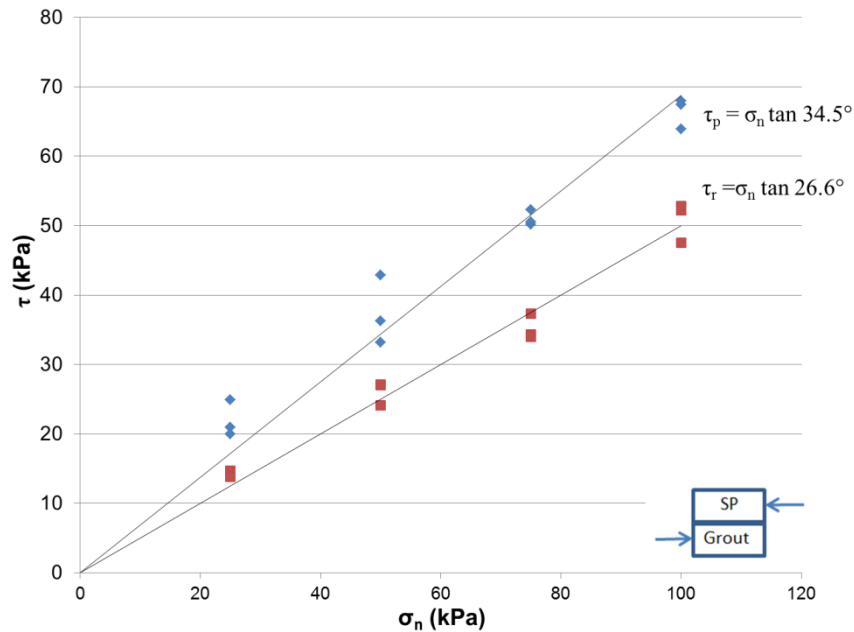


**Figure 5-19** Test 0015-0017 Mohr-Coulomb peak and residual shear strength envelope,  $\sigma_n$  25 to 100kPa

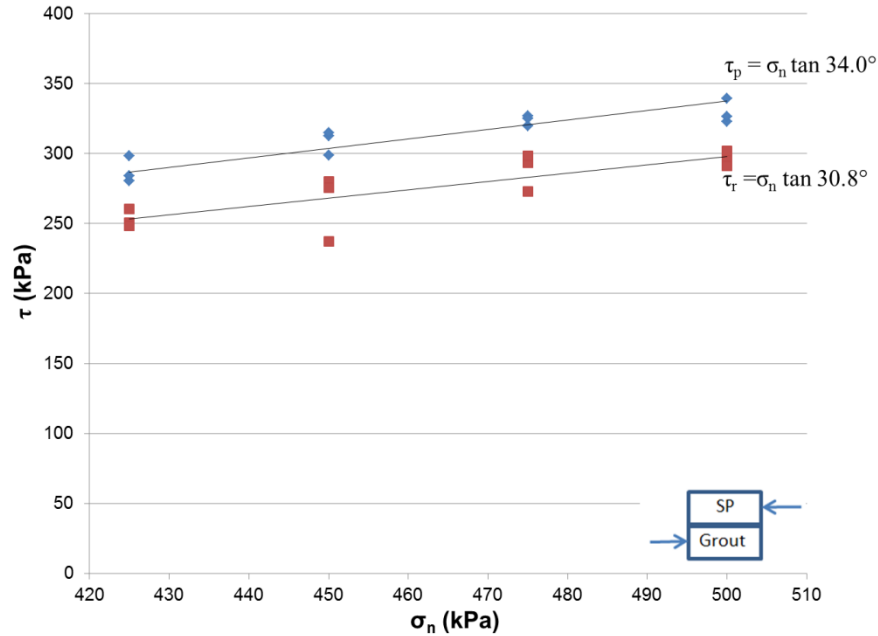


**Figure 5-20** Test 0024-0026 Mohr-Coulomb peak and residual shear strength envelope,  $\sigma_n$  425 to 500kPa

### 5.8 Shear Strength of Coburg Limestone and Steel

The shear strength of the Coburg limestone and steel interfaces presented different challenges than those of the Brighton sand because it was a solid block of material rather than granular particles. The shear stress versus horizontal displacement curves were found to be different in form from those of the Brighton sand. In these curves, a bi-linear behaviour was seen but did not have the distinct peak of the soil but instead had a break where the interface was mobilized and significant deformation began with relatively small increases or decreases in shear stress. This unusual behaviour made it challenging to establish what the shear strength was for the material. It was decided a reasonable procedure would be to take the average of the shear stress after the break as the shear strength for the determination of Mohr-Coulomb failure envelopes.

Selected defects were also seen forming in the rock samples during testing (**Figure 5-21**). These cracks were believed to form as a result of small asperities on the surface of the Coburg limestone samples causing bending moments to form within the sample from the normal load. This was a complication as using two monolithic materials in a direct shear test machine designed for soils is abnormal and was attempted to confirm whether it was a reasonable and more rapid alternative to using direct shear test machines specifically designed for direct shear

testing of rock. These cracks were not seen as making significant differences in the behaviour of the shear tests due to their close fit and negligible change in surface roughness. This, combined with limited rock samples available, meant the first rock sample was used until damage became significant enough to raise concerns that the damage would influence the results. It should be noted that the tests for the limestone and steel interfaces under low normal stress were conducted with the first rock sample. Conversely, during the first test serials of the limestone and steel interface at the 425 to 500 kPa normal stress range the rock sample was critically damaged after repeated tests (**Figure 5-22**) and was changed for the second rock sample before the first test of rock and steel at 500 kPa.

The vertical versus horizontal displacement graphs saw minimal displacements in the vertical direction (0.109mm at  $\sigma_n = 475$  kPa). There was no discernible pattern to the results as values went slightly up or slightly down without. It was likely from a minute buildup of powdered limestone between the two samples which was noticed and occasionally removed.

The Mohr-Coulomb failure envelopes seen in **Figure 5-27** and **Figure 5-28** show that, as the normal stress increases, the shear stress envelope plateaus gradually. The strength envelopes at 25-100 kPa and 425-500 kPa normal stress were  $\tau_p = \sigma_n \tan 32.8^\circ$  ( $r^2 = 0.998$ ) and  $\tau_p = \sigma_n \tan 28.1^\circ$  ( $r^2 = 0.974$ ) respectively. Despite this, at higher normal stress levels there were greater variations in the results between test serials of the same normal stress.

## 5.9 Shear Stiffness of Coburg Limestone and Steel

The shear stiffness of the Coburg limestone and steel interfaces was essential to numerical simulations and was determined using the chord method from the shear stress versus horizontal displacement curves for each test serial.

Generally, trends were the same as other tests where there were significant changes as normal stress increased in the 25 – 100 kPa range (56000 to 154000 kPa/m) but the stiffness values for the 425 to 500 kPa range were similar with no distinct pattern in the values (321000 to 419000 kPa/m).

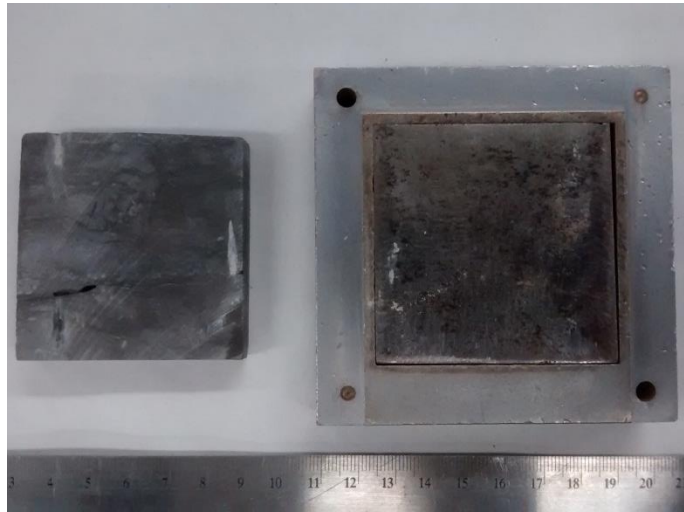


**Figure 5-21** Rock and steel sample after Test 0031



**Figure 5-22** First rock sample after damage in Test 0040 at 475 kPa

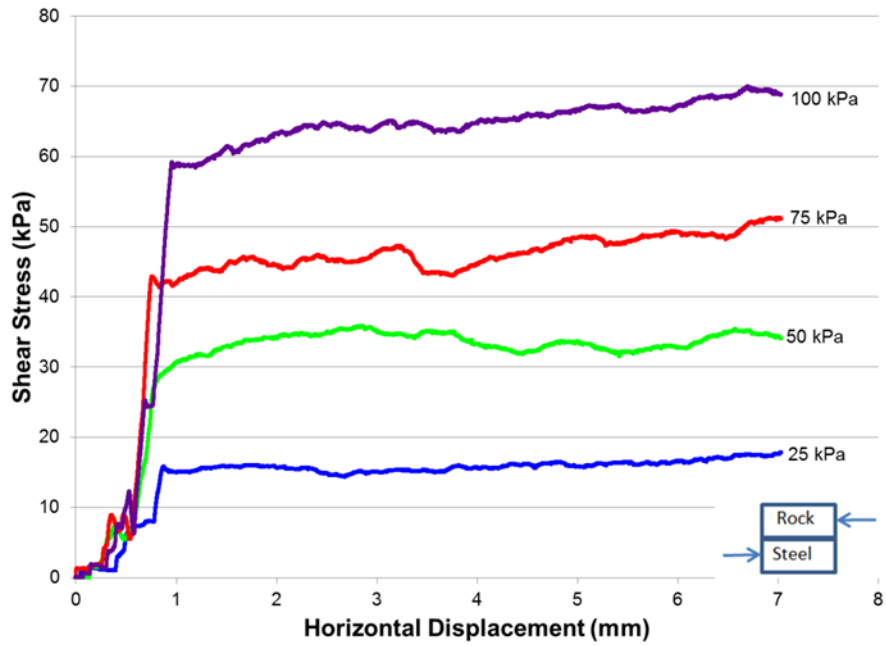


**Figure 5-23** Test 0032 limestone – steel sample,  $\tau$  versus horizontal displacement,  $\sigma_n$  25 to 100kPa

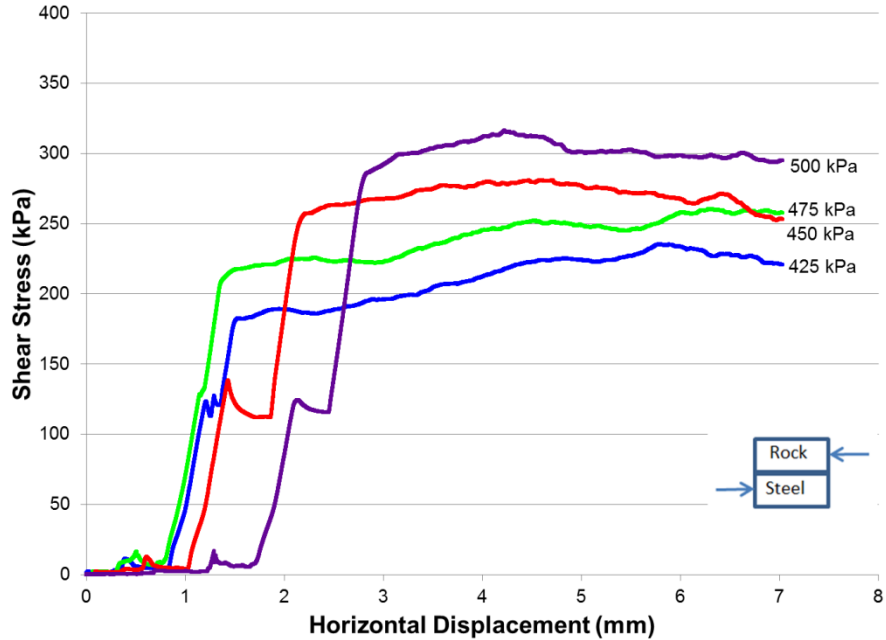


**Figure 5-24** Test 0041 limestone – steel sample,  $\tau$  versus horizontal displacement,  $\sigma_n$  425 to 500kPa

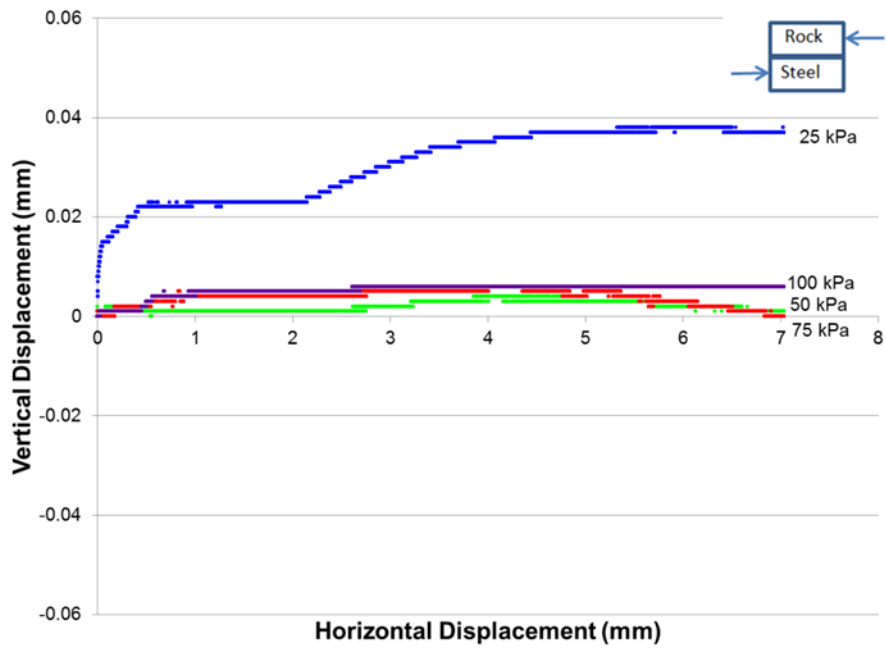


**Figure 5-25** Test 0032 limestone – steel sample, vertical versus horizontal displacement,  $\sigma_n$  25 to 100kPa

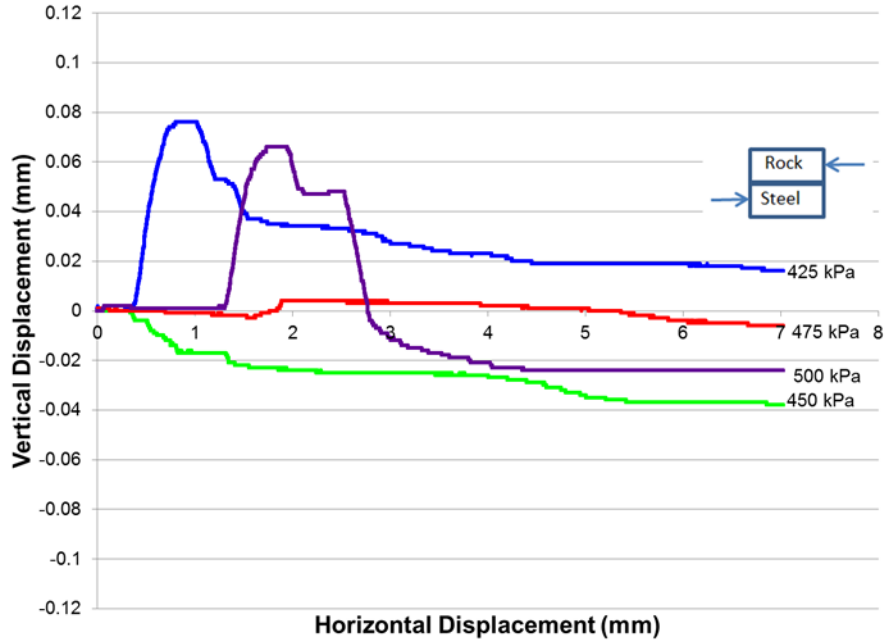


**Figure 5-26** Test 0041 limestone – steel sample, vertical versus horizontal displacement,  $\sigma_n$  425 to 500kPa

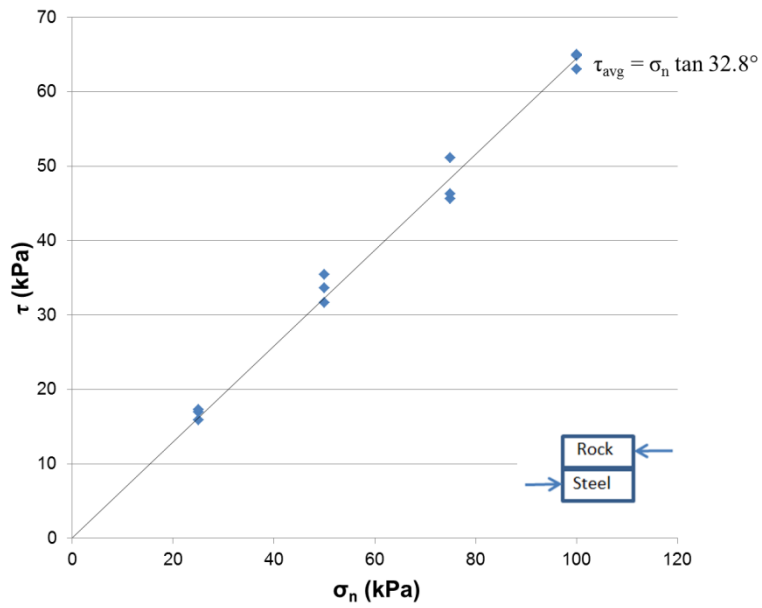


**Figure 5-27** Test 0031-0033 Mohr-Coulomb peak and residual shear strength envelope,  $\sigma_n$  25 to 100kPa

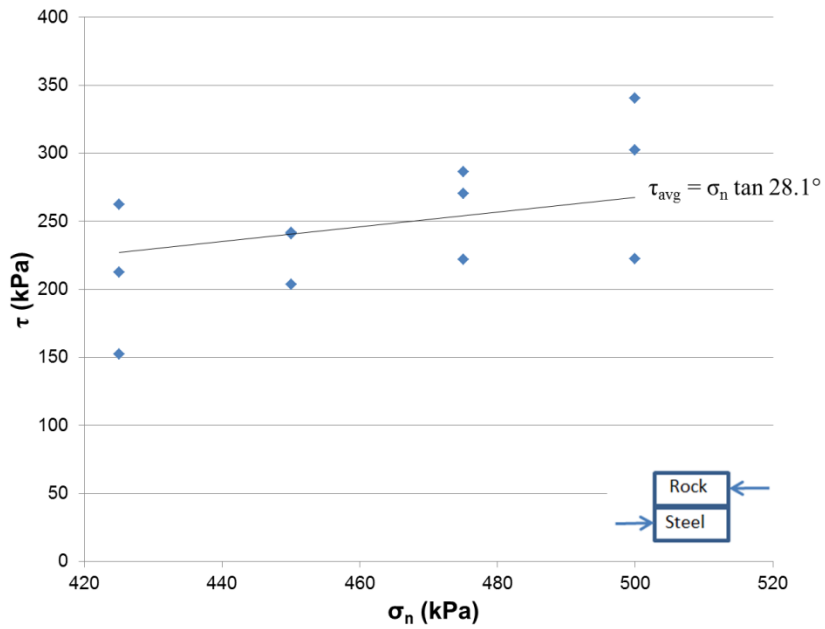


**Figure 5-28** Test 0040-0042 Mohr-Coulomb peak and residual shear strength envelope,  $\sigma_n$  425 to 500kPa

## 5.10 Shear Strength of Coburg Limestone and Grout

The shear strength of the Coburg limestone and grout varied similarly to that of the Coburg limestone and steel interfaces. The curves had the same form where no specific peak or residual value existed so an average of the post mobilization shear stress was taken as the shear strength.

The sample had some cracks for these tests as well since they had formed in the first rock sample during tests on the limestone and steel interfaces at the low normal stress range. One distinct mechanistic issue came up in the third test at the 425 kPa normal stress level (0039-03). At this point the front edge of the rock sample on top of the grout caught on the edge of the lower half of the shearbox allowing for a stress buildup to ~1000 kPa before the edge of the rock sample broke off a small chip allowing for the sample to deform further (**Figure 5-29**). The sample still seemed sufficiently intact for further tests but was assessed more frequently between tests to determine if replacement was prudent. When the average shear stress was calculated it was accomplished using the data points after the shear stress spike (beginning at approximately 3.3mm displacement).

Vertical versus horizontal displacement plots showed limited vertical movement of the samples (extremes of 0.029mm upward and 0.063mm downward). No specific pattern in the results were seen and as with the limestone and steel tests there was fine dust from the limestone and grout produced at the interface where material had been rubbed off, this was removed regularly from between the samples to prevent excessive buildup interfering with interface behaviour.

The Mohr-Coulomb failure envelope was produced from the average post mobilization shear stress determined from the shear stress versus horizontal displacement plots. The results for normal stresses of 25-100 kPa and 425-500 kPa were  $\tau_p = \sigma_n \tan 35.5^\circ$  ( $r^2 = 0.999$ ) and  $\tau_p = \sigma_n \tan 34.3^\circ$  ( $r^2 = 0.997$ ) respectively. This strength envelope was greater than that of steel. This was logical as the uneven and softer grout would have larger asperities which would create mechanical resistance to movement of the interface. The smooth hard steel would not provide the rock with the same amount or size of asperities due to its surface condition.

## 5.11 Shear Stiffness of Coburg Limestone and Grout

The shear stiffness of the Coburg limestone and grout interface was important for numerical simulations of interfaces. As such it was determined from the shear stress versus horizontal displacement plots using the chord method similar to the previous tests.

As with the previous stiffnesses, there was a noticeable positive trend in the results for the tests at the 25 to 100 kPa normal stress range (51000 to 145

kPa/m) but no specific trend when the stiffnesses were determined at the 425 kPa to 500 kPa normal stress level (408000 to 374000 kPa/m).

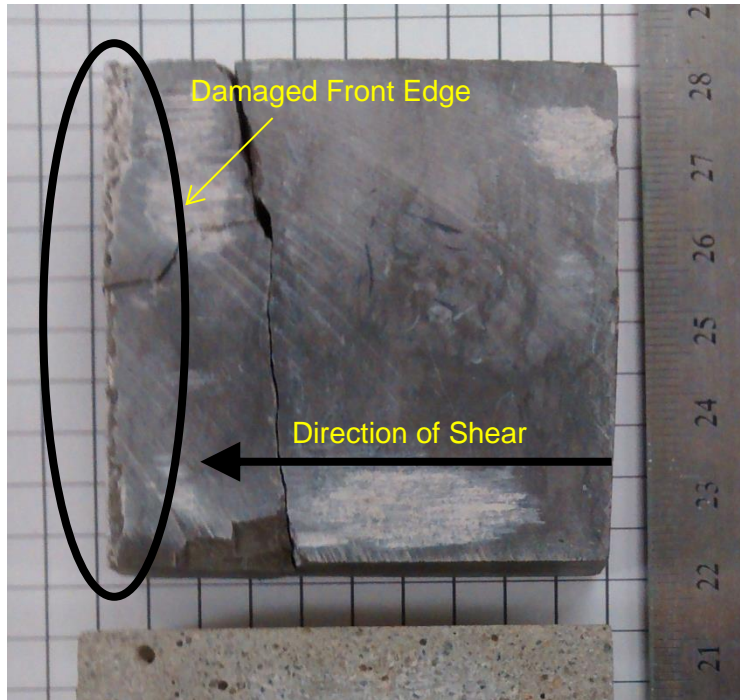


**Figure 5-29** First rock sample after Test 0039 at 475 kPa

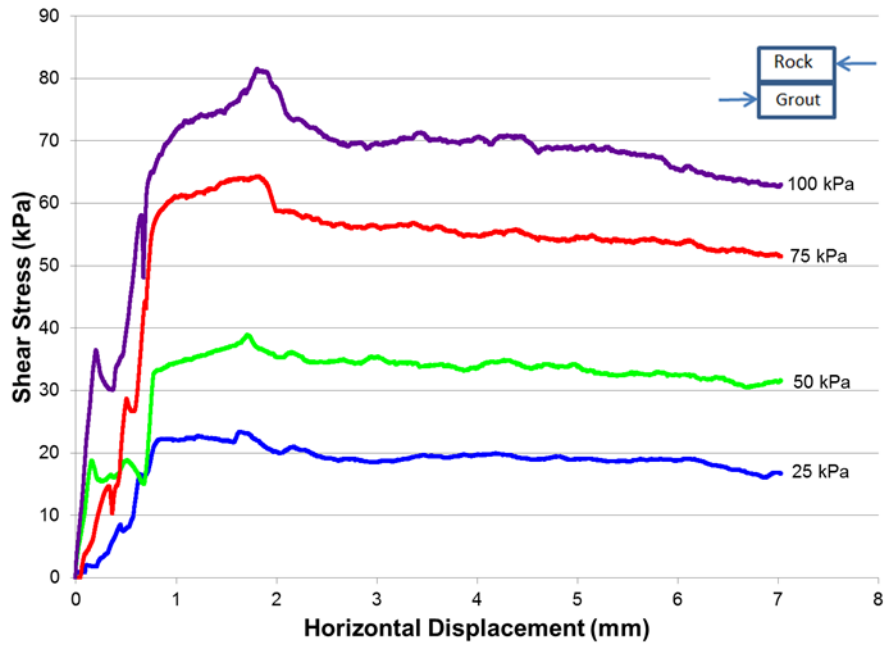


**Figure 5-30** Test 0035 limestone – grout sample,  $\tau$  versus horizontal displacement,  $\sigma_n$  25 to 100kPa

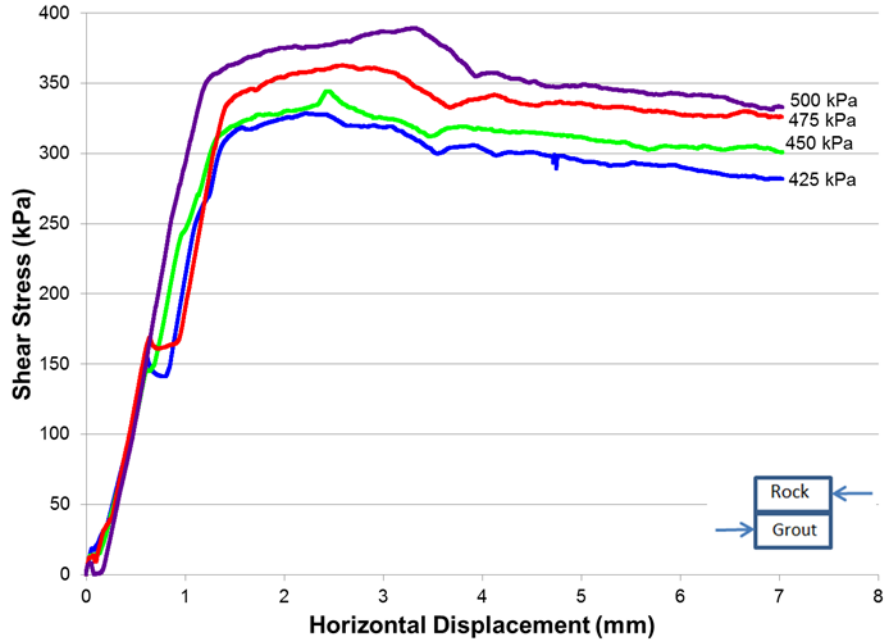


**Figure 5-31** Test 0038 limestone – grout sample,  $\tau$  versus horizontal displacement,  $\sigma_n$  425 to 500kPa

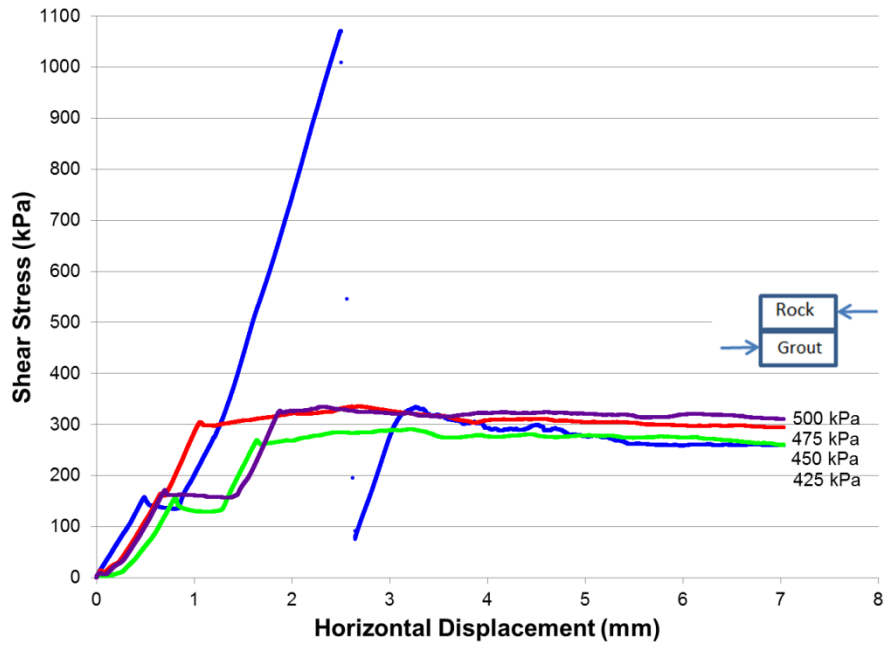


**Figure 5-32** Test 0039 limestone – grout sample,  $\tau$  versus horizontal displacement,  $\sigma_n$  425 to 500kPa

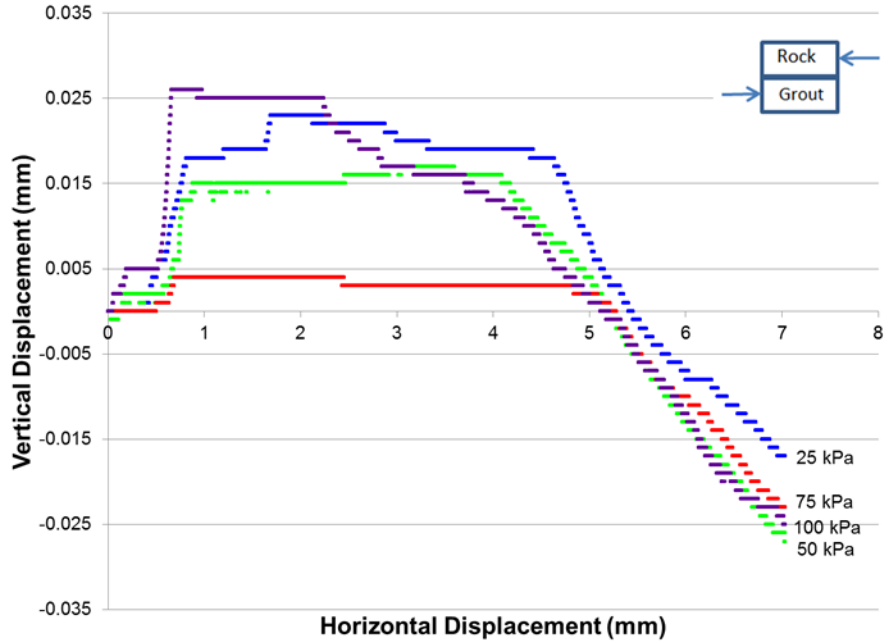


**Figure 5-33** Test 0035 limestone – grout sample, vertical versus horizontal displacement,  $\sigma_n$  25 to 100kPa

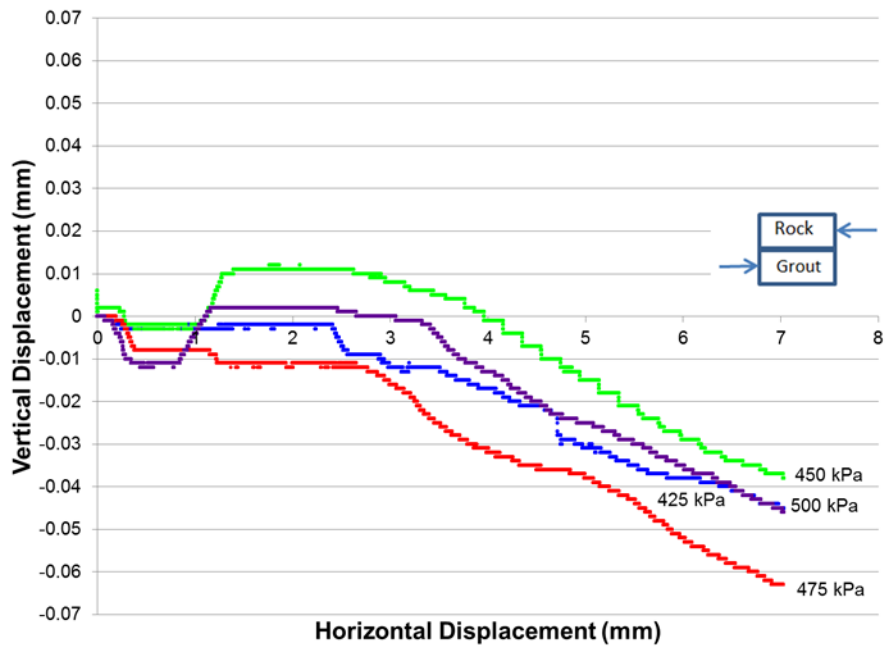


**Figure 5-34** Test 0038 limestone – grout sample, vertical versus horizontal displacement,  $\sigma_n$  425 to 500kPa

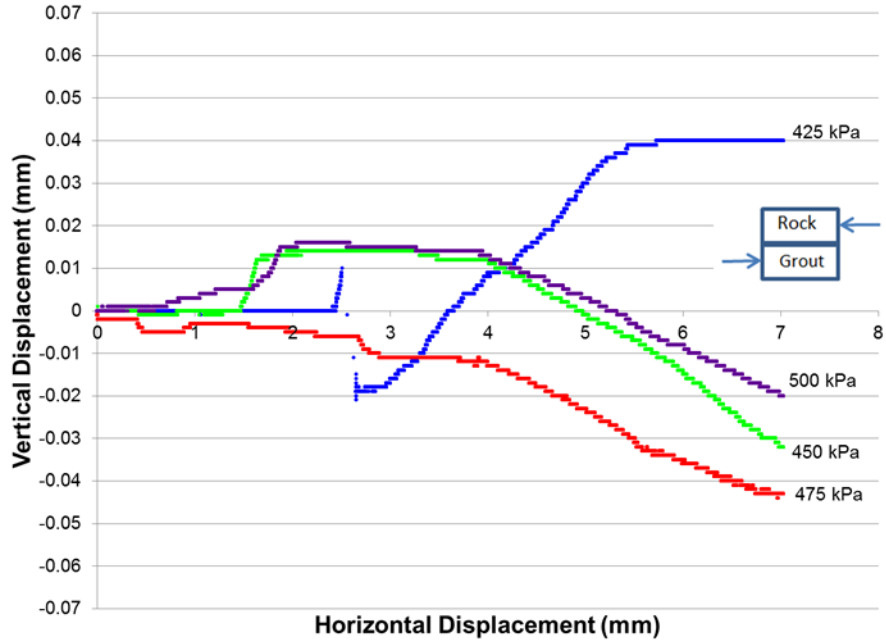


**Figure 5-35** Test 0039 limestone – grout sample, vertical versus horizontal displacement,  $\sigma_n$  425 to 500kPa

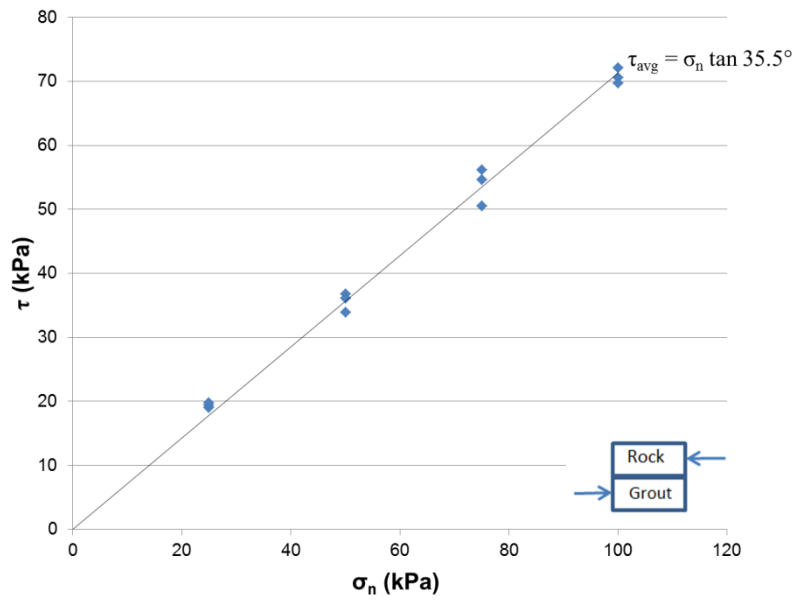


**Figure 5-36** Test 0034-0036 Mohr-Coulomb peak and residual shear strength envelope,  $\sigma_n$  25 to 100kPa

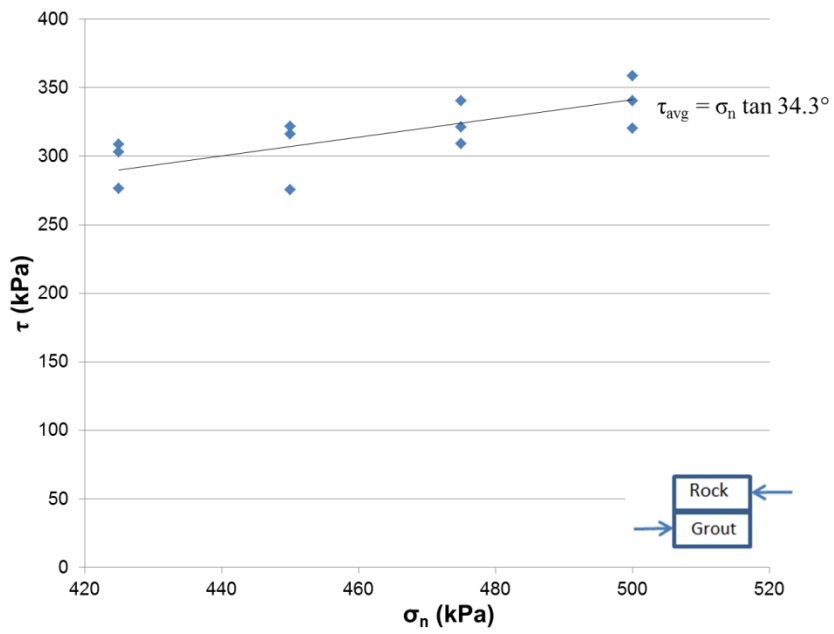


**Figure 5-37** Test 0037-0039 Mohr-Coulomb peak and residual shear strength envelope,  $\sigma_n$  425 to 500kPa

## 5.12 Shear Strength of Grout and Steel

The grout and steel had similar behaviour to that of the tests with rock. The curve had a bi-linear character like the rock samples so an average of the post mobilization section of the curve was taken as the shear strength rather than peak and residual values.

Vertical versus horizontal displacement graphs demonstrate minimal vertical movement during shearing (maximum of 0.075mm). The limited change is likely due to minor asperities and dust on the grout surface. It should also be noted that there was a flag in the vertical displacement data during test 0048-02 of -0.905 mm where the vertical LVDT was poorly positioned so it fell off the measurement point during testing resulting in an apparent downward direction.

The Mohr-Coulomb failure envelopes for both the 25-100 kPa level and the 425-500 kPa were plotted in **Figure 5-42** and **Figure 5-43** with results of  $\tau_p = \sigma_n \tan 21.9^\circ$  ( $r^2 = 0.966$ ) and  $\tau_p = \sigma_n \tan 27.9^\circ$  ( $r^2 = 0.996$ ) respectively. The shear strength of the grout-steel interface is one of the weakest of these tests and is only stronger than that of the SP and steel interface. There was also the unusual trend that the friction angle of the Mohr-Coulomb failure envelope increased as the normal stress increased. This could be due to some sensitivity of the friction angle to variance between the individual direct shear test results.

## 5.13 Shear Stiffness of Grout and Steel

The shear stiffness of the grout and steel interface behaved similarly to the previous tests. The general trend was that the shear stiffness increased as normal stress was raised over the 25 to 100 kPa range (90000 to 248000 kPa/m). No discernible pattern existed for the shear stiffness between 425 – 500 kPa (368000 to 391 kPa/m). These shear stiffness values were summarized in **Error! eference source not found.**

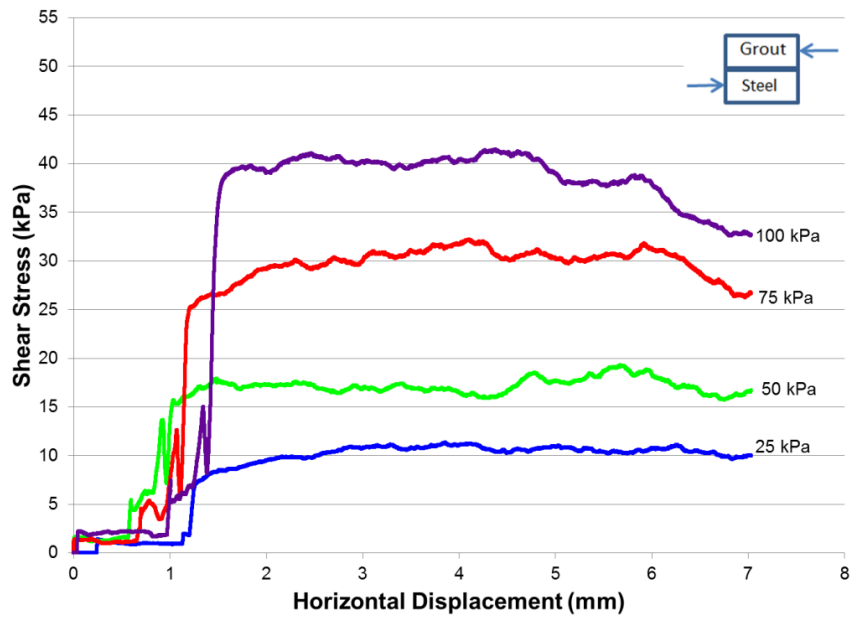


Figure 5-38 Test 0044 grout - steel sample,  $\tau$  versus horizontal displacement,  $\sigma_n$  25 to 100kPa

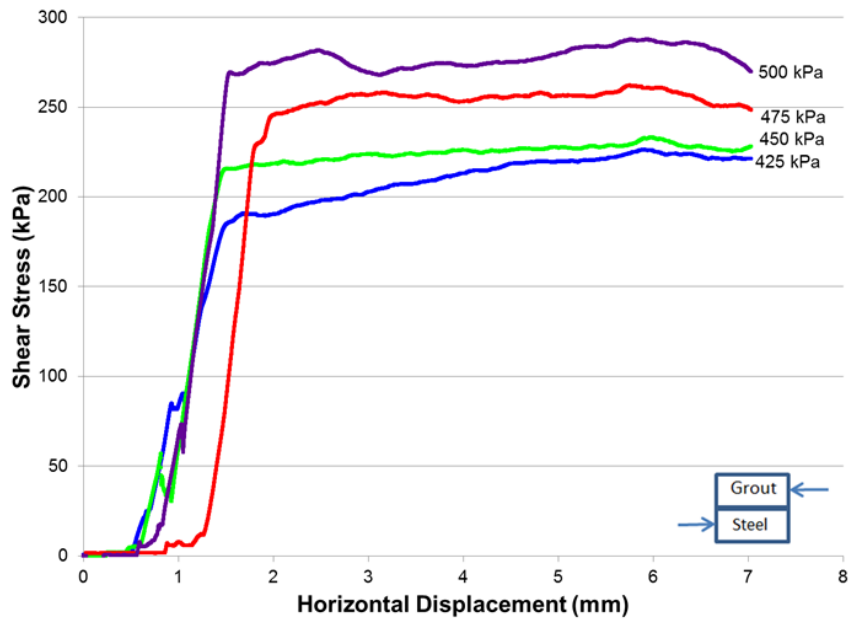
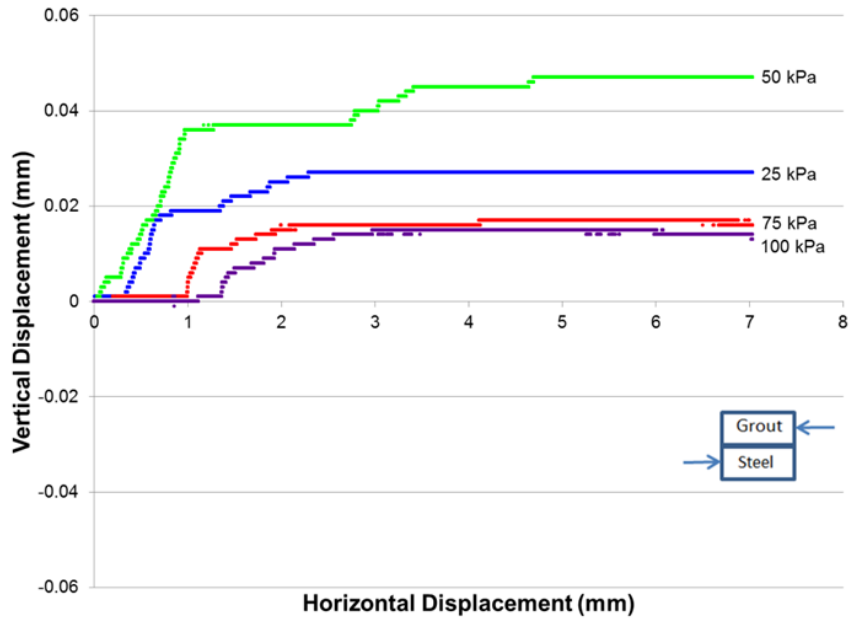
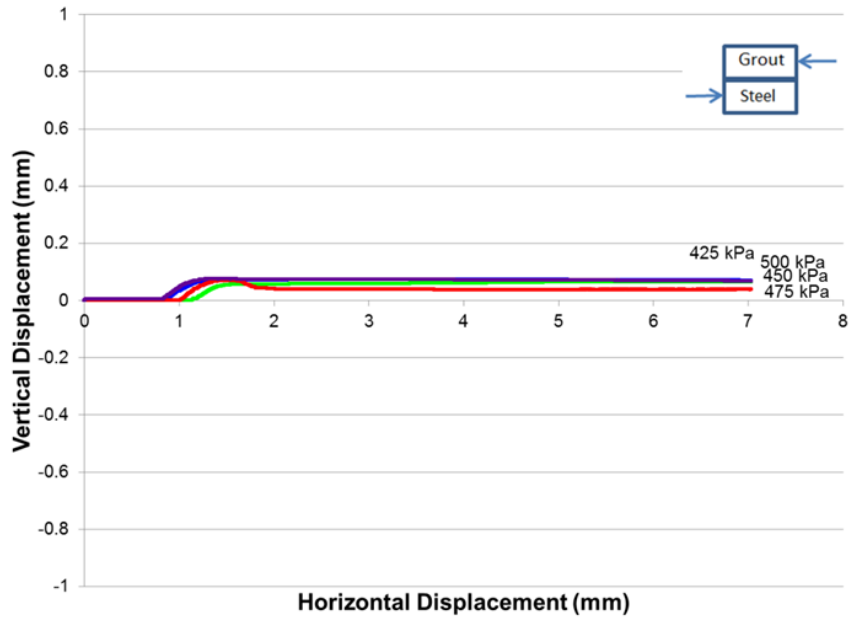


Figure 5-39 Test 0047 Grout - steel sample,  $\tau$  versus horizontal displacement,  $\sigma_n$  425 to 500kPa



**Figure 5-40** Test 0044 Grout - steel sample, vertical versus horizontal displacement,  $\sigma_n$  25 to 100kPa



**Figure 5-41** Test 0047 Grout - steel sample, vertical versus horizontal displacement,  $\sigma_n$  425 to 500kPa

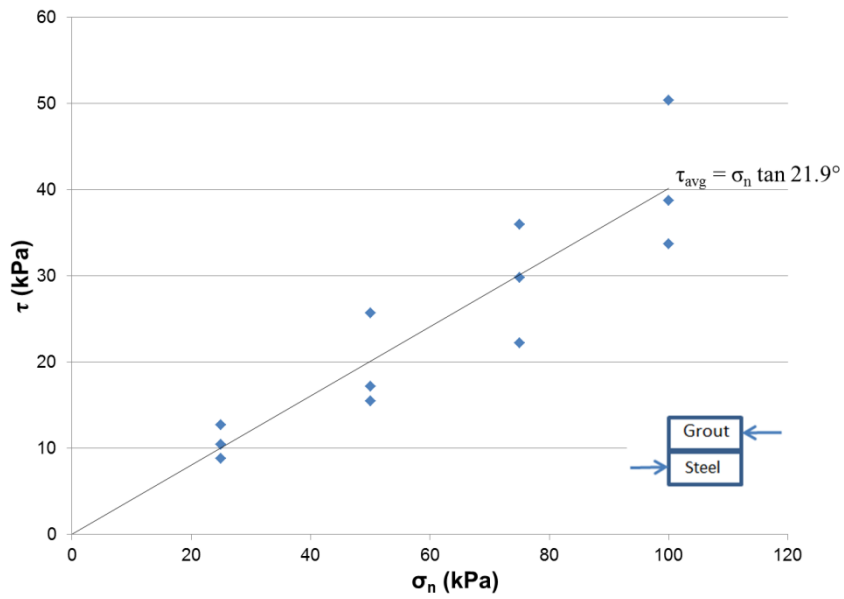


**Figure 5-42** Test 0043-0045 Mohr-Coulomb peak and residual shear strength envelope,  $\sigma_n$  25 to 100kPa

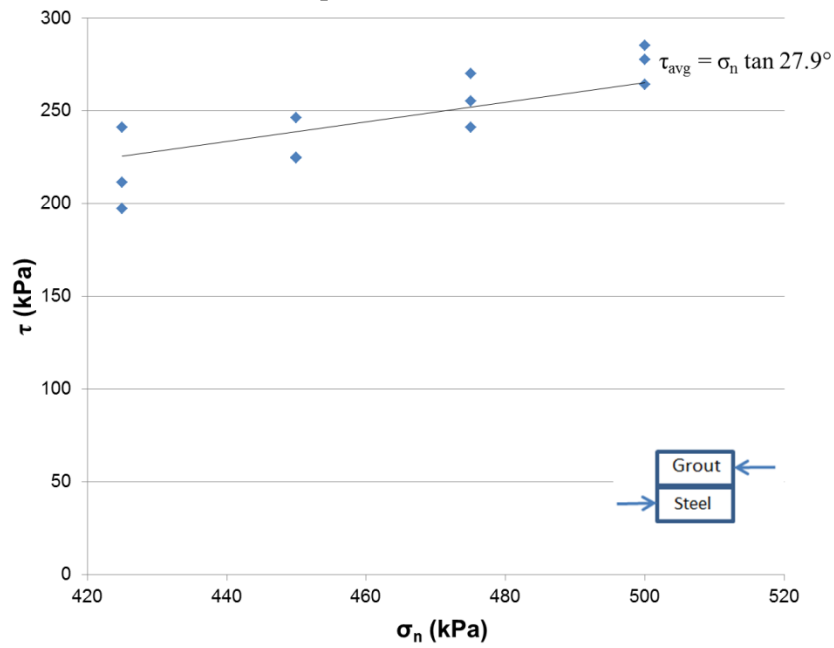


**Figure 5-43** Test 0046-0048 Mohr-Coulomb peak and residual shear strength envelope,  $\sigma_n$  425 to 500kPa

#### 5.14 Shear Strength of Concrete and Grout

The shear stress versus displacement plots of the concrete and grout tests were similar in their form to those of the other solid to solid interface scenarios. The behaviour was of a bi-linear type with no distinct peak or residual. As such the average of the post mobilization segment of the curve was taken as the shear strength for the interface.

Vertical displacement was minor (maximum of 0.113mm) and similar to the rock and grout tests. This was likely due to the similar surface of the concrete and grout surface to the rock and grout.

The Mohr-Coulomb envelope for the normal stress ranges of 25-100 kPa and 425-500kPa was determined from the shear stress versus displacement plots in **Figure 5-48** and **Figure 5-49** respectively. This provided the shear strength envelop for the 25-100 kPa and 425-500 kPa normal stress ranges of  $\tau_p = \sigma_n \tan 30.6^\circ$  ( $r^2 = 0.999$ ) and  $\tau_p = \sigma_n \tan 31.1^\circ$  ( $r^2 = 0.999$ ) respectively.

#### 5.15 Shear Stiffness of Concrete and Grout

Shear stiffness for the concrete and grout interface was calculated from the shear stress versus horizontal displacement graphs using the chord method. The results were important for the development of numerical simulations.

The shear stiffnesses for the concrete and grout interface followed a trend similar to the other tests in that a general increase of shear stiffness occurred from the 25-100 kPa normal stress (77000 – 171000 kPa/m). Conversely, at the 425-500 kPa normal stress level the shear stiffness had no specific pattern (297000 – 337000 kPa/m) though there was some variance between the different normal stresses.

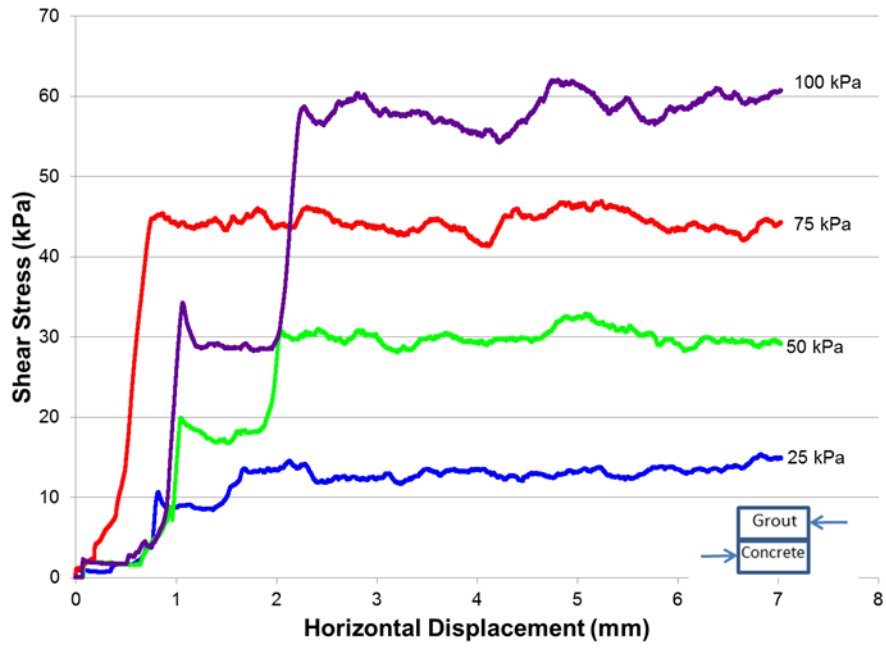


Figure 5-44 Test 0049 Grout - concrete sample,  $\tau$  versus horizontal displacement,  $\sigma_n$  25 to 100kPa

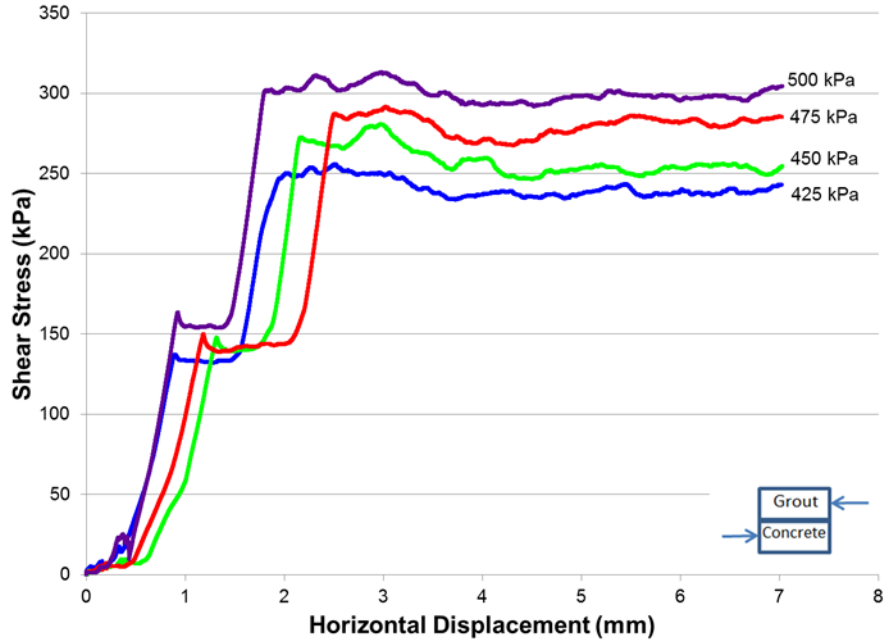
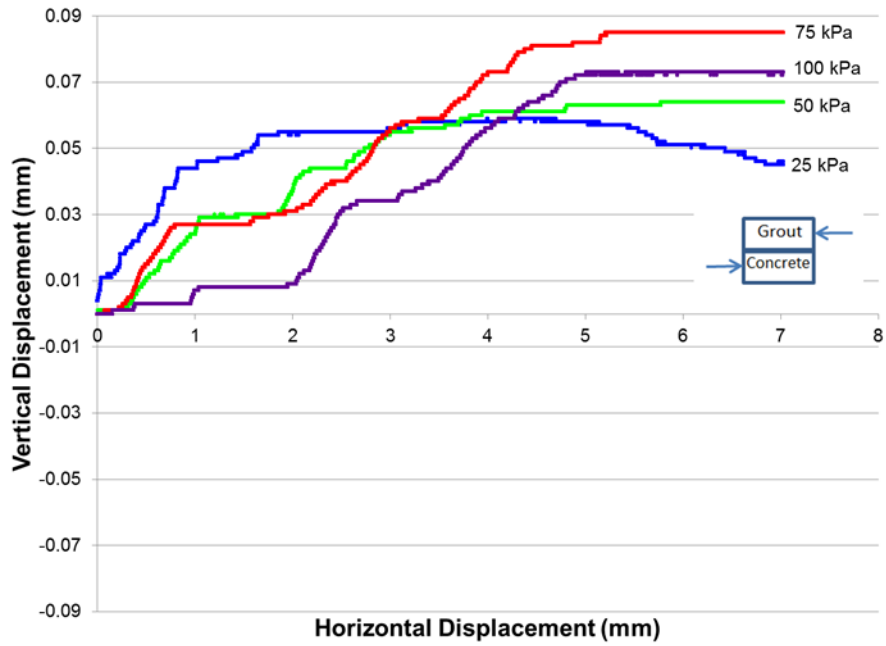
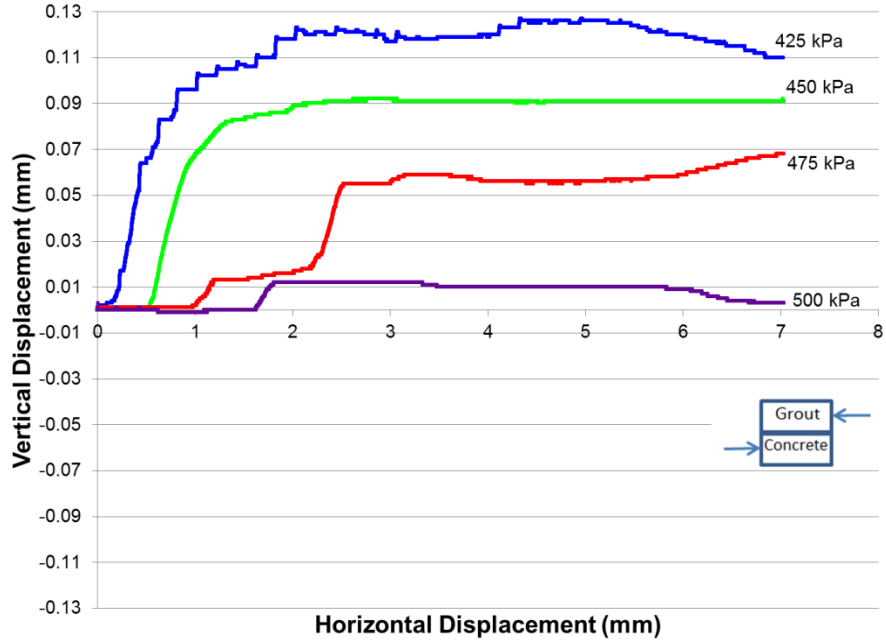


Figure 5-45 Test 0052 Grout - concrete sample,  $\tau$  versus horizontal displacement,  $\sigma_n$  425 to 500kPa



**Figure 5-46** Test 0049 Grout - steel sample, vertical versus horizontal displacement,  $\sigma_n$  25 to 100kPa



**Figure 5-47** Test 0052 Grout - steel sample, vertical versus horizontal displacement,  $\sigma_n$  425 to 500kPa

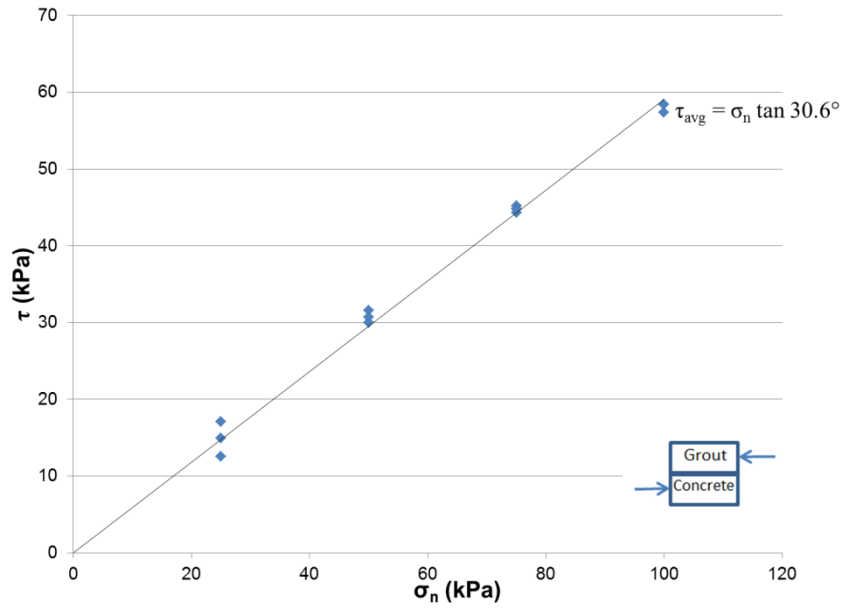


**Figure 5-48** Test 0049-0051 Mohr-Coulomb peak and residual shear strength envelope,  $\sigma_n$  25 to 100kPa

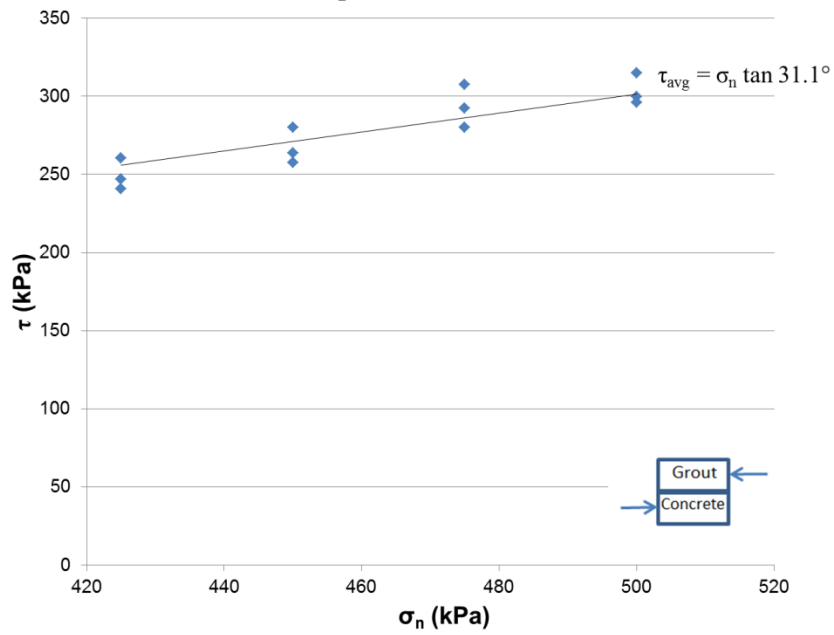


**Figure 5-49** Test 0052-0054 Mohr-Coulomb peak and residual shear strength envelope,  $\sigma_n$  425 to 500kPa

## 5.16 Summary of Results

The results of the tests cited above were summarized in **Table 5-1**. This data is not currently available within the scientific community and is a unique contribution from this thesis investigation. The results were consistent with literature for the Brighton sand. The results of the remaining interface tests were quantified. These results were anticipated, whereby the shear strength of the pure Brighton sand sample was greater than the shear strength of the Brighton sand interface with the other materials. As well, the tests with the relatively hard and smooth steel had lower shear strengths than tests with grout which was relatively softer and had more asperities. These results were similar to those cited in the work of Potyondy in 1961. He found that the pure soils used for testing had higher shear strength envelopes than the interfaces between soils and monolithic materials. A comparison of Potyondy's results and the relevant results of this research can be seen in **Figure 5-50**. The similarity of the results of this research to the limited previous research provided strong confidence in the accuracy of the data from the laboratory testing results.

**Table 5-1** Laboratory results for  $\Phi$ ,  $k_s$ , and  $R^2$

Interface Scenario	$\Phi_p$ ( $^\circ$ ) [ $R^2$ ]	$\Phi_r$ ( $^\circ$ ) [ $R^2$ ]	$\sigma_n$ (kPa)	Shear Stiffness (kPa/m)
SP Soil (25 – 100 kPa)	43.8 [0.997]	34.0 [0.997]	25	38000
			50	76000
			75	85000
			100	98000
SP Soil (425 – 500 kPa)	41.6 [0.998]	33.7 [0.990]	425	265000
			450	229000
			475	240000
			500	238000
SP Soil –Steel (25 – 100 kPa)	21.6 [0.969]	19.0 [0.988]	25	59000
			50	163000
			75	214000
			100	177000
SP Soil-Steel (425 – 500 kPa)	21.9 [0.997]	20.0 [0.995]	425	292000
			450	296000
			475	309000
			500	310000
SP Soil-Grout (25 – 100 kPa)	34.5 [0.993]	26.6 [0.996]	25	74000
			50	131000
			75	184000
			100	166000

Interface Scenario	$\Phi_p$ (°) [R <sup>2</sup> ]	$\Phi_r$ (°) [R <sup>2</sup> ]	$\sigma_n$ (kPa)	Shear Stiffness (kPa/m)
SP Soil-Grout (425 – 500 kPa)	34.0 [0.999]	30.8 [0.998]	425	259000
			450	287000
			475	259000
			500	274000
Limestone – Steel (25 – 100 kPa)	32.8 [0.998]		25	56000
			50	130000
			75	155000
			100	154000
Limestone – Steel (425 – 500 kPa)	28.1 [0.974]		425	321000
			450	338000
			475	430000
			500	419000
Limestone – Grout (25 – 100 kPa)	35.5 [0.999]		25	51000
			50	141000
			75	126000
			100	145000
Limestone – Grout (425 – 500 kPa)	34.3 [0.997]		425	408000
			450	318000
			475	373000
			500	374000
Grout – Steel (25 – 100 kPa)	21.9 [0.966]		25	90000
			50	69000
			75	206000
			100	248000
Grout – Steel (425 – 500 kPa)	27.9 [0.996]		425	368000
			450	356000
			475	464000
			500	391000
Grout – Concrete (25 – 100 kPa)	30.6 [0.999]		25	77000
			50	139000
			75	123000
			100	171000
Grout – Concrete (425 – 500 kPa)	31.1 [0.997]		425	297000
			450	398000
			475	362000
			500	337000

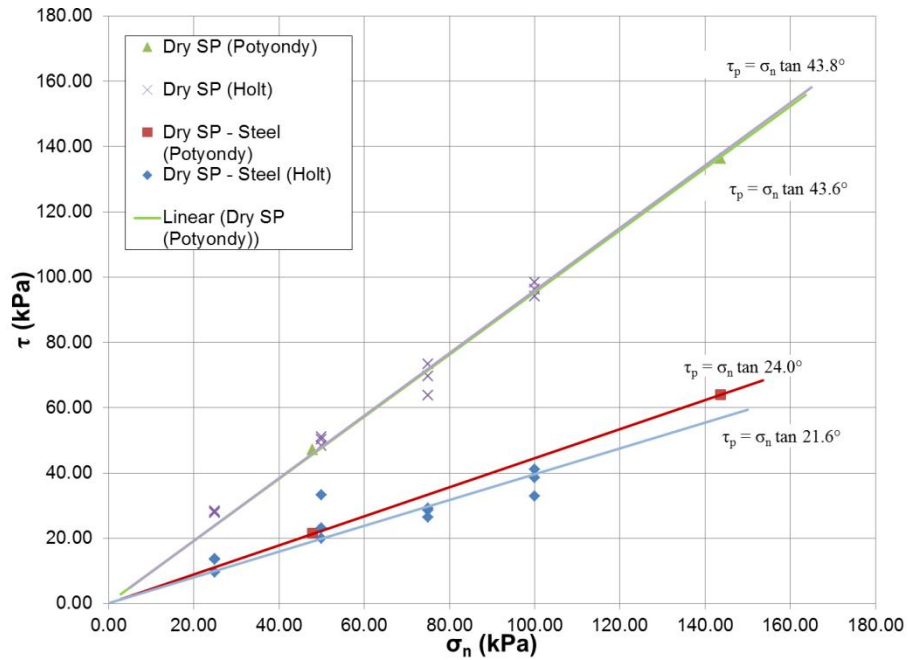


**Figure 5-50** Comparison of shear strength envelope results for pure sand samples and sand-steel samples between the author and (Potyondy, 1961)

Though not critical to the test results, it was also beneficial to take note of the vertical versus horizontal displacement plots (which can be seen in APPENDIX B). **Table 5-2** shows the most extreme results of the vertical displacements for each shear interface scenario. It should be noted that the extreme low result for the grout-steel interface was a flag in the data caused by a misplacement of the vertical displacement transducer on the edge of the measurement point on the load hanger. Otherwise, the most significant vertical displacements were seen in the pure Brighton sand tests. This was believed to be because of the freedom of movement of the soil particles relative to the shear plane allowing for dilation as the soil was sheared. This was a common result for dense poorly graded sands. Other results had relatively little vertical displacement. This was believed to be because the monolithic materials created a discrete failure plane where the soil does not experience as much dilation since the path of least resistance is moving across the material and not around grains of soil. For the testing of the monolithic samples with one another, though theoretically no displacement should occur, in practice, small dust particles which may be ground off the limestone or grout samples, as well as small asperities, could account for the small vertical displacements which occurred.

**Table 5-2** Maximum and minimum vertical displacements relative to starting position

Interface	Maximum Displacement (mm)	Minimum Displacement (mm)
Brighton sand	0.742	-0.129
Brighton sand – Grout	0.177	-0.105
Brighton sand – Steel	0.027	-0.092
Limestone - Steel	0.109	-0.041
Limestone – Grout	0.029	-0.064
Grout – Steel	0.075	-0.905
Concrete - Grout	0.127	-0.022

Coburg limestone samples provided unique complexities for testing on a conventional soil direct shear machine. The tests did not behave in the conventional peak and residual smooth curve manner of the soil samples but rather, there was a break where the shear plane mobilized instantaneously. This resulted in sharp changes in the relation between shear stress and displacement. As a result calculating peak and residual shear strength, as with the sand soil interfaces, was not possible. The solution was to take the average of the post failure shear stress values to create a singular shear strength data point for each shear stress versus horizontal displacement curve. The results (**Table 5-1**) demonstrated that surface condition and relative material properties can play a significant role in the shear strength of the materials. This was seen in the differences between the limestone-steel test results and the limestone-grout test results. In these tests the limestone-grout interface had higher shear strength than the limestone-steel interface. At lower normal stresses the difference was minimal being a difference of only 2.7°; however, as the normal stress increased to 425-500kPa, the difference increased to 6.2°. This change in normal stress also made both friction angles decrease where the limestone-grout friction angle decreased by 1.2° and the limestone-steel friction angle decreased by 4.7°.

The shear stiffnesses for all the tests were rather erratic due to the variation in the shear stress versus displacement curves. As such, averages at each normal stress level were taken. This demonstrated that in general, at the lower normal stress, there was an overall upward trend in the shear stiffnesses. At the higher normal stress level of 425-500 kPa the shear stiffnesses were greater than at the lower level but had no specific trend and relatively little variation.

Ultimately, these test results have provided a database of comprehensive and reliable values for the shear strength of diverse interface scenarios common to support and reinforcement systems in geotechnical engineering. With these values determined, future research can continue to build and refine the data on these shear strength parameters. Determining these shear strength parameters through laboratory tests was the first step in this research. The second objective (See

Chapter 1) was to assess how these shear strength parameters (once known) would influence numerical simulations in software commonly used in the field of geotechnical engineering.

## **6 Numerical Analysis Results and Discussion**

## 6.1 Introduction

The field of Geotechnical Engineering relies on a variety of tools during design, construction and operation and maintenance for predicting the behaviour of tunnels and surface excavations. One of these tools is computer based numerical simulation software. This software has evolved significantly over the years becoming more powerful, and providing more accurate predictions of overall ground behaviour with regards to geotechnical works. These numerical models have an inherent limitation in that accurate material parameters must be provided as input in order to yield accurate results. Currently, with regards to interaction associated with ground support, there is a limited amount of laboratory data available for input into these models (Oke et al., 2012a).

The two objectives of this research were intended to fill this knowledge gap. In Chapter 5, the first objective of this research was accomplished by conducting laboratory tests to determine the shear strength and stiffness parameters for diverse interface conditions related to ground support. This chapter now assesses if the numerical simulations can accurately handle or predict behaviour using the results from the laboratory tests in the previous chapter. This assessment was accomplished by creating a 2D numerical model of a direct shear test and then comparing these results the numerical simulations with the laboratory results.

## 6.2 Software Selection

There were a variety of different software available to chose in terms of the numerical analysis tools to be used as part of this research. Selected software is based on the use finite elements , for example Plaxis, Phase 2, FEMDEM (Plaxis, 2016; Rocscience Inc., 2014; Virtual Geoscience Simulation Tools, 2016). The Finite Difference Method is used in numerical analysis packages such as FLAC 2D and 3D (Itasca Consulting Group Inc., 2009). Finite element methods work by an iterative approach where mathematical relations between points are solved to within a certain level of convergence (Rocscience Inc., 2014). The Finite Difference Method uses differential equations to solve the problem from physical relations (Vlachopoulos, 2009).

It is also important to determine whether continuum or discontinuum models are best suited to model the problem. Generally, Continuum models such as Phase 2 or FLAC (Itasca Consulting Group Inc., 2009; Rocscience Inc., 2014), are the most common and are used for intact rocks, decomposed rocks, or soils where the material can be assumed to be generally homogeneous in nature. Discontinuum models are less common but apply for fractured rocks where homogeneous behaviour cannot be assumed (Oke et al., 2014).

When choosing between 3-dimensional (3D) software and 2-dimensional (2D) software for this research, there were several considerations:

- a. Suitability to simulate a direct shear test that would be comparable to the laboratory tests;
- b. Simplicity so focus could remain on testing the shear behaviour at the interface;
- c. Availability within RMC and the geotechnical community; and,
- d. The software's ability to accept a Mohr-Coulomb shear strength envelope.

In order to duplicate laboratory tests, it was necessary to create a numerical simulation of a direct shear test. This has been done effectively in 2D software by other researchers (Cui, 2012). The simplicity of a 2D model also reduces the overall complexity and run time for the simulations.

With this in mind, the two suites of 2D software for stress analysis available at RMC were GEO-SLOPE's SIGMA/W and Rocscience's Phase 2. These have been used commonly at RMC, in other academic institutions, and by different geotechnical engineering companies as these are industry-standard software packages. After considering the specifications it was decided to use the Phase 2 software because:

- a. It was able to model a direct shear machine;
- b. it was simple to use and input the shear behaviour of the interfaces;
- c. it was able to accept both the peak and residual Mohr-Coulomb shear strength inputs; and,
- d. it has been used for analysis of rock masses and tunnelling frequently within the field (Basarir, 2006; Cai, 2008; Oke et al., 2012a; Oke et al., 2012b).

Another consideration was the suitability of the plain-strain method used by the 2-D model. It was concluded that this is not a concern because the direct shearbox in the laboratory, just as in the numerical simulation, should not have had any stresses or deformations developing in the direction of the Z axis as shearing in the direction of the X axis occurred.

### 6.3 Phase 2 Software

Phase 2 is a 2D geotechnical modelling software developed by Rocscience. It uses the finite element method for predicting stress, strain, and displacement of the models. It has the ability to model various materials. The specific version used for this investigation was V8.0.

These materials can be modelled using various elastic property models (Rocscience Inc., 2014):

- a. Isotropic;
- b. Transverse Isotropic; and,
- c. Duncan-Chang Hyperbolic.

For the purposes of this research the Isotropic model was used alone as it was assumed the material properties were not directionally dependent.

The strength properties in Phase 2 can be modelled as elastic or plastic using diverse constitutive models (Rocscience Inc., 2014):

- a. Mohr-Coulomb;
- b. Hoek-Brown;
- c. Drucker-Prager;
- d. Generalized Hoek-Brown ;
- e. Cam-Clay;
- f. Modified Cam-Clay; and,
- g. Discrete Function.

For the purposes of this research only the Mohr-Coulomb and Hoek-Brown constitutive models were used. Materials can also be given hydraulic properties; however, this was not of concern for this research as samples were kept with a water contents no greater than 0.2%.

Within Phase 2, interfaces are called boundaries. There are seven types of boundaries (Rocscience Inc., 2014) but only three of them applied to this research. External boundaries form the closed outline of the model and its mesh. They do not have any set material properties (Rocscience Inc., 2014). Material boundaries

are internal boundaries which delimit a block of material. These also have no input parameters (Rocscience Inc., 2014). The third boundary type is a joint boundary which models a discontinuity within a material. The joint boundaries can be allocated properties of stiffness and strength input and even allow for residual strengths and other properties to be input for different types of joints. The stiffnesses are required inputs for the joint, however, the strength can be input using one of four constitutive models with optional values for residual strength (Rocscience Inc., 2014):

- a. None;
- b. Mohr-Coulomb;
- c. Barton-Bandis; and,
- d. Geosynthetic-Hyperbolic.

For the purpose of this research only the Mohr-Coulomb constitutive model was used for modelling of joints since all laboratory tests used this model. An example of how the rheological model of this joint is arranged can be seen in **Figure 6-1**. The ability to input these values was critical to the conduct of this research.

It should also be noted that other sources of stress (i.e. hydraulic forces) can be used but were not investigated specifically in this research.

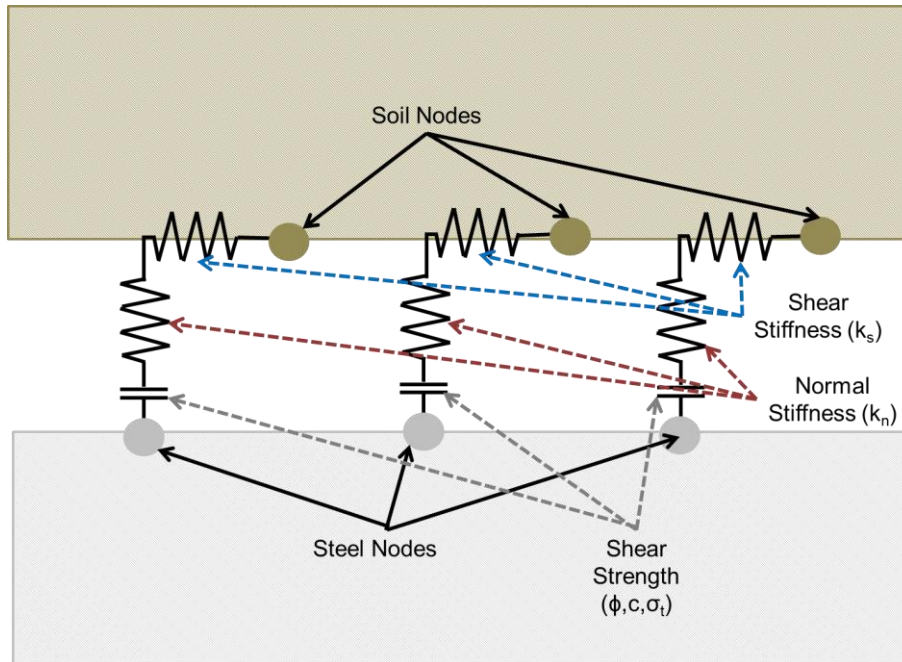


**Figure 6-1** Rheological model of joint boundary using a Mohr-Coulomb constitutive model based off description by Rocscience, 2014 ( $k_s$  = shear stiffness,  $k_n$  = normal stiffness  $\phi$  = friction angle,  $c$  = cohesion factor, and  $\sigma_t$  = tensile strength)

## 6.4 Direct Shearbox Simulation Preparation and Calibration of Numerical Model

The Phase 2 software was set-up to solve the modelled shearbox as a plain strain problem using Gaussian elimination allowing a maximum of 5000 iterations seeking a tolerance of 0.001. The simulated direct shearbox was originally created in three parts to be as true to the real shearbox as possible. These parts were the bottom half, the top half, and the top platen as per **Figure 6-3**. The box was made of brass so the material was given the same properties as brass listed in **Table 6-1** below.

### 6.4.1 Initial Model Design

It was then necessary to set boundary conditions to reproduce the constant rate of strain direct shearbox. The top half of the shearbox was held stationary in the X direction. Relative to this the lower half was displaced 7mm over 22 displacement steps (0.33mm/step) this was done by assigning the set displacements to the left and right exterior boundary of the lower half of the box. The bottom

boundary was held stationary in the Y direction. Normal loading was done by applying a uniform normal stress to the top of the direct shearbox (**Figure 6-2**).

With the shearbox boundary conditions set, the mesh was discretized. The mesh used was a graded 3 node triangle mesh. The number of exterior nodes was set to 500 nodes in the mesh setup dialogue box. After calibration of the models, as described in Section 6.4.2, the model had a total of 9292 nodes and 17993 elements.

This design allowed for the shear stress at the joint between the two halves of the sample to be determined at each displacement step to generate a shear stress versus displacement curve which could be compared to the laboratory results for the different arrangements of direct shear tests. Determining the shear stress could not be done directly as querying the joint produced a series of shear stress values which changed at each node. Due to this, it was necessary to integrate the shear stresses over the length of the joint in order to determine the shear force transmitted across the joint. This calculation was the same operation as averaging the shear stress along the length of the joint making it simple to export the queried joint data to MS EXCEL and calculate the average shear stress along the joint for each displacement step.

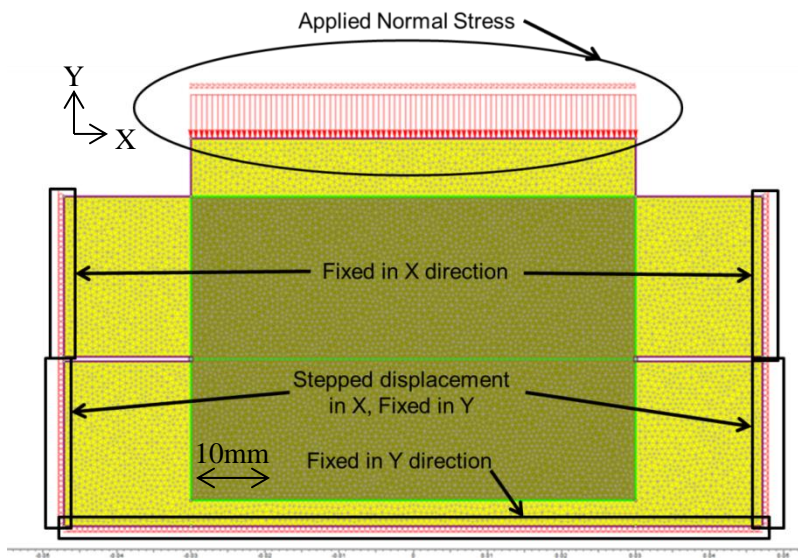


**Figure 6-2** Boundary conditions used in model of direct shearbox

#### 6.4.2 Model Calibration

With the model built, and a means to retrieve the desired data from the joint between the sample halves, it was necessary to begin calibration of the model. This was done by graphing the model results with respect to the direct shear test results at 25kPa normal stress during test 0007-01 (the first test of the Brighton

beach sand). Ideally, if the model and input parameters are all correct, the resulting shear stress at each displacement step should follow the shear stress versus displacement curve of the laboratory test. This was not the case, however. Initial numerically simulated test results had a different shape than the results from the laboratory results as well as a peak which was approximately 10 kPa lower than those obtained in the laboratory. This necessitated a parametric study to see how varying different parameters influenced the result.

It was decided to begin by using different means to model the boundary between the sand sample and the shearbox material. The two choices were to model the boundary as a joint, where inputs for strength and stiffness would be required, or as a material boundary where no user input was needed. Using a joint boundary was difficult and also not the most reliable as it required shear strength, shear stiffness, and horizontal stiffness inputs for the interface between the soil and the brass material of the shearbox. This information was not part of the laboratory testing regime. It seemed, based on the results in **Figure 6-5**, that the use of a material boundary, where no user input was required, provided better results than using a joint boundary. This was beneficial as it removed the need to input unverified parameters into the simulation. This assessment did not improve the difference in the peak shear strength drastically, however.

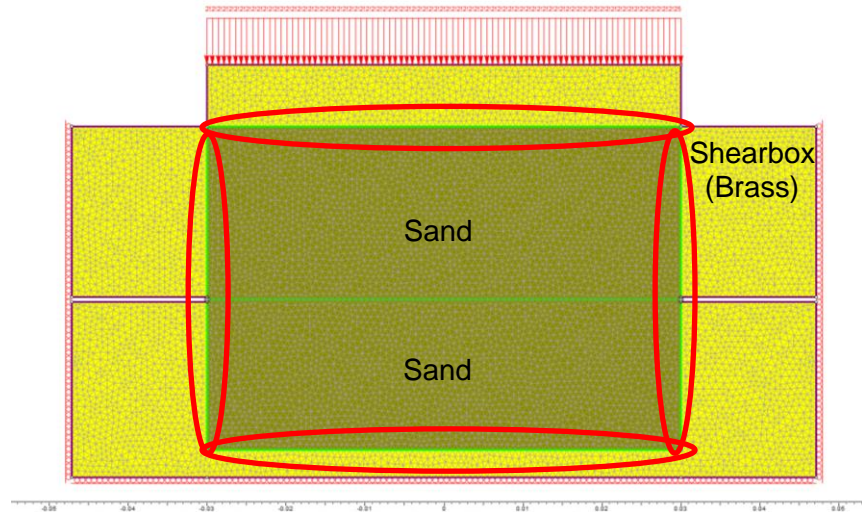


**Figure 6-3** First assessment of the direct shear test model using Brighton beach sand at 25 kPa normal stress and boundaries (circled in red) between the box and sand set as material boundaries

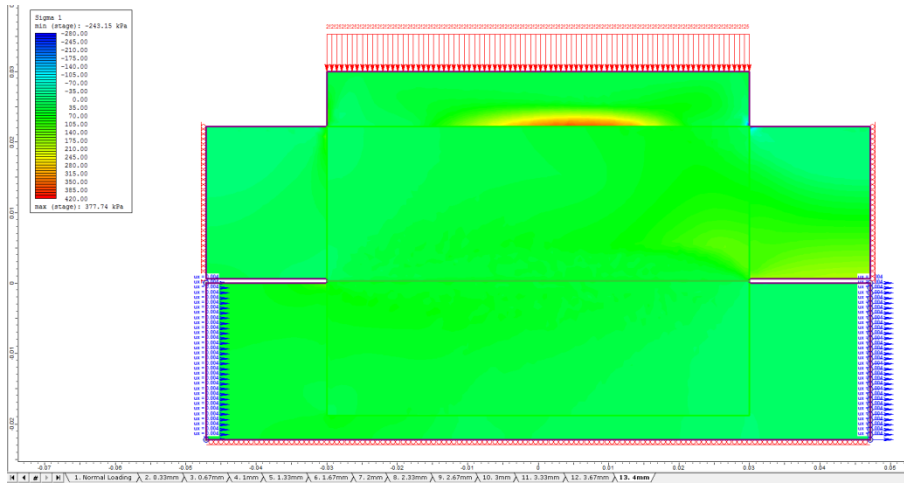


**Figure 6-4** Interpret results for  $\sigma_1$  principle stress within the model from **Figure 6-3** at 4mm displacement

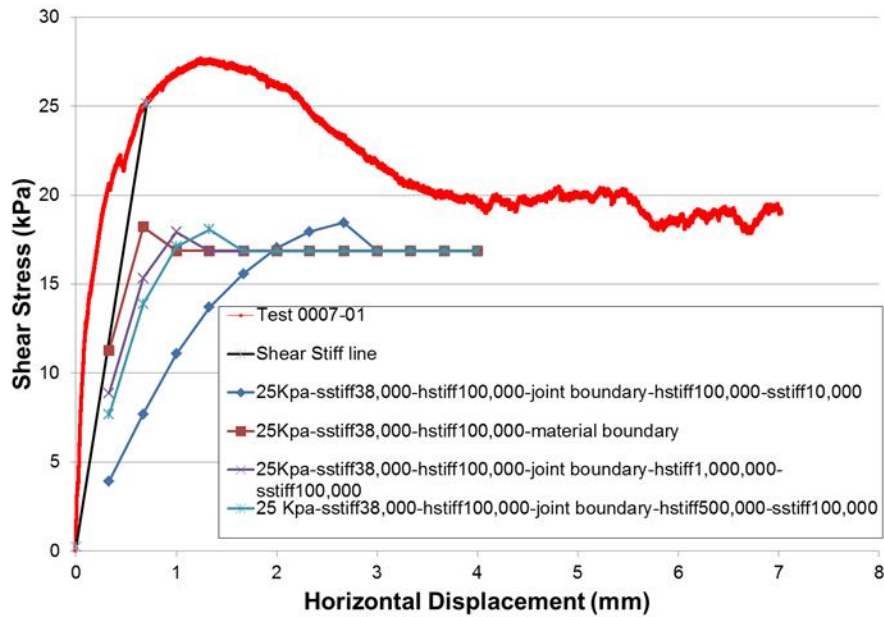


**Figure 6-5** 25 kPa laboratory test results (0007-01) compared with model average shear stress versus displacement varying shearbox and sample boundary type between material and joint types

The next parameter assessed was the size and design of the box. It was decided to change the box's design so instead of three pieces, the top shearbox half

and loading platen were combined into one continuous object which made it two pieces in total. This was done without changing the width or height of the shearbox walls. This arrangement was similarly used by Cui in 2012. Such an arrangement brought the test results closer to those of the laboratory tests; however, it was now over predicting the shear strength by approximately 5 kPa. In order to validate their influence, the height of the shearbox and the width of the shearbox walls were also varied and the results plotted. As seen in **Figure 6-9**, changing box height had no influence but changing the box width pushed the peak even higher and made the higher peak extend over the 1mm and 1.33mm displacement steps. It was decided to maintain the same width and height as the original dimensions but to model the box as two pieces rather than three.

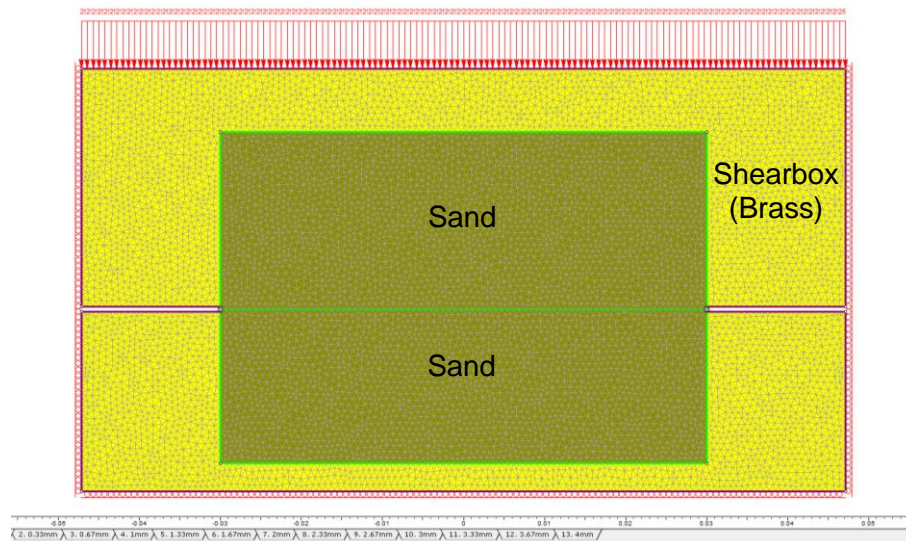


**Figure 6-6** Two part shearbox with same dimensions (wall thickness 17mm)

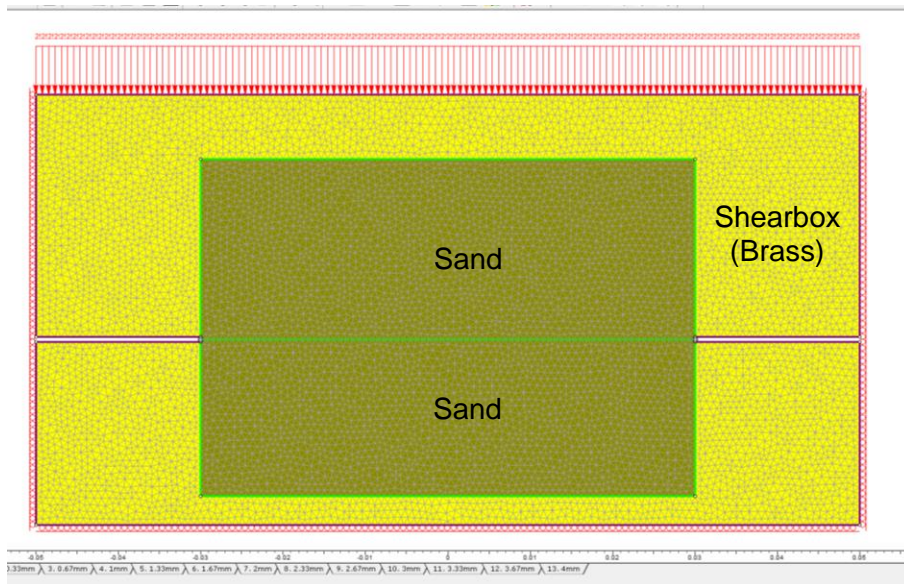


**Figure 6-7** Two part shearbox with thicker walls (20mm thick)

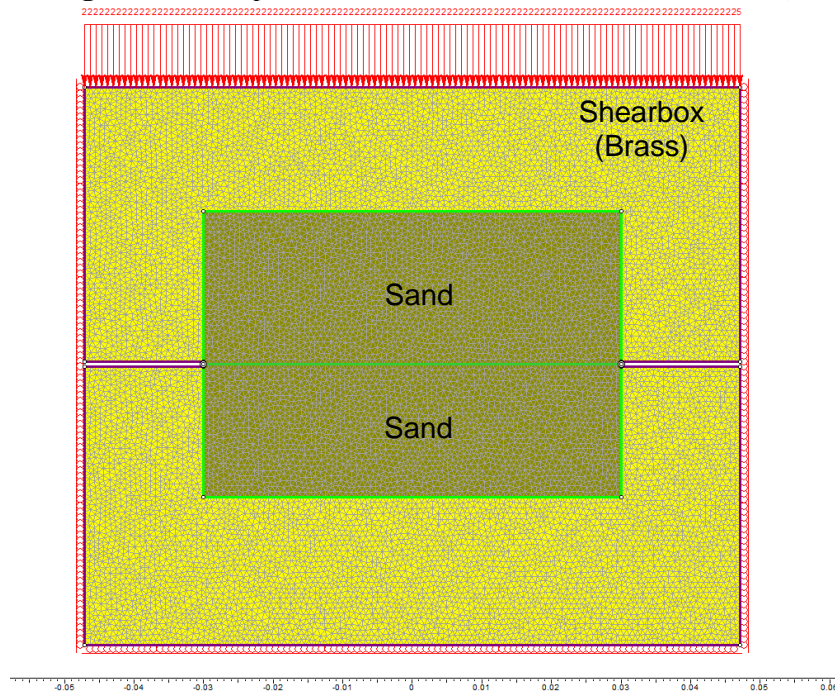


**Figure 6-8** Two part shearbox thicker top and bottom (walls 17mm thick) (top and bottom 20mm thick)

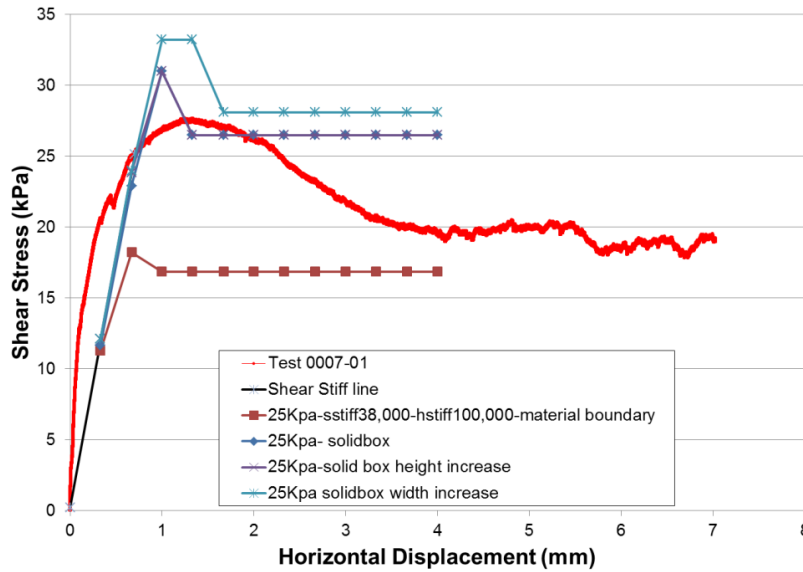


**Figure 6-9** Laboratory test of sand at 25 KPa normal stress (0007-01) compared to model results of the two part shearbox, and changes to shearbox dimensions

The last parameter which had to be assessed for its influence was the normal stiffness at the joint between the two sample halves. For these tests, the joint had been given the peak and residual shear strength and stiffness parameters determined from the laboratory tests. However, the normal stiffness of the material was not a parameter which could be determined as it would require taking an undisturbed sample from within the direct shear test sample which was not possible. As such, the normal stiffness was calibrated at the 25 kPa normal stress level to carefully match the curve from the laboratory results. Varying the stiffness between  $1 \times 10^5$  kPa/m (the default value) and  $3 \times 10^6$  kPa/m revealed that the higher normal stiffness values of  $2 \times 10^6$  kPa/m and  $3 \times 10^6$  kPa/m made the numerical simulation results match the laboratory result more accurately, as seen in **Figure 6-11**. It was also noted that none of the above variations had any serious impact on the residual part of the numerical results matching with those from the laboratory. Potentially this was due to changes in the effective stiffness as the shear failure was beginning to mobilize. Such changes are not accounted for in any of the joint inputs.

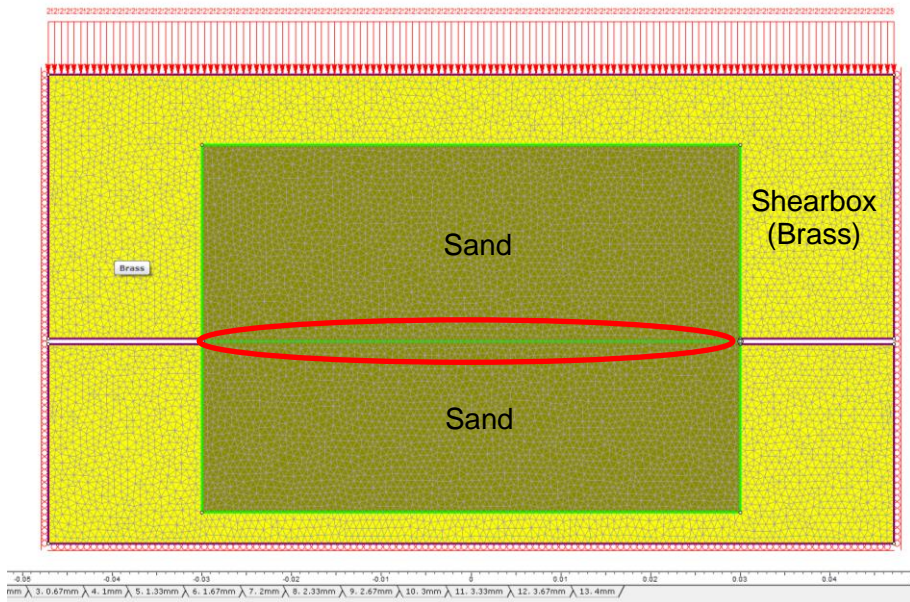


**Figure 6-10** Model for shear test normal stiffness at the joint (circled in red) set to  $3 \times 10^6$  kPa/m

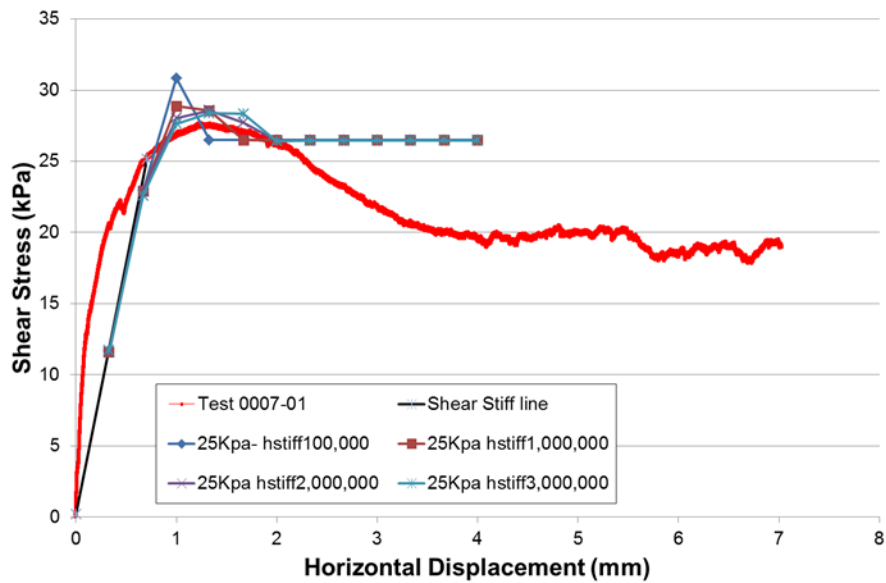


**Figure 6-11** Laboratory test at 25 kPa normal stress (0007-01) compared with model results at different normal stiffnesses for the joint between the two shearbox halves

### 6.4.3 Final Model Design and Run

With the above calibration completed, the models could now be built and run for the various interface scenarios. The final model boundaries were set up as described in **Figure 6-12** below. The only boundary used which required input parameters was the joint boundary between the two halves of the shearbox sample.

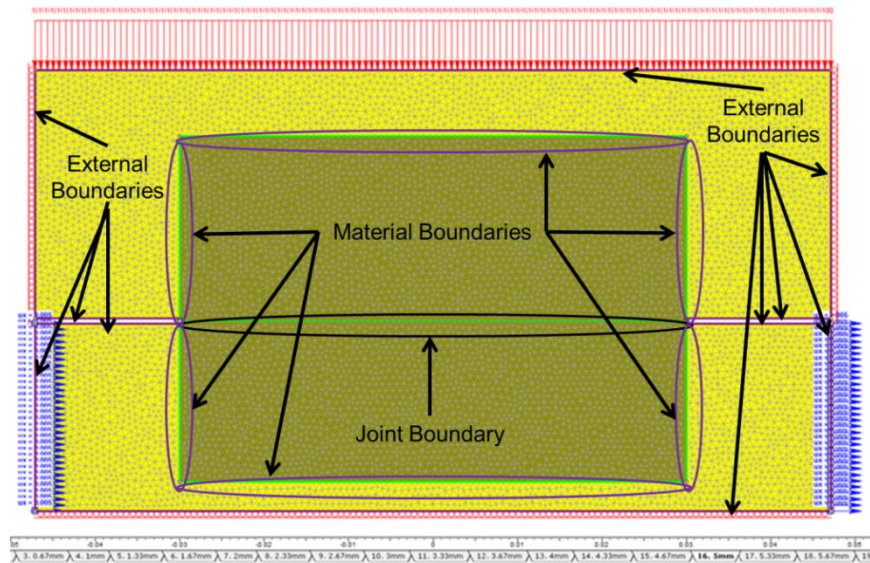


**Figure 6-12** Diagram of boundary types in model

The material properties also had to be determined and input for the model to function. The material parameters used are listed in **Table 6-1** below for all the materials. It should be noted the properties for the joint between the halves of the shearbox varied from test to test except for the normal stiffness which was set at  $3 \times 10^6$  kPa/m as determined during the calibration at 25 kPa. All other model properties were kept as discussed in Sections 6.4.1 and 6.4.2.

**Table 6-1** Material strength and elastic parameters <sup>1</sup>(MatWeb, 2016)  
<sup>2</sup>(Geotechdata, 2013) <sup>3</sup>(King Packaged Materials Company, 2016) <sup>4</sup>(Ghazvinian et al., 2015) <sup>5</sup>(EngineeringToolBox, 2016)

Material [Constitutive Model]	Parameter	Value
Brass (Shearbox) [Elastic Isotropic, Mohr-Coulomb]	Tensile Strength (kPa) <sup>1</sup>	25.5 x 10 <sup>5</sup>
	Friction Angle (°)	90
	Cohesion (kPa) <sup>1</sup>	10.5
	E (kPa) <sup>1</sup>	1.1 x 10 <sup>8</sup>
	$\nu$ <sup>1</sup>	0.3
Brighton Beach Sand [Plastic-isotropic, Mohr-Coulomb]	Tensile Strength (kPa)	0
	Peak [Residual] Friction Angle (°)	43.8 [34]
	Cohesion (kPa)	0
	E (kPa) <sup>2</sup>	6.5 x 10 <sup>4</sup>
	$\nu$ <sup>2</sup>	0.3
Grout [Elastic – Isotropic, Hoek-Brown]	UCS (kPa)	4.8 x 10 <sup>4</sup>
	E (kPa) <sup>3</sup>	2.45 x 10 <sup>7</sup>
	$\nu$ <sup>3</sup>	0.14
Steel [Elastic-Isotropic, Hoek Brown]	UCS (kPa) <sup>5</sup>	1.86 x 10 <sup>5</sup>
	E (kPa) <sup>5</sup>	2 x 10 <sup>8</sup>
	$\nu$ <sup>5</sup>	0.3
Coburg Limestone [Elastic-Isotropic, Hoek-Brown]	UCS (kPa) <sup>4</sup>	7.246 x 10 <sup>4</sup>
	E (kPa) <sup>4</sup>	3.7 x 10 <sup>7</sup>
	$\nu$ <sup>4</sup>	0.18
Concrete [Elastic-Isotropic, Hoek-Brown]	UCS (kPa)	4.68 x 10 <sup>4</sup>
	E (kPa) <sup>5</sup>	3 x 10 <sup>7</sup>
	$\nu$ <sup>5</sup>	0.18

This calibration at 25 kPa for the sand sample should allow for the results from the numerical simulation to match the shear stress versus displacement curves from the laboratory results.

## 6.5 Brighton Beach Sand

The numerical simulations for the Brighton sand were created using the material properties in **Table 6-1**. The joint was given properties as per the laboratory results from Chapter 5. All properties not listed were left in their default values. Below are a sample of results for the 25 kPa to 100 kPa and 425 kPa to 500 kPa range in **Figure 6-15** and **Figure 6-16** respectively.

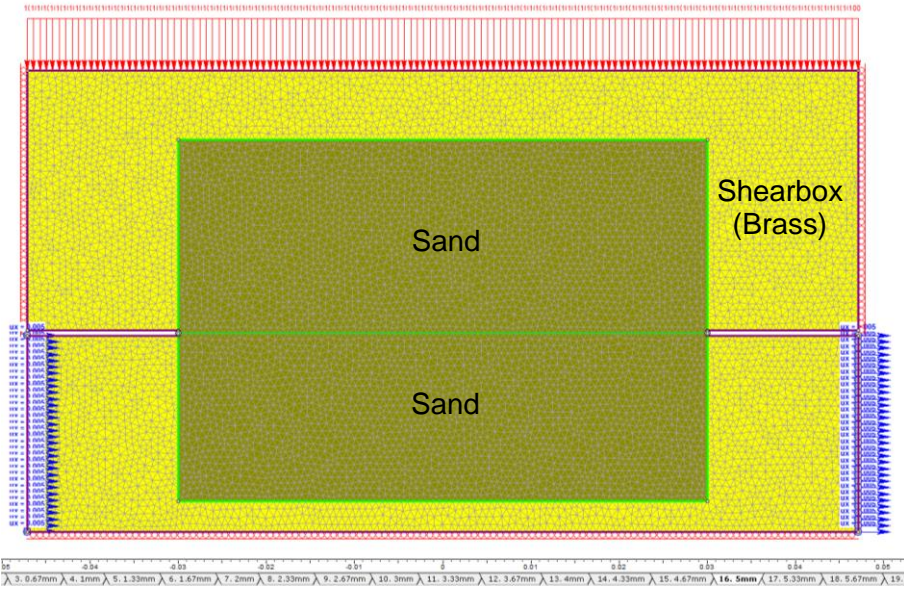


**Figure 6-13** Model of Brighton sand test at 100 kPa normal stress and 5mm displacement

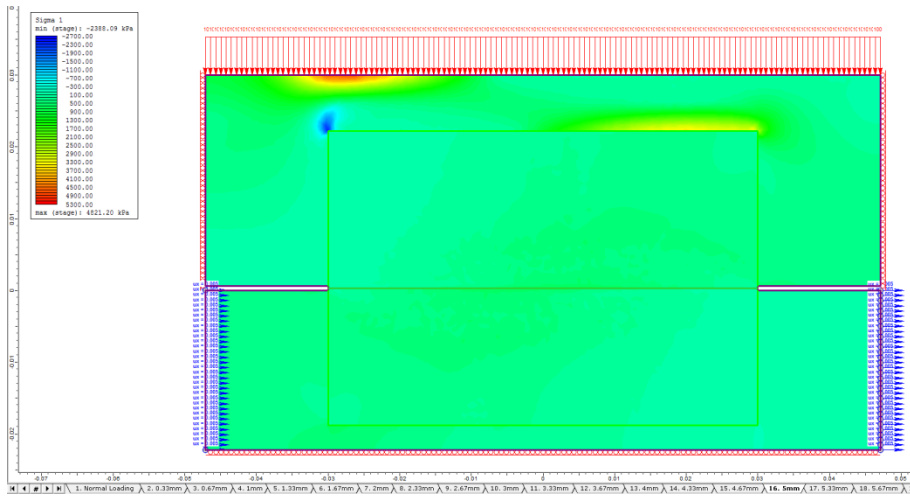


**Figure 6-14** Contoured results for  $\sigma_1$  principle stress of model from **Figure 6-13** at 5mm displacement

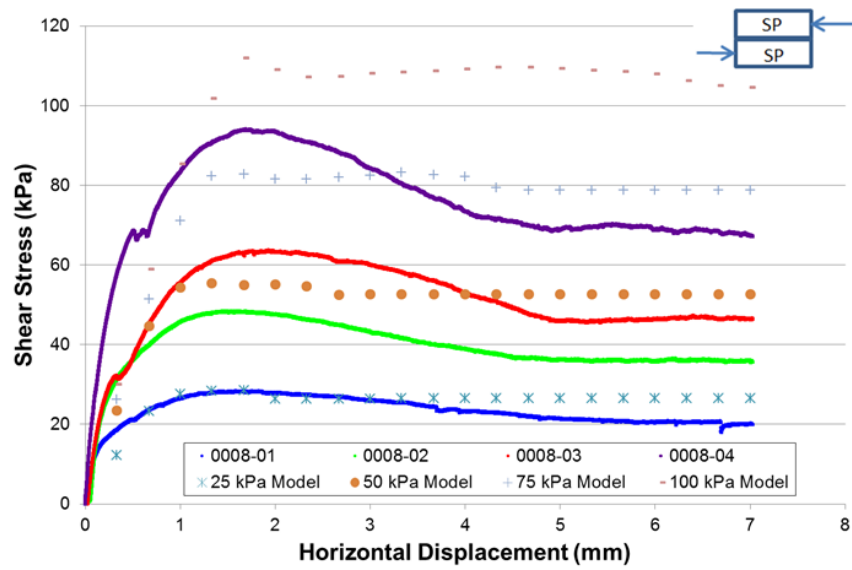


Figure 6-15 Select laboratory results for direct shear Brighton sand at 25 kPa to 100 kPa compared to model results

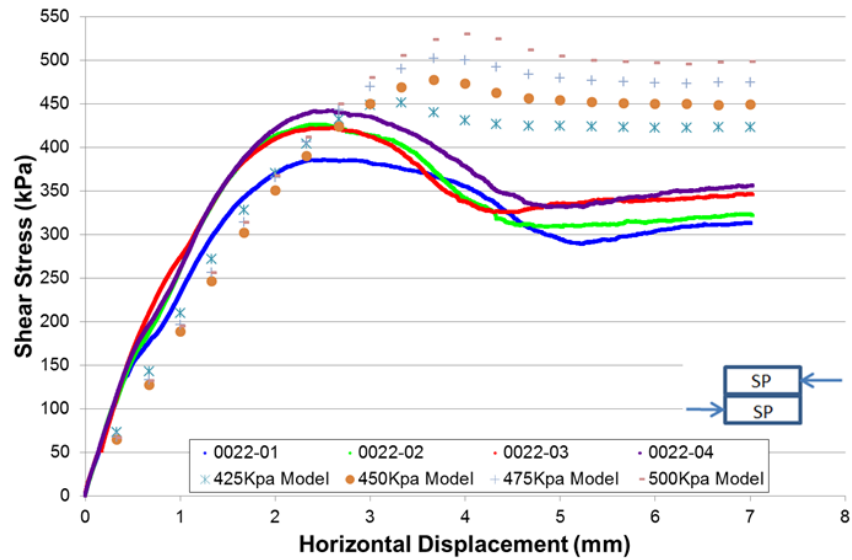
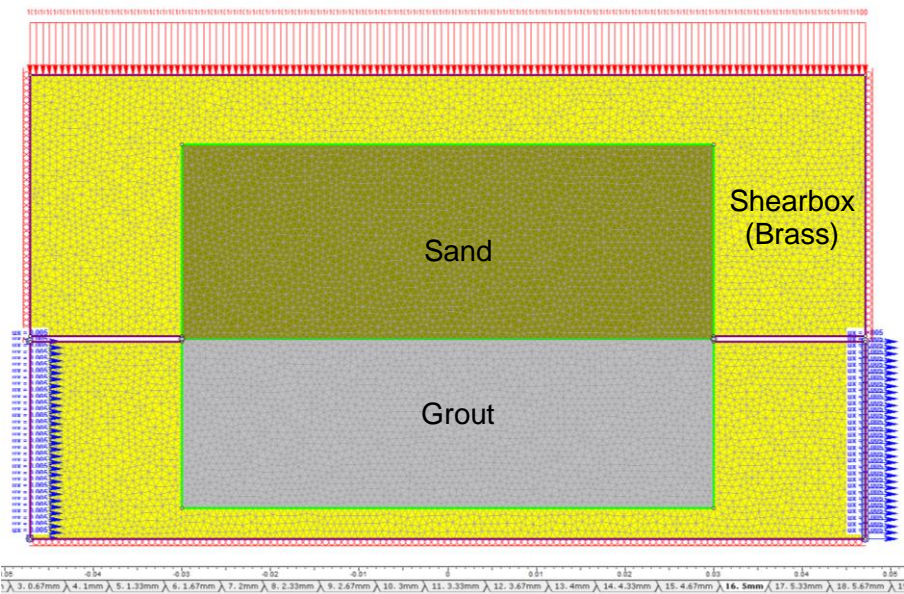


Figure 6-16 Select laboratory results for direct shear of Brighton sand 425 kPa to 500 kPa compared to model results

The results did not meet with expectations. Though the calibration at 25 kPa yielded good agreement at that normal stress level, the normal stress of applied to the simulation increased so did the discrepancy between the laboratory values and the numerical simulation results. This led to an overestimation of the peak shear strength by 20 kPa and the 100 kPa normal stress level, and 75 kPa at the 500 kPa normal stress level. It was also noted that the peak failure occurred at greater displacements than the laboratory results as the normal stress increased.

## 6.6 Brighton Beach Sand and Grout

The numerical simulations for the Brighton sand and grout were created using the material properties in **Table 6-1**. The joint was given properties as per the laboratory results from Chapter 5. All properties not listed were left in their default values. Below are selected results for the 25 kPa to 100 kPa and 425 kPa to 500 kPa range in **Figure 6-19** and **Figure 6-20** respectively.



**Figure 6-17** Model of Brighton sand and grout test at 100 kPa normal stress and 5mm displacement

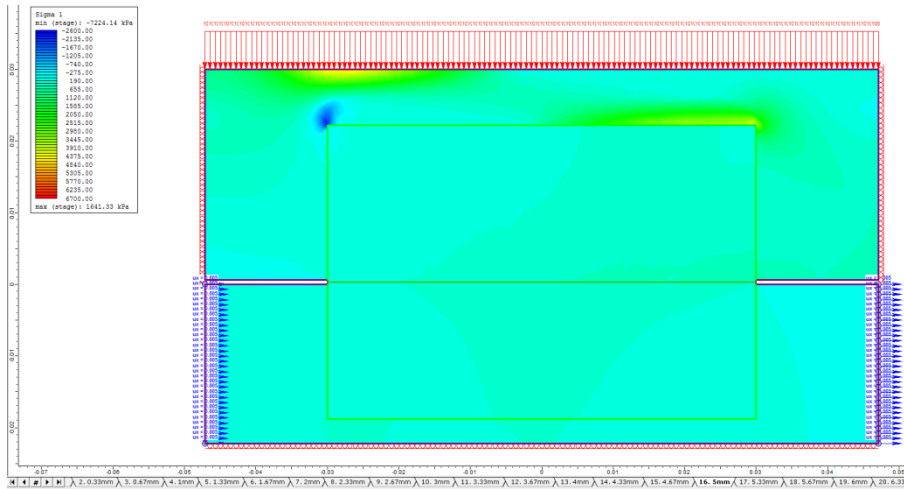


**Figure 6-18** Contoured results for  $\sigma_1$  principle stress of model from **Figure 6-17** at 5mm displacement

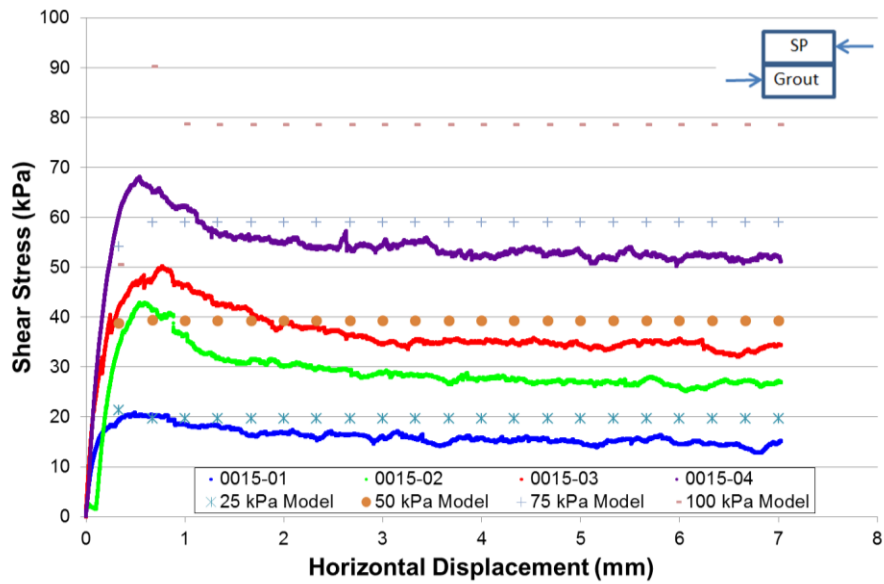


**Figure 6-19** Select laboratory results for direct shear Brighton sand and grout at 25 kPa to 100 kPa compared to model results

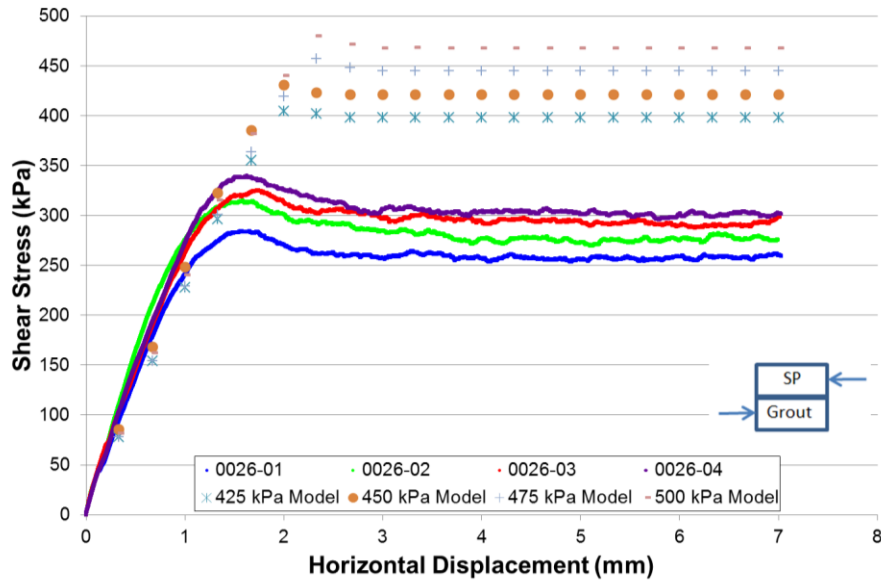


**Figure 6-20** Select laboratory results for direct shear Brighton sand and grout at 425 kPa to 500 kPa compared to model results

The model and laboratory results for the Brighton sand and grout interface agreed at lower normal stresses but diverged significantly as the normal stresses increased. The difference in peak shear strength approached 150 kPa at 500kPa normal stress. This means the models drastically over predicted the strength of the interface.

### 6.7 Brighton Beach Sand and Steel

The numerical simulations for the Brighton sand and steel were created using the material properties in **Table 6-1**. The joint was given properties as per the laboratory results from Chapter 5. All properties not listed were left at their default values. Below are samples of results for the 25 kPa to 100 kPa and 425 kPa to 500 kPa range in **Figure 6-23** and **Figure 6-24** respectively.

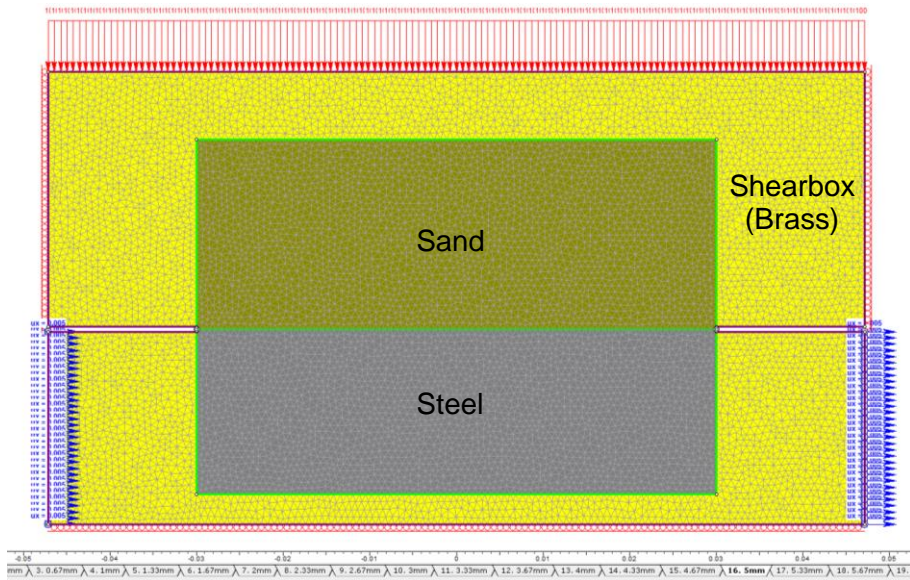


**Figure 6-21** Model of Brighton sand and steel test at 100 kPa normal stress and 5mm displacement

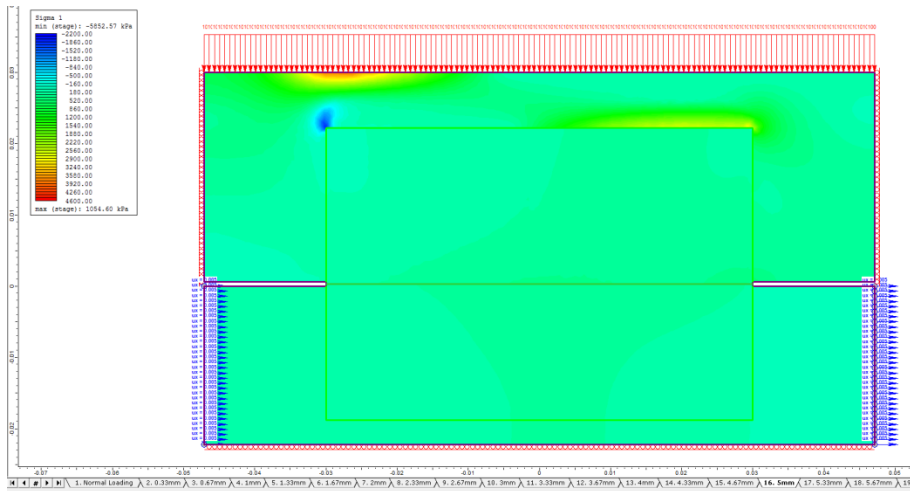


**Figure 6-22** Contoured results for  $\sigma_1$  principle stress of model from **Figure 6-21** at 5mm displacement

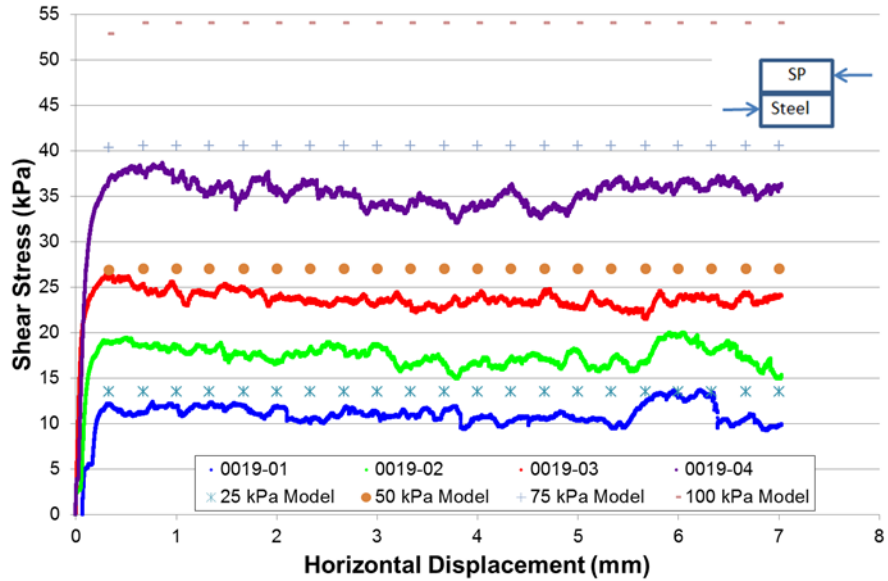


**Figure 6-23** Select laboratory results for direct shear Brighton sand and steel at 25 kPa to 100 kPa compared to model results

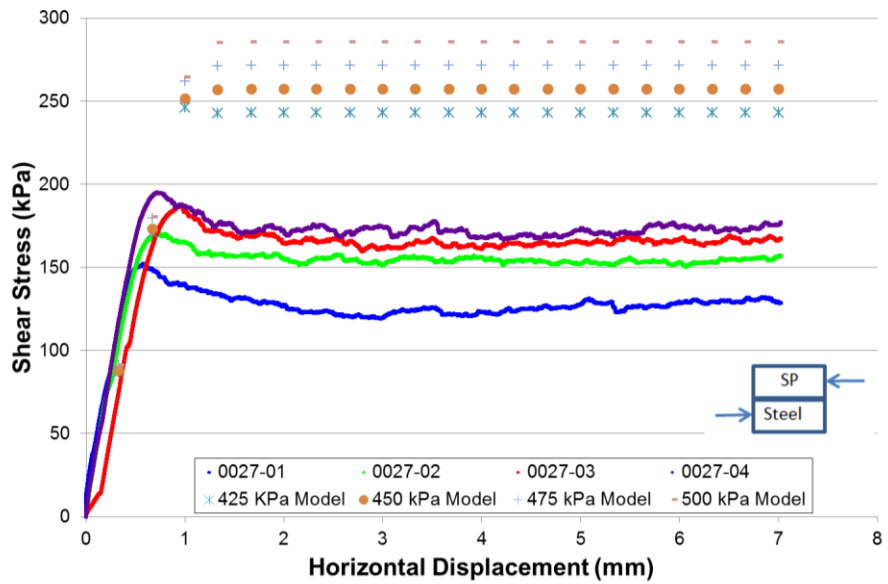


**Figure 6-24** Select laboratory results for direct shear Brighton sand and steel at 425 kPa to 500 kPa compared to model results

The model and laboratory results for the Brighton sand and steel interface had a small difference of 2 kPa at 25 kPa normal stress but diverged drastically as the normal stresses increased. The difference in peak shear strength approached 90kPa at 500kPa normal stress meaning the models drastically over predicted the strength of the interface.

## 6.8 Coburg Limestone and Grout

The numerical simulations for the Coburg limestone and grout were created using the material properties in **Table 6-1**. The joint was given properties as per the laboratory results from Chapter 5. All properties not listed were left in their default values. Below are samples of results for the 25 kPa to 100 kPa and 425 kPa to 500 kPa range in **Figure 6-27** and **Figure 6-28** respectively.

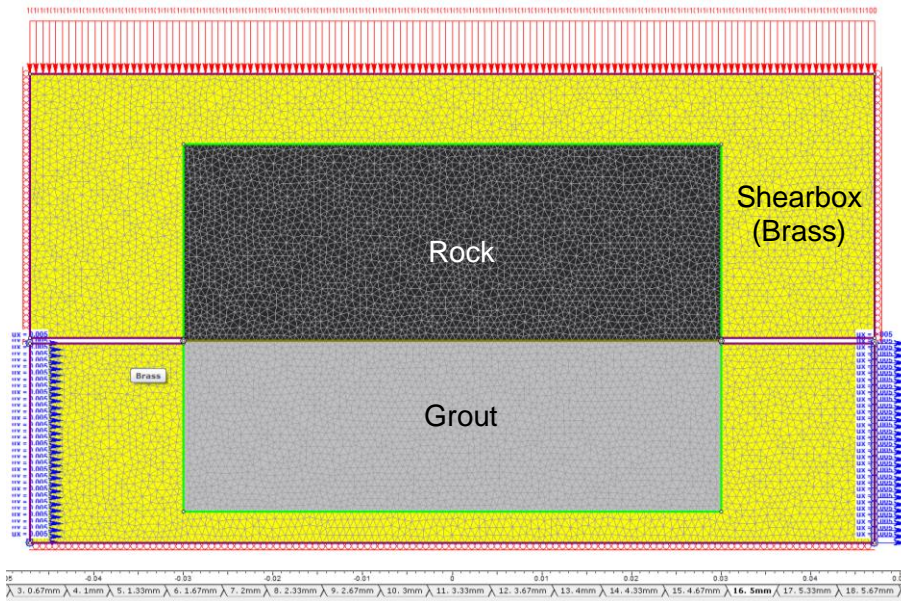


**Figure 6-25** Model of Coburg limestone and grout test at 100 kPa normal stress and 5mm displacement

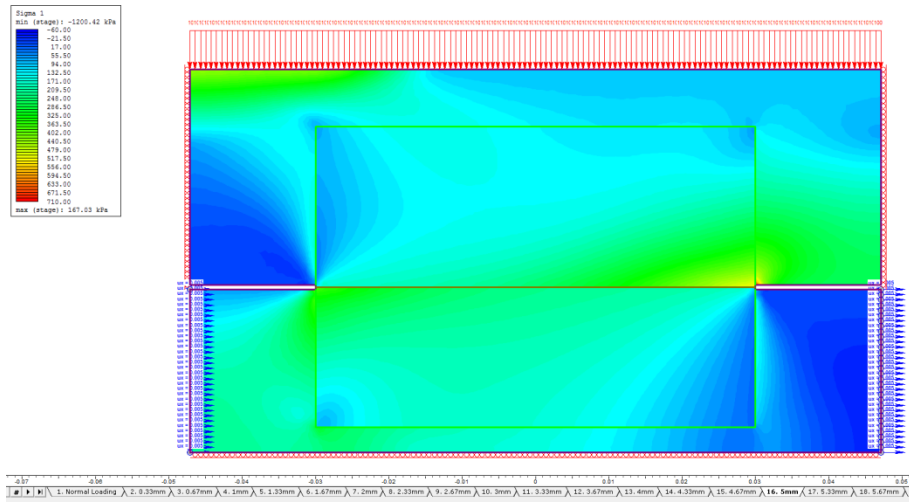


**Figure 6-26** Contoured results for  $\sigma_1$  principle stress of model from **Figure 6-25** at 5mm displacement

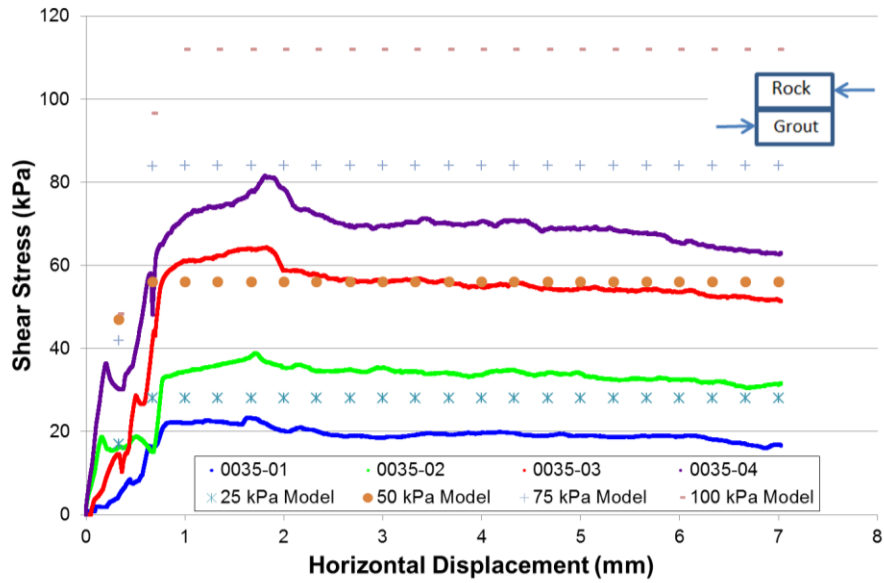


**Figure 6-27** Select laboratory results for direct shear Coburg limestone and grout at 25 kPa to 100 kPa compared to model results

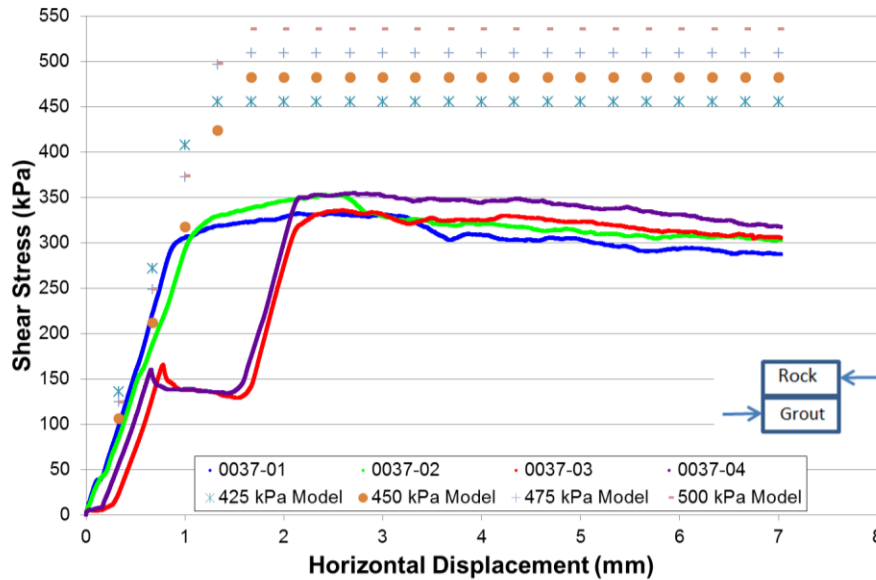


**Figure 6-28** Select laboratory results for direct shear Coburg limestone and grout at 425 kPa to 500 kPa compared to model results

The model and laboratory results for the Coburg limestone and grout interface differed by 10 kPa at 25 kPa normal stresses and diverged drastically as the normal stresses increased. The difference in peak shear strength approached 190 kPa at 500kPa. There was a consistent over estimation of shear strength by the numerical simulation.

## 6.9 Coburg Limestone and Steel

The numerical simulations for the Coburg limestone and steel were created using the material properties in **Table 6-1**. The joint was given properties as per the laboratory results from Chapter 5. All properties not listed were left in their default values. Below are samples of results for the 25 kPa to 100 kPa and 425 kPa to 500 kPa range in **Figure 6-31** and **Figure 6-32** respectively.

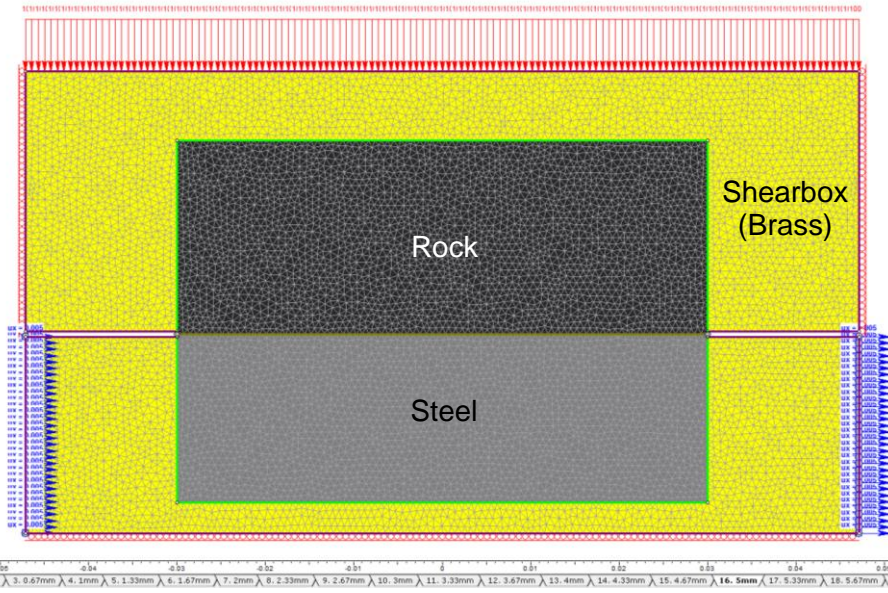


**Figure 6-29** Model of Coburg limestone and steel test at 100 kPa normal stress and 5mm displacement

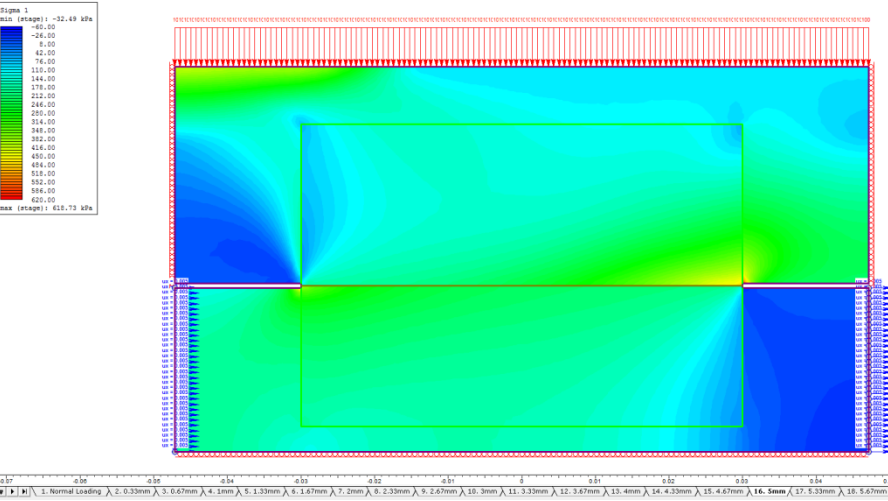


**Figure 6-30** Contoured results for  $\sigma_1$  principle stress of model from **Figure 6-29** at 5mm displacement

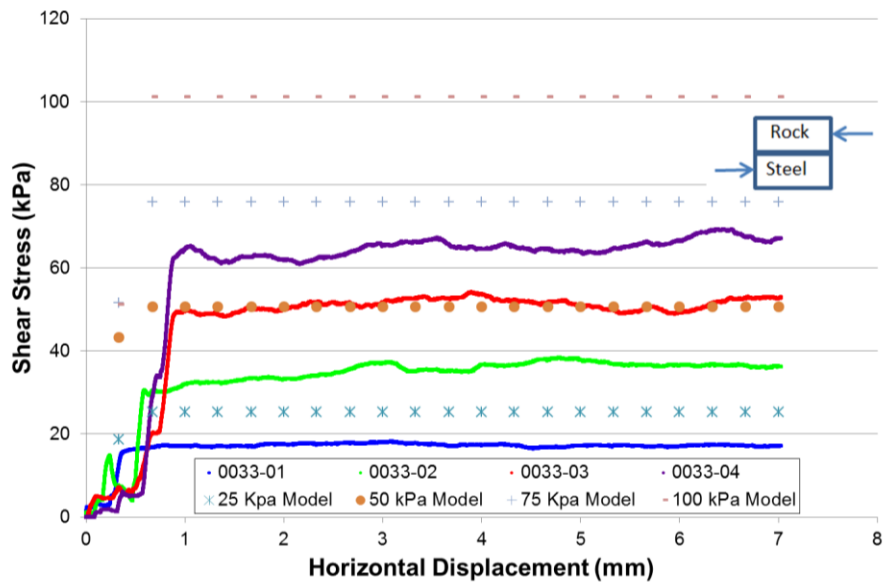


**Figure 6-31** Select laboratory results for direct shear Coburg limestone and steel at 25 kPa to 100 kPa compared to model results

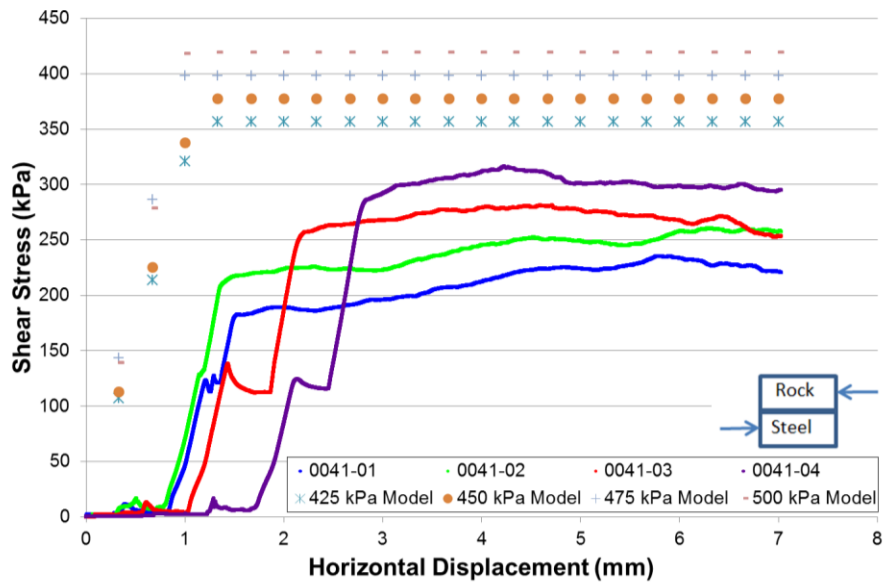


**Figure 6-32** Select laboratory results for direct shear Coburg limestone and steel at 425 kPa to 500 kPa compared to model results

The model and laboratory results for the Coburg limestone and steel interface differed by 10 kPa at 25 kPa normal stress and diverged drastically as the normal stresses increase. The difference in peak shear strength approached 125 kPa at 500kPa. There was a consistent over estimation of shear strength by the numerical simulation.

## 6.10 Grout and Steel

The numerical simulations for the grout and steel were created using the material properties in **Table 6-1**. The joint was given properties as per the laboratory results from Chapter 5. All properties not listed were left in their default values. Below are samples of results for the 25 kPa to 100 kPa and 425 kPa to 500 kPa range in **Figure 6-35** and **Figure 6-36** respectively.

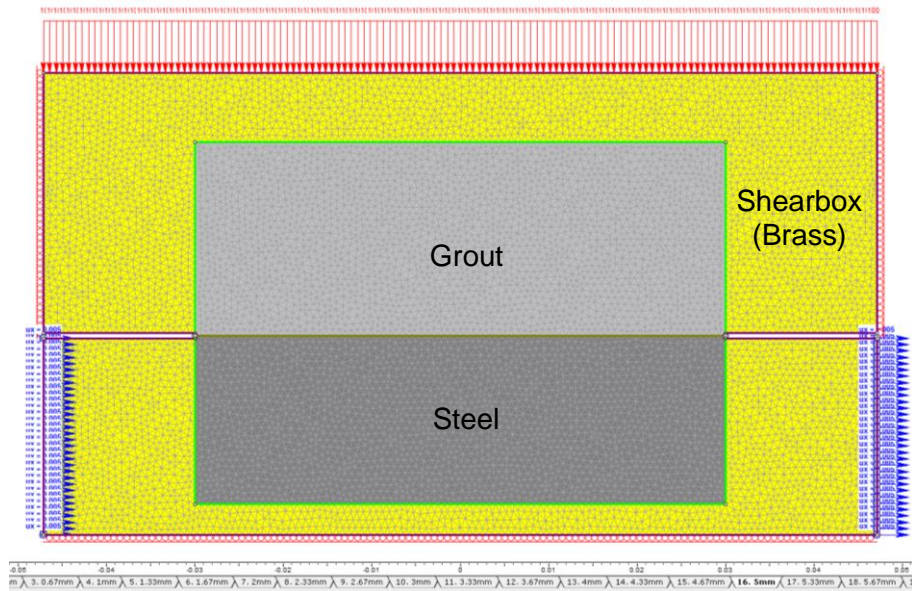


**Figure 6-33** Model of grout and steel test at 100 kPa normal stress and 5mm displacement

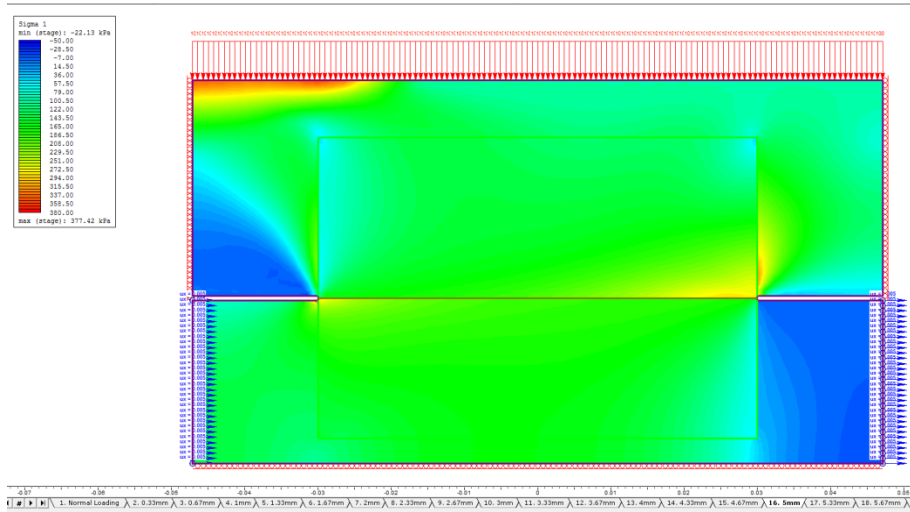


**Figure 6-34** Contoured results for  $\sigma_1$  principle stress of model from **Figure 6-33** at 5mm displacement

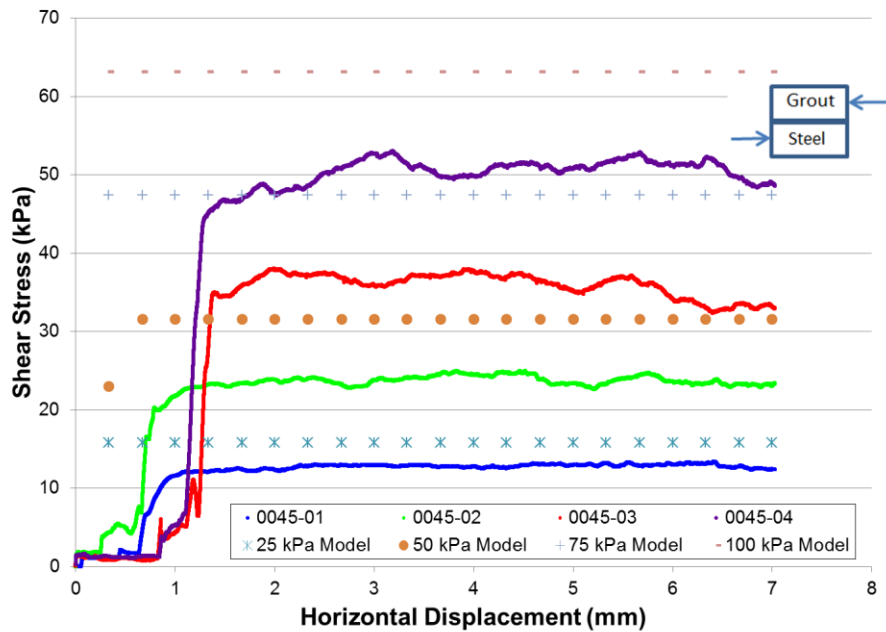


**Figure 6-35** Select laboratory results for direct shear tests of grout and steel at 25 kPa to 100 kPa compared to model results

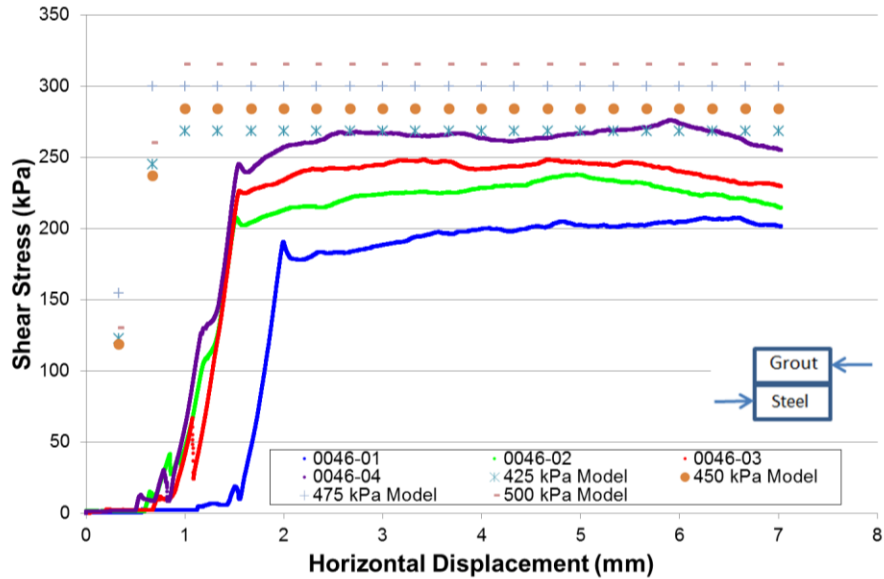


**Figure 6-36** Select laboratory results for direct shear tests of grout and steel at 425 kPa to 500 kPa compared to model results

The model and laboratory results for the steel and grout interface differed by 3 kPa at 25 kPa normal stress and diverged significantly as the normal stress increased. The difference in peak shear strength approached 50 kPa at 500kPa though a greater difference was seen at 425 kPa where the model result was 75 kPa higher than the laboratory results. This meant that the shear strength was consistently over estimated by the models.

### 6.11 Grout and Concrete

The numerical simulations for the grout and concrete were created using the material properties in **Table 6-1**. The joint was given properties as per the laboratory results from Chapter 5. All properties not listed were left in their default values. Below are samples of results for the 25 kPa to 100 kPa and 425 kPa to 500 kPa range in **Figure 6-39** and **Figure 6-40** respectively.

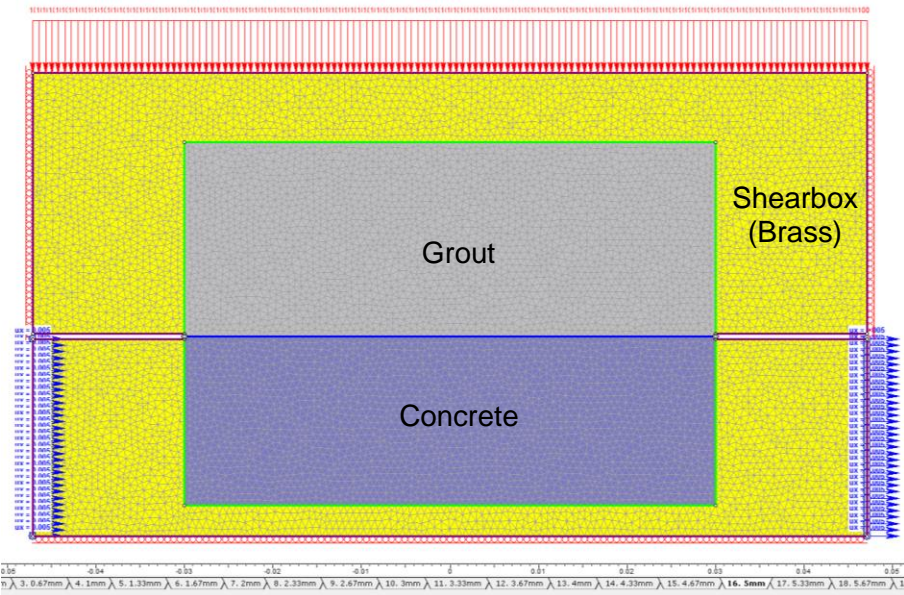


**Figure 6-37** Model of grout and concrete test at 100 kPa normal stress and 5mm displacement

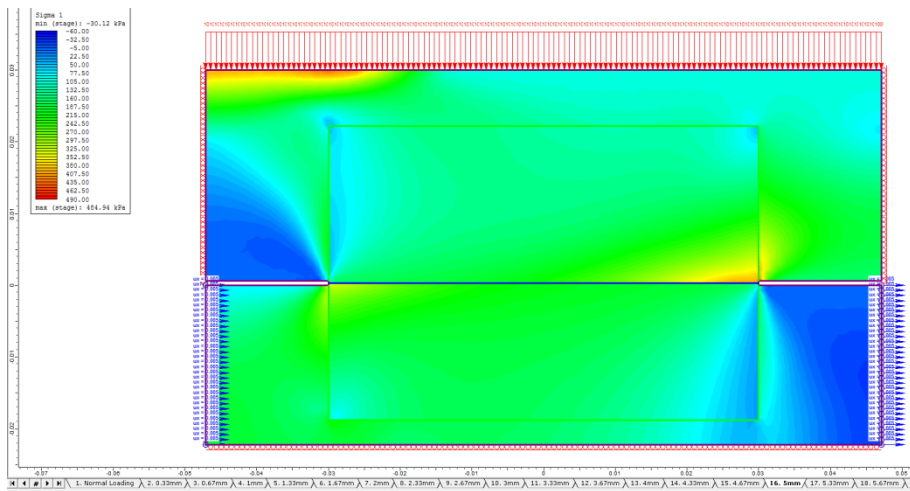


**Figure 6-38** Contoured results for  $\sigma_1$  principle stress of model from **Figure 6-37** at 5mm displacement

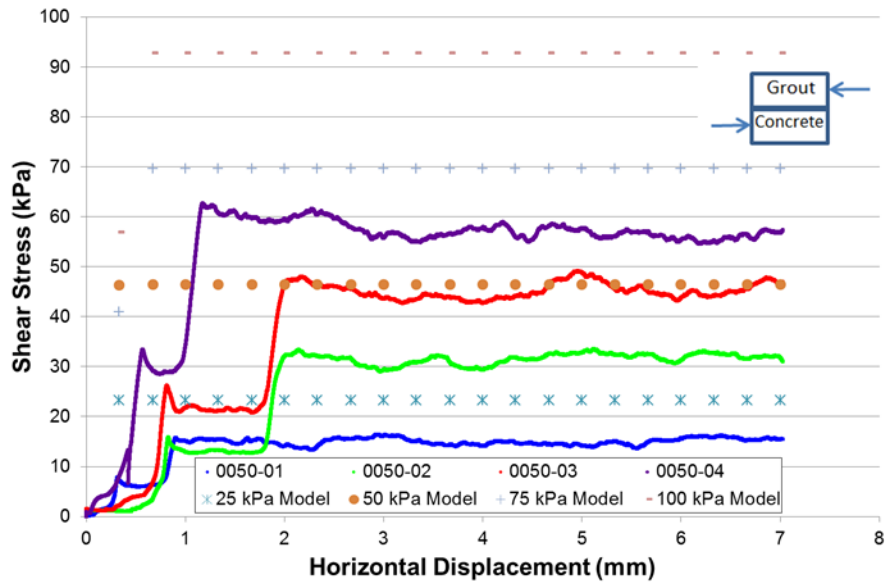


**Figure 6-39** Select laboratory results for direct shear tests of grout and concrete at 25 kPa to 100 kPa compared to model results

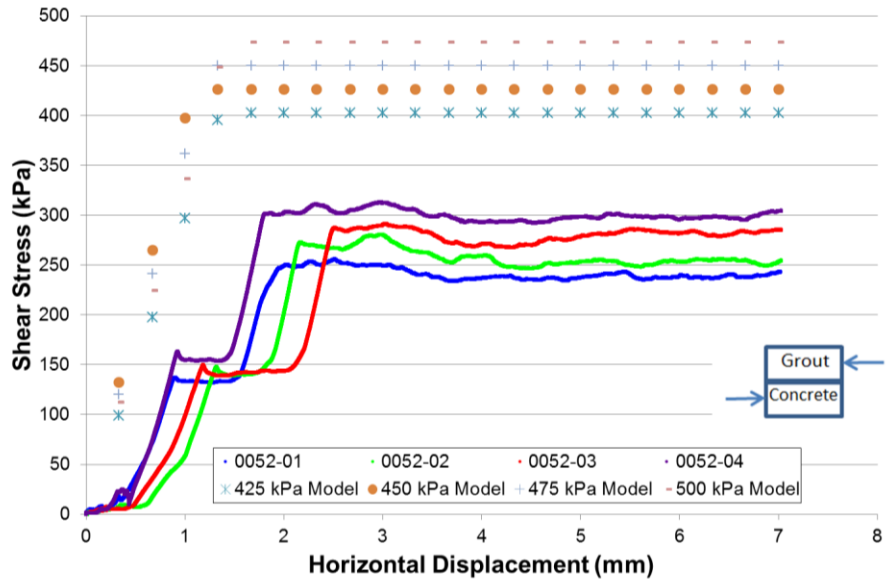


**Figure 6-40** Select laboratory results for direct shear tests of grout and concrete at 425 kPa to 500 kPa compared to model results

The model and laboratory results for the grout and concrete interface differed by 10 kPa at 25 kPa normal stresses but diverged drastically as the normal

stress increased. The difference in peak shear strength approaches 175 kPa at 500kPa. The model consistently over-estimated the shear strength.

## 6.12 Discussion

Though there was some variation in laboratory results, the model results consistently predicted higher shear strength than the laboratory results. The specific values of which can be seen in **Table 6-2**. The general trend was that as normal stress increased the over-estimation of the model's shear strength increased. This result brought into question the suitability of the modelling program's ability to analyze such shearbox arrangements and, particularly, the geo-mechanics involved at the interface.

Despite differences in predicted shear strength between the laboratory and model results, there was good agreement between the shear stiffness of the model with the chord used to determine shear stiffness from the laboratory results. An example of this was seen in **Figure 6-9**.

At present, it is not advisable to directly use laboratory values for the shear strength of interfaces as input parameters for modelling in design due to the discrepancies between the model results and the laboratory results. There are several possible solutions to determine the reasons for this and resolve the differences between them. The first would be to develop a variable reduction factor for the inputs related to the normal stress. This would be the simplest and work well for the direct shearbox models. Another option available for refining the interface behaviour is to reassess how the rheological models of these joints are constructed within the numerical software itself. Currently, the interfaces are modelled very simply using two springs and one slider in the arrangement shown in **Figure 6-1**. The design and performance of these rheological models ought to be carefully reassessed and modified. It is considered likely that as the shearing takes place some of the parameters do not remain constant and using a factor to reduce the shear strength as displacement occurs could overcome some of the discrepancies between the laboratory and numerical model results.

For the Brighton sand, an area of interest is the discrepancy between the residual shear strength behaviour of the models when compared to the laboratory results. The models seemed to not alter the shape of the residual portion of the output regardless of parametric changes made during calibration. This is likely due to variations in physical testing from the particle to particle interaction during test which would influence the stiffness of the interface as particles began to flow during shearing. Testing focused on the different factors influencing the residual shear behaviour could provide better insight into how to improve the input for such residual shear parameters and provide more accurate stiffness values.

It would also be valuable to investigate 3D modelling of the interfaces and the use of different modelling software in order to assess which programs offer

better predictions of interface shear behaviour. Future research must be conducted since it is the only means of discerning how best to improve modelling software.

**Table 6-2** Summary of model and laboratory peak and residual shear strengths

Interface	Normal Stress (kPa)	Model Peak (kPa)	Lab Peak (kPa)	Model Residual (kPa)	Lab Residual (kPa)
Sand – Sand	25	28.5	27.7	26.5	19.2
			28.3		20
			27.9		19.7
	50	55.4	51	52.7	36.96
			48.4		35.9
			50.2		32.7
	75	83.2	73.3	78.8	51.4
			63.7		46.3
			69.7		49.1
	100	112.0	96.2	104.7	70.4
			94.1		67.4
			98.5		64.7
	425	451.5	384.7	423.4	255.6
			385.8		312.9
			338.9		256.2
	450	477.8	399.4	449.5	341.1
			426.1		322.9
			388.1		264.9
475	502.2	450.2	474.6	342.7	
		422.2		346.2	
		399.5		260	
500	530.1	448.4	498.9	327.7	
		442		355.6	
		440.1		312.9	
Sand – Grout	25	21.4	20.9	19.7	14.7
			24.9		14
			20		13.8
	50	39.4	42.9	39.3	27
			36.3		27.1
			33.2		24.1
	75	59.1	50.2	59	34.3
			50.5		37.3

Interface	Normal Stress (kPa)	Model Peak (kPa)	Lab Peak (kPa)	Model Residual (kPa)	Lab Residual (kPa)
Sand – Grout	100	90.3	52.3	78.7	34
			68		52.2
			63.9		47.5
	425	404.8	67.4	398.0	250.7
			280.4		248.5
			298.2		260.3
	450	431.1	284.1	421.4	237.2
			298.8		280.1
			312.7		275.6
	475	457.3	314.8	444.8	272.8
			326.8		293.4
			319.8		298.4
	500	480.1	325.3	468.2	295.1
			322.9		291
			326.4		302
Sand - Steel	25	13.5	9.5	13.5	7
			13.6		9.7
			13.4		11.2
	50	27.0	23	27.0	20.8
			20		15.1
			33.3		18.4
	75	40.6	28.5	40.6	24.5
			26.4		23.7
			29.2		26.3
	100	54.1	32.8	54.1	29.7
			38.6		35.6
			41		38.8
	425	246.2	151.9	243.0	129
			168.1		153.3
			172.8		157
450	257.4	170.7	257.3	156.5	
		185.8		164.1	
		187.7		173	
475	271.6	187.8	271.5	166.2	
		186.2		167.1	

Interface	Normal Stress (kPa)	Model Peak (kPa)	Lab Peak (kPa)	Model Residual (kPa)	Lab Residual (kPa)
	500	285.8	206.7	285.8	194.5
			195		175.5
			186.2		182.1
			215		198.4
Rock – Steel	25	25.3	16.99		
			15.89		
			17.26		
	50	50.6	31.69		
			33.64		
			35.44		
	75	75.9	45.6		
			46.3		
			51.11		
	100	101.2	63.06		
			65		
			64.88		
	425	356.4	152.26		
			212.27		
			262.36		
	450	377.4	203.73		
			240.68		
			241.85		
	475	398.4	221.67		
			270.39		
			286.25		
	500	419.3	222.44		
			302.09		
			340.56		
Rock – Grout	25	28.0	18.98		
			19.41		
			19.78		
	50	56.0	36.73		
			33.91		
			36.13		
	75	84.0	50.54		
			56.15		

Interface	Normal Stress (kPa)	Model Peak (kPa)	Lab Peak (kPa)	Model Residual (kPa)	Lab Residual (kPa)
Rock – Grout	100	112.0	54.66		
			70.54		
			69.75		
			72.06		
	425	455.4	308.8		
			303.15		
			276.35		
	450	482.1	321.49		
			315.98		
			275.56		
	475	508.9	321.21		
			340.13		
			309.16		
	500	535.7	340.33		
358.61					
320.17					
Grout – Steel	25	15.8	8.81		
			10.42		
			12.74		
	50	31.6	15.46		
			17.16		
			25.69		
	75	47.4	22.23		
			29.81		
			35.94		
	100	63.1	33.69		
			38.73		
			50.38		
	425	268.3	197.27		
			211.44		
			241		
	450	284.1	224.55		
			224.76		
			246.13		
475	299.9	241.03			
		255.18			

Interface	Normal Stress (kPa)	Model Peak (kPa)	Lab Peak (kPa)	Model Residual (kPa)	Lab Residual (kPa)
	500	315.7	270.14		
			264.31		
			277.53		
			285.33		
Grout - Concrete	25	23.2	12.52		
			14.97		
			17.11		
	50	46.4	29.98		
			31.58		
			30.67		
	75	69.7	44.32		
			45.18		
			44.75		
	100	92.9	58.39		
			57.39		
			58.43		
	425	402.6	240.88		
			246.73		
			260.39		
	450	426.4	257.35		
			263.89		
			280.23		
	475	450.1	280.07		
			292.2		
			307.41		
	500	473.7	299.77		
			295.87		
			314.9		

### 6.13 Summary

Modern developments in geotechnical engineering with respect to excavation and tunnel design have been aided by the use of computer based numerical simulations. These tools have provided designers and researchers with new insight into how real world engineering projects may behave before they are

constructed. They have been especially helpful in designing excavations and tunnels which employ ground reinforcement and support systems. Beneficial as these tools have been to advancements in geotechnical engineering field, there is still a need to validate their predictions of the behaviour of both the ground and the support and reinforcement systems. Until recently, there was limited focus on predicting the shear behaviour of the interfaces where reinforcement members and the ground meet. In selected cases the interface shear behaviour was not considered but rather an estimated pullout load for a support or reinforcement member was used. Though it has worked in past, in the interest of more accurate numerical simulations, it is important to better understand the real world interface shear behaviour and compare it to these numerical simulations to refine and validate them.

The results of the laboratory tests have provided a starting point for the assessment of these numerical models with regards to support-ground interfaces. The laboratory results were used to provide input parameters for these interface conditions and subsequently, the behaviour of the models was compared to the behaviour of the laboratory tests. From the laboratory tests and computer simulations done in this research, the results showed that the numerical simulations over-estimated the strength of the interface between the support and ground materials. It is recommended that any design conducted using modelling software be used with caution taking into account the possible inaccuracies associated with the noted interface issues and arrangements. In addition, the laboratory shear strength and shear stiffness results cannot be used as direct inputs for modelling at this time; this highlights the limitations associated with current software packages in this regard.

## **7 Conclusions and Recommendations**

## 7.1 Conclusion

This research has been a critical first step to better understanding shear interface behaviour, performance of ground support materials with surrounding ground, and the modelling of these interfaces. Previous research on these shear interfaces was limited and not particularly focused on support or reinforcement systems for tunnelling or surface excavations. This lack of accurate shear interface parameters has an influence on modelling. Computer based modelling software is a relatively new tool within the geoen지니어ing field and has undergone significant development over the past several decades. The numerical simulations have been used extensively for tunnelling and excavations which employ support and reinforcement systems. Despite their common use inaccuracies have been explicitly determined concerning the ability to model accurately without empirical determined values for input. This lack of input data is especially problematic for modelling the shear interfaces of support systems. These knowledge gaps are filled by the two objectives of this research paper:

- I. Obtain, document and provide interface shear behaviour parameters for various support materials and geomaterials; and,
- II. Asses the performance of numerical models using the shear parameters determined from laboratory tests with a view to determine the suitability or relevance of default inputs and experimental results as inputs.

The first objective was accomplished using a modified ASTM D3080 constant rate of strain direct shear test. In previous research this method was used for interface testing of support interface with geo-materials (Hossain and Yin 2014). Through the performance of over 192 constant rate of strain direct shear tests, a database of shear strength parameters for diverse interface scenarios was developed. This data was then processed to determine the Mohr-Coulomb shear strength envelope for these various interface conditions which is the most common way to display such shear strength information. The Mohr-Coulomb shear strength envelope and the shear stiffness were critical inputs for effective modelling of these interfaces.

To accomplish the second objective, it was necessary to take the laboratory results and asses a model's capacity to replicate the test behaviour. A model of the direct shearbox and samples was constructed and run using the laboratory data from the direct shear tests. From these models shear stress versus displacement graphs were taken from the joint between the two simulated shearbox halves. This model output was then compared to the data from the laboratory tests to confirm that the model was accurately simulating the laboratory behaviour.

## 7.2 Contributions

Four significant contributions were made by this research to the body of knowledge about ground support and reinforcement.

- a. The 192 modified ASTM D3080 direct shear tests have produced a significant database of shear behaviours (both shear strength and shear stiffness) for the diverse interface scenarios found in support and reinforcement systems;
- b. The research confirmed that the direct shear test is a practical method to obtain accurate shear strength parameters from interfaces;
- c. A means of evaluating the accuracy of numerical simulations using the laboratory results was developed; and,
- d. It was determined that the numerical simulations were not accurately predicting the shear behaviour of the interfaces between the support materials and the geomaterials even through real input values were utilized – highlighting the need for improved interface arrangements within numerical modelling software packages.

These contributions are a critical first step in better understanding these interfaces and improving modelling and design for tunnels and other excavations.

## 7.3 Recommendations

This research was a significant step toward filling knowledge gaps regarding the shear behaviour of support-ground interfaces. It also assessed the accuracy of common modelling programs and their performance at predicting the shear behaviour of these interfaces. This work has led to several recommendations for future areas of study.

- a. Further shear testing is needed to expand the database to include different rock types, moisture contents, grout types, and soils;
- b. Conduct of shear tests using a direct shear machine for rock samples would be advantageous in order to remove some of the variability when testing samples of two monolithic materials and further refine the database;
- c. Currently, engineers must exercise caution when using laboratory data as an input for numerical simulations and,
- d. Further development of the numerical simulation software systems is necessary in order to improve their ability to accurately model these interface shear behaviours providing better information to designers.



## References

Archibald, J. 2012. MINE 325 applied rock mechanics. Department of Mining Engineering Queen's University, Kingston.

ASTM D2487. 2011. *Standard practice for classification of soils for engineering purposes (unified soil classification system)*. ASTM International, West Conshohocken, PA.

ASTM D3080. 2011. *Test method for direct shear test of soils under consolidated drained conditions*. ASTM International.

ASTM D5607. 2008. *Standard test method for performing laboratory direct shear strength tests of rock specimens under constant normal force*. ASTM International.

ASTM D6913. 2004. *Standard test methods for particle-size distribution (gradation) of soils using sieve analysis*. ASTM International.

Basarir, H. 2006. *Engineering geological studies and tunnel support design at sulakyurt dam site, turkey*, *Engineering Geology*, **86**(4): 225-237.

Bathurst, R.J., Blatz, J.A., and Burger, M.H. 2003. *Performance of instrumented large-scale unreinforced and reinforced embankments loaded by a strip footing to failure* *Canadian Geotechnical Journal*, **40**: 1067.

Bathurst, R.J., Vlachopoulos, N., Walters, D.L., Burgess, P.G., and Allen, T.M. 2006. *The influence of facing stiffness on the performance of two geosynthetic reinforced soil retaining walls* *Canadian Geotechnical Journal*, **43**: 1225.

Brady, B.H.G. and Brown, E.T. 1993. *Rock mechanics for underground mining*. Chapman & Hall, London.

Cai, M. 2008. *Influence of stress path on tunnel excavation response – numerical tool selection and modeling strategy*, *Tunnelling and Underground Space Technology*, **23**(6): 618-628.

CFEM. 2007. *Canadian foundation engineering manual*. Canadian Geotechnical Society, Richmond, B.C.

D. Cruz, B. Forbes and N. Vlachopoulos. *Summary of Lab Results for Axial Strain Testing of Optically Instrumented Rebar* 2016.

Cui, Y. 2012. *Direct shear failure of a synthetic rock containing discontinuous joints*. MSc, University of Alberta, Edmonton.

Data Track Pi. 2014. *Figure of signal changes and core position [online]*. Available from [http://www.datatrackpi.com/images/stories/article\\_images/technical\\_papers/LVDT\\_II.jpg](http://www.datatrackpi.com/images/stories/article_images/technical_papers/LVDT_II.jpg) [cited 12 2014].

Doucet, C. and Voyzelle, B. 2012. Technical information data sheets. Natural Resources Canada, Canada.

Dunnicliff, J. and Green, G.E. 1988. *Geotechnical instrumentation for monitoring field performance* /. Wiley, New York.

Durham Instruments. 2015. *Data acquisition and analysis software [online]*. Available from <https://www.hbm.com/en/2290/catman-data-acquisition-software/> [cited 06/07 2015].

Durham Instruments. 2014. *HBM quantum X MX440A universal amplifier data sheet [online]*. Available from [http://www.disensors.com/downloads/products/QuantumX%20MX440A%20-channel%20Universal%20Amplifier\\_828\\_271375.pdf](http://www.disensors.com/downloads/products/QuantumX%20MX440A%20-channel%20Universal%20Amplifier_828_271375.pdf) [cited 11/19 2014].

EngineeringToolBox. 2016. *Poisson's ratio for common materials [online]*. Available from [http://www.engineeringtoolbox.com/poissons-ratio-d\\_1224.html](http://www.engineeringtoolbox.com/poissons-ratio-d_1224.html) [cited 03/01 2016].

Ezzein, F. and Bathurst, R. 2011. *A transparent sand for geotechnical laboratory modeling, Geotechnical Testing Journal*, **34**(6).

Forbes, B. 2015. THE APPLICATION OF DISTRIBUTED OPTICAL SENSING FOR MONITORING SUPPORT IN UNDERGROUND EXCAVATIONS. MASc, Queen's University, Kingston.

geomat. 2015. *Image of triaxial geogrid [online]*. Available from [http://www.geomat.eu/en/images/vyrobky/45\\_01\\_01\\_tensar-triax\\_monolithic-polypropylene-triaxial-geogrid-for-reinforcement.jpg?h=600](http://www.geomat.eu/en/images/vyrobky/45_01_01_tensar-triax_monolithic-polypropylene-triaxial-geogrid-for-reinforcement.jpg?h=600) [cited March 2015].

Geotechdata. 2013. *Soil elastic young's modulus [online]*. Available from <http://www.geotechdata.info/parameter/soil-young's-modulus.html> [cited 02/17 2016].

Gervais, J.R.D. 2003. *Customs and traditions of the canadian military engineers*. DND, Ottawa.

Ghazvinian, E., Diederichs, M.S., Labrie, D., and Martin, C.D. 2015. *An investigation on the fabric type dependency of the crack damage thresholds in brittle rocks*, *Geotechnical Geologic Engineering*, **33**(July): 1409.

Goodhue, M., Edil, T., and Benson, C. 2001. *Interaction of foundry sands with geosynthetics*, *Journal of Geotechnical and Geoenvironmental Engineering*, **127**(4): 353-362.

Grasso, P., Scotti, G., Blasini, Pescara, M., Floria, V., and Kazilis, N. 2003. *Successful application of the observational design method to difficult tunnel conditions - driskos tunnel*. Geodata S.A.

HBM GmbH. 2015. *Catman AP professional measurement made easy [online]*. Available from [http://www.durhaminstruments.com/downloads/products/Catman%20AP\\_460.pdf](http://www.durhaminstruments.com/downloads/products/Catman%20AP_460.pdf) [cited 08/10 2015].

Heyman, J., Coulomb, C. A. (Charles Augustin), 1736-1806. *Essai sur une application des regles de maximis & minimis a quelques problemes de statique, relatifs a l, and Essai sur une application des regles de maximis & minimis a quelques problemes de statique, relatifs a l'architecture*. 1972. *Coulomb's memoir on statics; an essay in the history of civil engineering*. University Press, Cambridge Eng.

Hoek, E. 2014. *Rockbolts and cables*. Unknown, Unknown.

Hoek, E. and Marinos, P. 2007. *A brief history of the development of the hoek-brown failure criterion*, *Brazilian Journal of Soil and Rocks*, **2**(November): 1-8.

Hoffman, K. 1986. *Applying the wheatstone bridge circuit [online]*. Available from [http://paginas.fisica.uson.mx/horacio.munguia/aula\\_virtual/Cursos/Instrumentacion%20II/Documentos/Teoria%20Ctos%20Puentes.PDF](http://paginas.fisica.uson.mx/horacio.munguia/aula_virtual/Cursos/Instrumentacion%20II/Documentos/Teoria%20Ctos%20Puentes.PDF) 2015].

Holtz, R.D.(.D.). and Kovacs, W.D. 2011. *Introduction to geotechnical engineering*. Prentice-Hall, Englewood Cliffs, N.J.

Honeywell. 2009. *Model AL-JP high output load cell [online]*. Available from [https://measurementsensors.honeywell.com/ProductDocuments/Load/Model\\_AL-JP\\_Datasheet.pdf](https://measurementsensors.honeywell.com/ProductDocuments/Load/Model_AL-JP_Datasheet.pdf) [cited 11/19 2014].

Hossain, M. and Yin, J. 2014. *Behaviour of a pressure-grouted soil-cement interface in direct shear tests*, *International Journal of Geomechanics*, **14**(1): 101-109.

Hottinger Baldwin Messtechnik GmbH. 2015. *MGC plus data acquisition system [online]*. Available from [http://www.durhaminstruments.com/downloads/products/MGC%20Plus%20Data%20Acquisition%20System%20\(overview\)\\_362.pdf](http://www.durhaminstruments.com/downloads/products/MGC%20Plus%20Data%20Acquisition%20System%20(overview)_362.pdf) [cited 08/10 2015].

Hudson, J.A. and Harrison, J.P. 1997. *Engineering rock mechanics an introduction to the principles*. Elsevier Science Ltd., Oxford.

Itasca Consulting Group Inc. 2009. *Fast lagrangian analysis of continua in 3 dimensions, version 4.0*. Itasca Consulting Group Inc., Minneapolis.

King Packaged Materials Company. 2016. *Material properties of non-shrink grout*. King Packaged Materials Company, Burlington.

Kopczynski, P. 1992. *LVDTs. theory & application*, *Sensors*, **9**(3).

Macro Sensors. 2014. *LVDT output signal [online]*. Available from [http://www.macrosensors.com/images/tutorial\\_page\\_images/images/fig3.jpg](http://www.macrosensors.com/images/tutorial_page_images/images/fig3.jpg) [cited 12 2014].

Marco Sensors. 2014. *LVDT cross section [online]*. Available from [http://www.macrosensors.com/images/tutorial\\_page\\_images/images/fig1.jpg](http://www.macrosensors.com/images/tutorial_page_images/images/fig1.jpg) [cited 12 2014].

Marinos, P. and Hoek, E. 2001. *The appropriate use of geological information in the design and construction of the egnatia motorway tunnels*, *Egnatia Odos A.E.*

MatWeb, L. 2016. *Overview of materials for brass [online]*. Available from <http://www.matweb.com> [cited 02/17 2016].

Microsoft. 2010. *MS excel*. Microsoft.

National Instruments. 2016. *How is temperature affecting your strain measurement accuracy? [online]*. Available from <http://www.ni.com/white-paper/3432/en/> 2016].

Oke, J., Vlachopoulos, N., and Diederichs, M.S. 2012a. Improved input parameters and numerical analysis techniques for temporary support of underground excavation in weak rock. *In* RockEng, Edmonton.

Oke, J., Vlachopoulos, N., and Marinos, P. 2014a. *Umbrella arch nomenclature and selection methodology for temporary support systems for design and construction of tunnels*, *Geotechnical and Geological Engineering Journal*, **32**(1): 97-130.

Oke, J., Vlachopoulos, N., and Vazaios, I. 2014b. Procedure and considerations when creating a geomechanical three dimensional numerical analysis for construction of tunnel infrastructure. *In* GeoRegina 2014, Regina, SK.

Oke, J., Vlachopoulos, N., and Diederichs, M.S. 2013. Pre-support nomenclature and support selection methodology for temporary support systems within weak rock masses. *In* World Tunnel Congress 2013: Underground - the way of the future!, Geneva, Switzerland.

Oke, J., Vlachopoulos, N., and Diederichs, M.S. 2012b. Sensitivity numerical analysis of orientations and sizes of forepoles for underground excavations in weak rock. *In* 46th US Rock Mechanics / Geomechanics Symposium, Chicago.

O'Rourke, T., Druschel, S., and Netravali, A. 1990. *Shear strength characteristics of Sand- Polymer interfaces*, *Journal of Geotechnical Engineering*, **116**(3): 451-469.

Plaxis. 2016. *Plaxis geotechnical software [online]*. Available from <http://www.plaxis.nl/about/> [cited 04/28 2016].

Potyondy, J.G. 1961. *Skin friction between various soils and construction materials*, *Geotechnique*, **11**(4): 339-353.

RDP Group. 2014a. *How it works - LVDT [online]*. Available from <http://www.rdpelectrosense.com/displacement/lvdt/lvdt-principles.htm> [cited 10/15 2014].

RDP Group. 2014b. *DC-DC LVDT displacement transducers*. RDP Group, .

Rocscience Inc. 2014. *Phase 2 version 8.020*. Rocscience Inc., Toronto.

T. Krahn, J. Blatz, M. Alfaro, and R. J. Bathurst. 2007. *Large-scale interface shear testing of sandbag dyke materials*, *Geosynthetics International*, **14**(2): 119-126.

Terzaghi, K., Peck, R.B., and Mesri, G. 1996. Soil mechanics in engineering practice. Wiley.

Thiel, R. 2009. *A technical note regarding interpretation of cohesion (or adhesion) and friction angle in direct shear tests* [online]. Available from <http://geosyntheticsmagazine.com/2009/04/01/cohesion-or-adhesion-and-friction-angle-in-direct-shear-tests/> [cited 05/10 2015].

Virtual Geoscience Simulation Tools. 2016. *3D FEMDEM* [online]. Available from <http://vgest.net/technology/3d-femdem/> [cited 04/28 2016].

Vlachopoulos, N. 2009. Back Analysis of a Tunnelling Case Study In Weak Rock of the Alpine System In Northern Greece: Validation and Optimization of Design Analysis Based on Ground Characterization and Numerical Simulation. Doctor of Philosophy, Queen's University, Kingston, ON, Canada.

Vlachopoulos, N. 2000. Performance of two full-scale model geosynthetic - reinforced retaining walls: Segmental and wrapped - faced. MASC, Royal Military College of Canada, Kingston, ON.

Vlachopoulos, N., Forbes, B., Oke, J., and Hyatt, A. 2014. The development of a technique in order to measure the distributed optical sensing of a forepole temporary support element employed within an umbrella arch system. *In* EUROCK international Symposium, Vigo, Spain.

Wykeham Farrance Engineering Limited. 1968. *WF 2500 constant rate of strain shear box handbook*. Wykeham Farrance Engineering Limited, Slough, England.

Yasitli, N. 2012. *Numerical modelling of surface settlements at the transition zone excavated by new austrian tunnelling method and umbrella arch method*.

## **APPENDIX A**

This appendix presents the shear stress versus horizontal displacement curves and the vertical versus horizontal displacement curves for all of the Direct Shear tests performed as part of this research. The Mohr Coulomb failure envelopes are also presented below. **Table A-1** Test Index contains a guide to the location of the diagrams within this appendix.

**Table A-1** Test Index

Test Type	Page number
Brighton Sand – Brighton Sand on WF 2500	162-165, 176-179
Brighton Sand – Brighton Sand WF 25403 Validation	165-168
Brighton Sand – Grout	169-172, 179-182
Brighton Sand – Steel	172-175, 183-186
Rock – Steel	186-189, 197-200
Rock - Grout	190-193, 193-196
Grout –Steel	200-207
Grout - Concrete	207-214

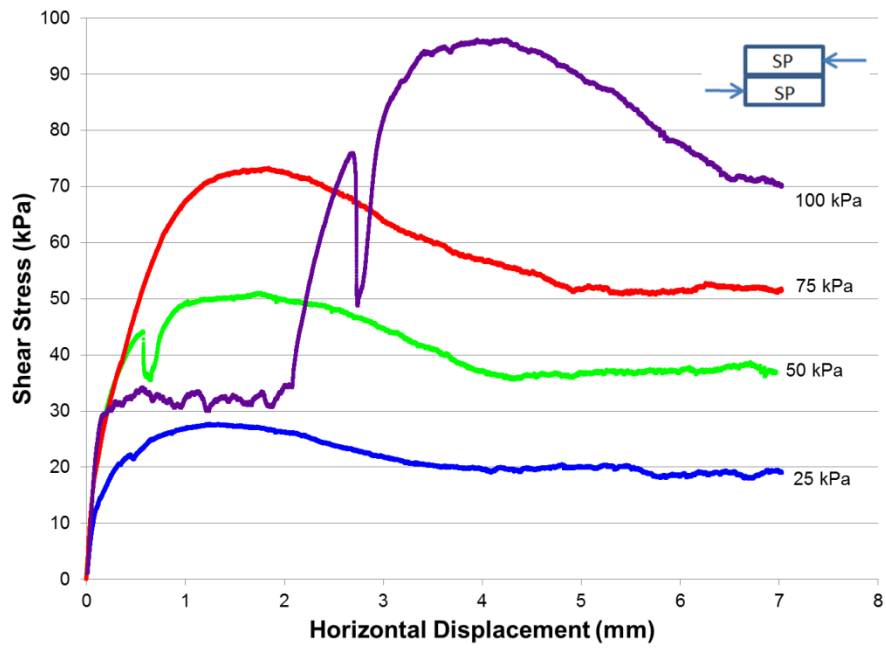


Figure A-1 Test 0007 sand 25-100kPa shear stress versus horizontal displacement

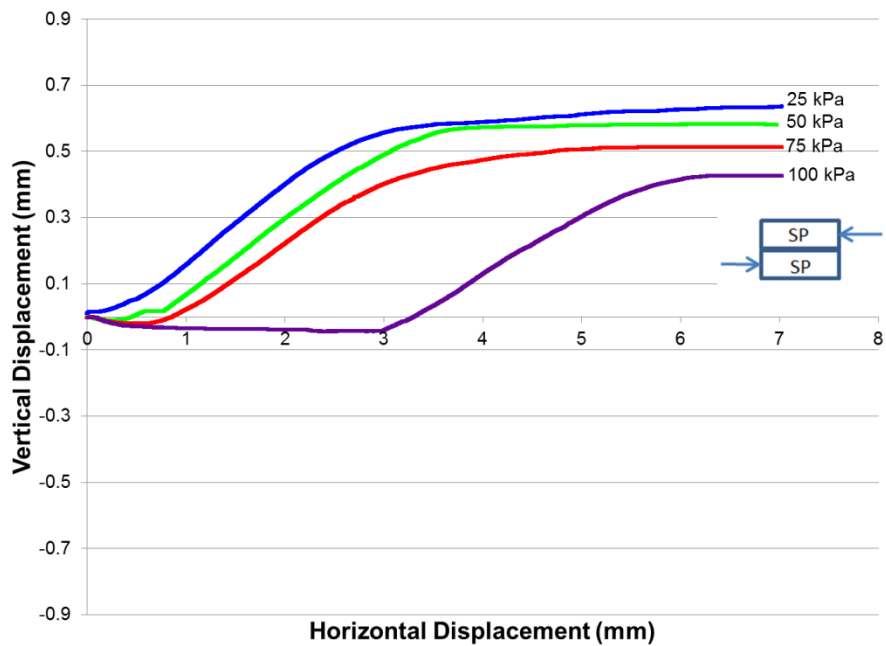


Figure A-2 Test 0007 sand 25-100 kPa vertical versus horizontal displacement

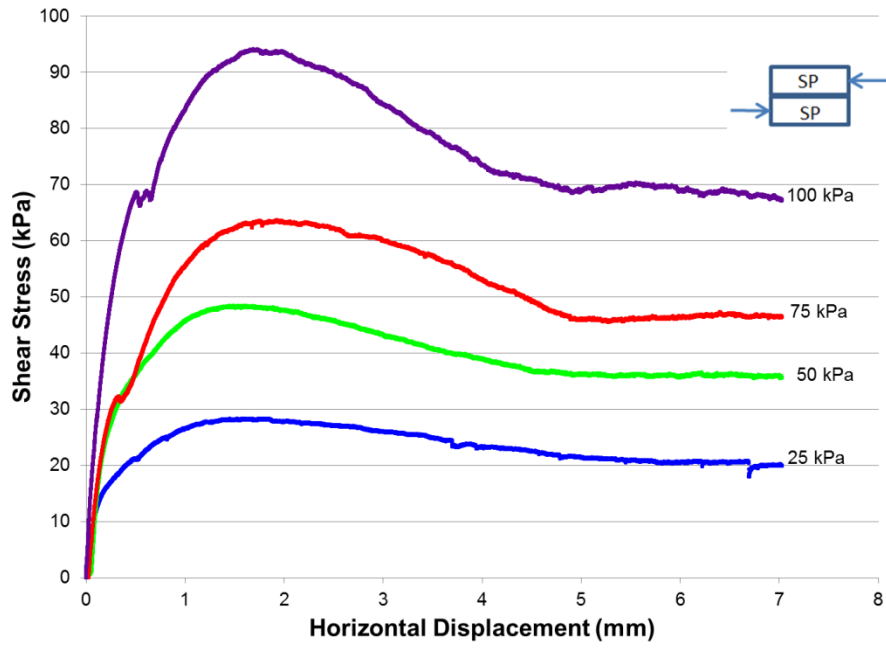


Figure A-3 Test 0008 sand 25-100kPa shear stress versus horizontal displacement

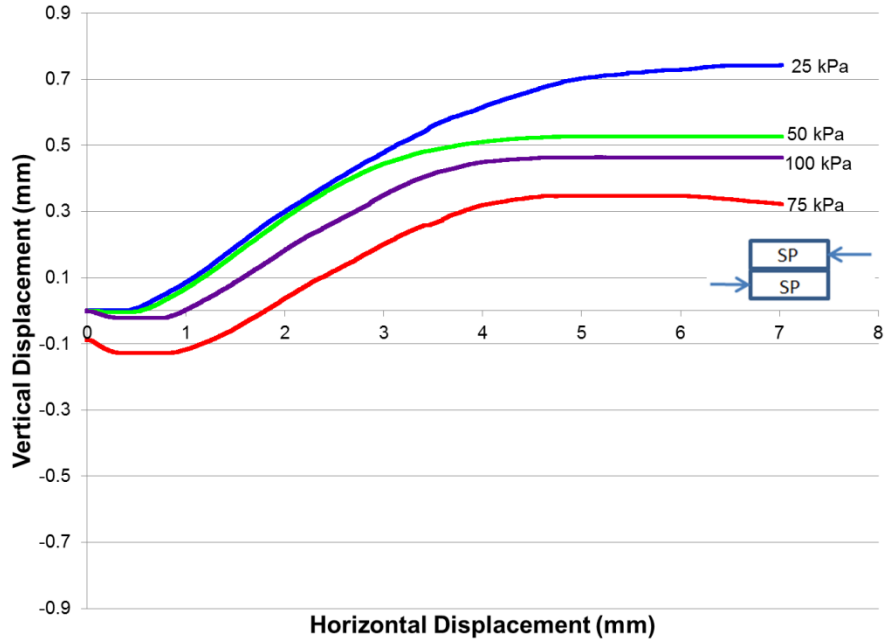


Figure A-4 Test 0008 sand 25-100 kPa vertical versus horizontal displacement

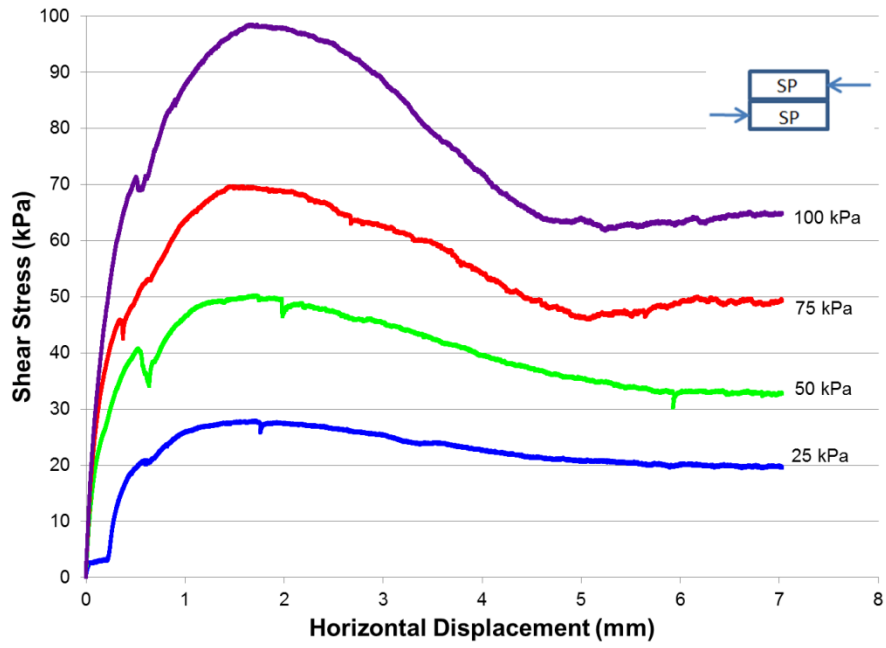


Figure A-5 Test 0009 sand 25-100kPa shear stress versus horizontal displacement

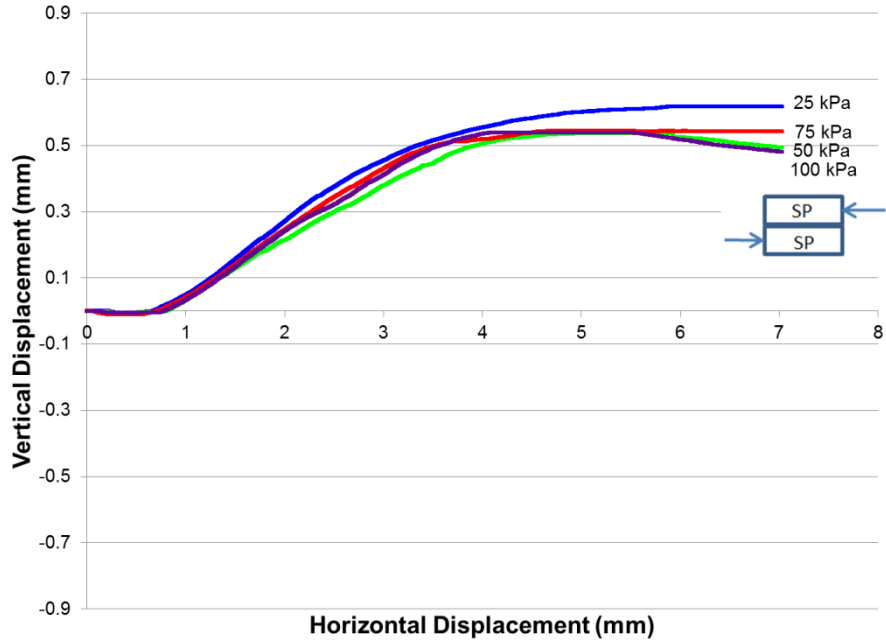


Figure A-6 Test 0009 sand 25-100 kPa vertical versus horizontal displacement

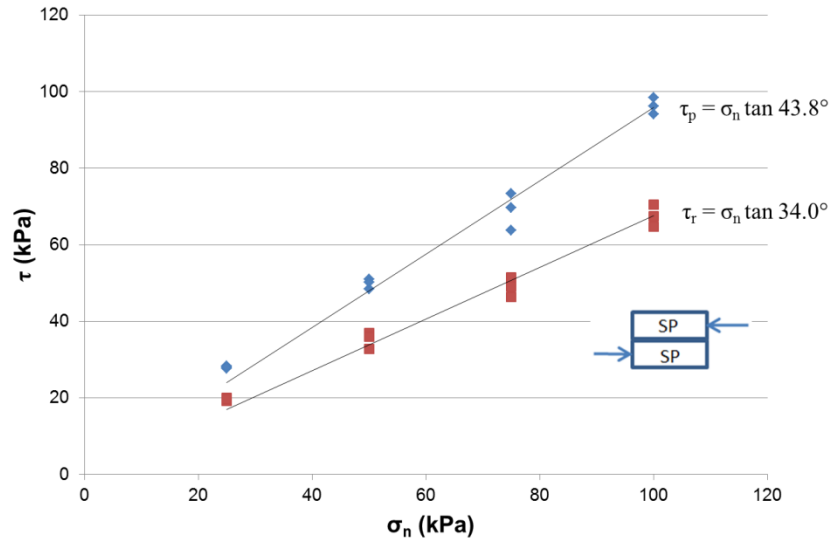


Figure A-7 Mohr-Coulomb shear strength 25-100 kPa Brighton Sand WF 2500

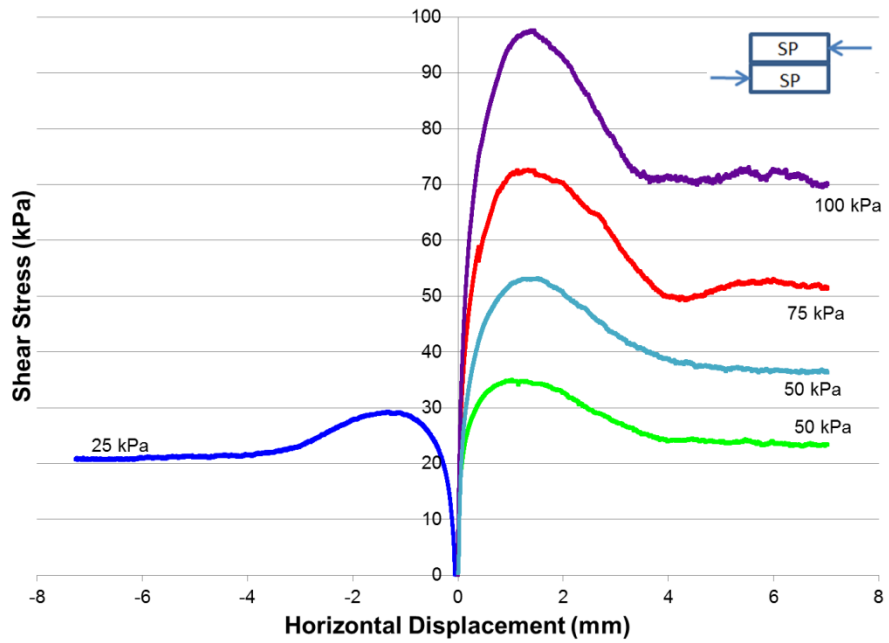
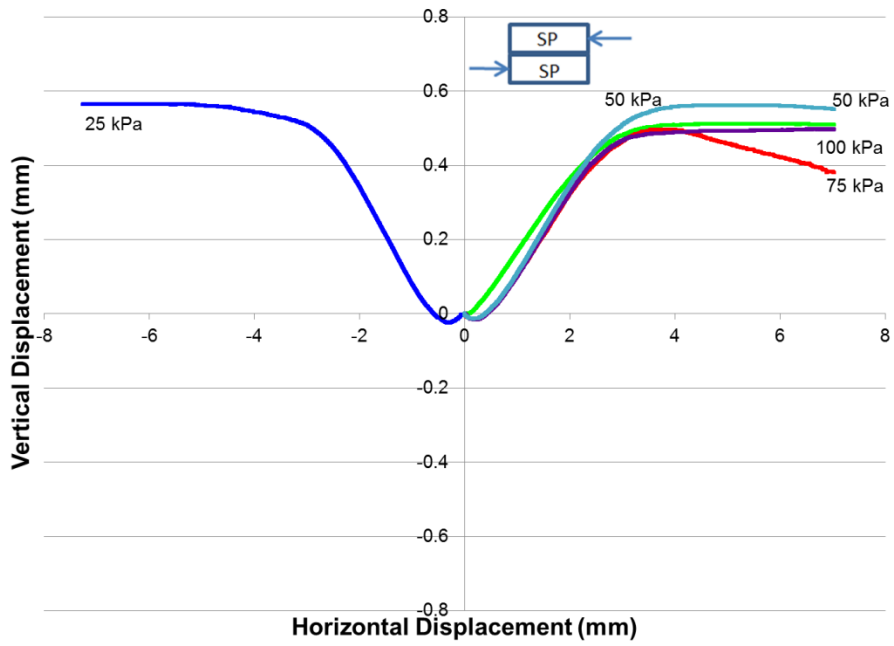
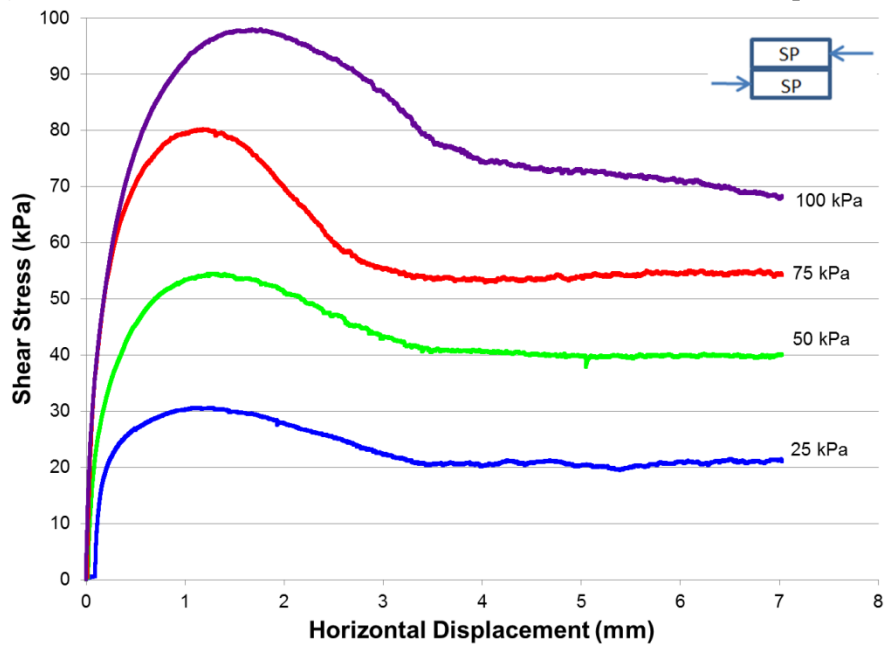


Figure A-8 Test 0010 sand 25-100kPa shear stress versus horizontal displacement



**Figure A-9** Test 0010 sand 25-100 kPa vertical versus horizontal displacement



**Figure A-10** Test 0011 sand 25-100kPa shear stress versus horizontal displacement

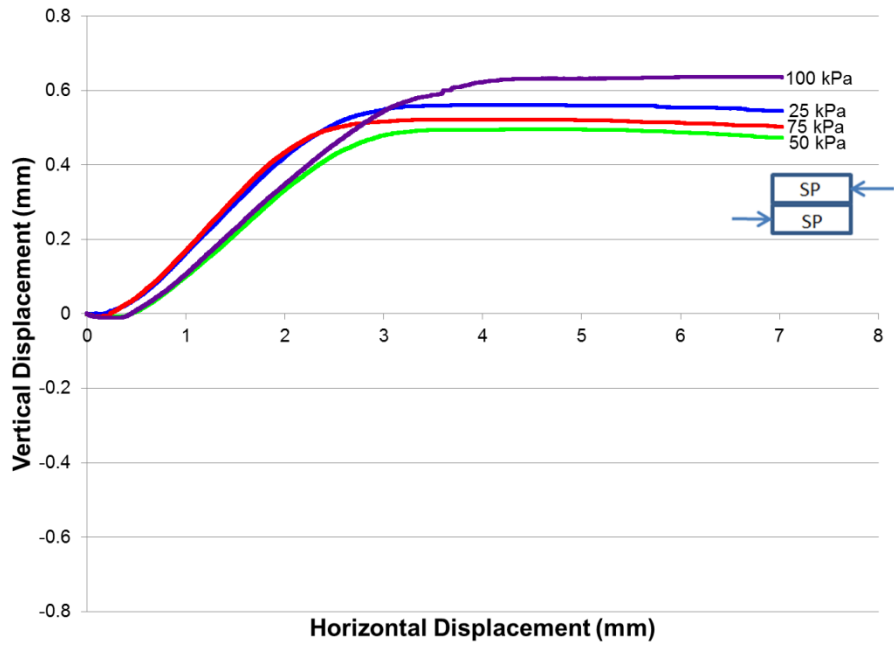


**Figure A-11** Test 0011 sand 25-100 kPa vertical versus horizontal displacement

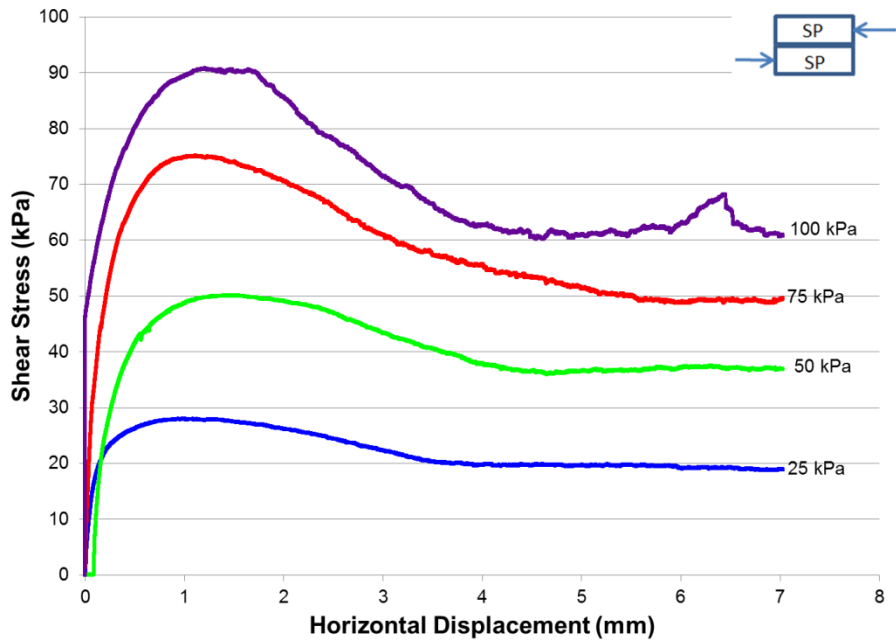


**Figure A-12** Test 0012 sand 25-100kPa shear stress versus horizontal displacement

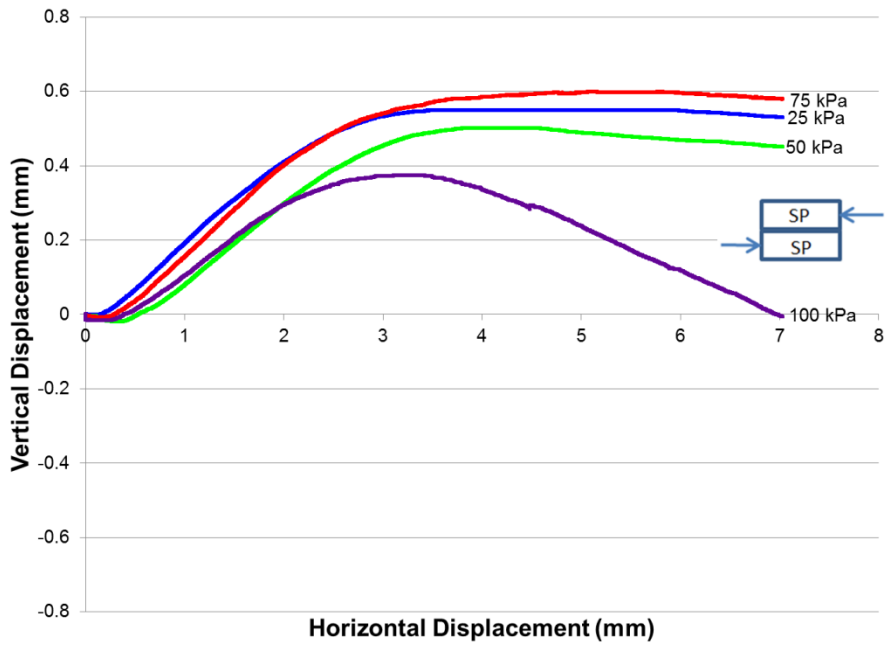


Figure A-13 Test 0012 sand 25-100 kPa vertical versus horizontal displacement

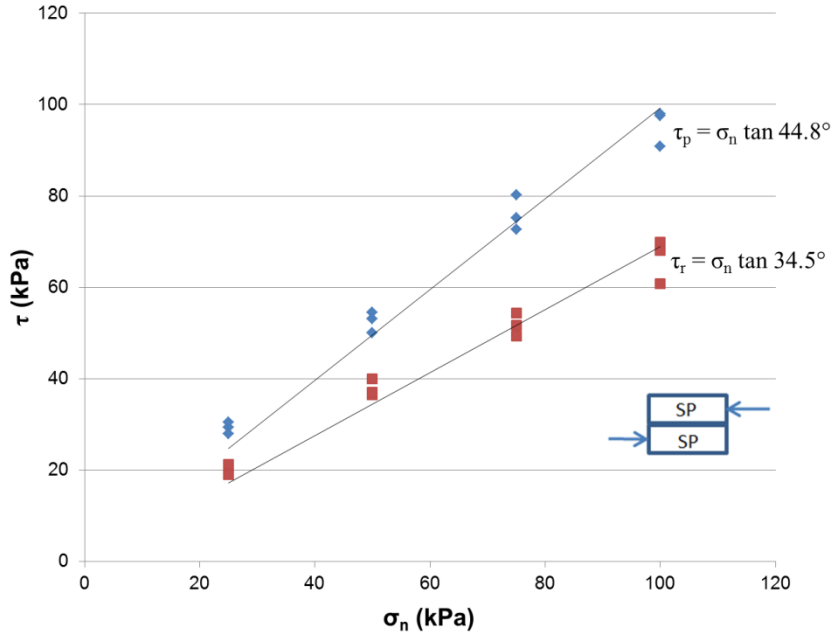
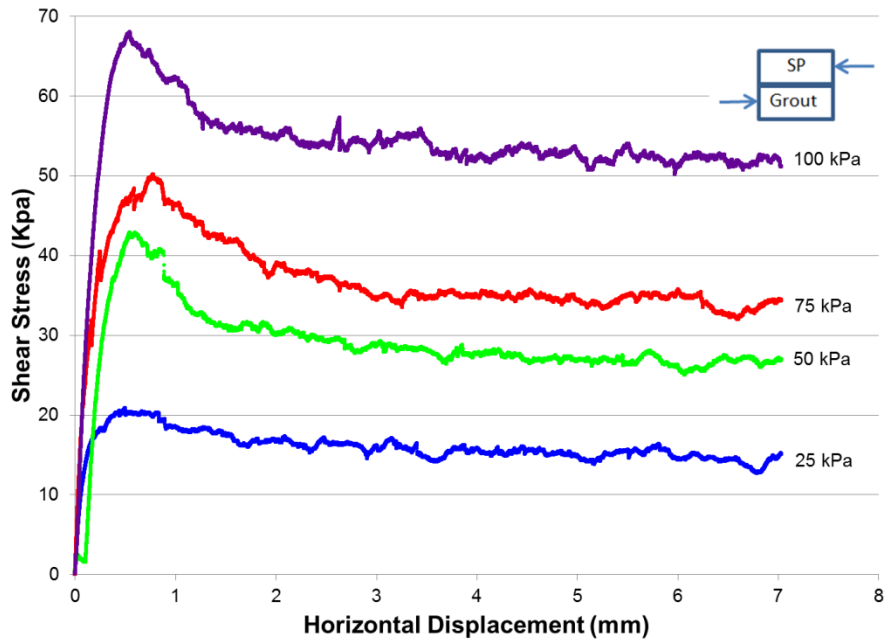
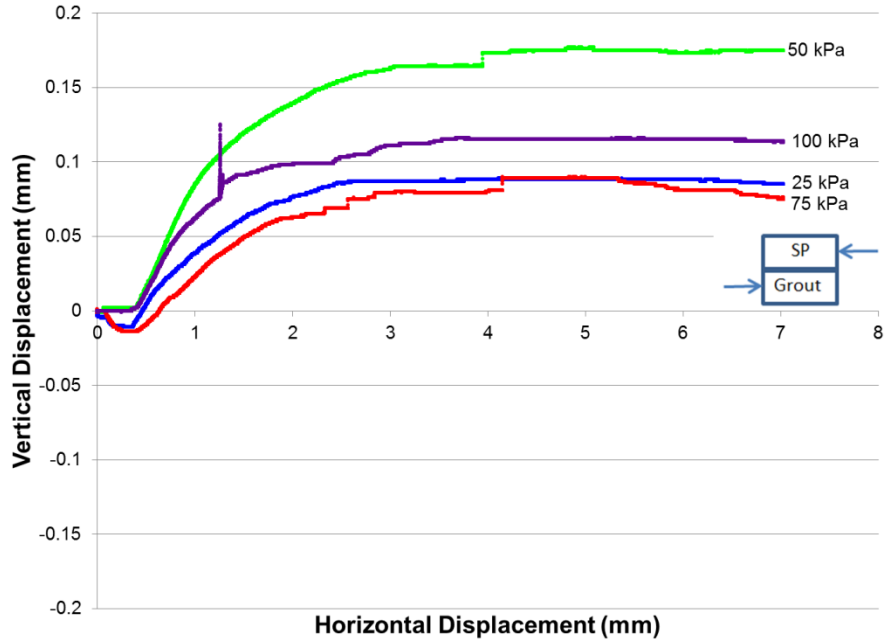


Figure A-14 Mohr-Coulomb shear strength 25-100 kPa Brighton Sand WF 25403



**Figure A-15** Test 0015 sand-grout 25-100kPa shear stress versus horizontal displacement



**Figure A-16** Test 0015 sand-grout 25-100 kPa vertical versus horizontal displacement

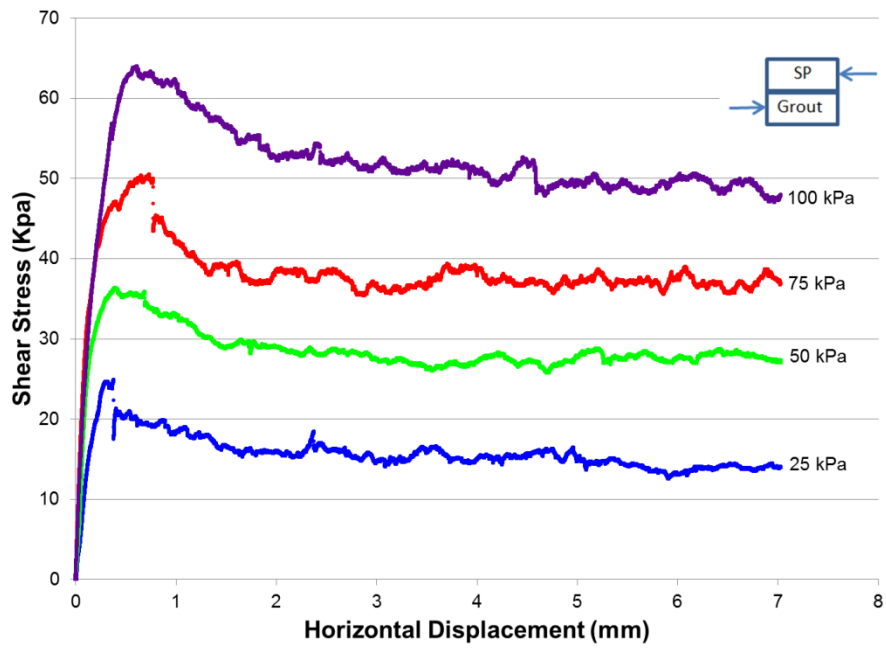


**Figure A-17** Test 0016 sand-grout 25-100kPa shear stress versus horizontal displacement

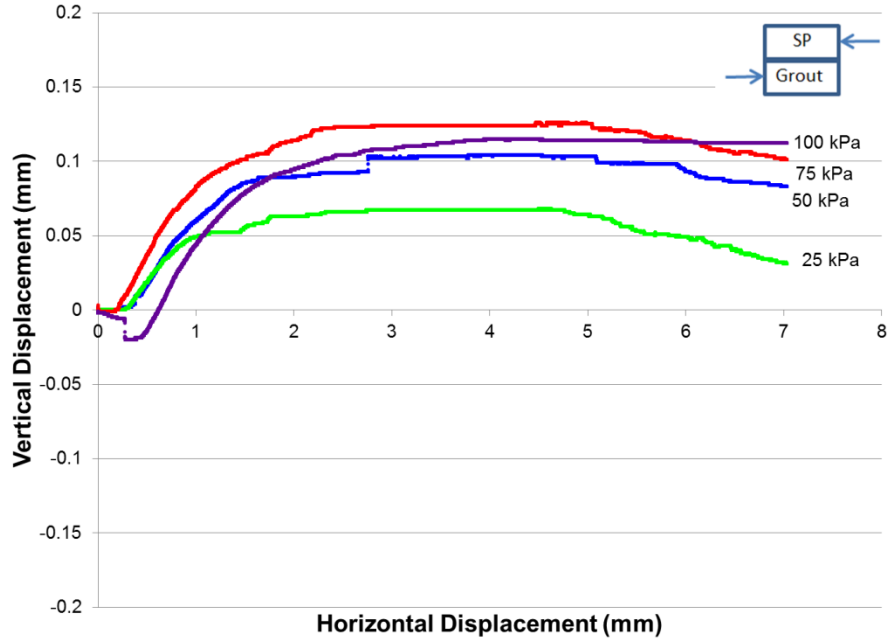


**Figure A-18** Test 0016 sand-grout 25-100 kPa vertical versus horizontal displacement

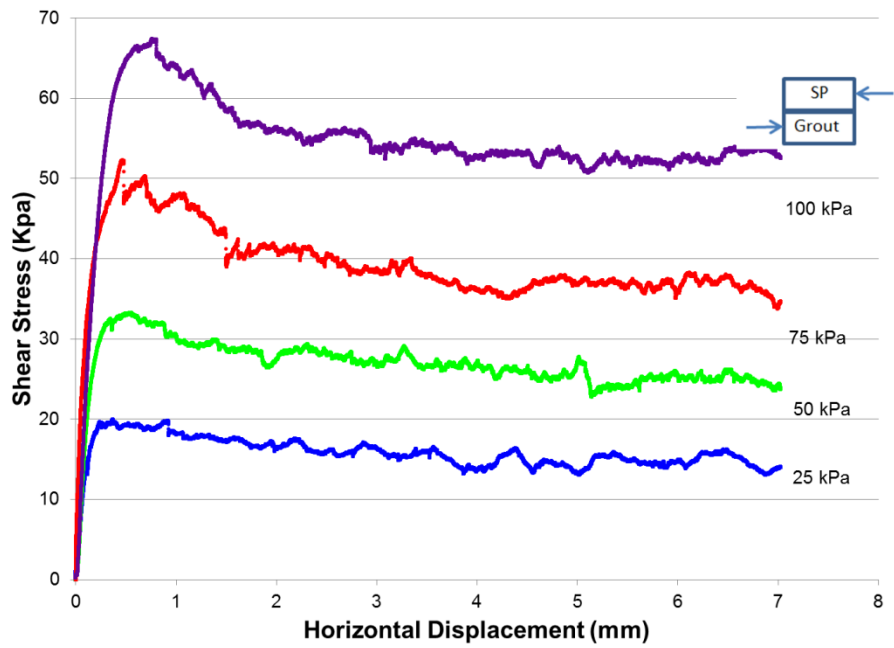


**Figure A-19** Test 0017 sand-grout 25-100kPa shear stress versus horizontal displacement

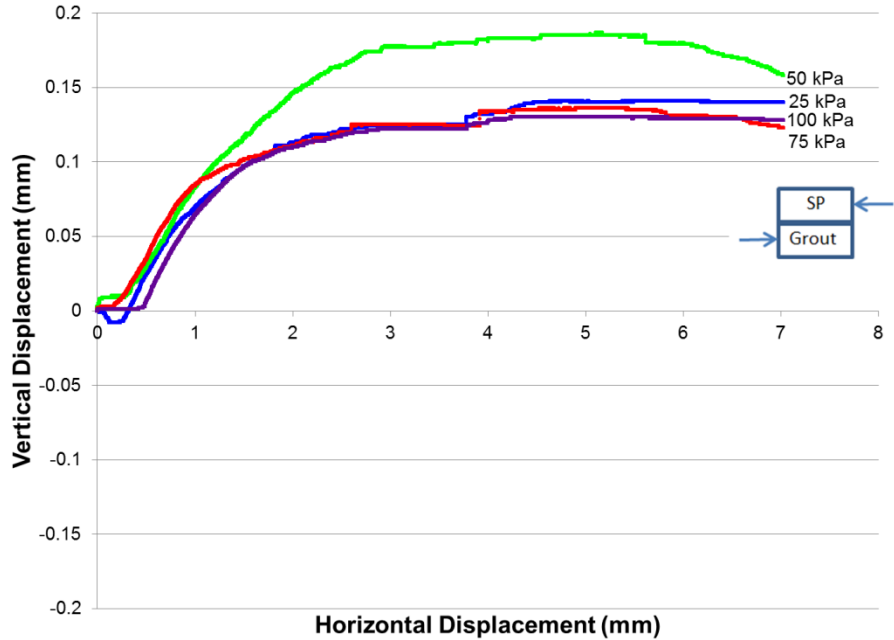


**Figure A-20** Test 0017 sand-grout 25-100 kPa vertical versus horizontal displacement

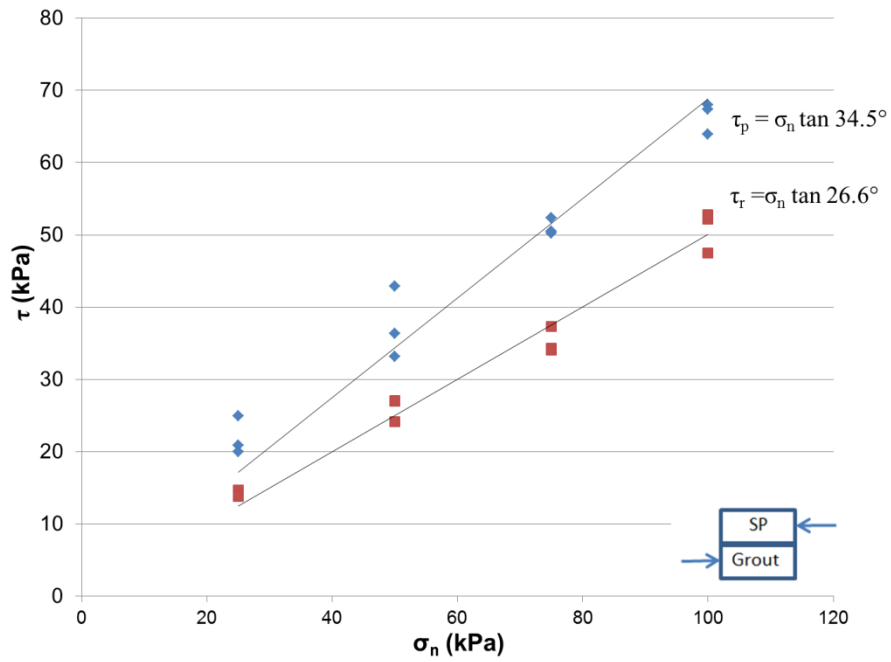


Figure A-21 Mohr-Coulomb shear strength 25-100 kPa sand and grout

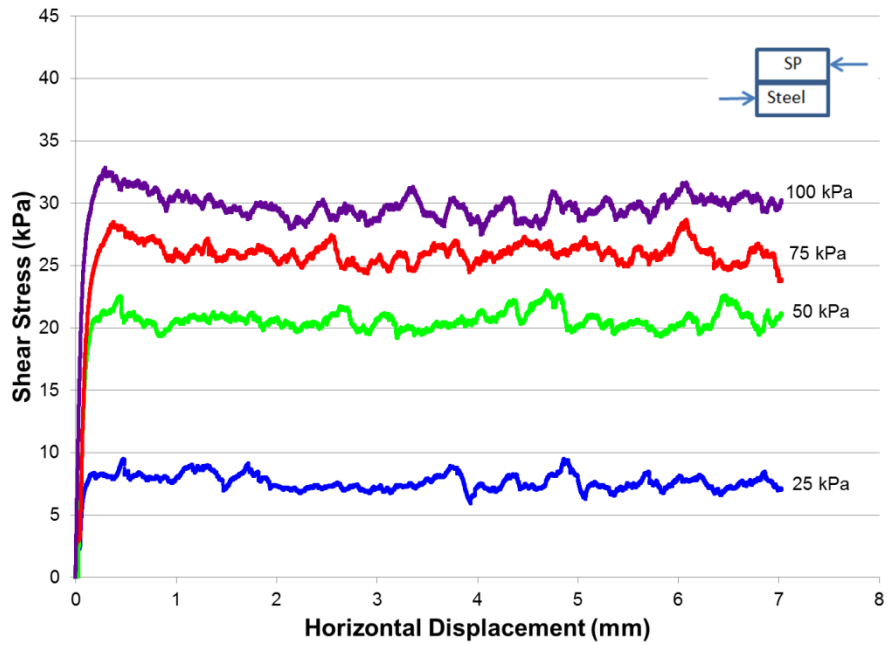
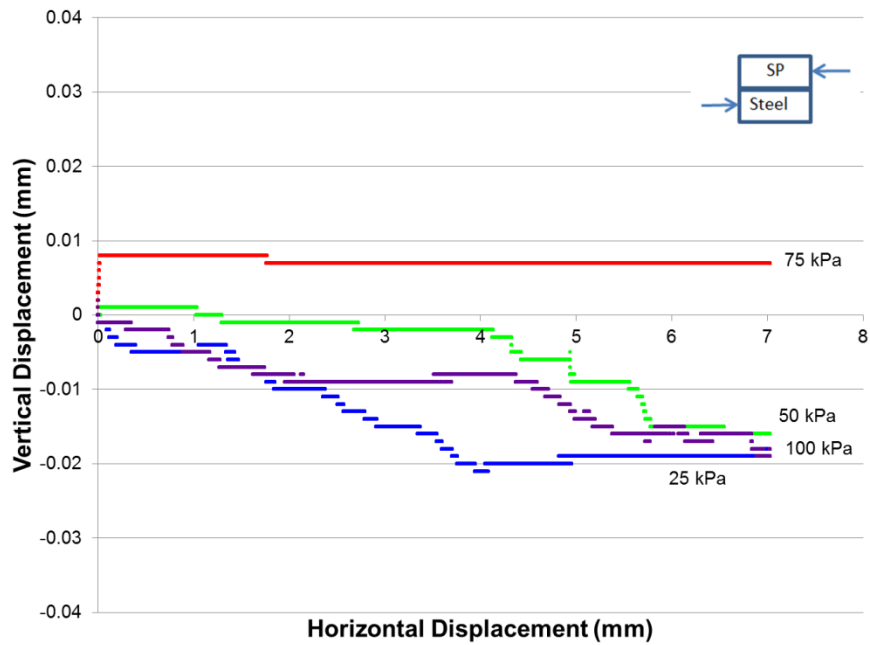
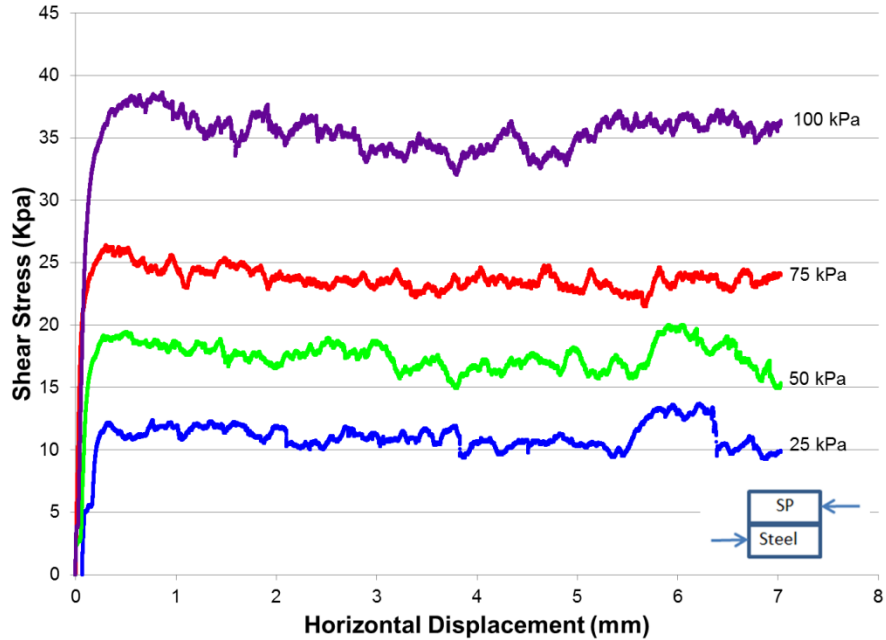


Figure A-22 Test 0018 sand-steel 25-100kPa shear stress versus horizontal displacement



**Figure A-23** Test 0018 sand-steel 25-100 kPa vertical versus horizontal displacement



**Figure A-24** Test 0019 sand-steel 25-100kPa shear stress versus horizontal displacement

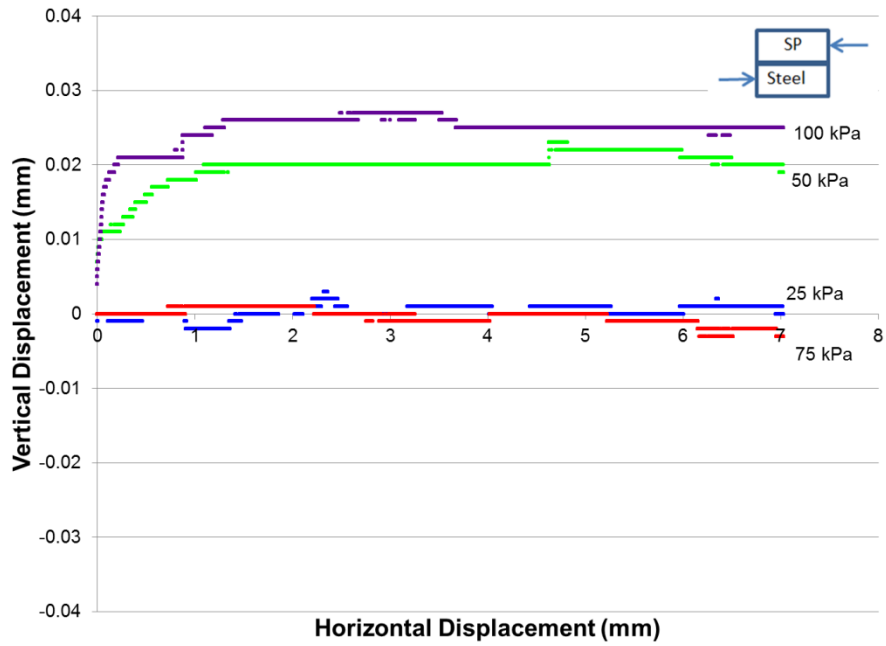


**Figure A-25** Test 0019 sand-steel 25-100 kPa vertical versus horizontal displacement

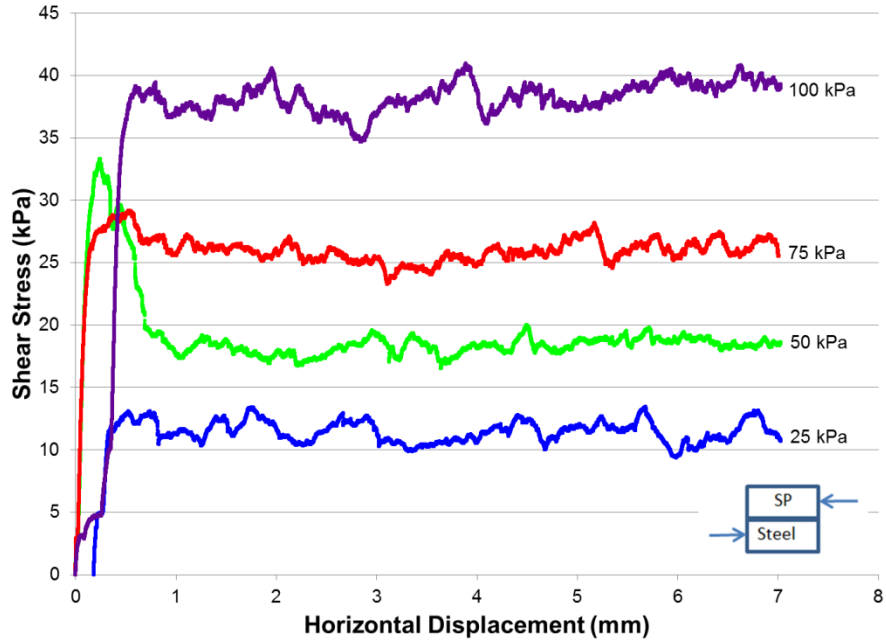


**Figure A-26** Test 0020 sand-steel 25-100kPa shear stress versus horizontal displacement

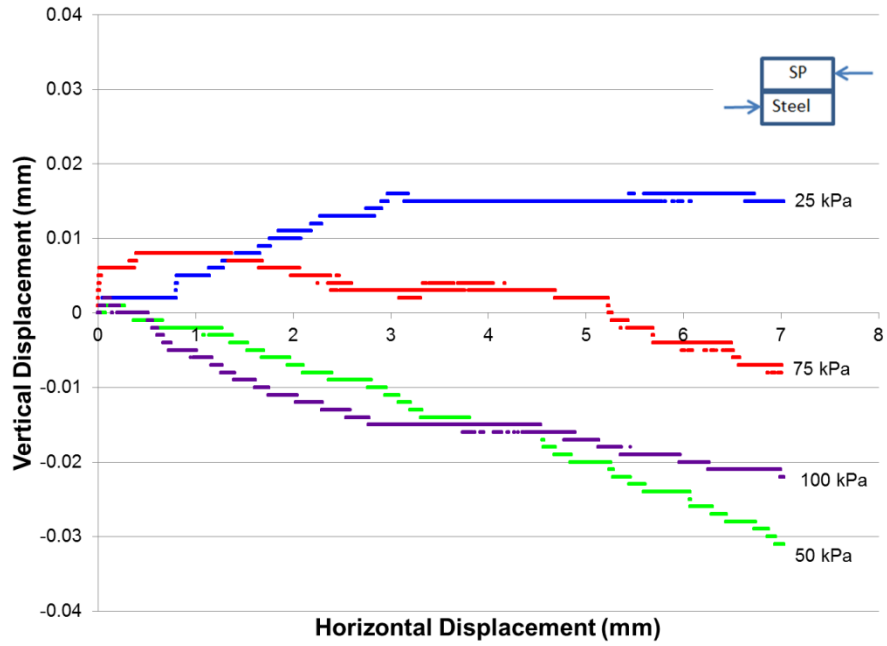


**Figure A-27** Test 0020 sand-steel 25-100 kPa vertical versus horizontal displacement

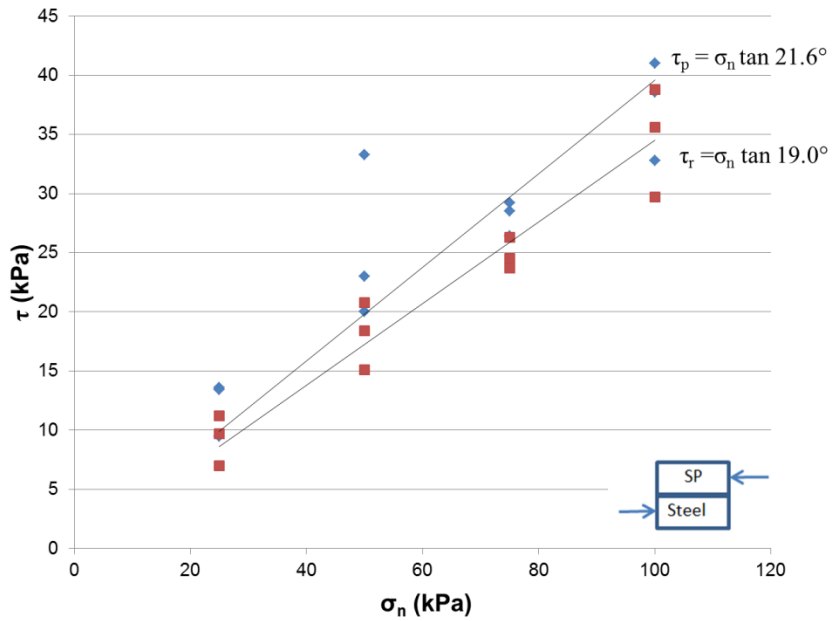


**Figure A-28** Mohr-Coulomb shear strength 25-100 kPa sand and steel

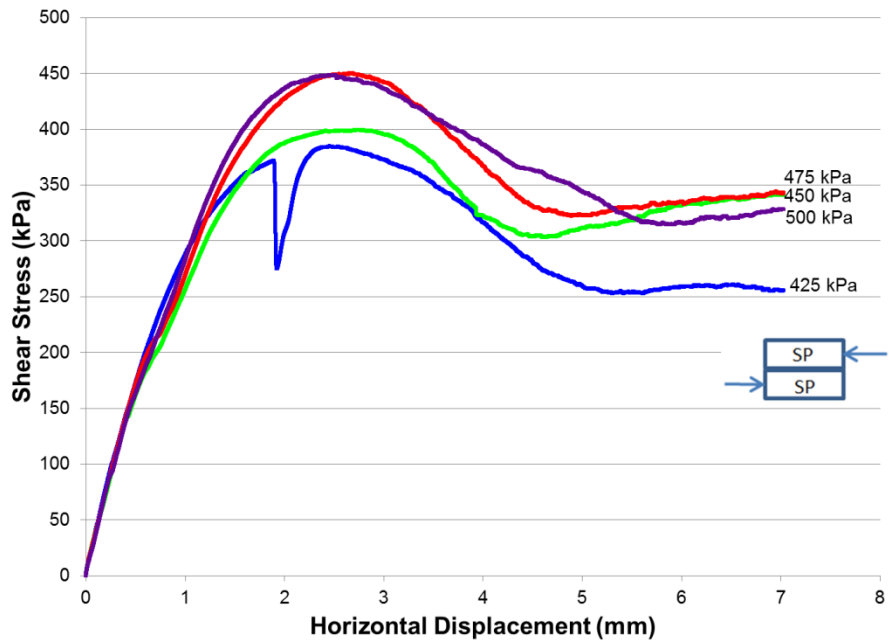


Figure A-29 Test 0021 sand 425-500kPa shear stress versus horizontal displacement

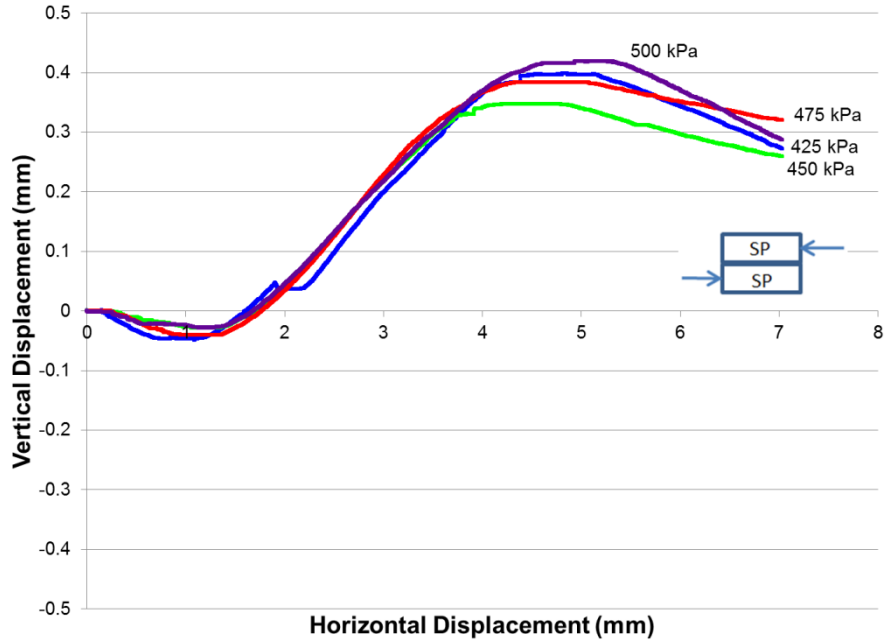


Figure A-30 Test 0021 sand 425-500 kPa vertical versus horizontal displacement

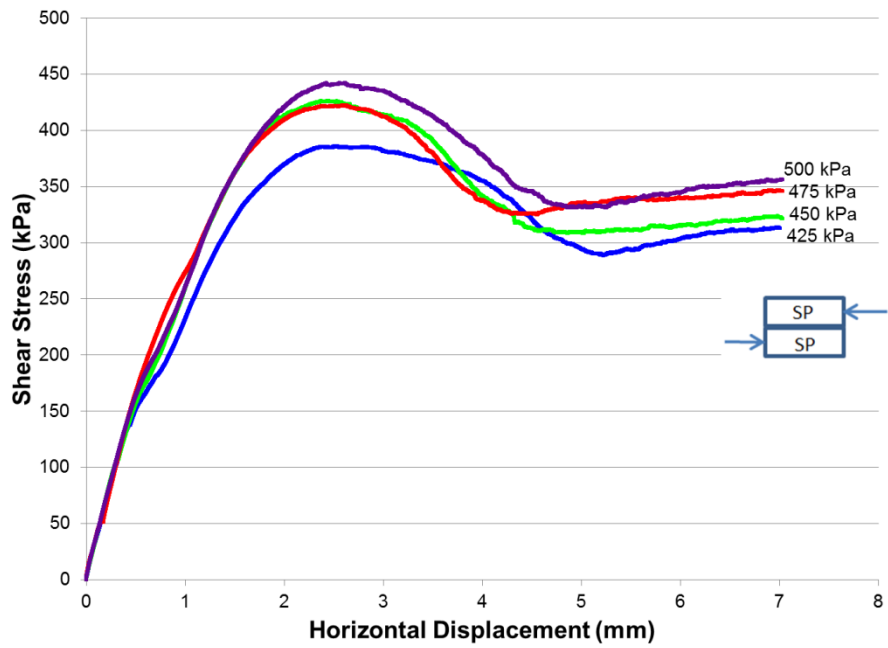


Figure A-31 Test 0022 sand 425-500kPa shear stress versus horizontal displacement

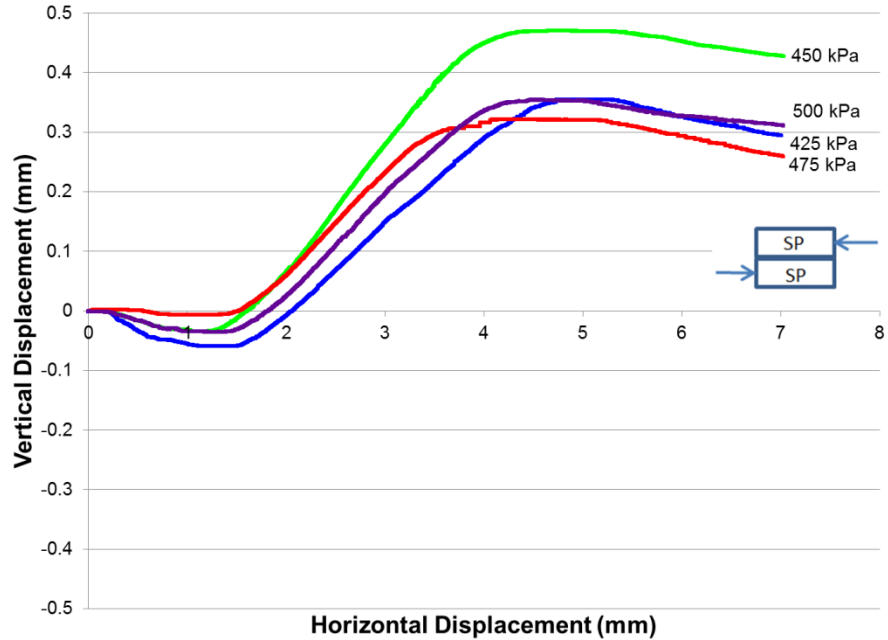
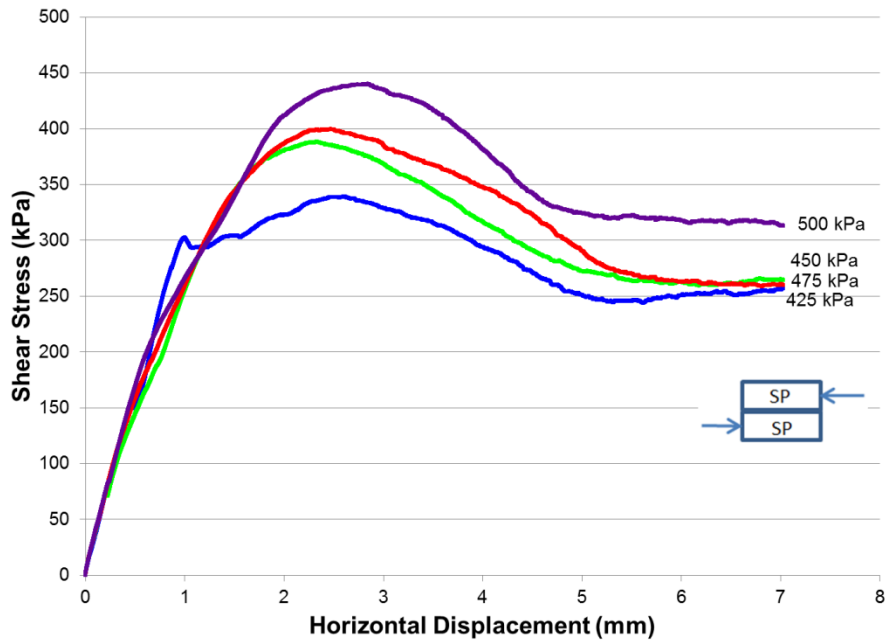
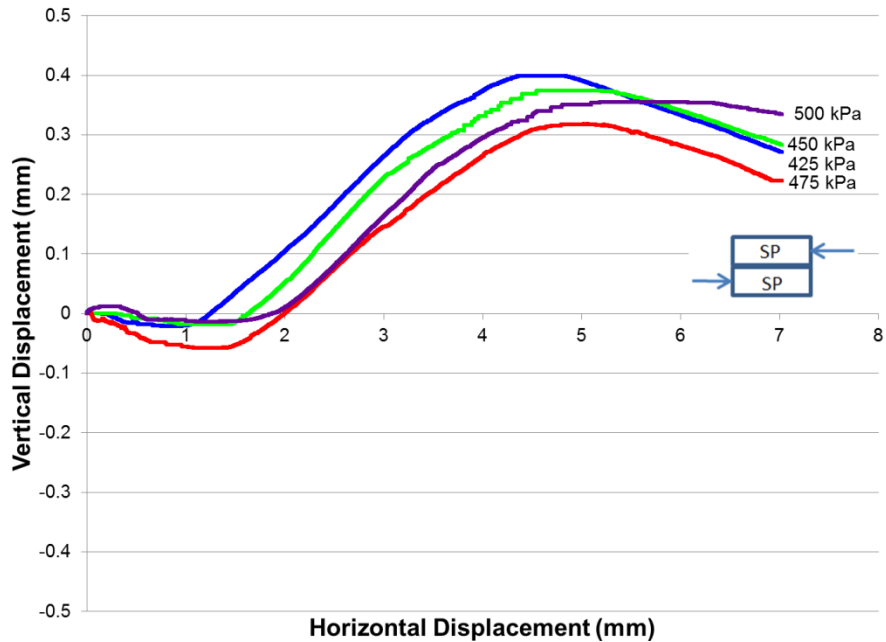


Figure A-32 Test 0022 sand 425-500 kPa vertical versus horizontal displacement



**Figure A-33** Test 0023 sand 425-500kPa shear stress versus horizontal displacement



**Figure A-34** Test 0023 sand 425-500 kPa vertical versus horizontal displacement

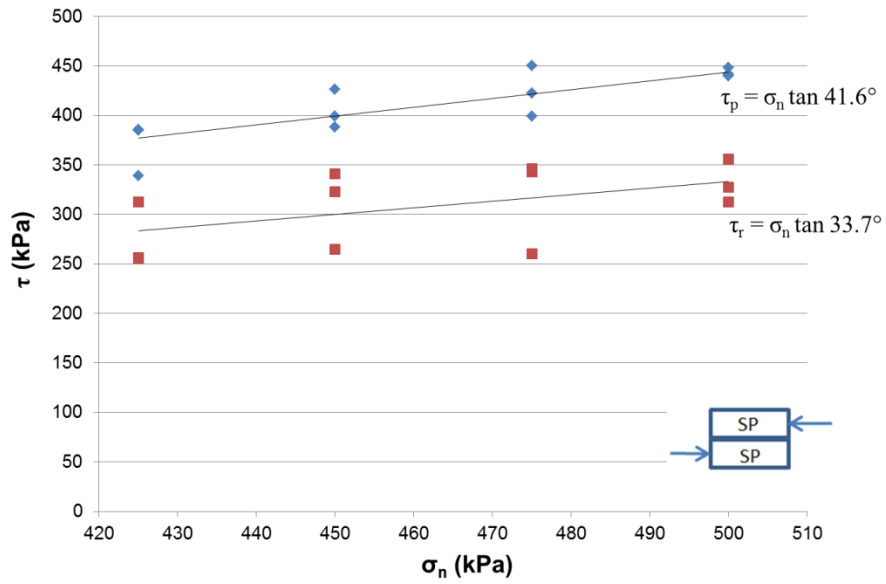


**Figure A-35** Mohr-Coulomb shear strength 425-500 kPa Brighton sand

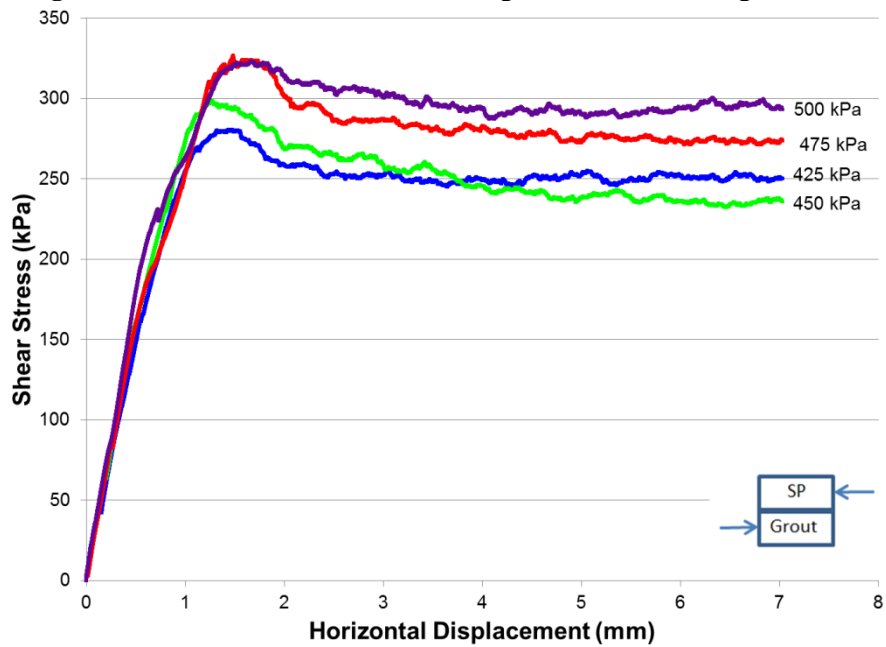


**Figure A-36** Test 0024 sand-grout 425-500kPa shear stress versus horizontal displacement

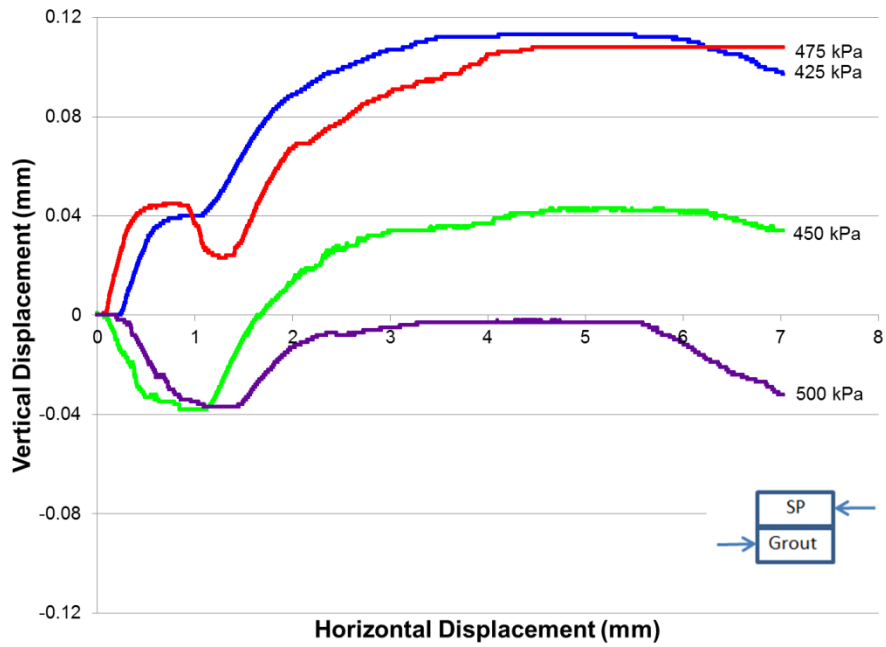


**Figure A-37** Test 0024 sand-grout 425-500 kPa vertical versus horizontal displacement

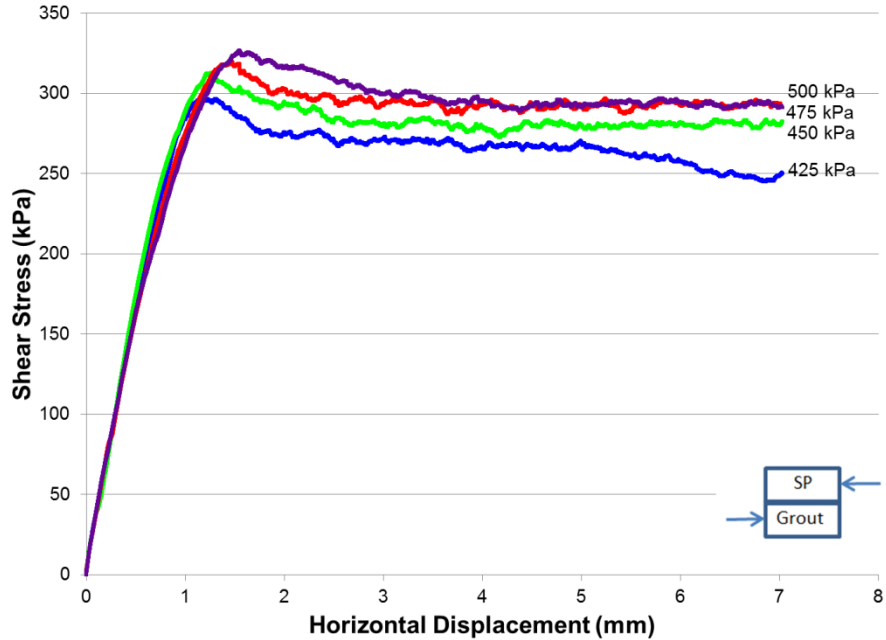


**Figure A-38** Test 0025 sand-grout 425-500kPa shear stress versus horizontal displacement

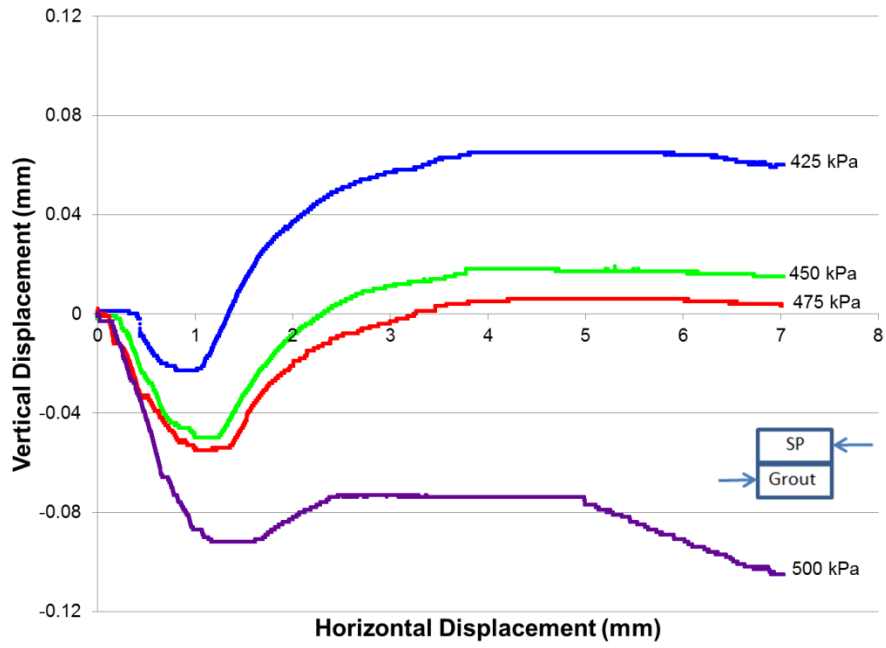


**Figure A-39** Test 0025 sand-grout 425-500 kPa vertical versus horizontal displacement

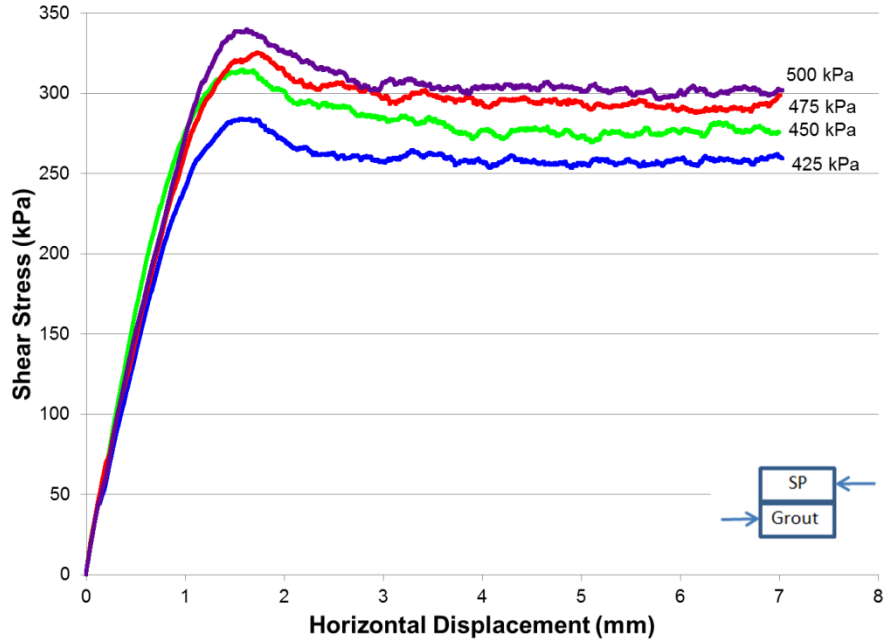


**Figure A-40** Test 0026 sand-grout 425-500kPa shear stress versus horizontal displacement

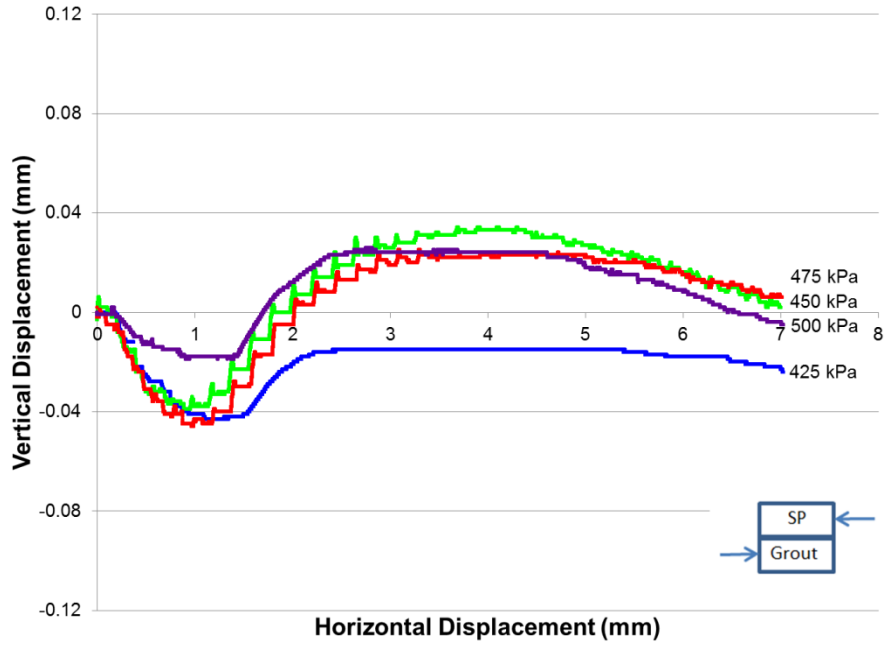


**Figure A-41** Test 0026 sand-grout 425-500 kPa vertical versus horizontal displacement

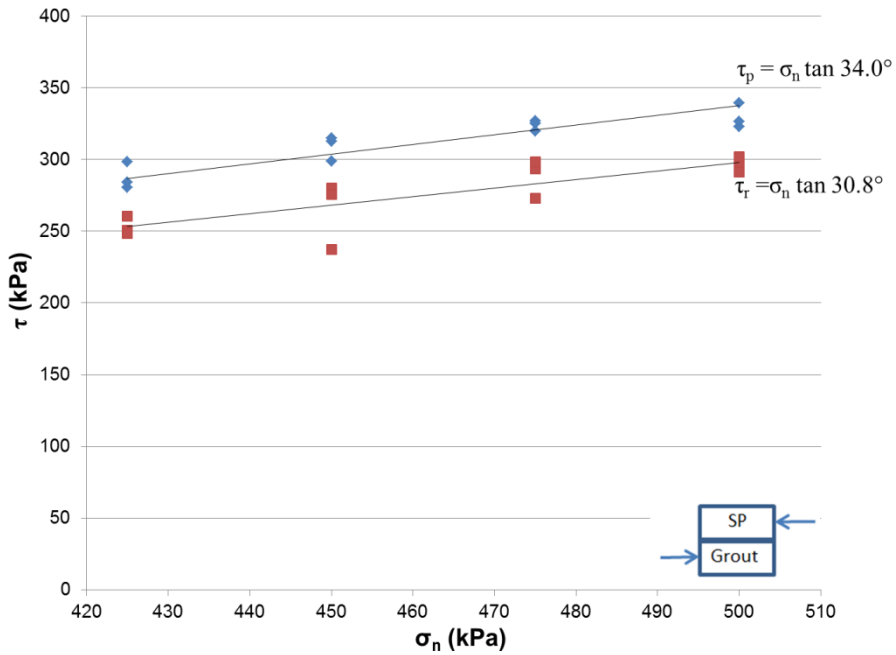


**Figure A-42** Mohr-Coulomb shear strength 425-500 kPa sand and grout

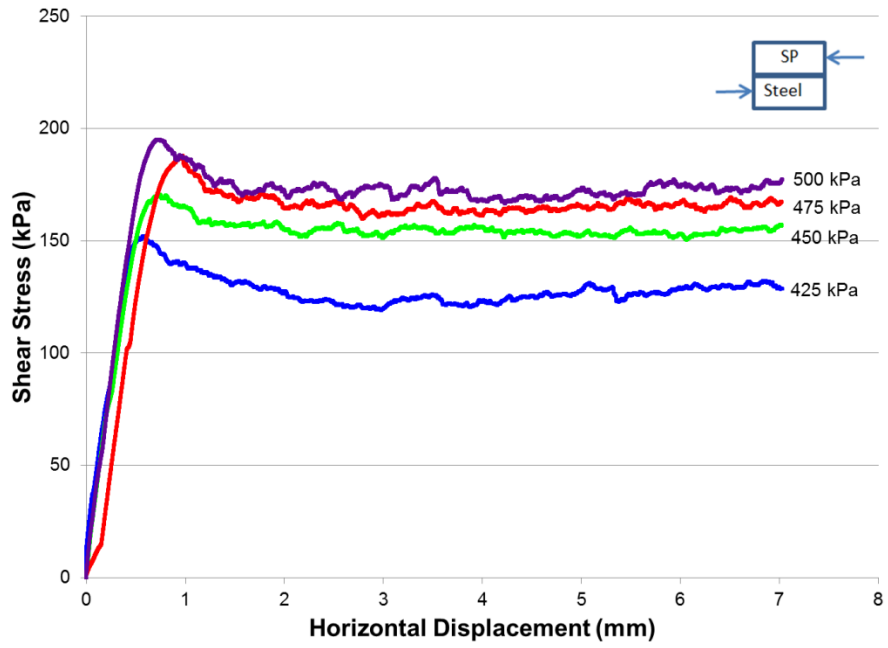


**Figure A-43** Test 0027 sand-steel 425-500kPa shear stress versus horizontal displacement

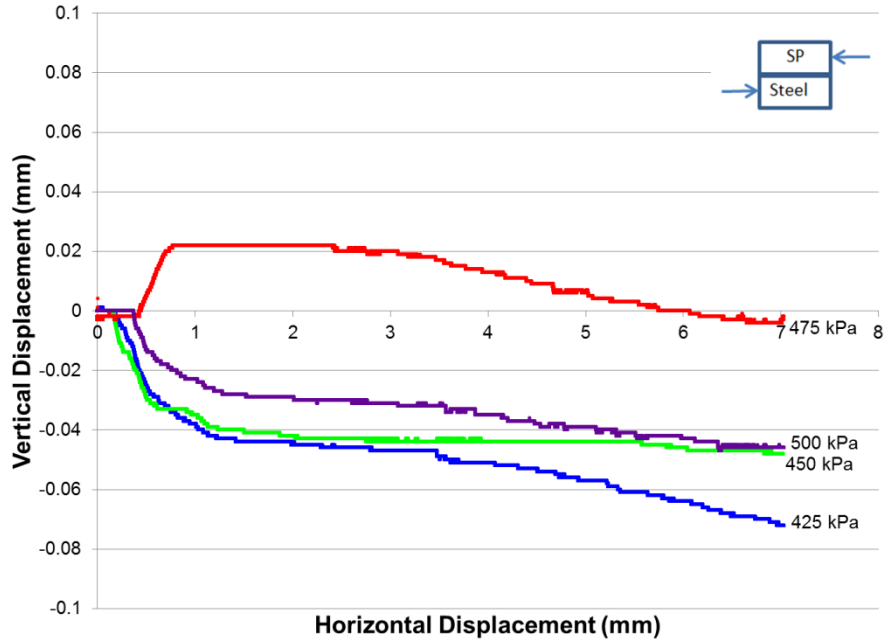


**Figure A-44** Test 0027 sand-steel 425-500 kPa vertical versus horizontal displacement

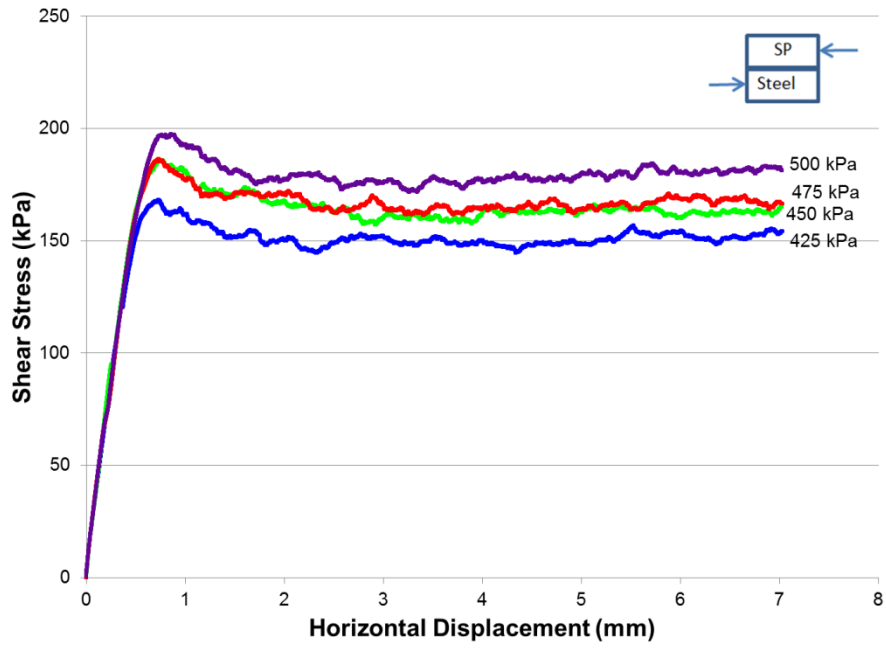


**Figure A-45** Test 0028 sand-steel 425-500kPa shear stress versus horizontal displacement

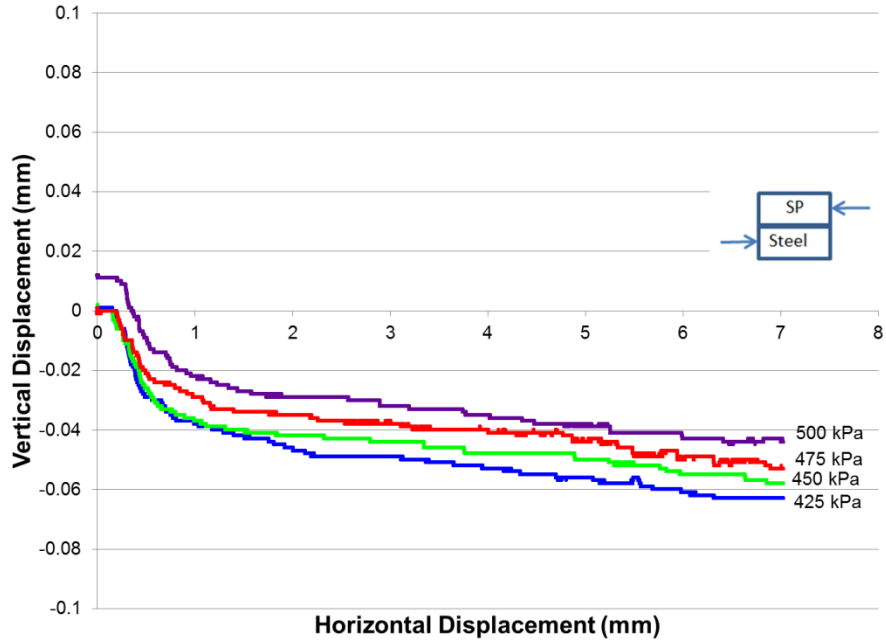


**Figure A-46** Test 0028 sand-steel 425-500 kPa vertical versus horizontal displacement

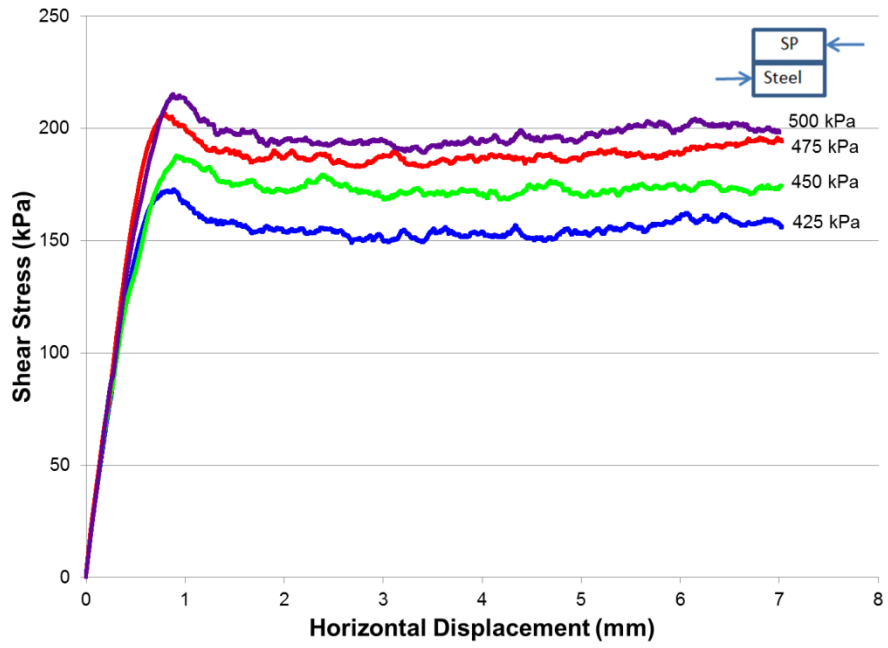


**Figure A-47** Test 0029 sand-steel 425-500kPa shear stress versus horizontal displacement

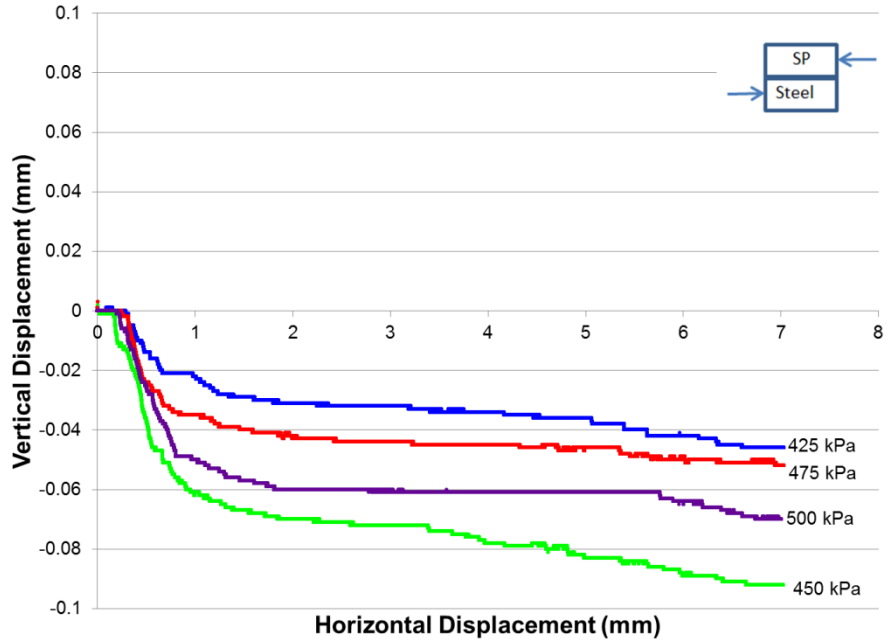


**Figure A-48** Test 0029 sand-steel 425-500 kPa vertical versus horizontal displacement

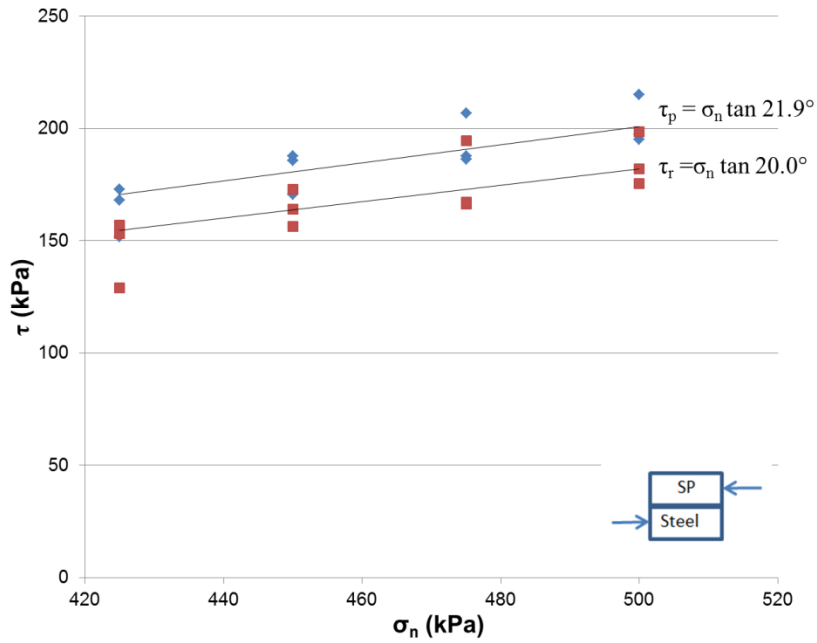


Figure A-49 Mohr-Coulomb shear strength 425-500 kPa sand and steel

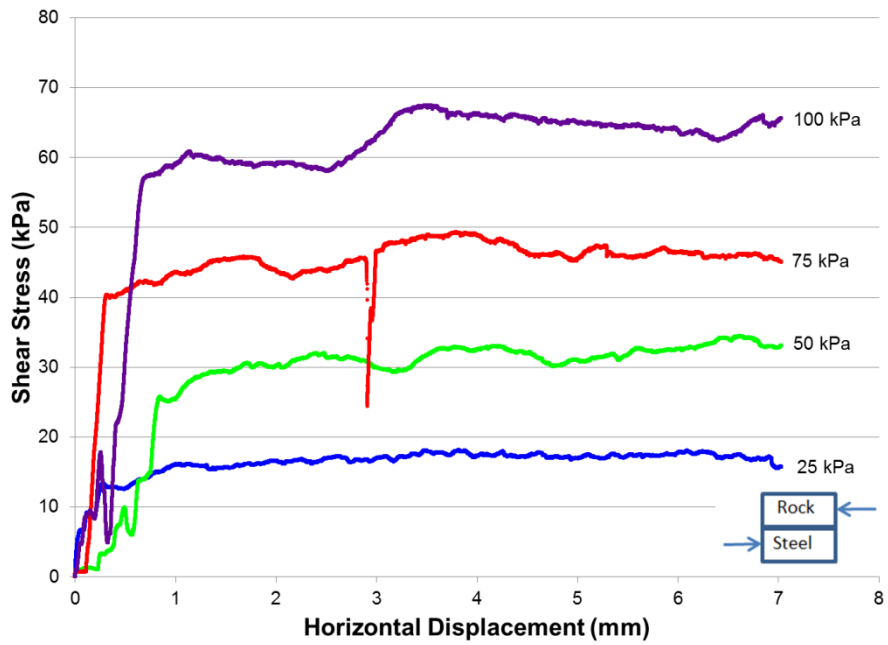
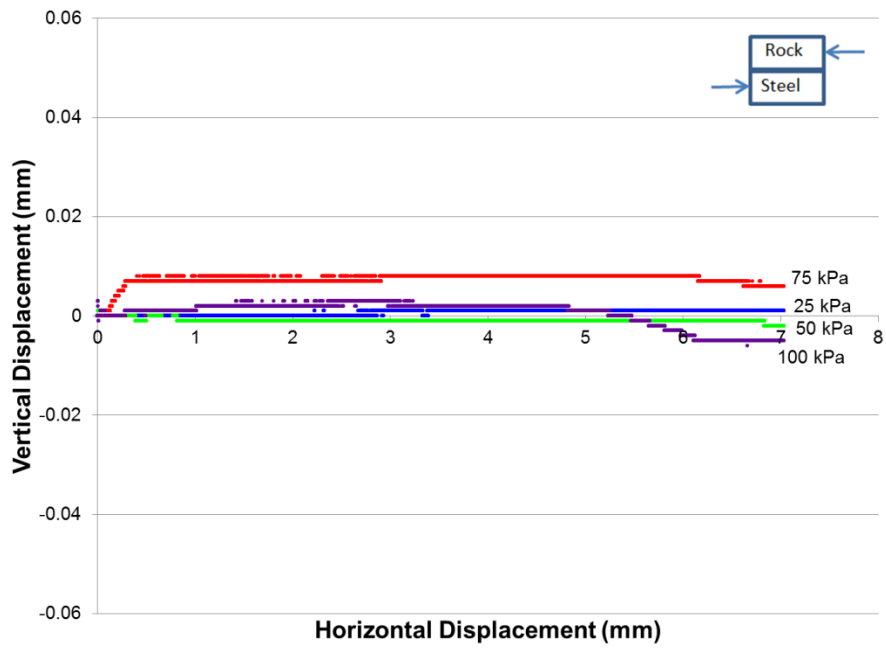
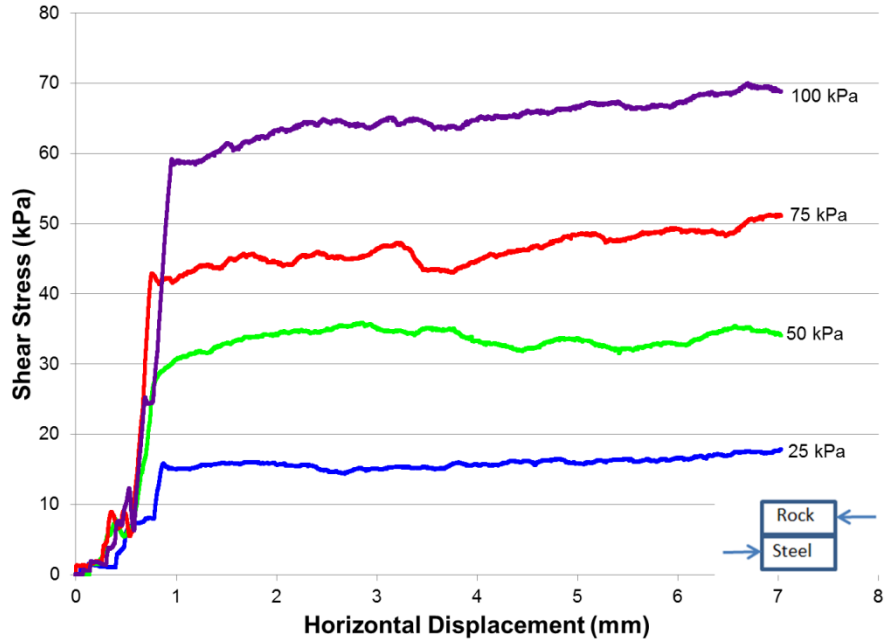


Figure A-50 Test 0031 rock-steel 25-100 kPa shear stress versus horizontal displacement



**Figure A-51** Test 0031 rock-steel 25-100 kPa vertical versus horizontal displacement



**Figure A-52** Test 0032 rock-steel 25-100 kPa shear stress versus horizontal displacement

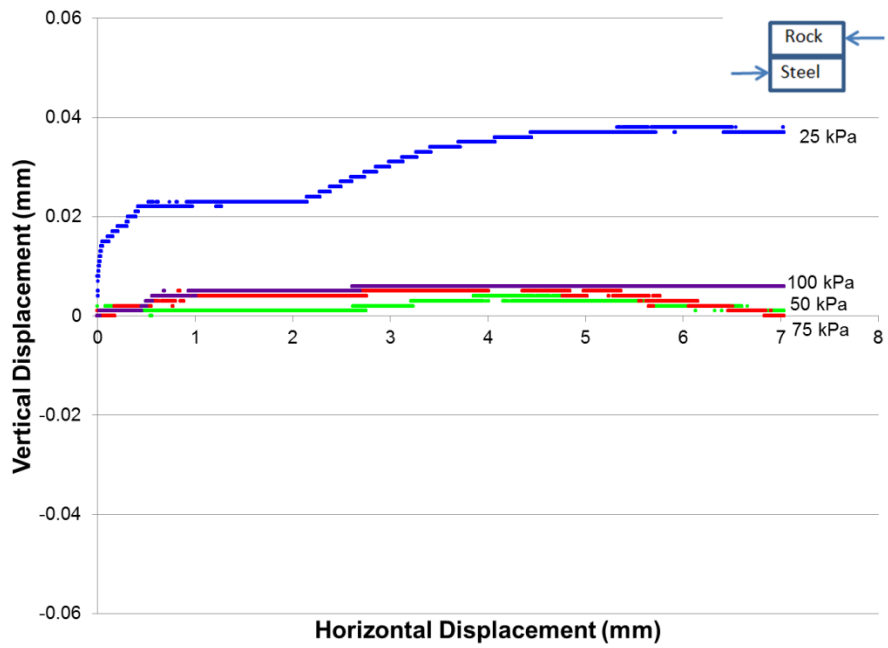


**Figure A-53** Test 0032 rock-steel 25-100 kPa vertical versus horizontal displacement

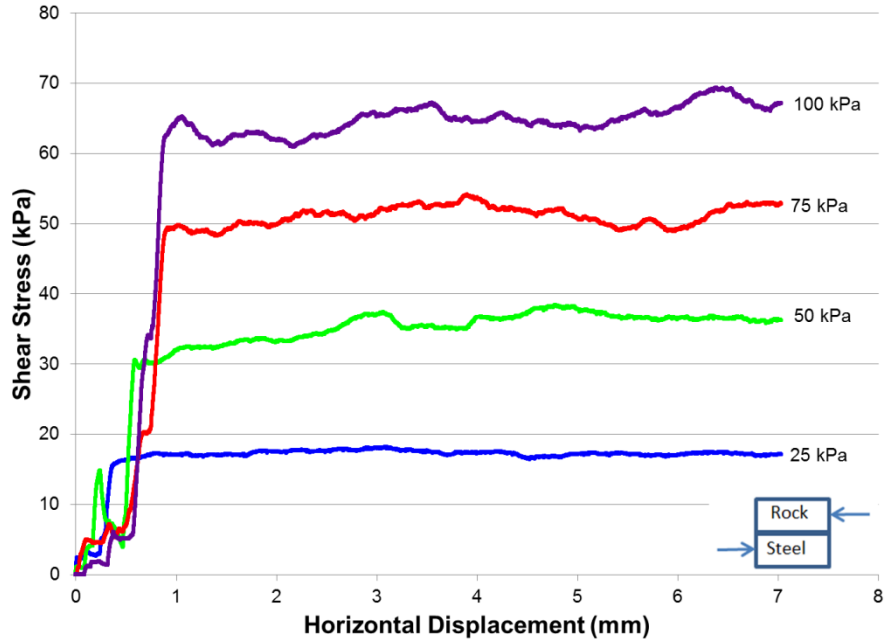


**Figure A-54** Test 0033 rock-steel 25-100 kPa shear stress versus horizontal displacement

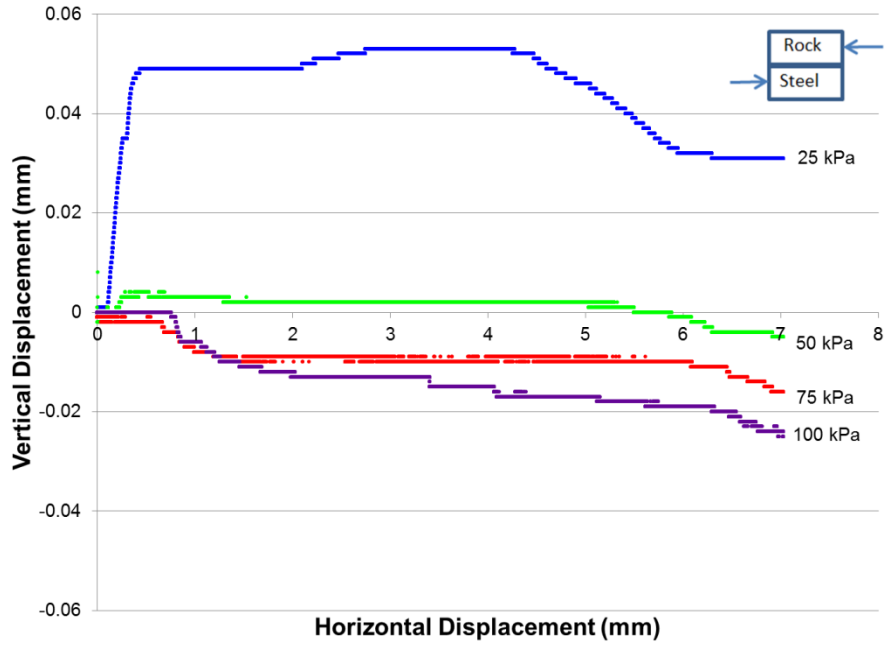


Figure A-55 Test 0033 rock-steel 25-100 kPa vertical versus horizontal displacement

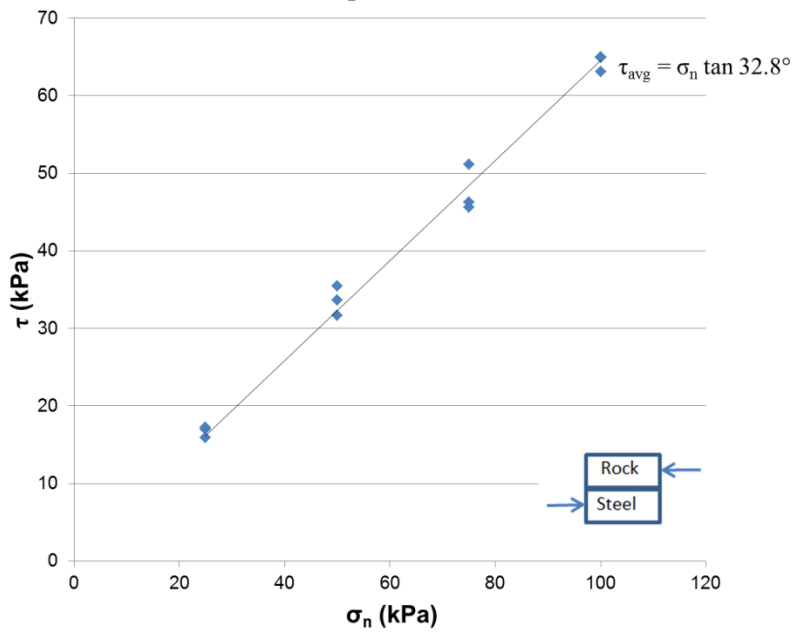


Figure A-56 Mohr-Coulomb shear strength 25-100 kPa rock and steel

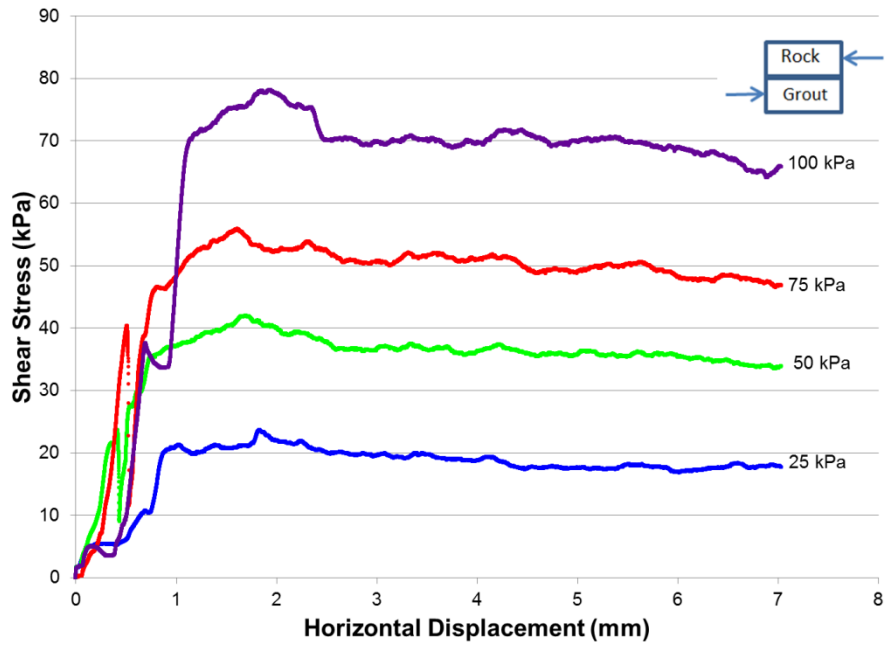


Figure A-57 Test 0034 rock-grout 25-100 kPa shear stress versus horizontal displacement

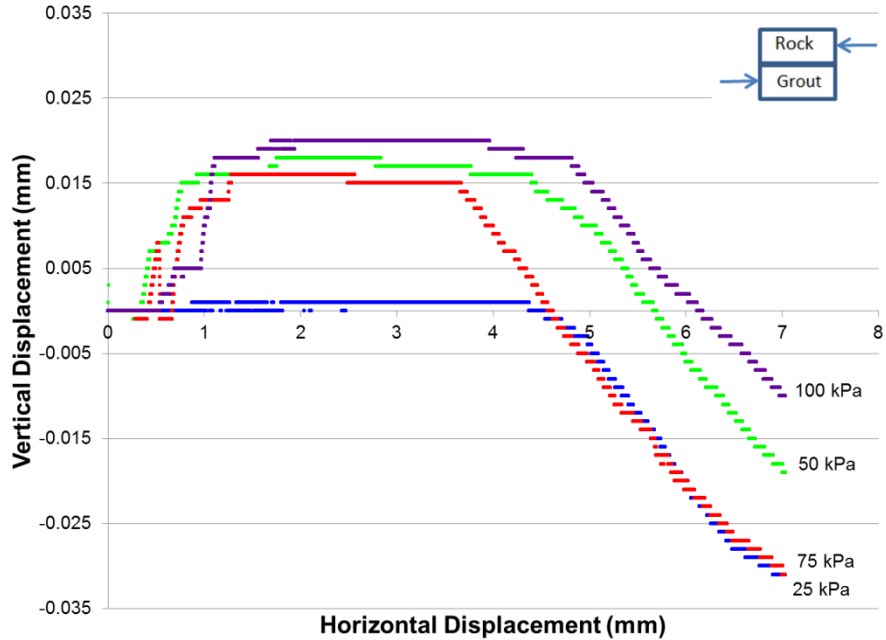
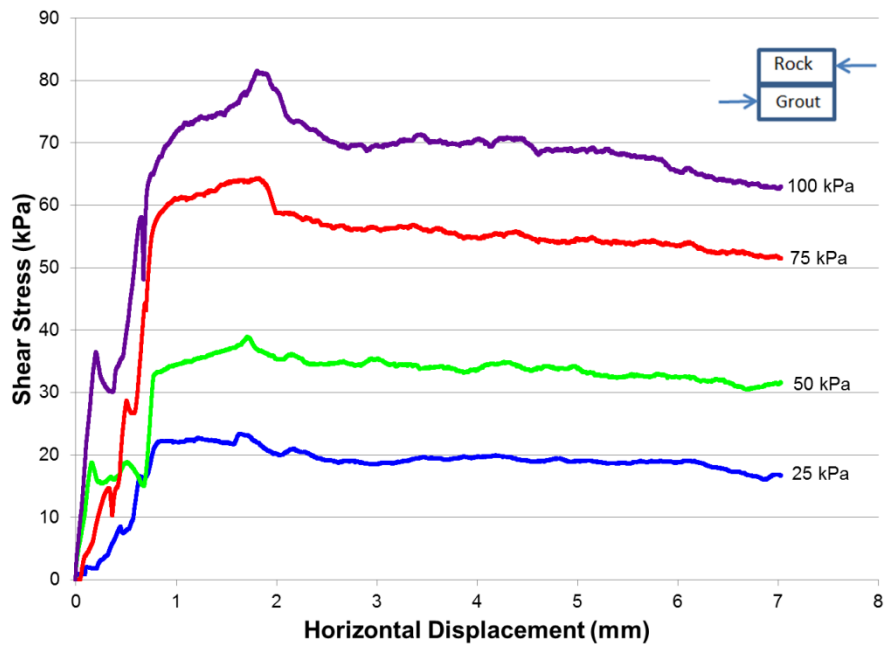
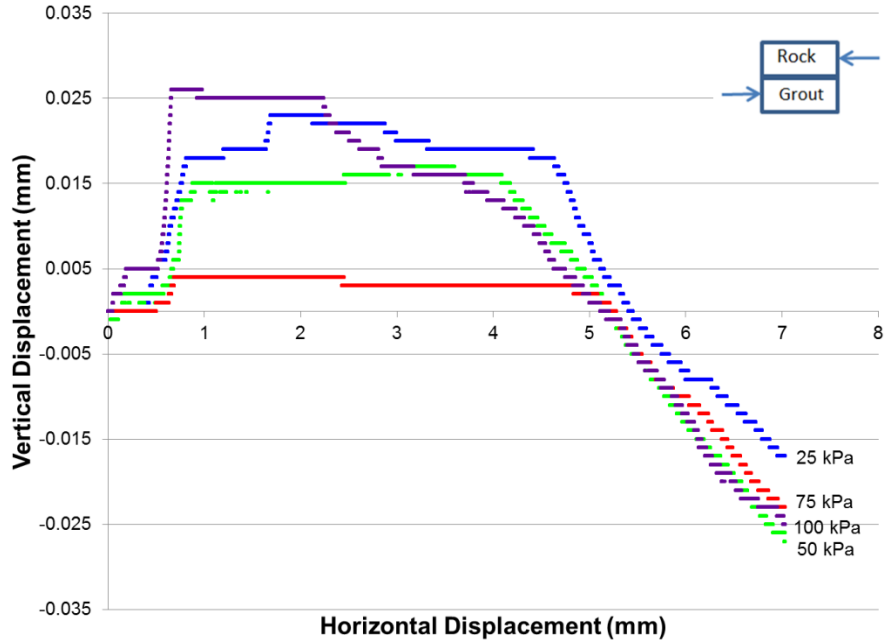


Figure A-58 Test 0034 rock-grout 25-100 kPa vertical versus horizontal displacement



**Figure A-59** Test 0035 rock-grout 25-100 kPa shear stress versus horizontal displacement



**Figure A-60** Test 0035 rock-grout 25-100 kPa vertical versus horizontal displacement

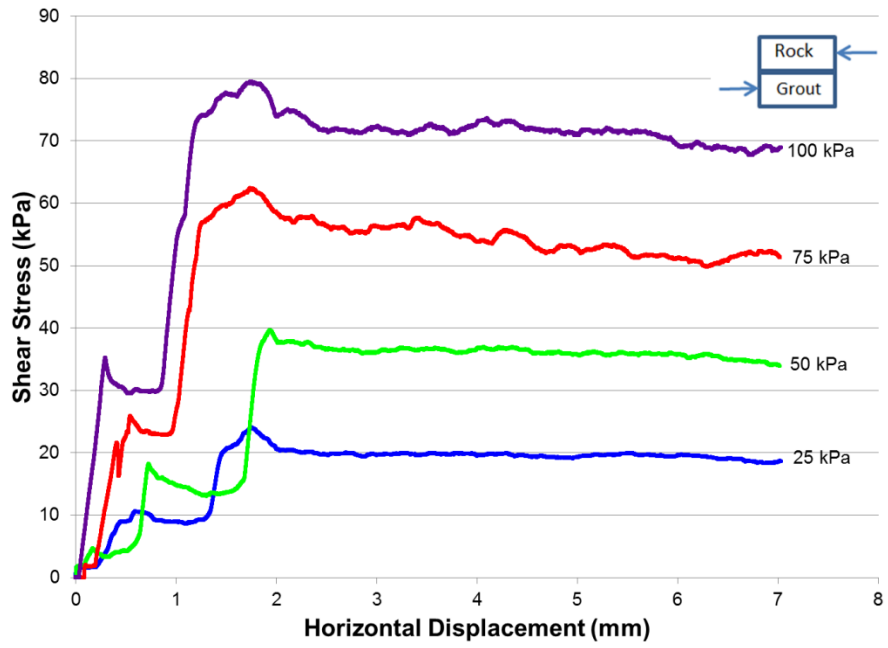


**Figure A-61** Test 0036 rock-grout 25-100 kPa shear stress versus horizontal displacement

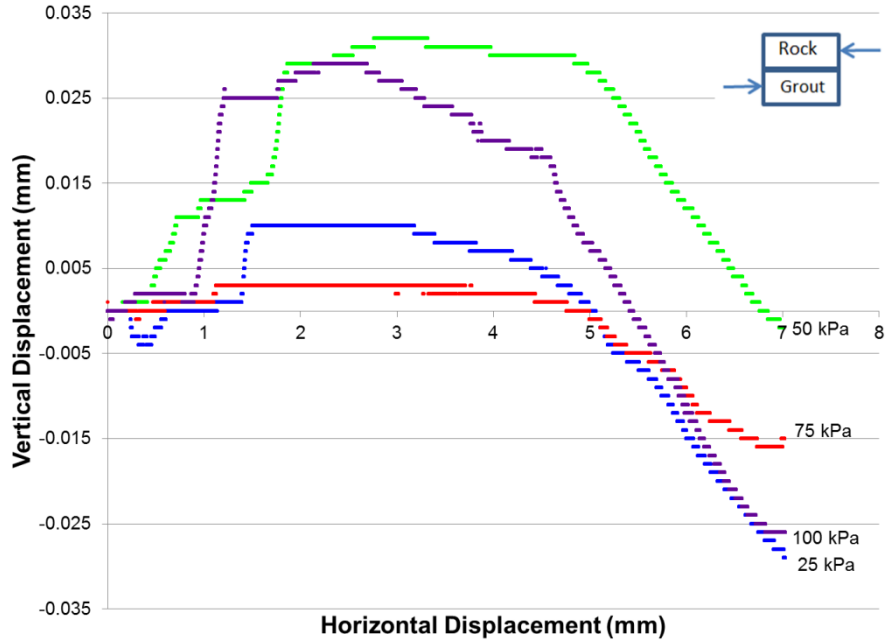


**Figure A-62** Test 0036 rock-grout 25-100 kPa vertical versus horizontal displacement

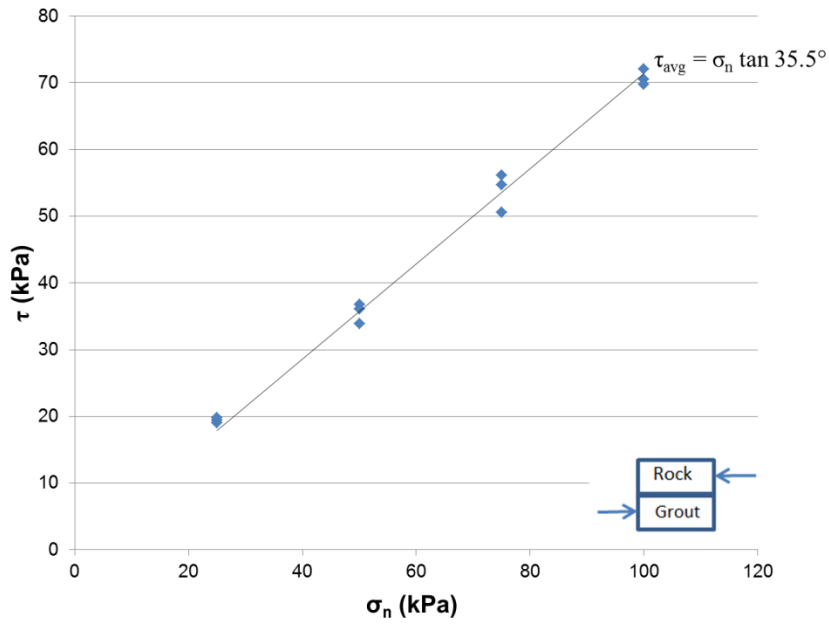


**Figure A-63** Mohr-Coulomb shear strength 25-100 kPa rock and grout

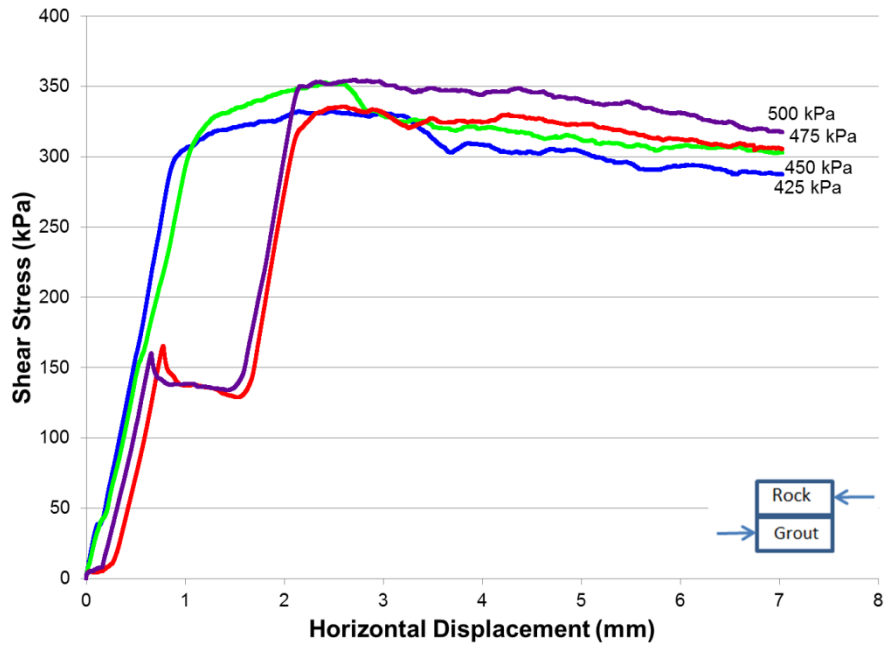


**Figure A-64** Test 0037 rock-grout 425-500 kPa shear stress versus horizontal displacement

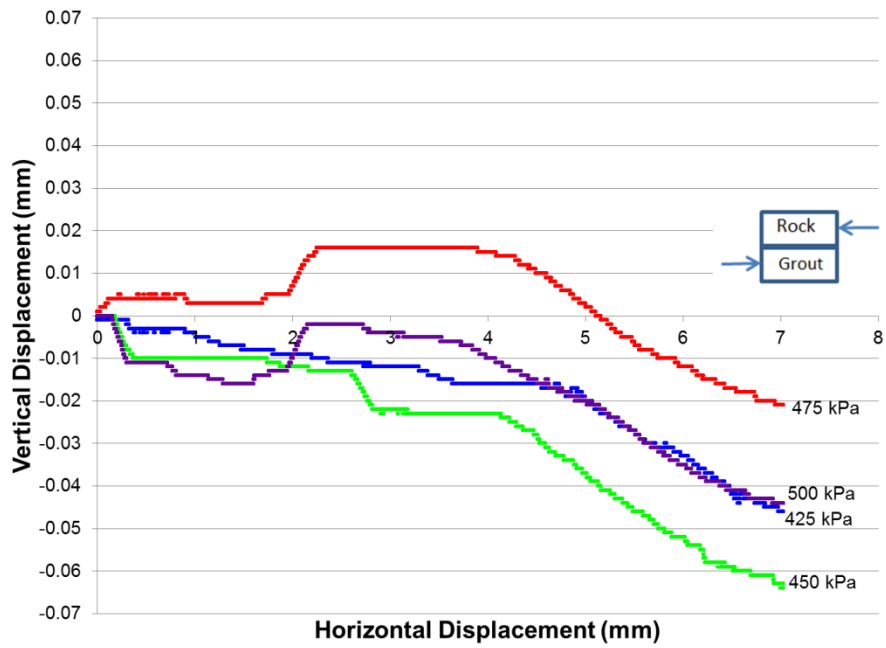


**Figure A-65** Test 0037 rock-grout 425-500 kPa vertical versus horizontal displacement

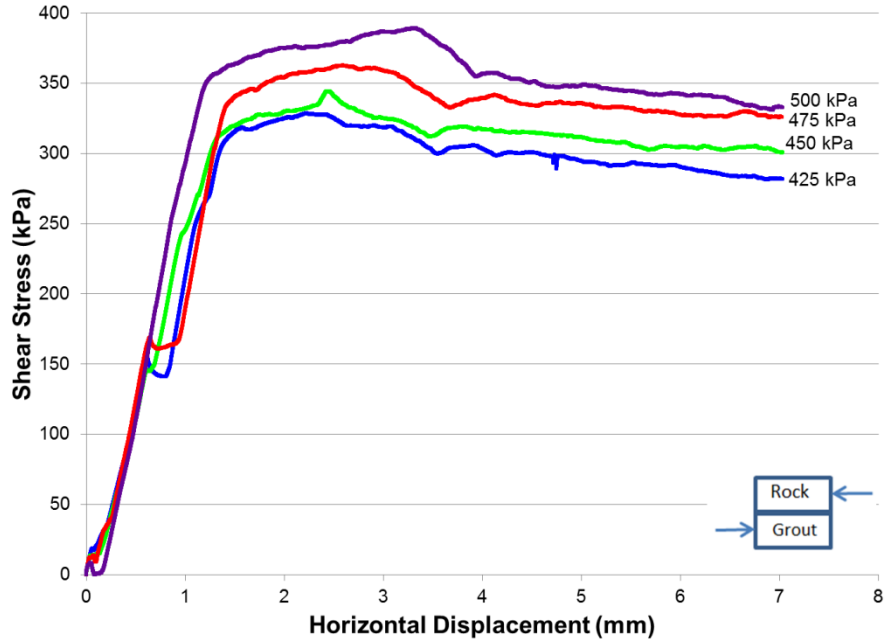


**Figure A-66** Test 0038 rock-grout 425-500 kPa shear stress versus horizontal displacement

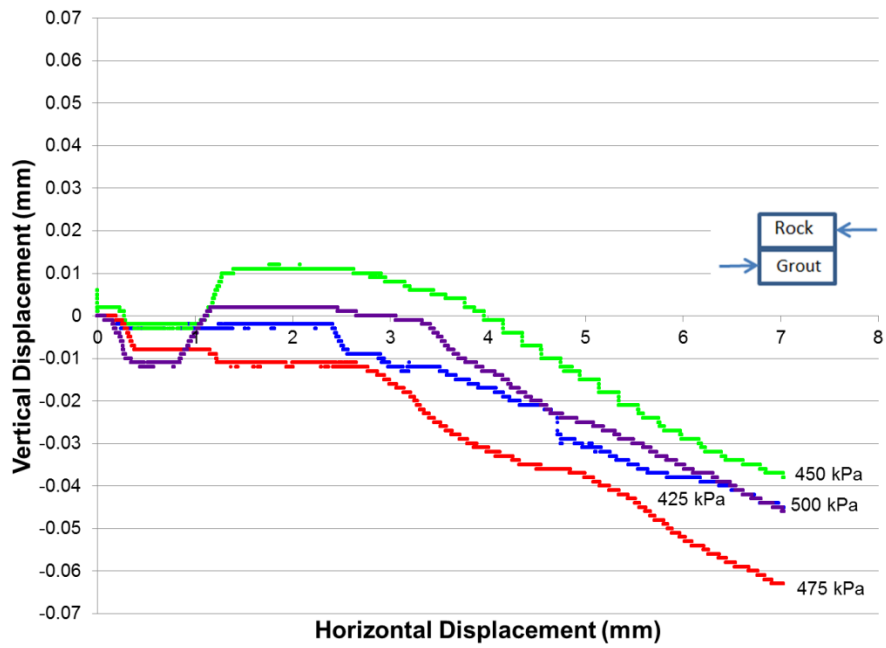


**Figure A-67** Test 0038 rock-grout 425-500 kPa vertical versus horizontal displacement

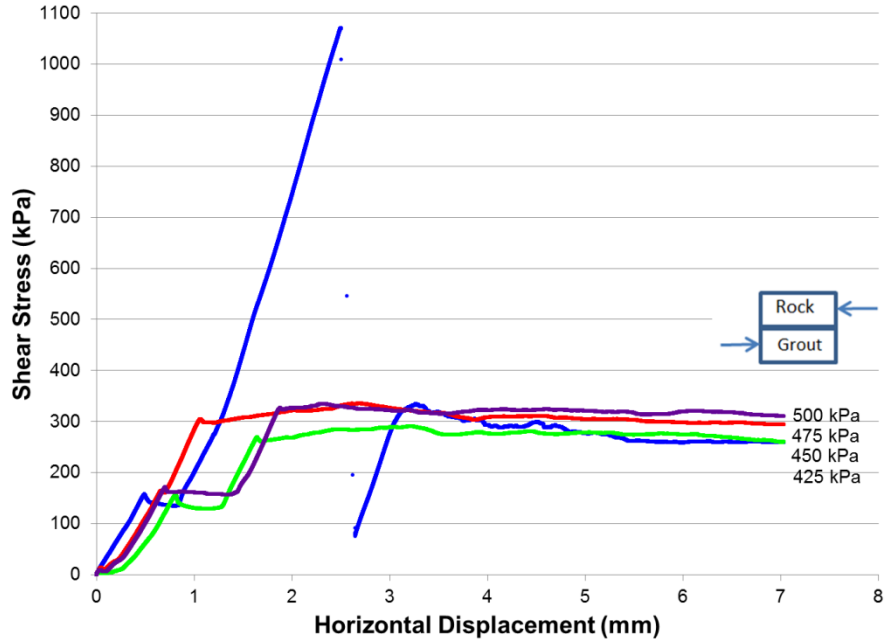


**Figure A-68** Test 0039 rock-grout 425-500 kPa shear stress versus horizontal displacement

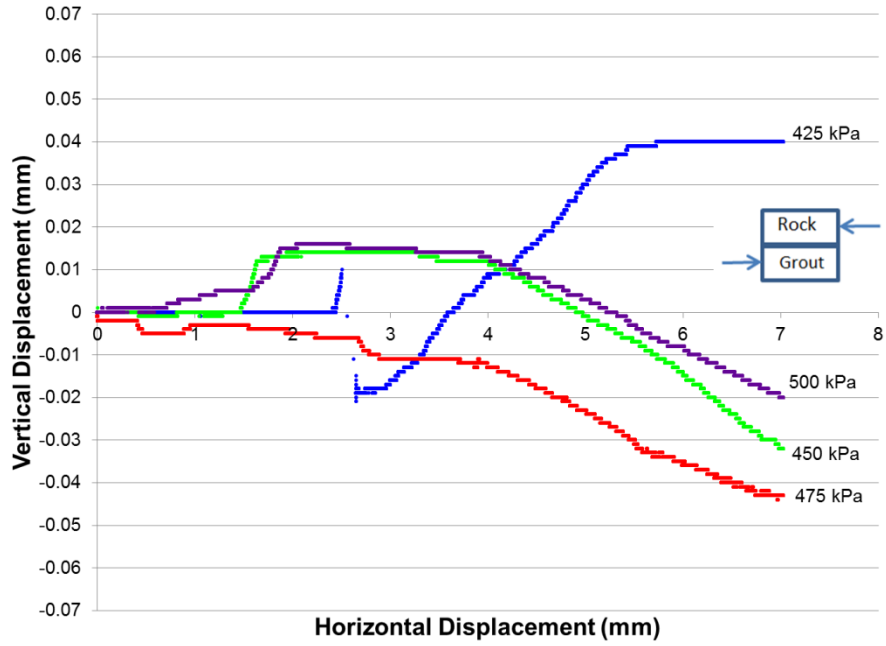


**Figure A-69** Test 0039 rock-grout 425-500 kPa vertical versus horizontal displacement

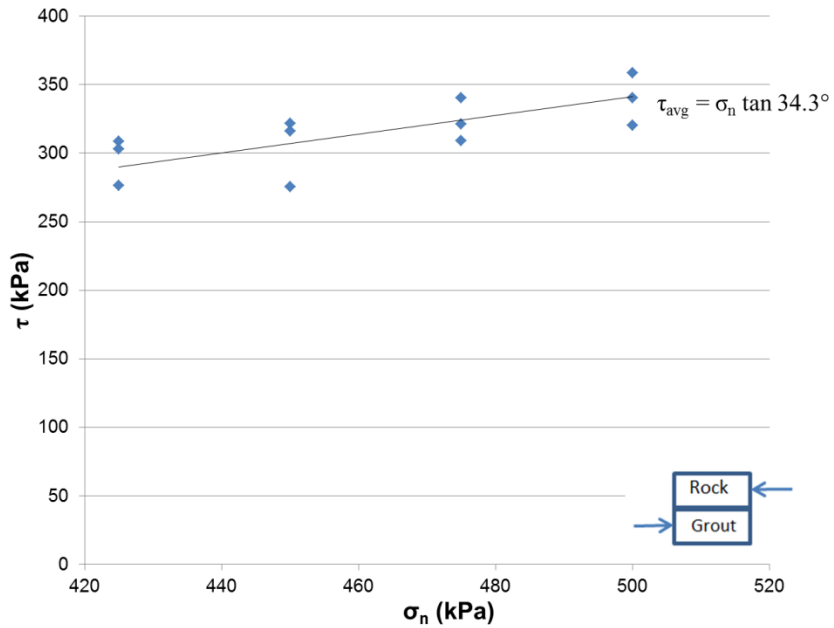


**Figure A-70** Mohr-Coulomb shear strength 425-500 kPa rock and grout

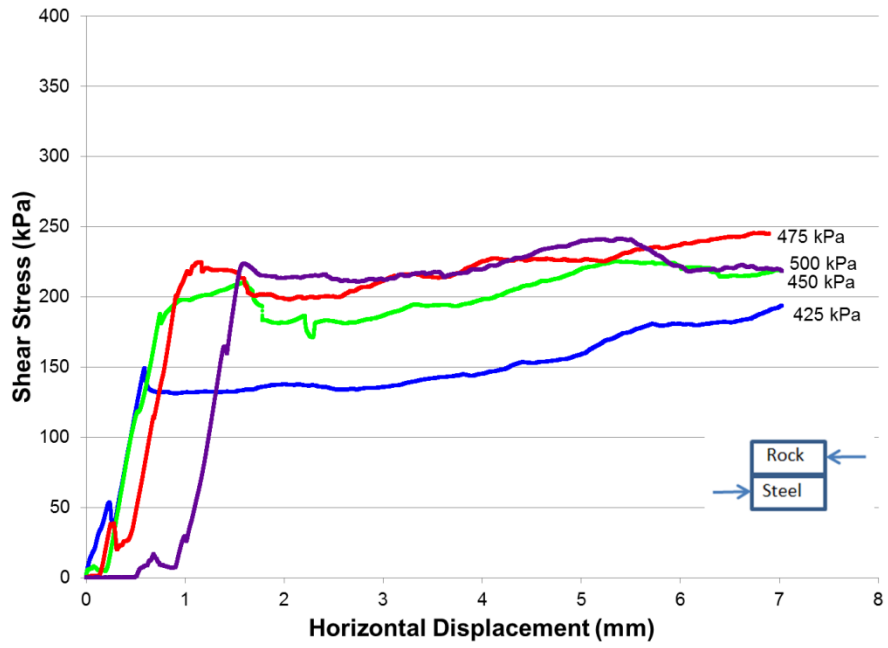


**Figure A-71** Test 0040 rock-steel 425-500 kPa shear stress versus horizontal displacement

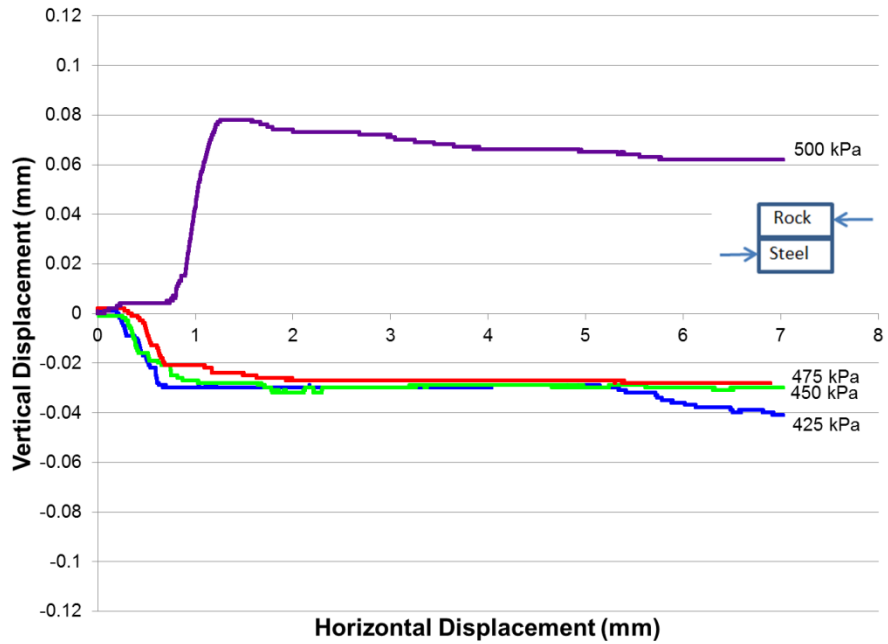


**Figure A-72** Test 0040 rock-steel 425-500 kPa vertical versus horizontal displacement

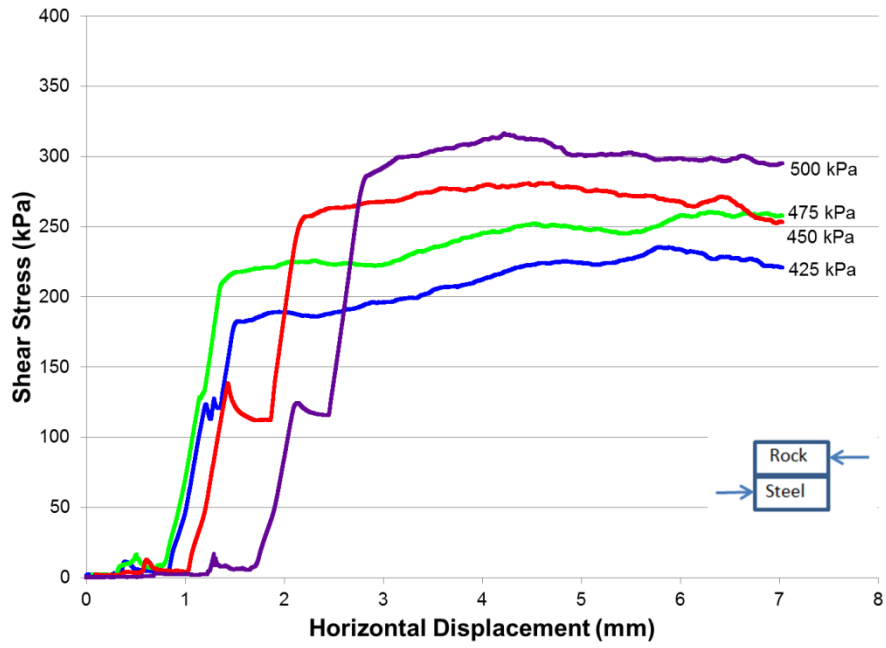


**Figure A-73** Test 0041 rock-steel 425-500 kPa shear stress versus horizontal displacement

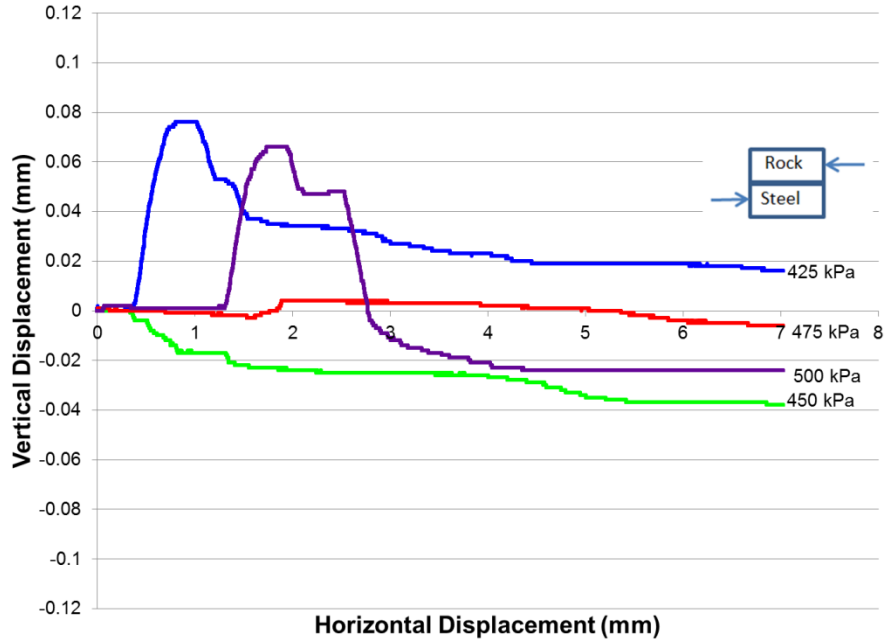


**Figure A-74** Test 0041 rock-steel 425-500 kPa vertical versus horizontal displacement

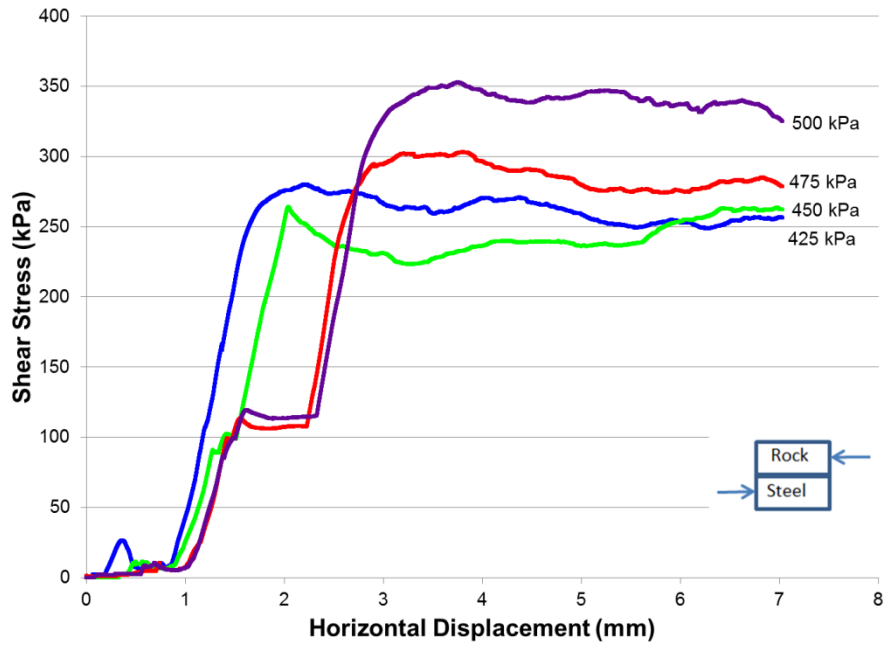


**Figure A-75** Test 0042 rock-steel 425-500 kPa shear stress versus horizontal displacement

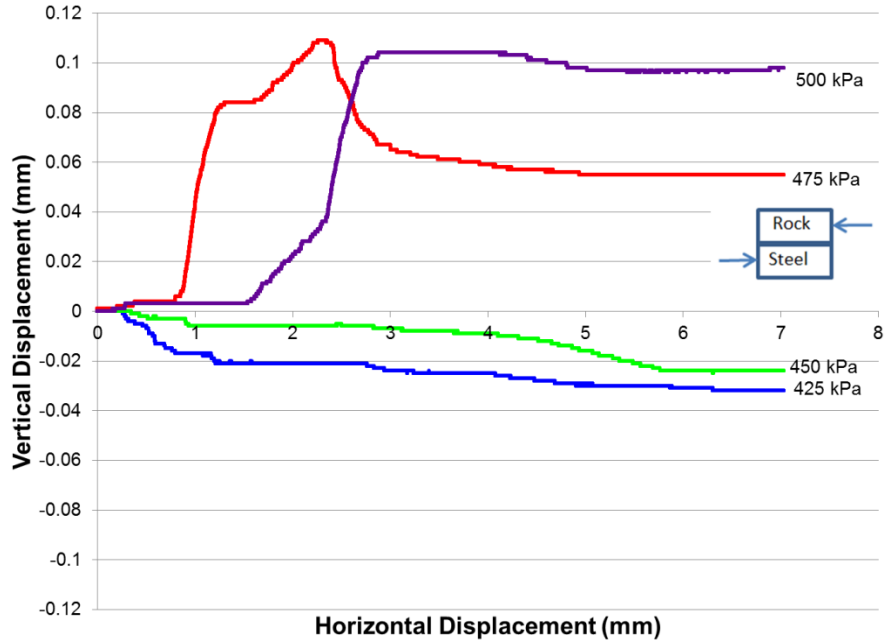


**Figure A-76** Test 0042 rock-steel 425-500 kPa vertical versus horizontal displacement

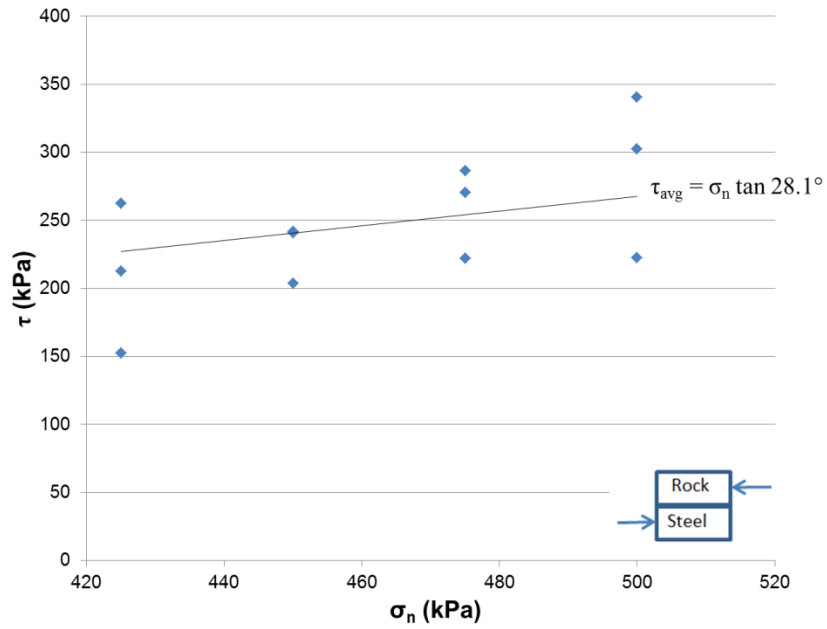


Figure A-77 Mohr-Coulomb shear strength 425-500 kPa rock and steel

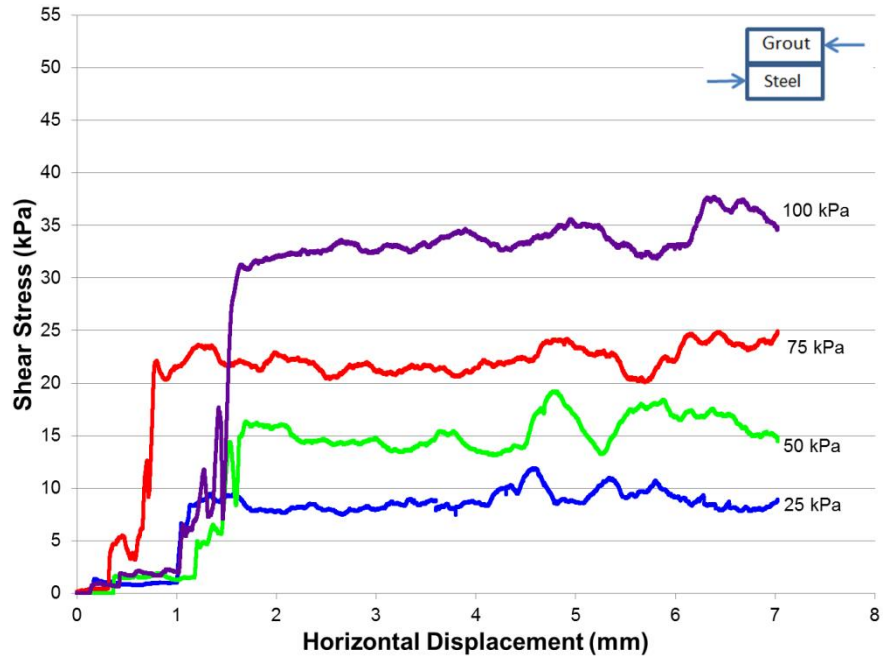
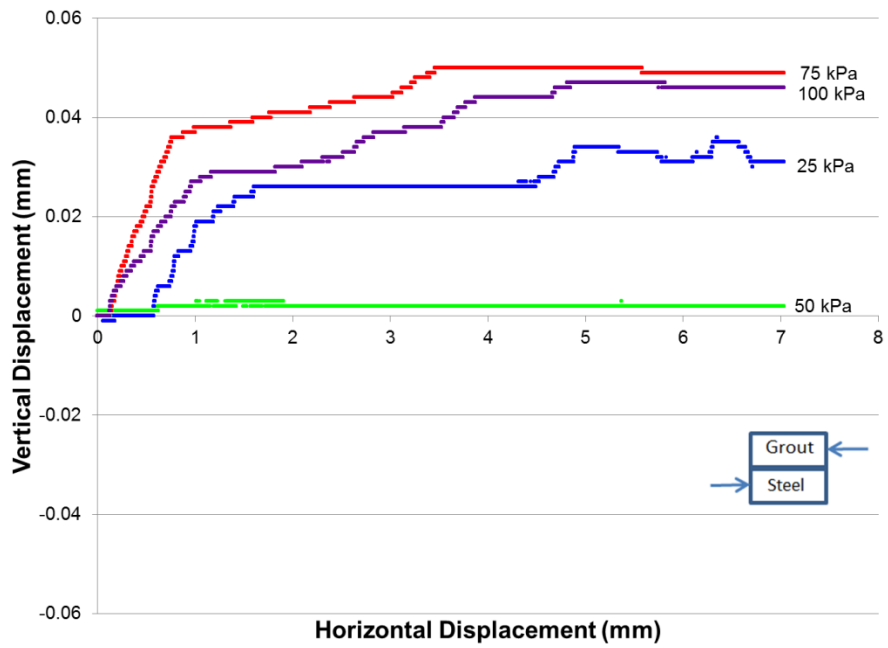
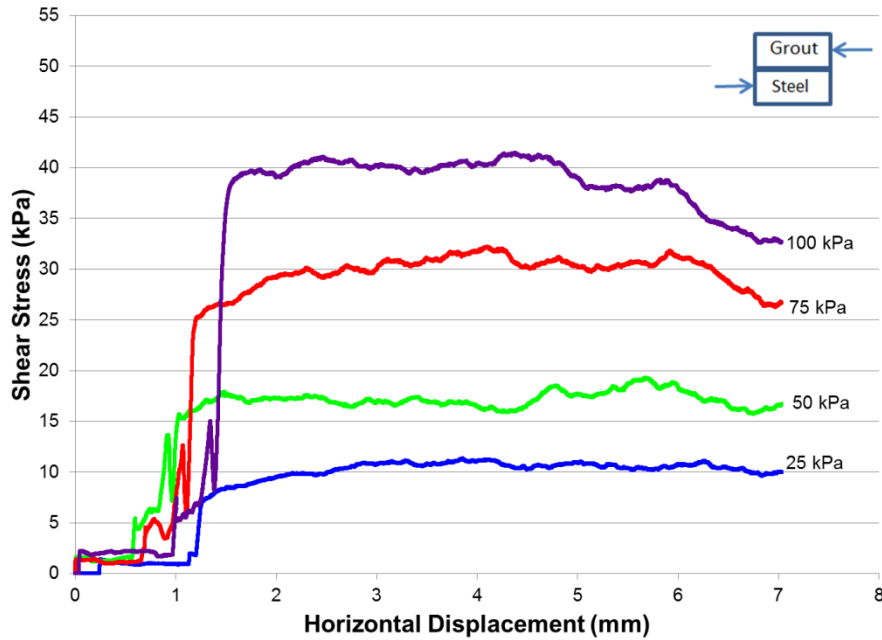


Figure A-78 Test 0043 grout-steel 25-100 kPa shear stress versus horizontal displacement



**Figure A-79** Test 0043 grout-steel 25-100 kPa vertical versus horizontal displacement



**Figure A-80** Test 0044 grout-steel 25-100 kPa shear stress versus horizontal displacement

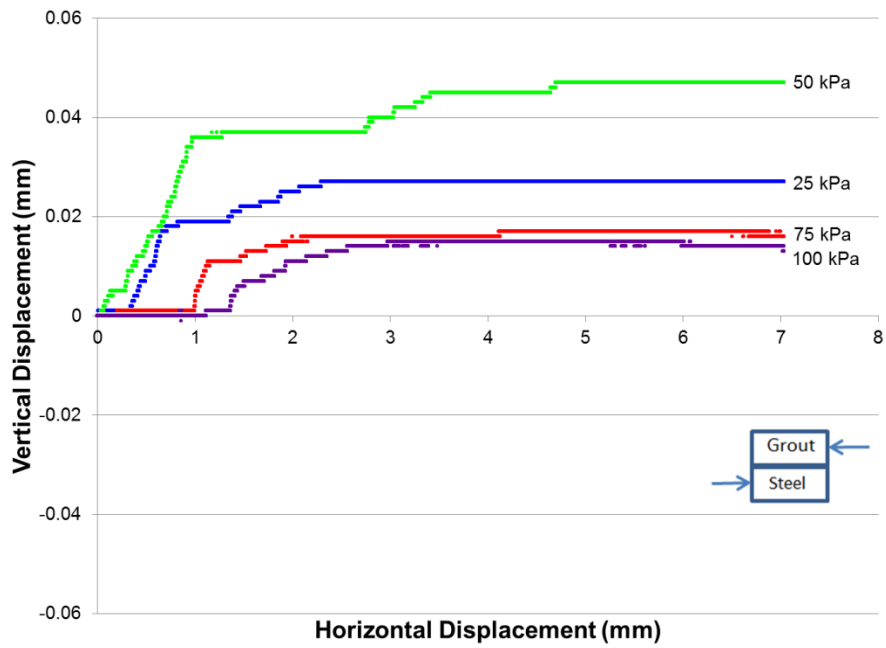


**Figure A-81** Test 0044 grout-steel 25-100 kPa vertical versus horizontal displacement

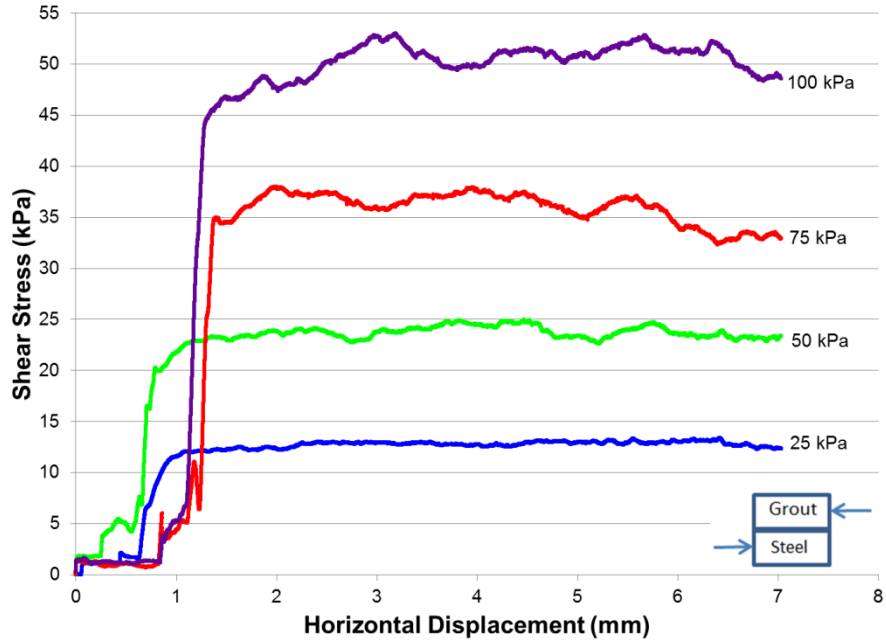


**Figure A-82** Test 0045 grout-steel 25-100 kPa shear stress versus horizontal displacement

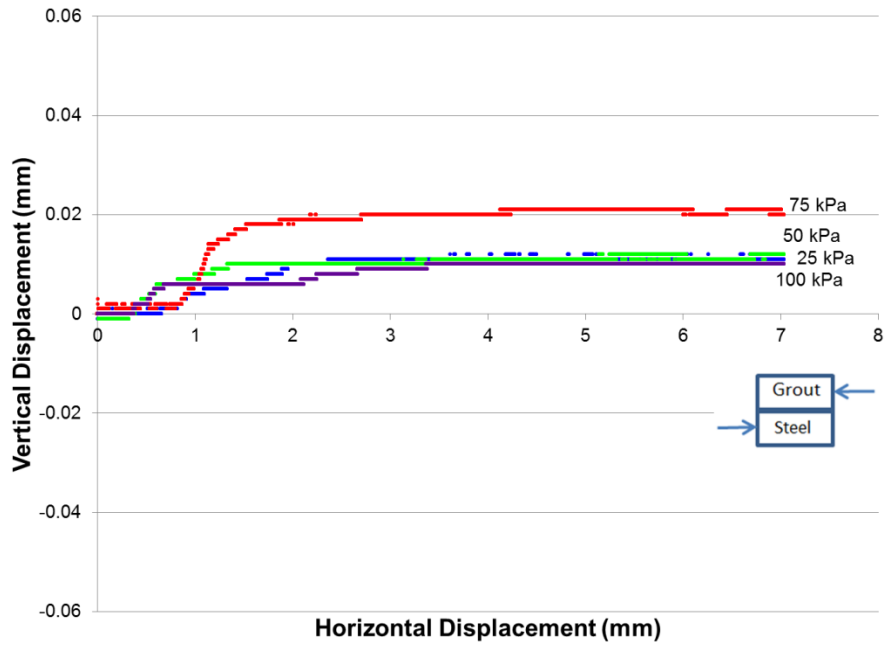


**Figure A-83** Test 0045 grout-steel 25-100 kPa vertical versus horizontal displacement

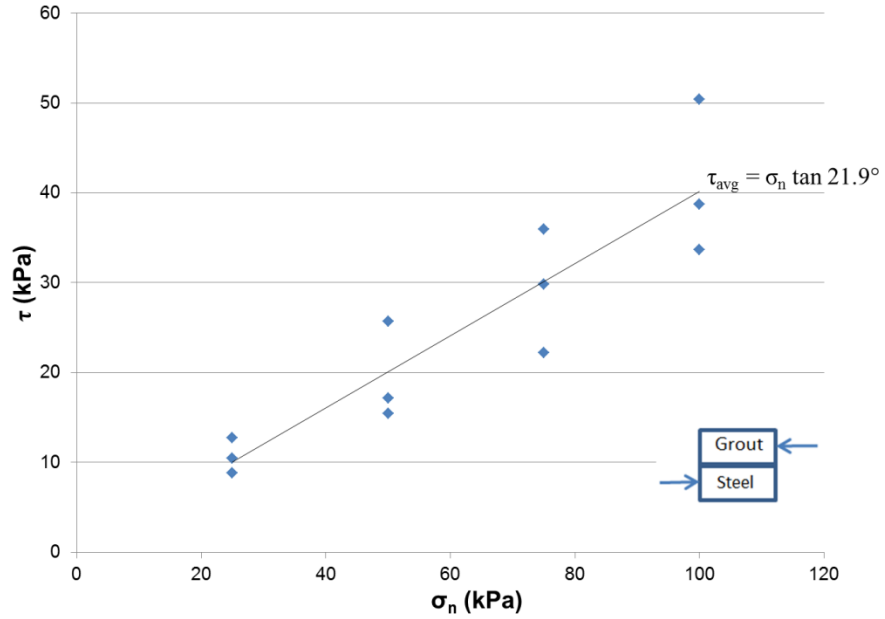


**Figure A-84** Mohr-Coulomb shear strength 25-100 kPa grout and steel

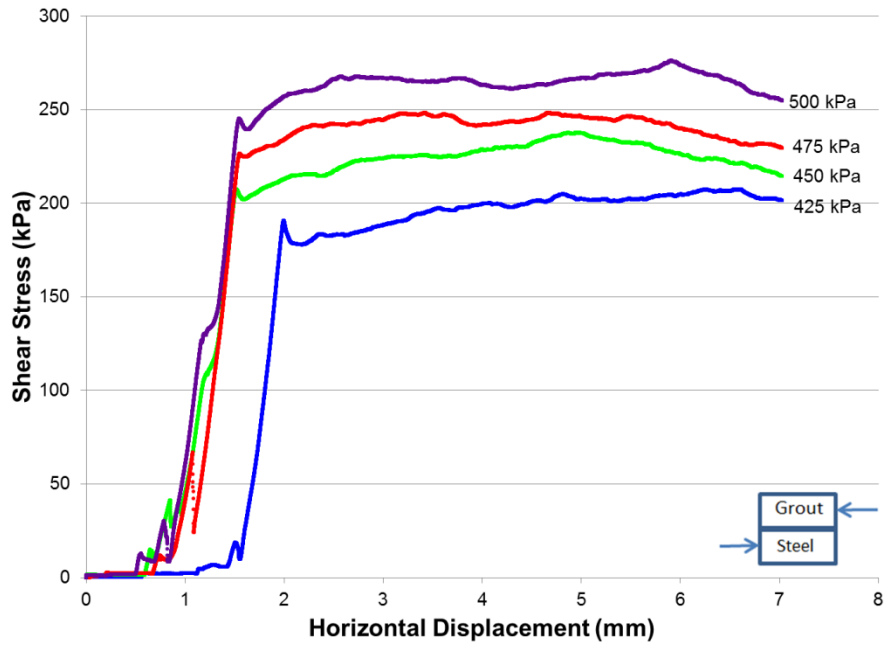


Figure A-85 Test 0046 grout-steel 425-500 kPa shear stress versus horizontal displacement

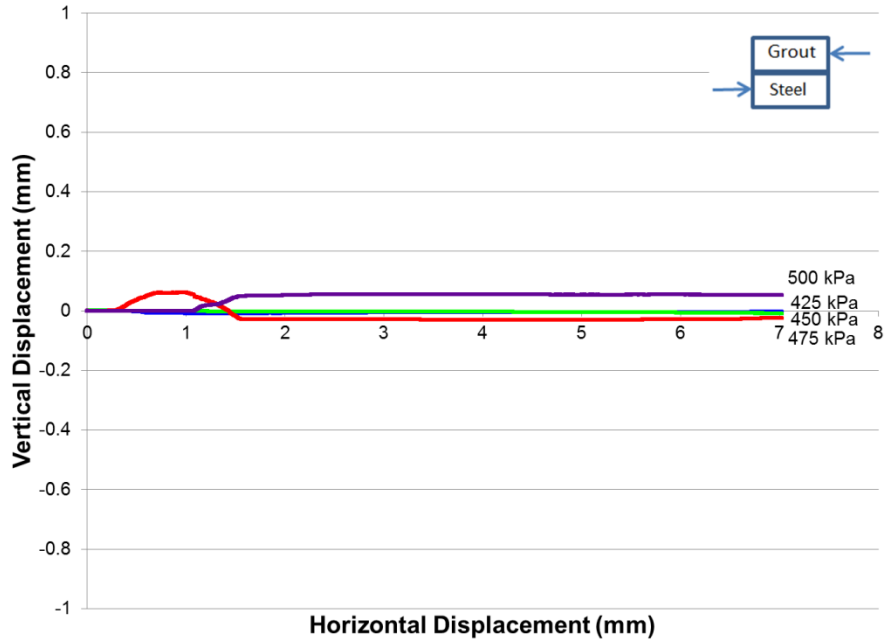


Figure A-86 Test 0046 grout-steel 425-500 kPa vertical versus horizontal displacement

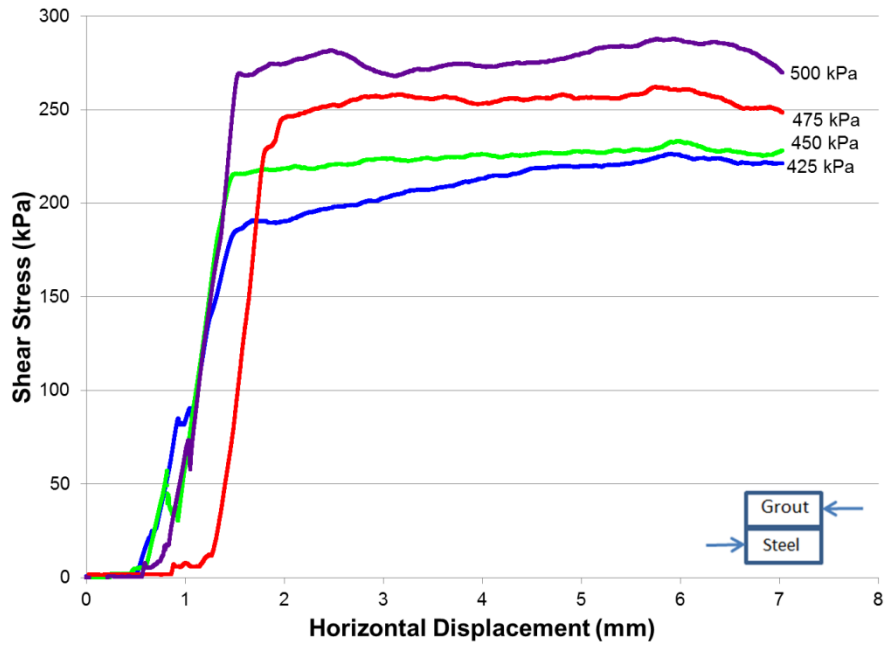


Figure A-87 Test 0047 grout-steel 425-500 kPa shear stress versus horizontal displacement

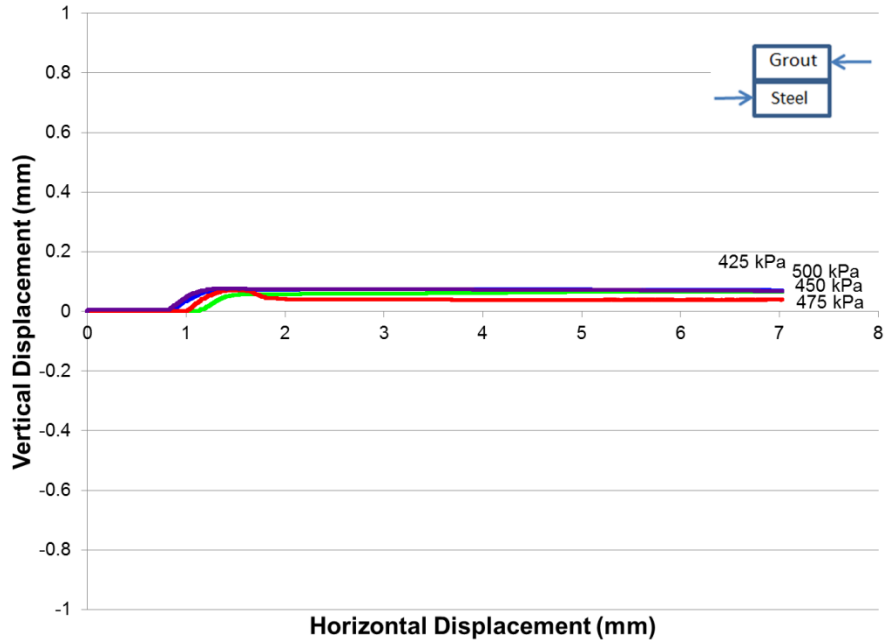


Figure A-88 Test 0047 grout-steel 425-500 kPa vertical versus horizontal displacement

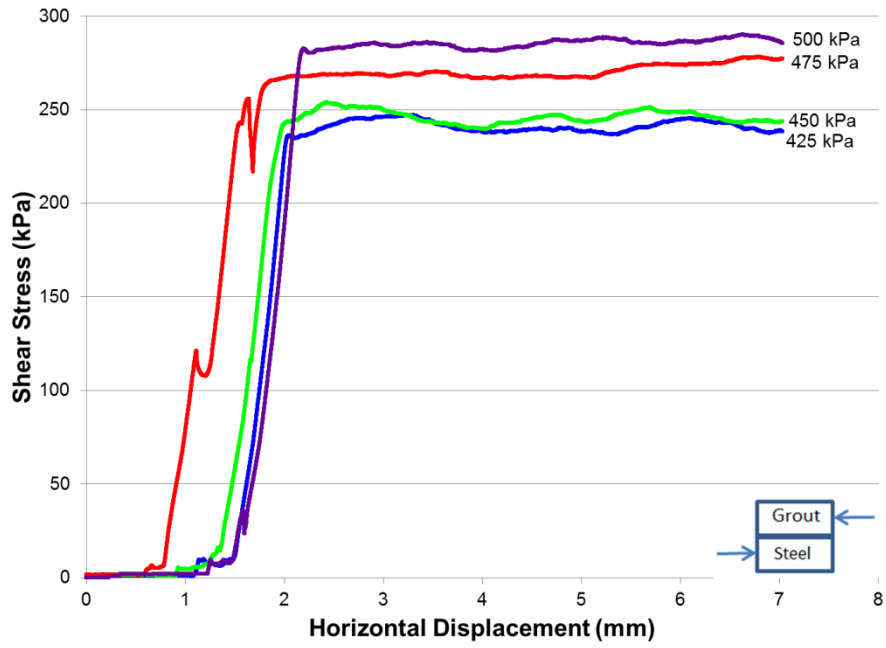


Figure A-89 Test 0048 grout-steel 425-500 kPa shear stress versus horizontal displacement

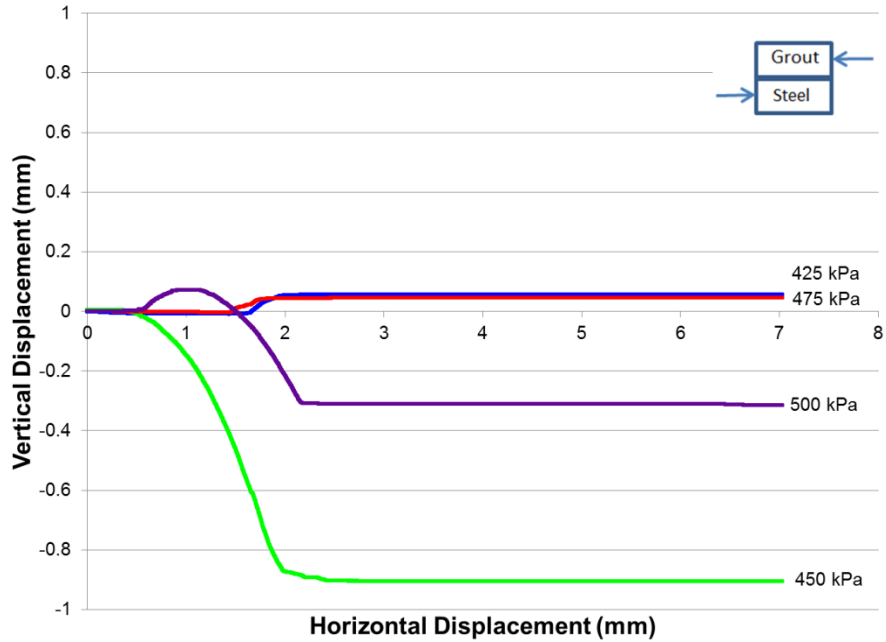
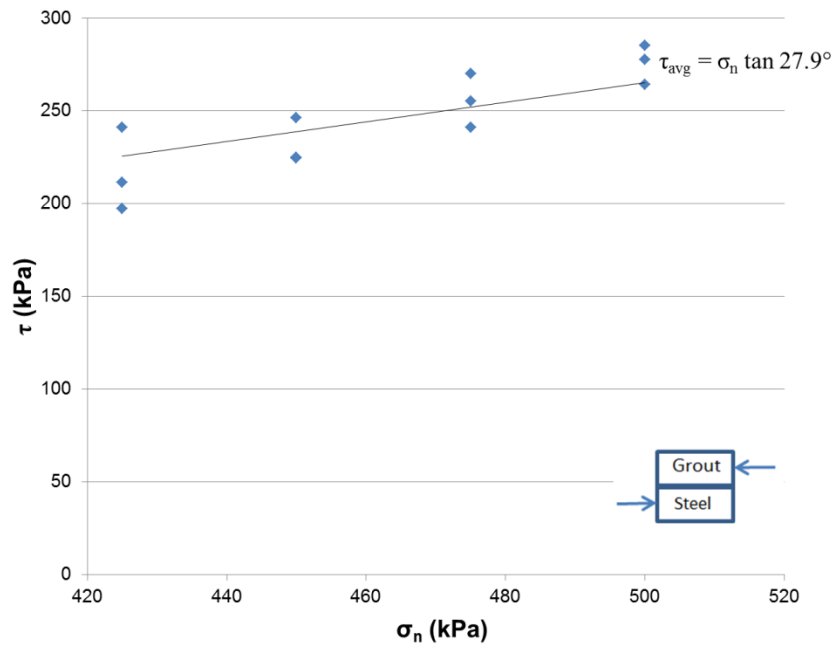
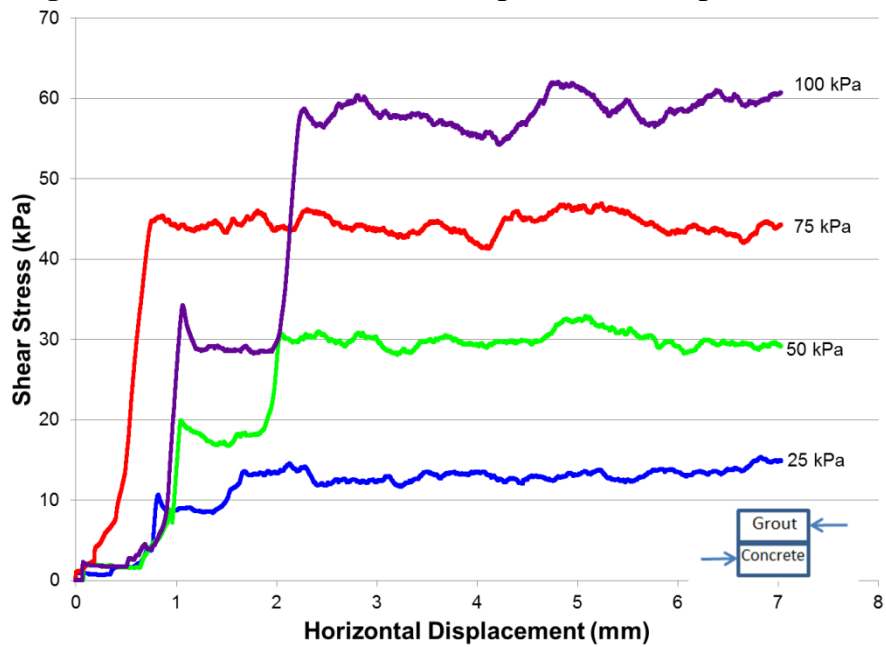


Figure A-90 Test 0048 grout-steel 425-500 kPa vertical versus horizontal displacement



**Figure A-91** Mohr-Coulomb shear strength 425-500 kPa grout and steel



**Figure A-92** Test 0049 grout-concrete 25-100 kPa shear stress versus horizontal displacement

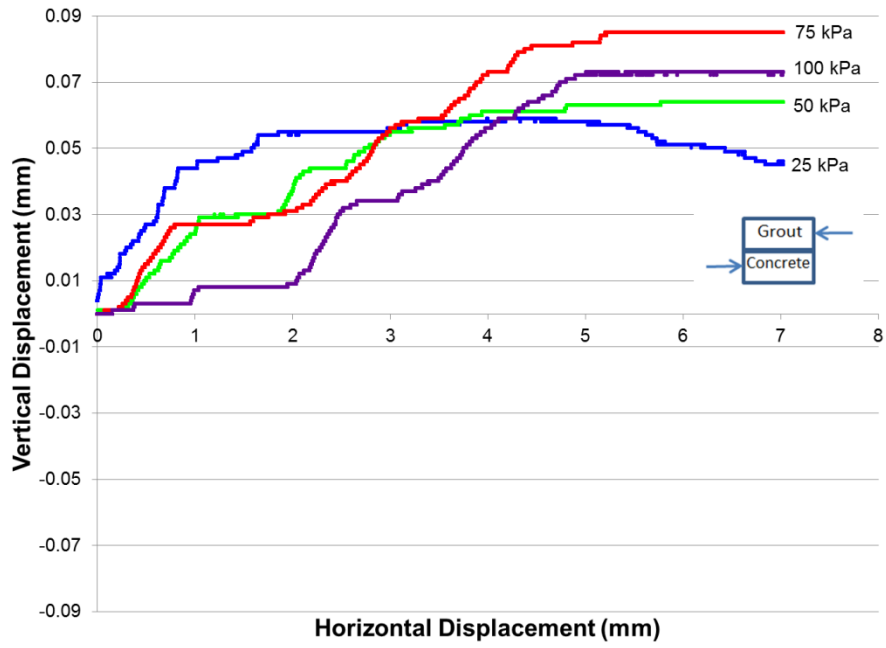


**Figure A-93** Test 0049 grout-concrete 25-100 kPa vertical versus horizontal displacement

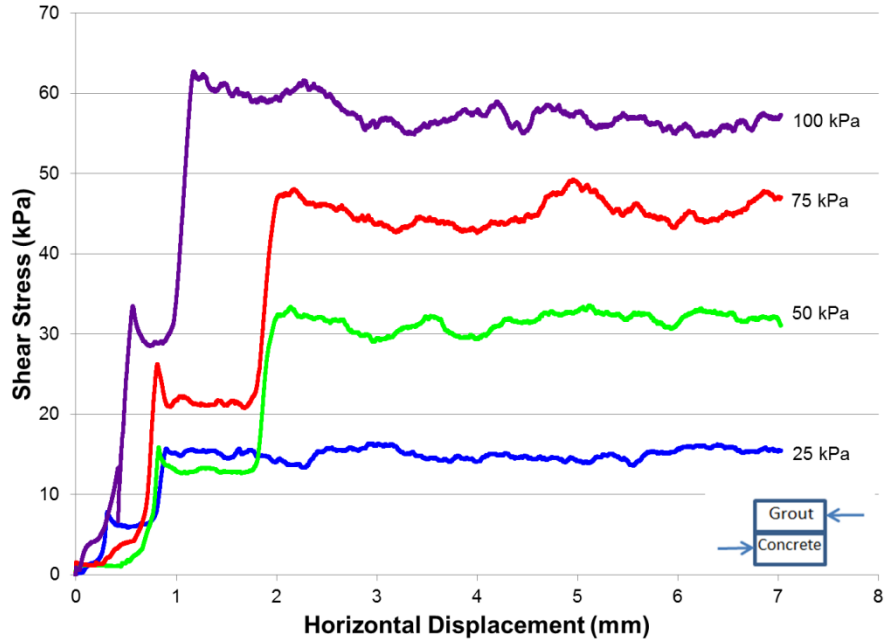


**Figure A-94** Test 0050 grout-concrete 25-100 kPa shear stress versus horizontal displacement

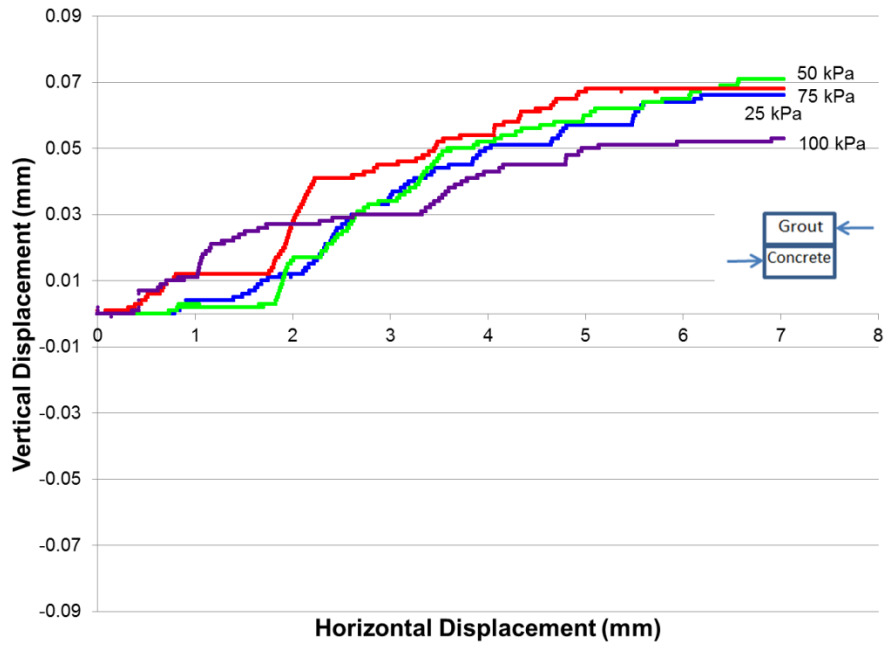


**Figure A-95** Test 0050 grout-concrete 25-100 kPa vertical versus horizontal displacement

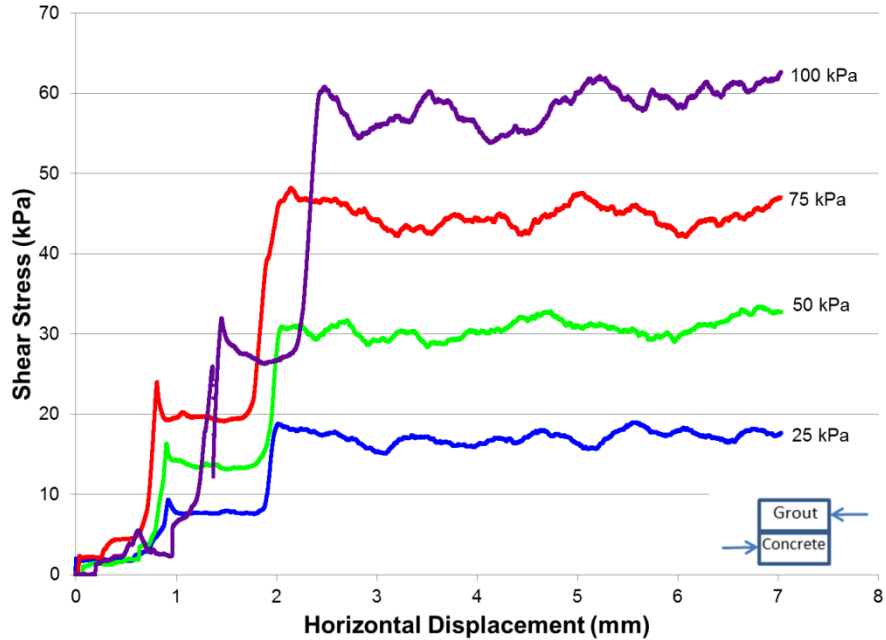


**Figure A-96** Test 0051 grout-concrete 25-100 kPa shear stress versus horizontal displacement

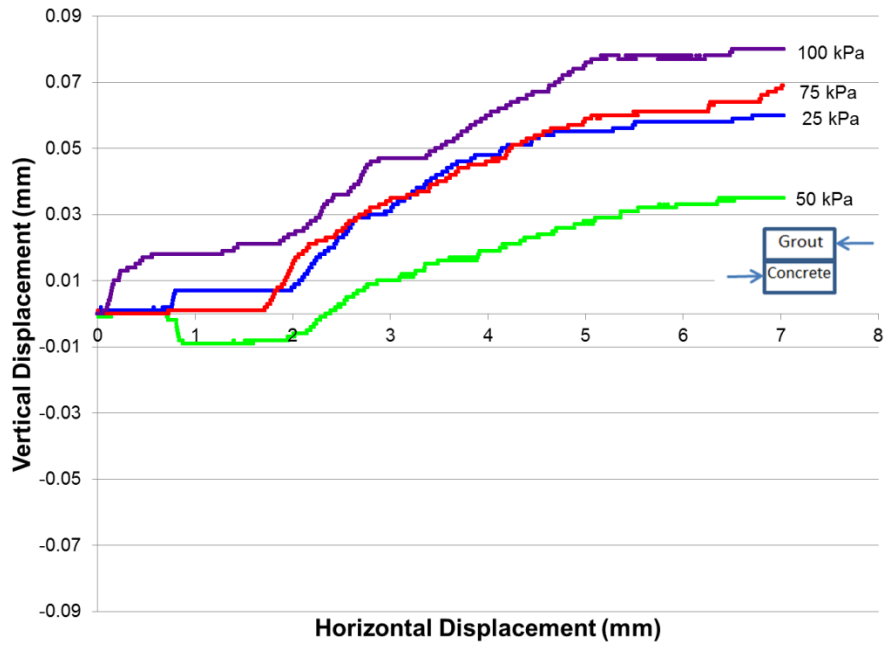


**Figure A-97** Test 0051 grout-concrete 25-100 kPa vertical versus horizontal displacement

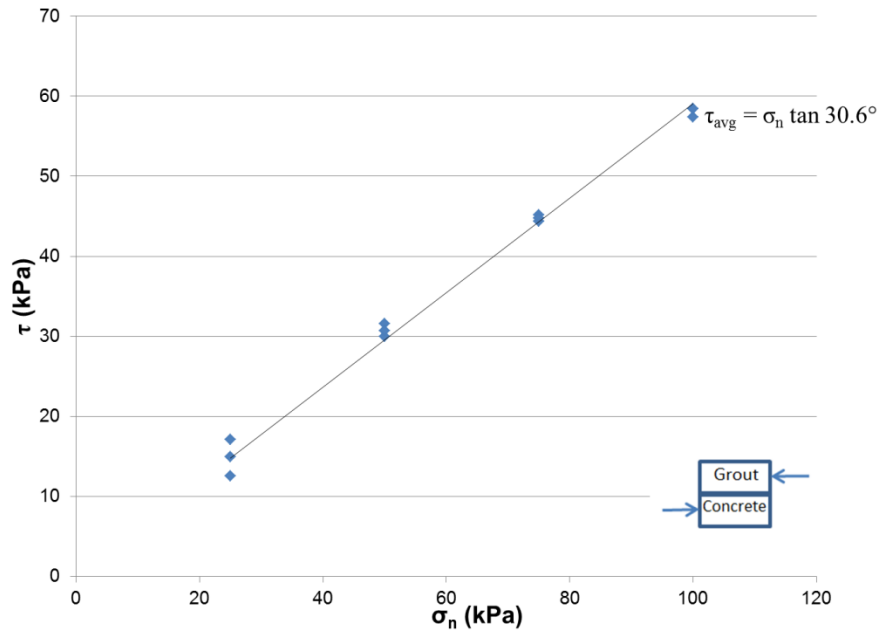


**Figure A-98** Mohr-Coulomb shear strength 25-100 kPa grout and concrete

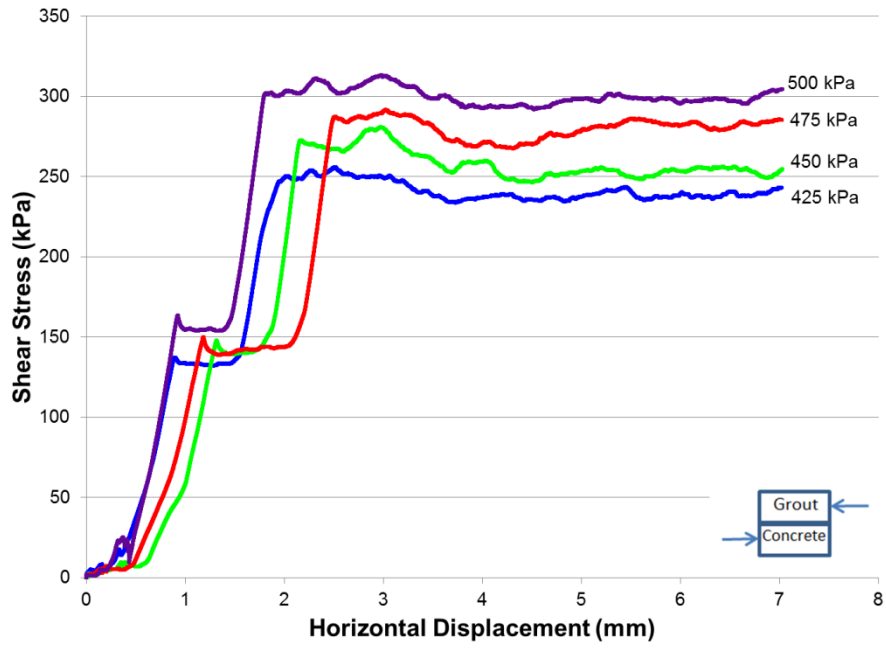


**Figure A-99** Test 0052 grout-concrete 425-500 kPa shear stress versus horizontal displacement

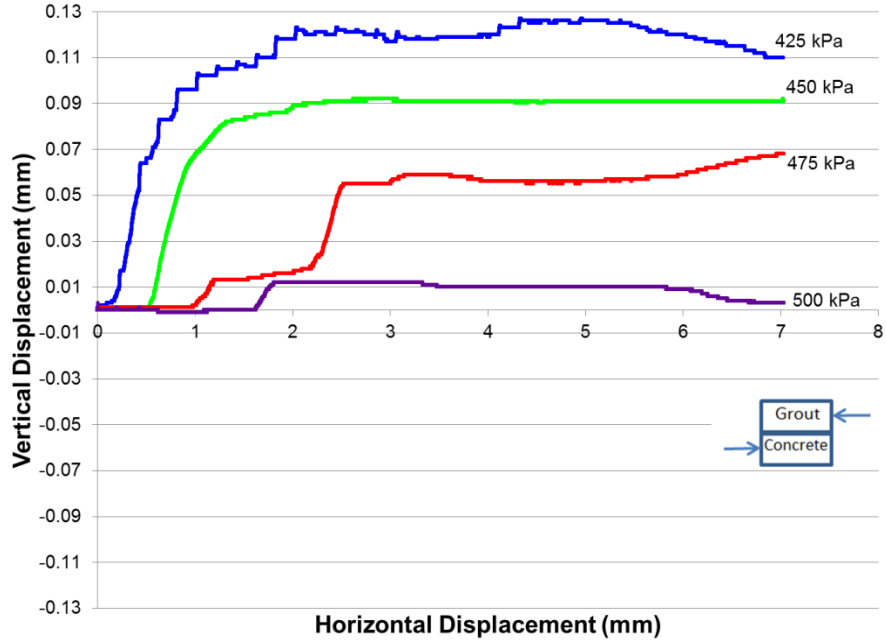


**Figure A-100** Test 0052 grout-concrete 425-500 kPa vertical versus horizontal displacement

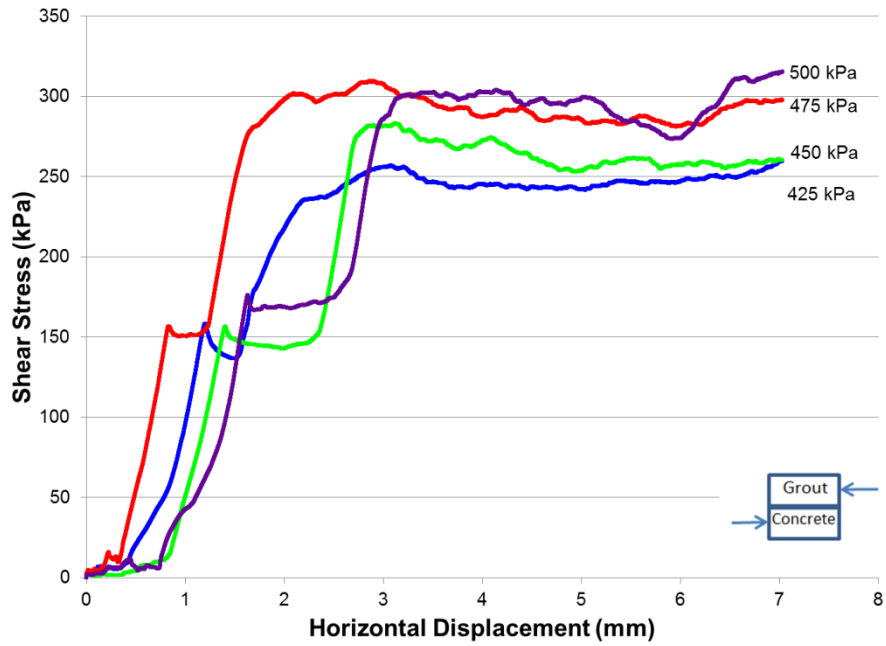


**Figure A-101** Test 0053 grout-concrete 425-500 kPa shear stress versus horizontal displacement

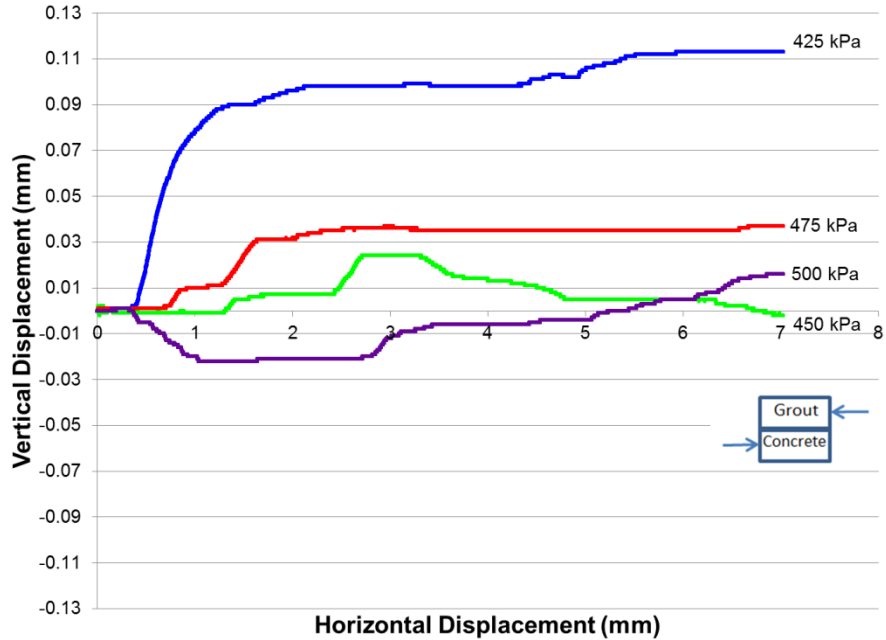


**Figure A-102** Test 0053 grout-concrete 425-500 kPa vertical versus horizontal displacement

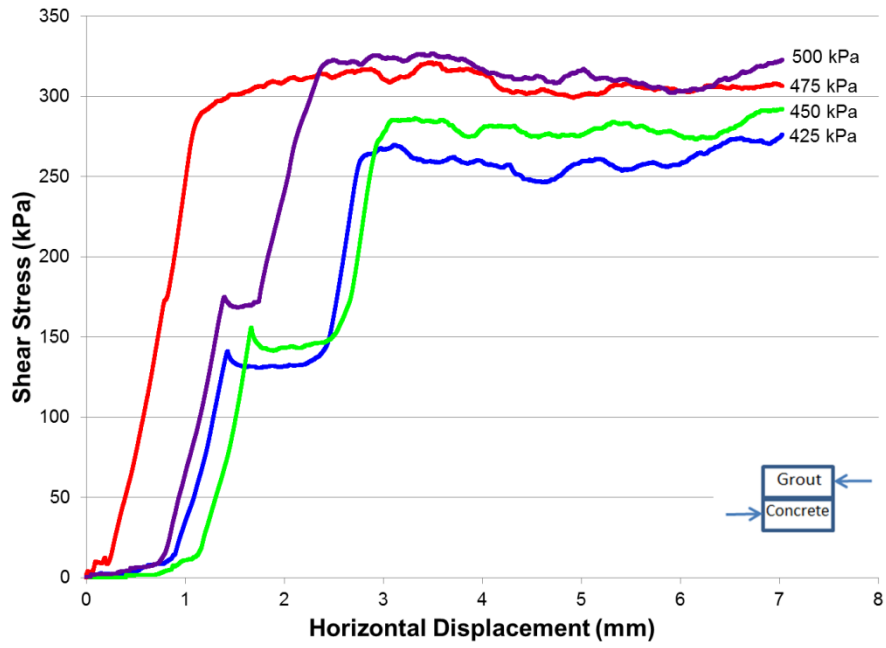


**Figure A-103** Test 0054 grout-concrete 425-500 kPa shear stress versus horizontal displacement

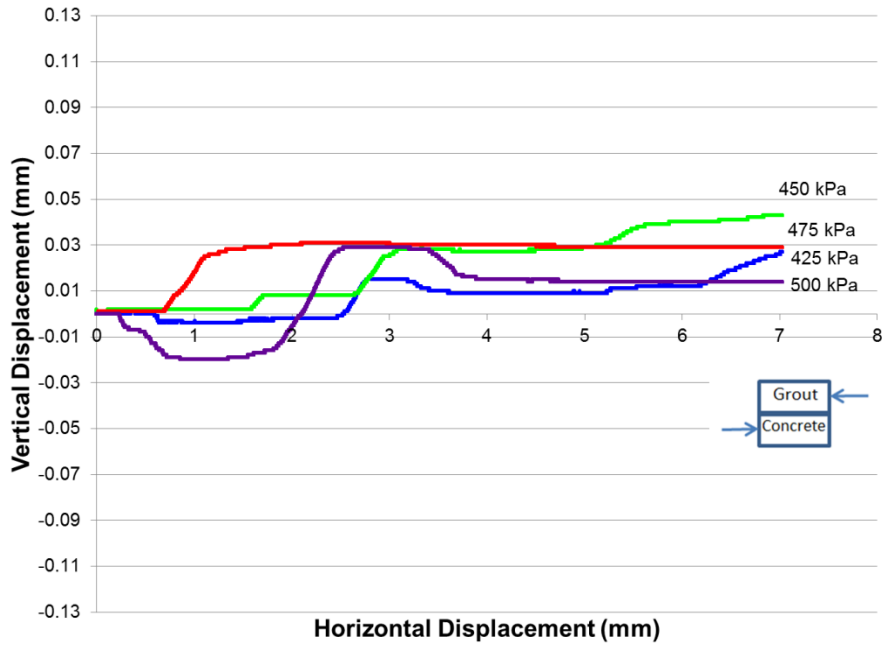


**Figure A-104** Test 0054 grout-concrete 425-500 kPa vertical versus horizontal displacement

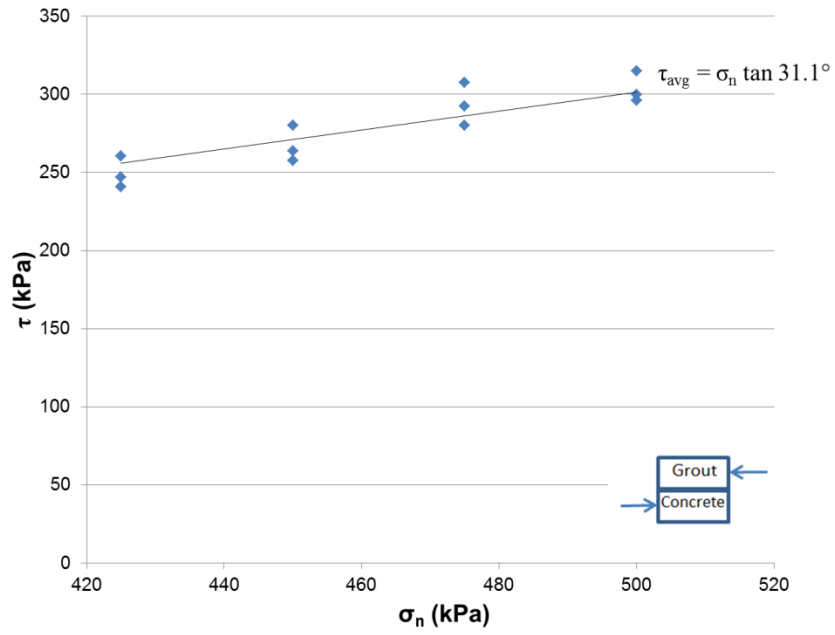


**Figure A-105** Mohr-Coulomb shear strength 425-500 kPa grout and concrete

## **APPENDIX B**

This appendix contains **Table B-1** summarizing the maximum and minimum vertical displacements from the laboratory results.

**Table B-1** Vertical displacements from laboratory results

Material	Test	$\sigma_n$ (kPa)	Max Vertical $\delta$ (mm)	Horizontal Positon at max (mm)	Min Vertical $\delta$ (mm)	Horizontal Positon at min (mm)
Brighton Sand	0007	25	0.636	7.018	0	0
		50	0.581	5.994	-0.01	0.171
		75	0.513	5.84	-0.021	0.391
		100	0.425	6.265	-0.045	2.348
	0008	25	0.742	7.01	-0.001	0.082
		50	0.526	4.865	-0.004	0.154
		75	0.347	4.642	-0.129	0.491
		100	0.464	5.144	-0.023	0.312
	0009	25	0.617	5.866	-0.006	0.298
		50	0.537	5.261	-0.005	0.243
		75	0.543	4.655	-0.012	0.237
		100	0.539	4.303	-0.007	0.279
	0021	425	0.398	4.804	-0.049	1.086
		450	0.347	4.183	-0.029	1.055
		475	0.384	4.377	-0.041	0.973
		500	0.419	4.933	-0.029	1.127
	0022	425	0.354	4.732	-0.059	1.106
		450	0.47	4.636	-0.035	1.02
		475	0.321	4.077	-0.007	0.816
		500	0.354	4.467	-0.036	1.169
	0023	425	0.399	4.496	-0.022	0.746
		450	0.374	4.548	-0.019	1.097
		475	0.318	5.022	-0.058	1.076
		500	0.355	5.181	-0.014	1.098

Material	Test	$\sigma_n$ (kPa)	Max Vertical $\delta$ (mm)	Horizontal Positon at max (mm)	Min Vertical $\delta$ (mm)	Horizontal Positon at min (mm)
Brighton Sand - Grout	0015	25	0.089	4.109	-0.011	0.251
		50	0.177	4.823	-0.001	0
		75	0.09	4.149	-0.014	0.253
		100	0.125	1.256	-0.001	0.003
	0016	25	0.104	3.782	0	0
		50	0.068	4.499	0	0
		75	0.126	4.471	-0.001	0.01
		100	0.115	3.939	-0.02	0.282
	0017	25	0.141	4.633	-0.008	0.124
		50	0.187	5.105	0	0
		75	0.136	4.525	0	0
		100	0.13	4.23	0	0
	0024	425	0.113	4.114	0	0
		450	0.043	4.638	-0.038	0.84
		475	0.108	4.455	0	0
		500	0	0	-0.037	1.087
	0025	425	0.065	3.8	-0.023	0.805
		450	0.019	5.303	-0.05	1
		475	0.006	4.203	-0.055	0.999
		500	0	0	-0.105	6.902
	0026	425	0.001	0.001	-0.043	1.104
		450	0.034	3.683	-0.039	0.886
		475	0.025	3.086	-0.046	0.968
		500	0.026	2.748	-0.019	0.909

Material	Test	$\sigma_n$ (kPa)	Max Vertical $\delta$ (mm)	Horizontal Positon at max (mm)	Min Vertical $\delta$ (mm)	Horizontal Positon at min (mm)
Brighton Sand - Steel	0018	25	0	0	-0.021	3.943
		50	0.002	0.001	-0.016	6.542
		75	0.008	0.021	0	0
		100	0.002	0.002	-0.019	6.886
	0019	25	0.003	2.317	-0.002	0.906
		50	0.023	4.626	0	0
		75	0.001	0.72	-0.003	6.168
		100	0.027	2.481	0	0
	0020	25	0.016	2.97	0	0
		50	0.001	0.073	-0.031	6.94
		75	0.008	0.392	-0.008	6.862
		100	0.002	0.063	-0.022	6.996
	0027	425	0.001	0.013	-0.072	6.962
		450	0	0	-0.048	6.832
		475	0.022	0.771	-0.004	6.651
		500	0	0	-0.047	6.368
	0028	425	0.001	0	-0.063	6.317
		450	0.002	0.003	-0.058	6.859
		475	0.001	0.001	-0.053	6.895
		500	0.012	0	-0.045	6.475
	0029	425	0.001	0.001	-0.046	6.602
		450	0.003	0.001	-0.092	6.648
		475	0.003	0.002	-0.052	6.942
		500	0	0	-0.07	6.74

Material	Test	$\sigma_n$ (kPa)	Max Vertical $\delta$ (mm)	Horizontal Positon at max (mm)	Min Vertical $\delta$ (mm)	Horizontal Positon at min (mm)
Limestone and Steel	0031	25	0.001	2.223	0	0
		50	0.001	0.001	-0.002	6.83
		75	0.008	0.406	0	0
		100	0.003	0.006	-0.006	6.658
	0032	25	0.038	5.325	0	0
		50	0.004	3.852	0	0
		75	0.006	3.996	0	0
		100	0.006	2.609	0	0
	0033	25	0.053	2.746	0	0
		50	0.008	0.002	-0.005	6.915
		75	0	0	-0.016	6.905
		100	0	0	-0.025	6.976
	0040	425	0.001	0	-0.041	6.918
		450	0	0	-0.032	1.791
		475	0.002	0.002	-0.028	5.301
		500	0.078	1.257	0	0
	0041	425	0.076	0.802	0	0
		450	0	0	-0.038	6.858
		475	0.004	1.886	-0.006	6.667
		500	0.066	1.733	-0.024	4.35
	0042	425	0	0	-0.032	6.304
		450	0.001	0.001	-0.025	6.308
		475	0.109	2.255	0	0
		500	0.104	2.877	0	0

Material	Test	$\sigma_n$ (kPa)	Max Vertical $\delta$ (mm)	Horizontal Positon at max (mm)	Min Vertical $\delta$ (mm)	Horizontal Positon at min (mm)
Limestone – Grout	0034	25	0.001	0.874	-0.031	6.905
		50	0.018	1.752	-0.019	7.004
		75	0.016	1.283	-0.031	7.002
		100	0.02	1.694	-0.01	6.975
	0035	25	0.023	1.687	-0.017	6.954
		50	0.017	2.859	-0.027	7.024
		75	0.004	0.688	-0.023	6.955
		100	0.026	0.658	-0.025	7.011
	0036	25	0.01	1.502	-0.029	7.013
		50	0.032	2.763	-0.002	6.969
		75	0.003	1.126	-0.016	6.734
		100	0.029	2.136	-0.026	6.821
	0037	425	0.001	0.002	-0.046	6.977
		450	0	0	-0.064	6.994
		475	0.016	2.245	-0.021	6.941
		500	0	0	-0.044	6.91
	0038	425	0.002	0.002	-0.045	6.975
		450	0.012	1.759	-0.038	7.025
		475	0	0	-0.063	6.908
		500	0.002	1.155	-0.046	7.015
	0039	425	0.04	5.729	-0.021	2.649
		450	0.014	1.94	-0.032	6.984
		475	0	0	-0.044	6.968
		500	0.016	2.037	-0.02	6.985

Material	Test	$\sigma_n$ (kPa)	Max Vertical $\delta$ (mm)	Horizontal Positon at max (mm)	Min Vertical $\delta$ (mm)	Horizontal Positon at min (mm)
Grout - Steel	0043	25	0.036	6.345	-0.001	0.059
		50	0.003	1.013	0	0
		75	0.05	3.456	0	0
		100	0.047	4.813	0	0
	0044	25	0.027	2.288	0	0
		50	0.047	4.692	0	0
		75	0.017	4.108	0	0
		100	0.015	2.973	-0.001	0.858
	0045	25	0.012	3.61	-0.002	-0.01
		50	0.012	5.141	-0.001	0.011
		75	0.021	4.127	0	0
		100	0.01	3.366	0	0
	0046	425	0.001	0	-0.01	1.879
		450	0.001	0.006	-0.009	6.75
		475	0.062	0.901	-0.031	3.86
		500	0.054	2.26	-0.001	0.423
	0047	425	0.073	2.01	0	0
		450	0.065	6.207	0	0
		475	0.068	1.398	0	0
		500	0.075	1.275	0	0
	0048	425	0.056	2.818	-0.01	1.431
		450	0.005	0.118	-0.905	2.64
		475	0.046	3.116	-0.005	1.161
		500	0.071	0.904	-0.316	6.874

Material	Test	$\sigma_n$ (kPa)	Max Vertical $\delta$ (mm)	Horizontal Positon at max (mm)	Min Vertical $\delta$ (mm)	Horizontal Positon at min (mm)
Grout- Concrete	0049	25	0.059	3.991	0	0
		50	0.064	5.774	0	0
		75	0.085	5.203	0	0
		100	0.073	5.01	0	0
	0050	25	0.066	6.187	0	0
		50	0.071	6.57	0	0
		75	0.068	4.999	0	0
		100	0.053	6.905	-0.001	0.14
	0051	25	0.06	6.713	0	0
		50	0.035	6.371	-0.009	0.873
		75	0.069	7.015	0	0
		100	0.08	6.503	0	0
	0052	425	0.127	4.327	0	0
		450	0.092	2.615	0	0
		475	0.068	6.956	0	0
		500	0.012	1.802	-0.001	0.619
	0053	425	0.113	5.927	0	0
		450	0.024	2.71	-0.002	0.02
		475	0.037	2.939	0	0
		500	0.016	6.858	-0.022	1.036
	0054	425	0.027	7.009	-0.004	0.64
		450	0.043	6.829	0	0
		475	0.031	2.09	0	0
		500	0.029	2.527	-0.02	0.858

## **APPENDIX C**

This appendix contains all plots comparing the laboratory shear stress versus horizontal displacement. IT also contains plots produced for the model calibration. **Table C-1** is an index for quick reference to the location of given test results.

**Table C-1** Index by interface test type

Test Type	Page number
Brighton Sand – Brighton Sand	225-227
Brighton Sand – Grout	228-230
Brighton Sand – Steel	230-233
Rock - Grout	234-236
Rock – Steel	237-239
Grout –Steel	240-242
Grout - Concrete	243-245
Calibration	246-247

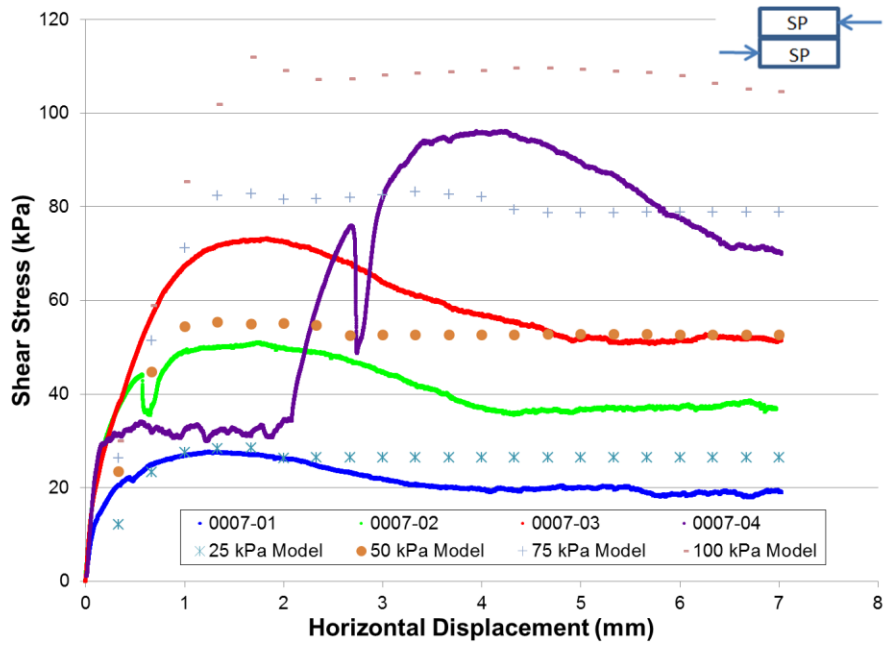


Figure C-1 Sand sample model versus test 0007

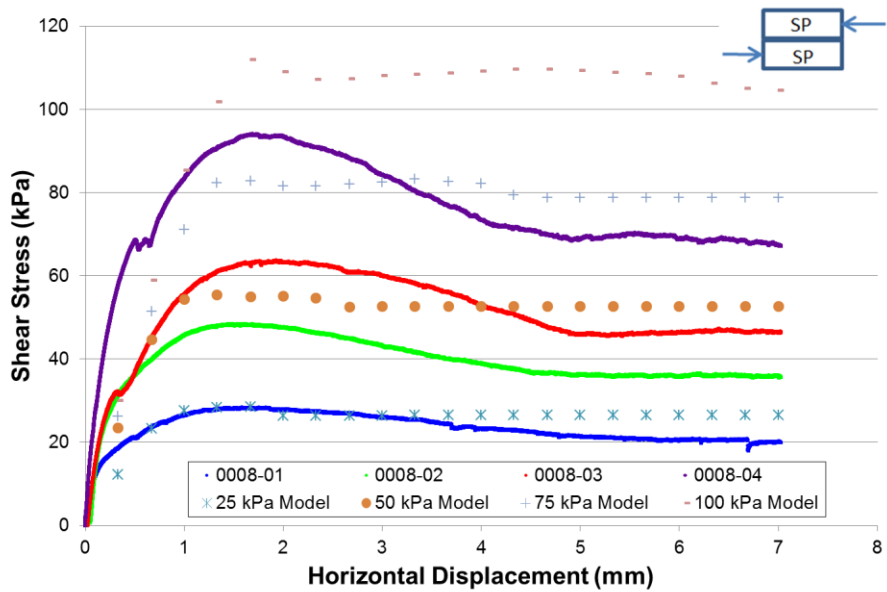


Figure C-2 Sand sample model versus test 0008

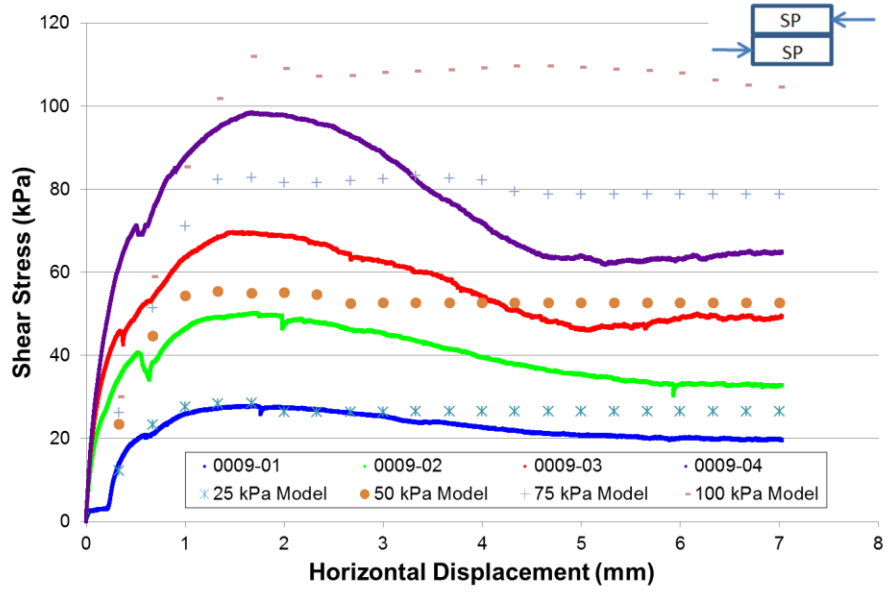


Figure C-3 Sand sample model versus test 0009

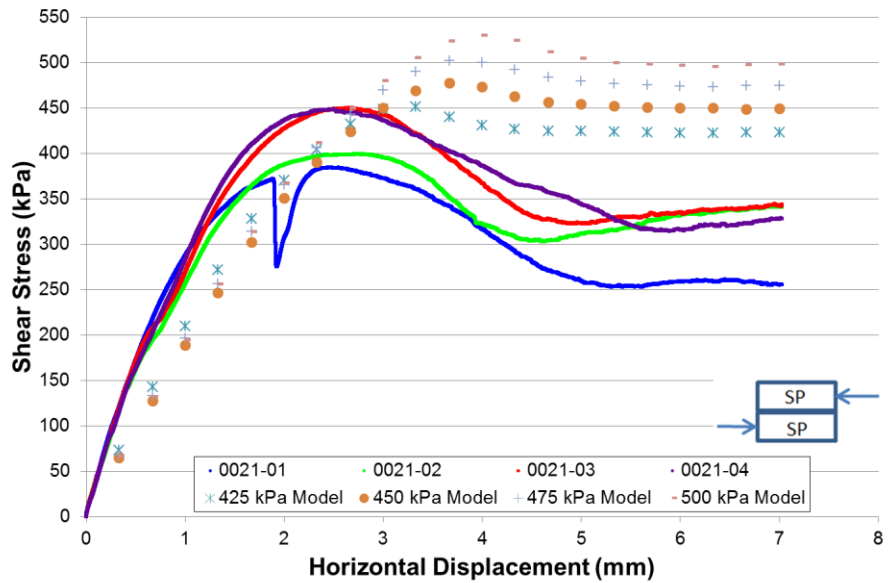


Figure C-4 Sand sample model versus test 0021

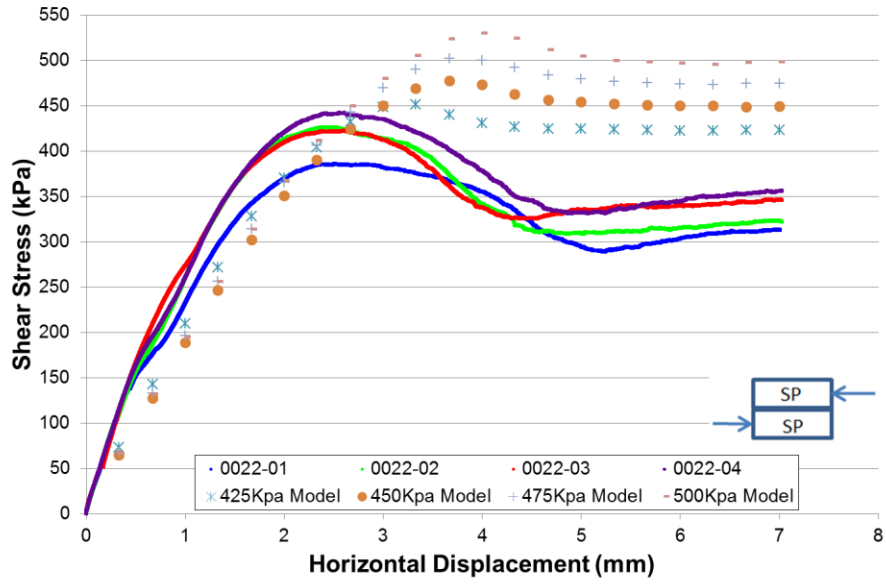


Figure C-5 Sand sample model versus test 0022

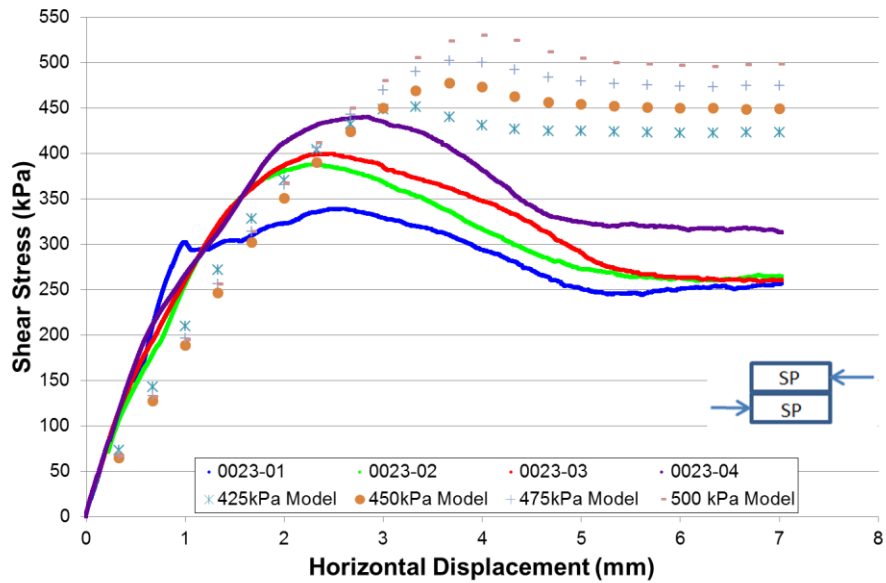


Figure C-6 Sand sample model versus test 0023

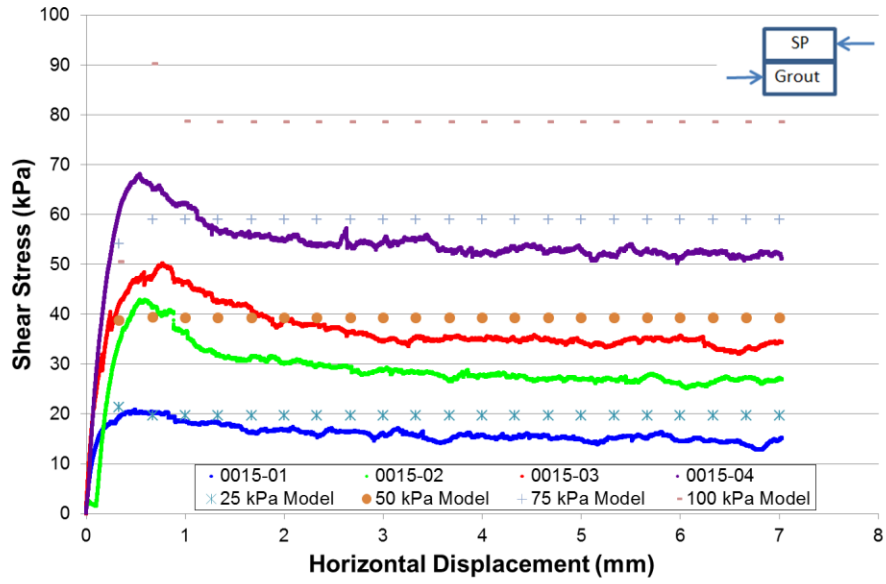


Figure C-7 Sand-grout sample, model versus test 0015

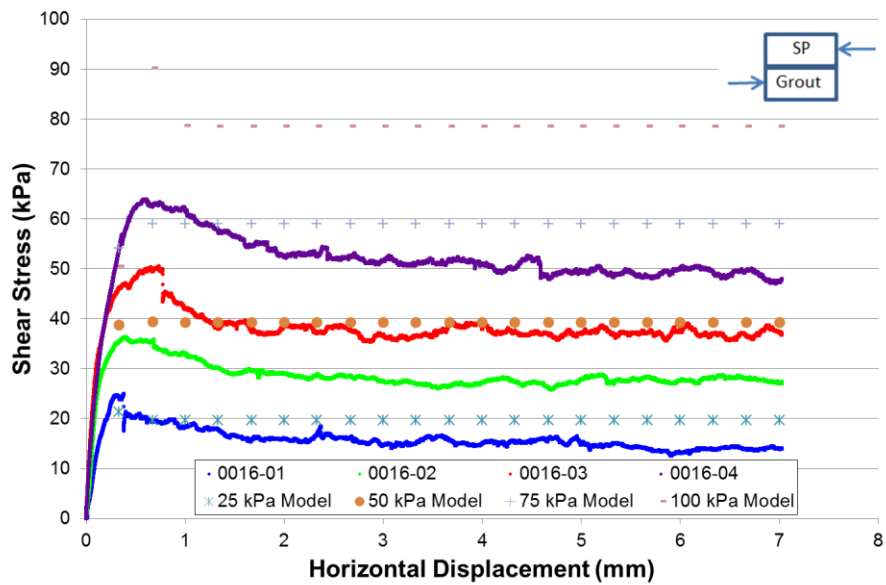


Figure C-8 Sand-grout sample, model versus test 0016

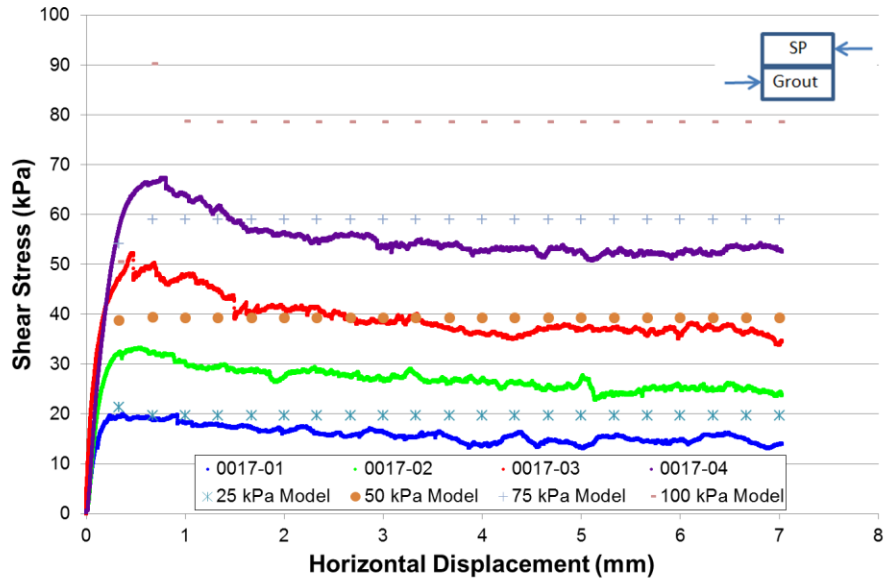


Figure C-9 Sand-grout sample, model versus test 0017

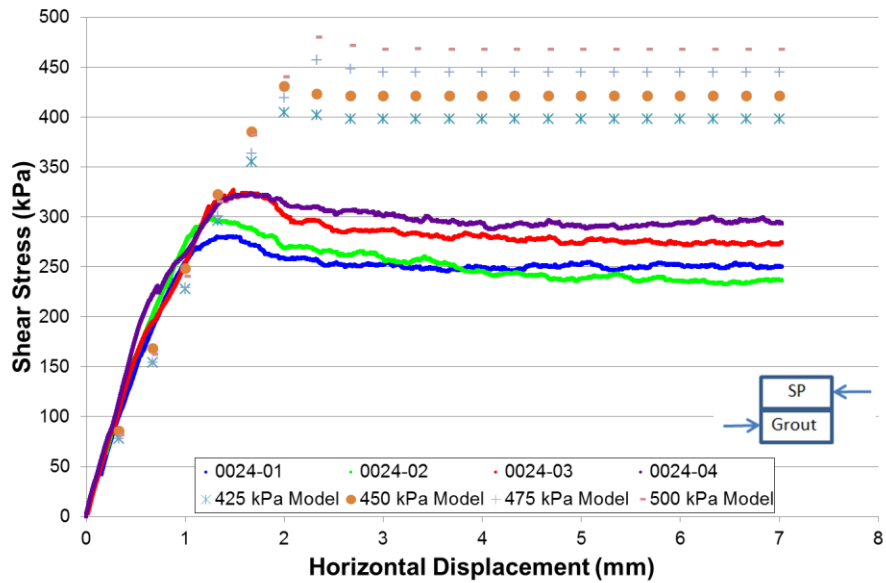


Figure C-10 Sand-grout sample, model versus test 0024

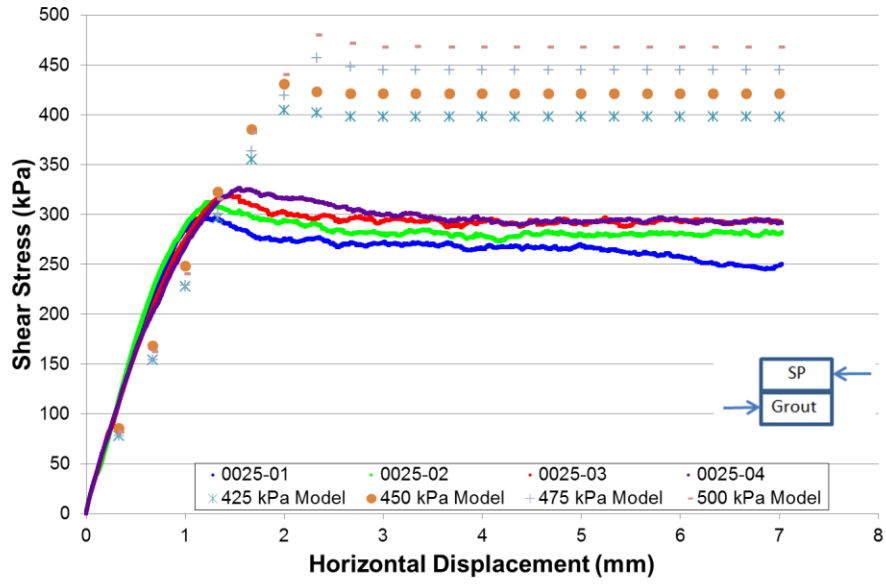


Figure C-11 Sand-grout sample, model versus test 0025

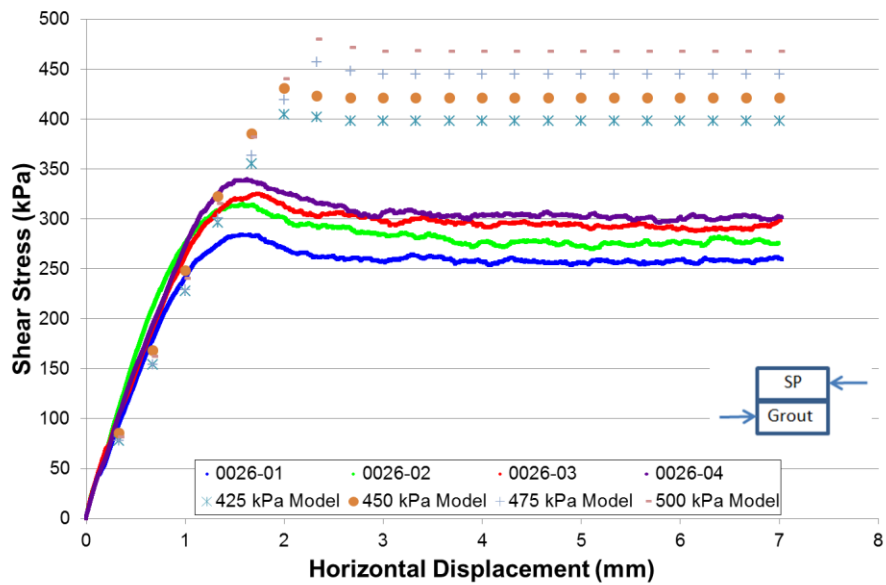


Figure C-12 Sand-grout sample, model versus test 0026

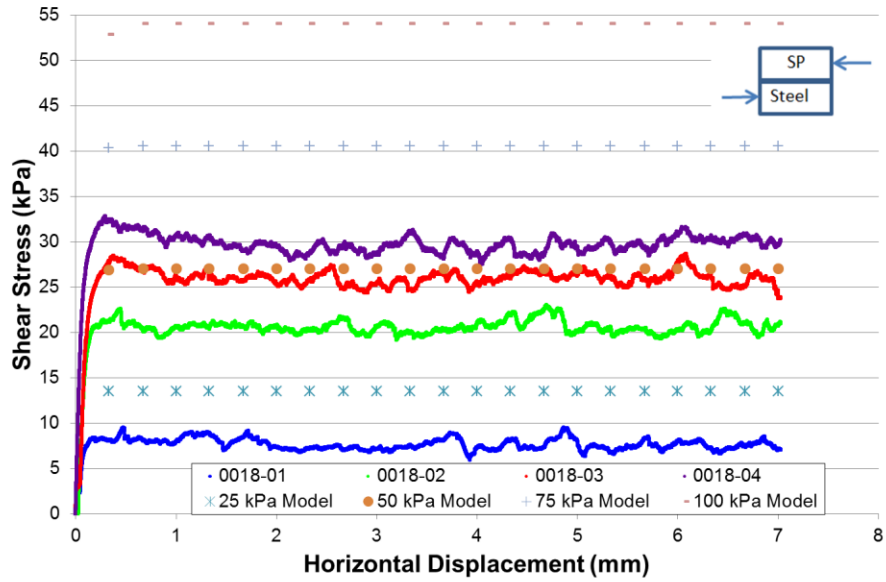


Figure C-13 Sand-steel sample, model versus test 0018

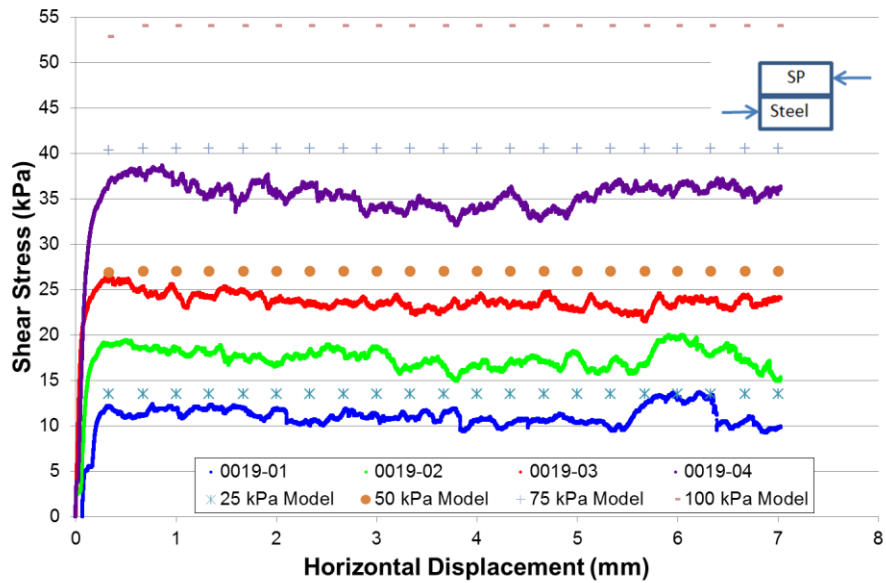


Figure C-14 Sand-steel sample, model versus test 0019

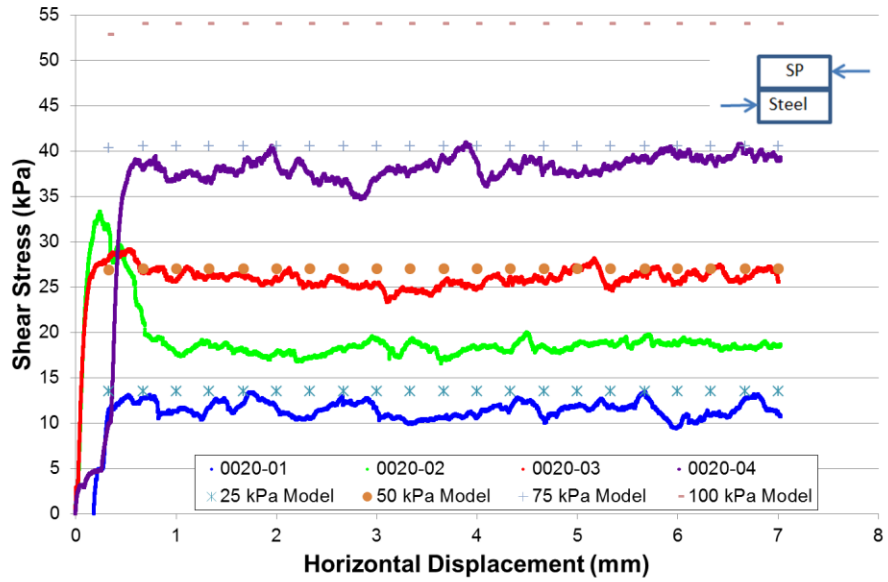


Figure C-15 Sand-steel sample, model versus test 0020

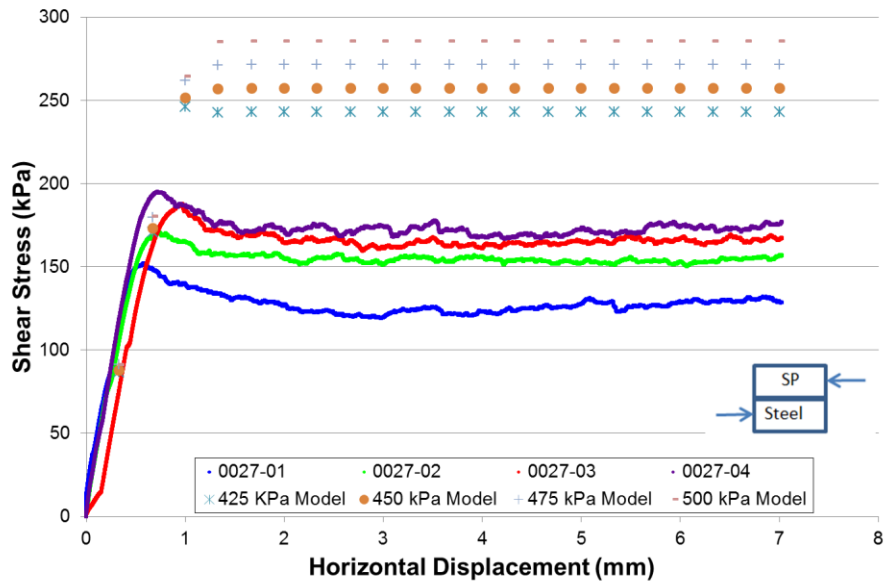


Figure C-16 Sand-steel sample, model versus test 0027

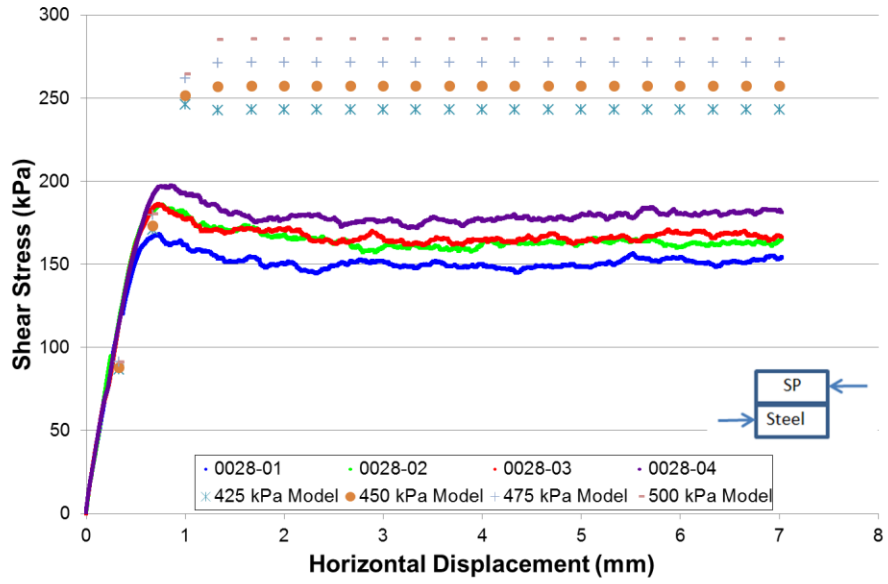


Figure C-17 Sand-steel sample, model versus test 0028

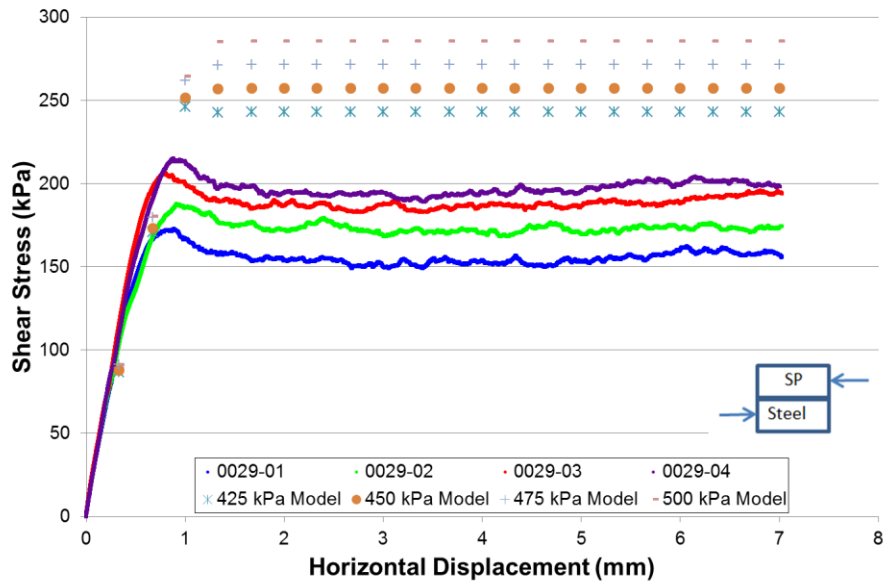


Figure C-18 Sand-steel sample, model versus test 0029

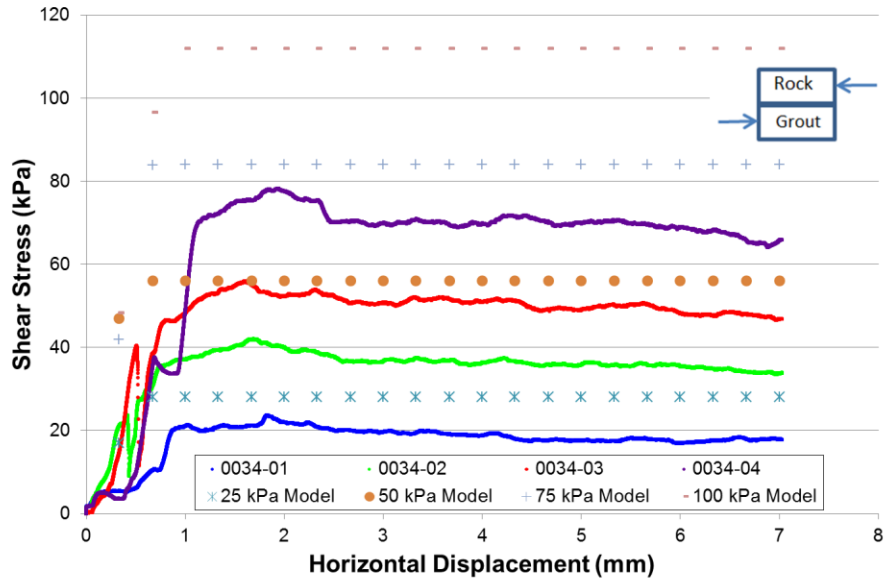


Figure C-19 Rock-grout sample, model versus test 0034

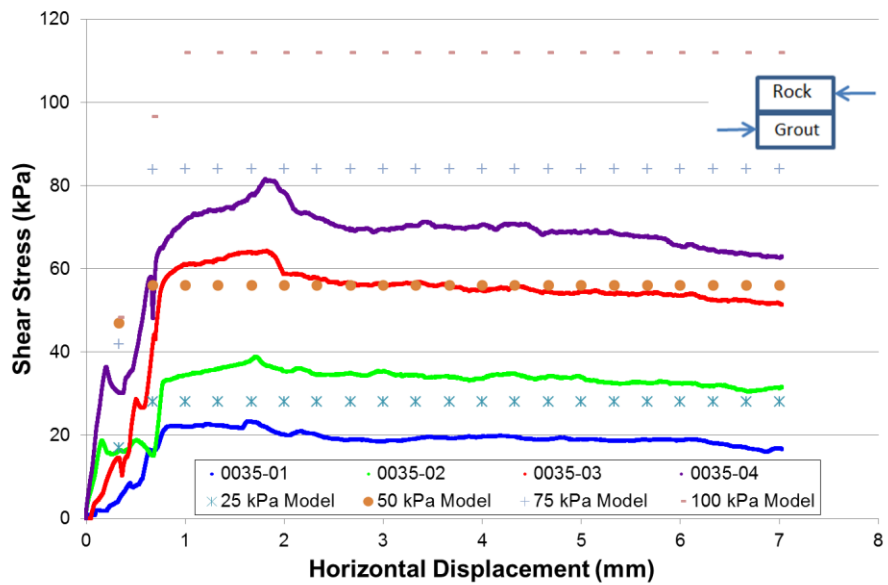


Figure C-20 Rock-grout sample, model versus test 0035

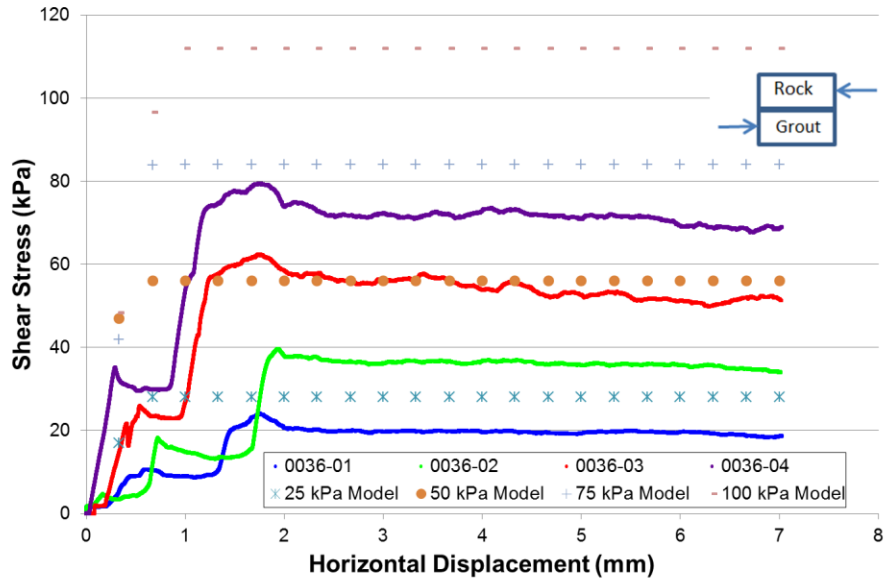


Figure C-21 Rock-grout sample, model versus test 0036

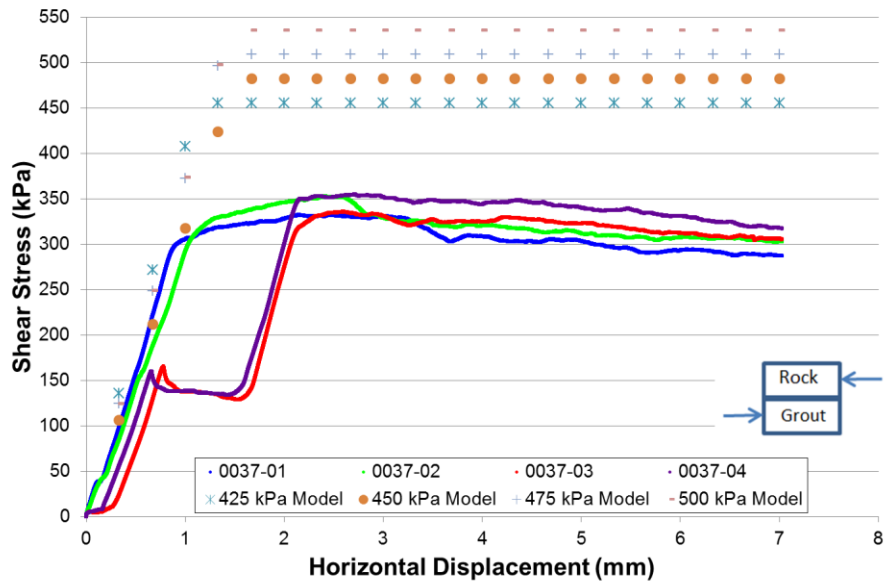


Figure C-22 Rock-grout sample, model versus test 0037

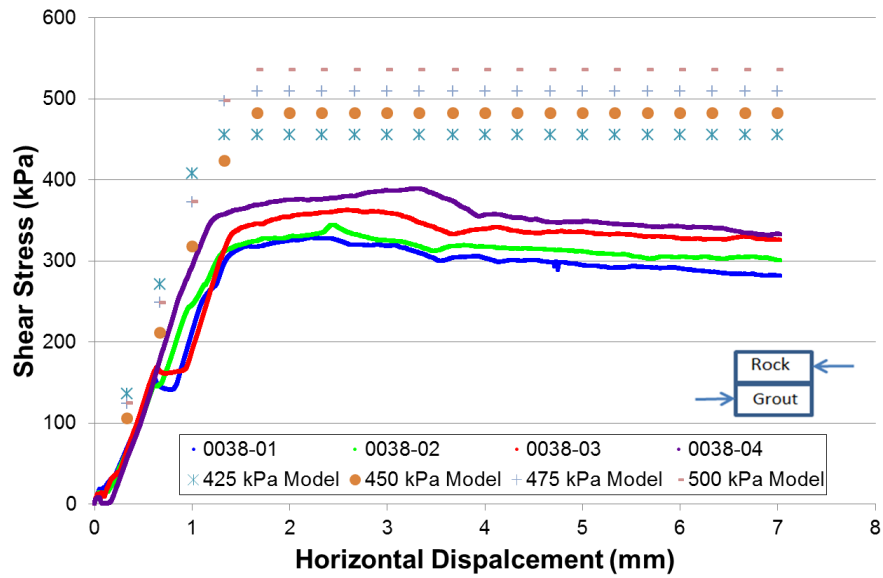


Figure C-23 Rock-grout sample, model versus test 0038

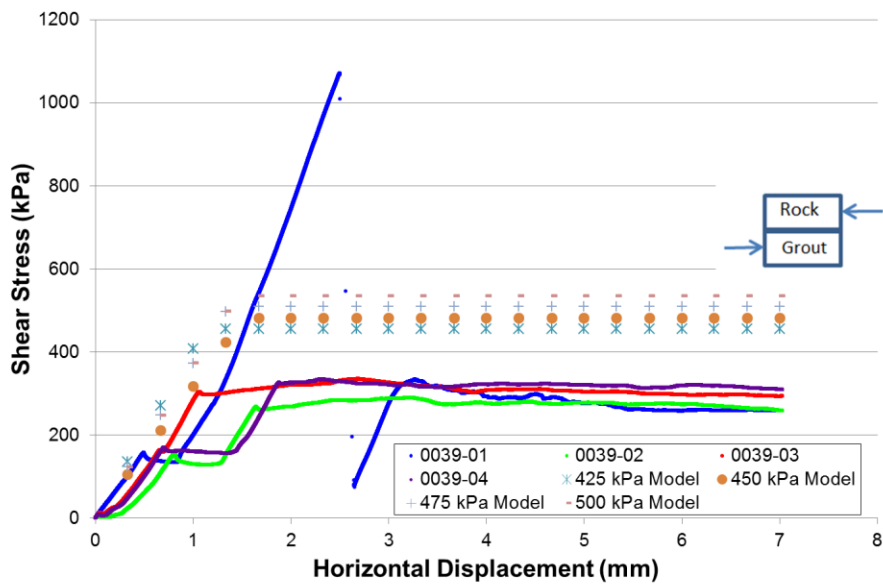


Figure C-24 Rock-grout sample, model versus test 0039

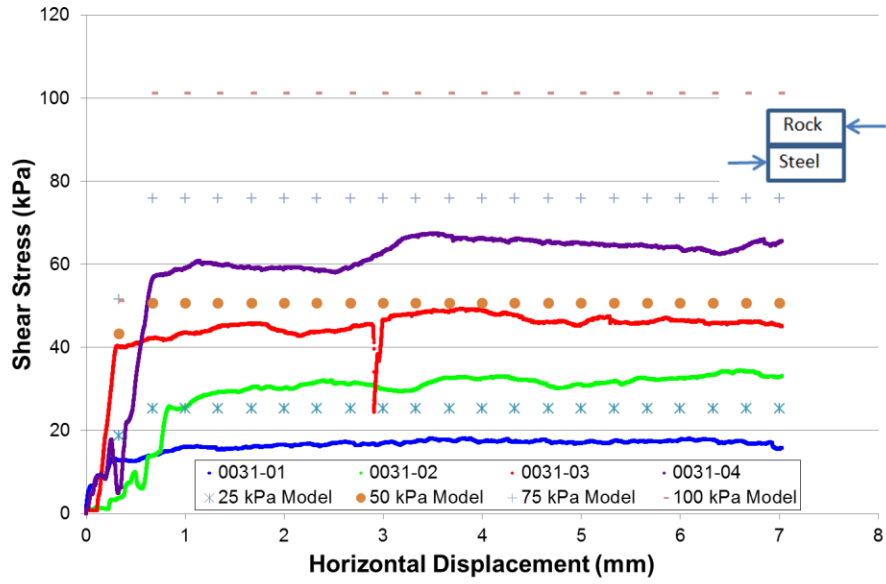


Figure C-25 Rock-steel sample, model versus test 0031

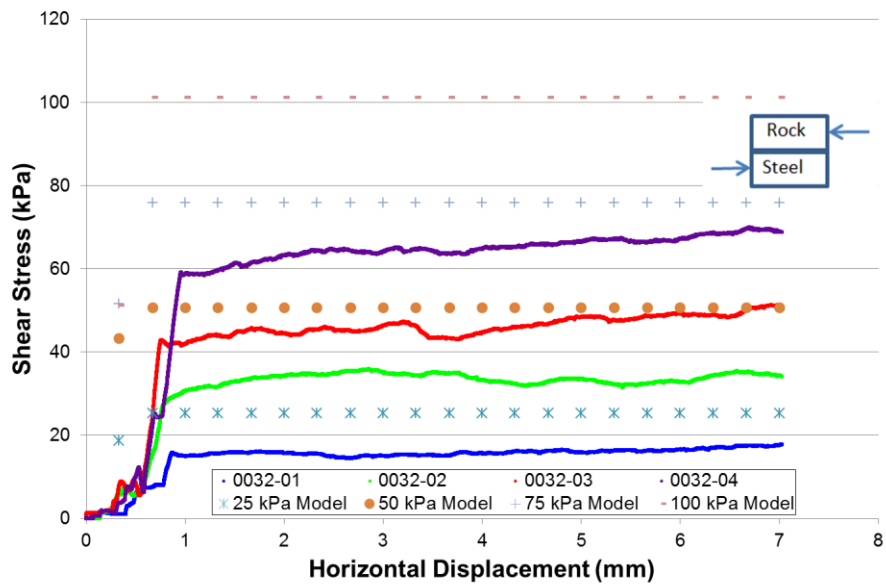


Figure C-26 Rock-steel sample, model versus test 0032

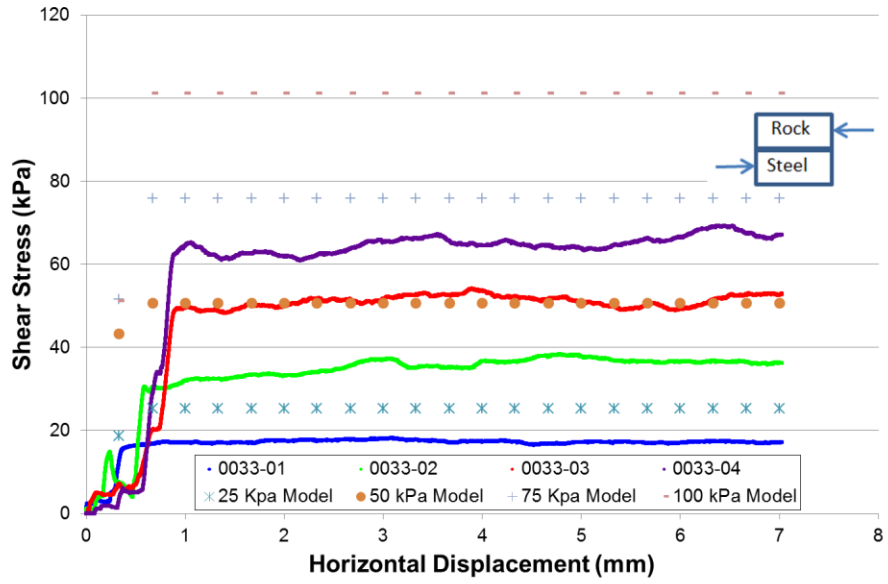


Figure C-27 Rock-steel sample, model versus test 0033

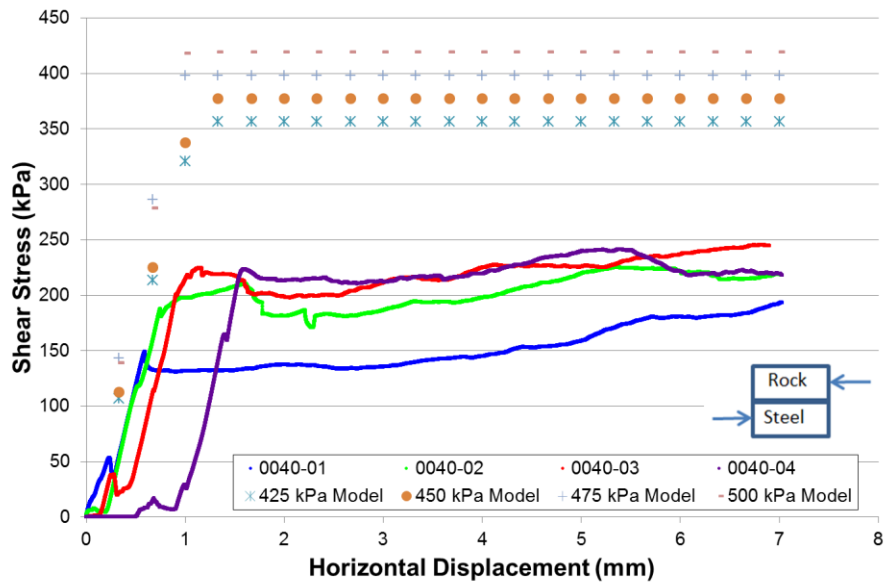


Figure C-28 Rock-steel sample, model versus test 0040

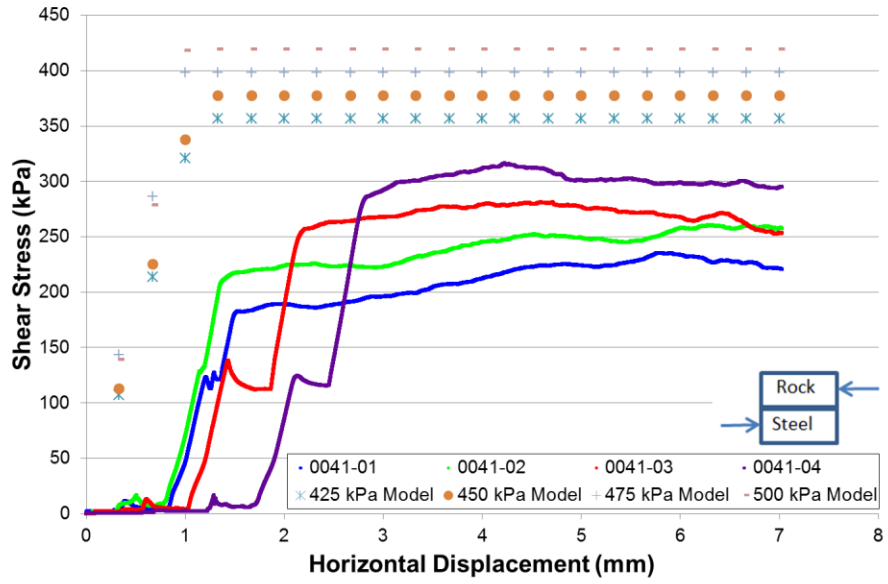


Figure C-29 Rock-steel sample, model versus test 0041

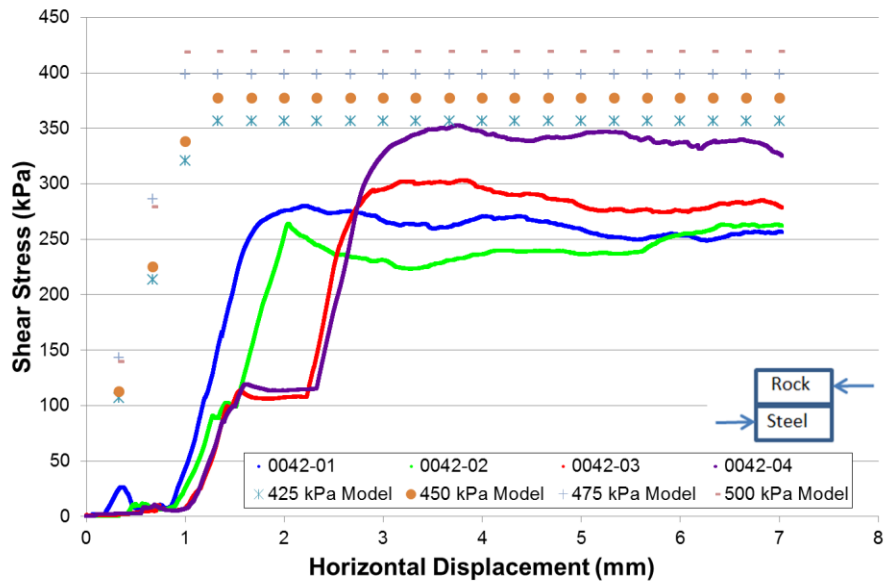


Figure C-30 Rock-steel sample, model versus test 0042

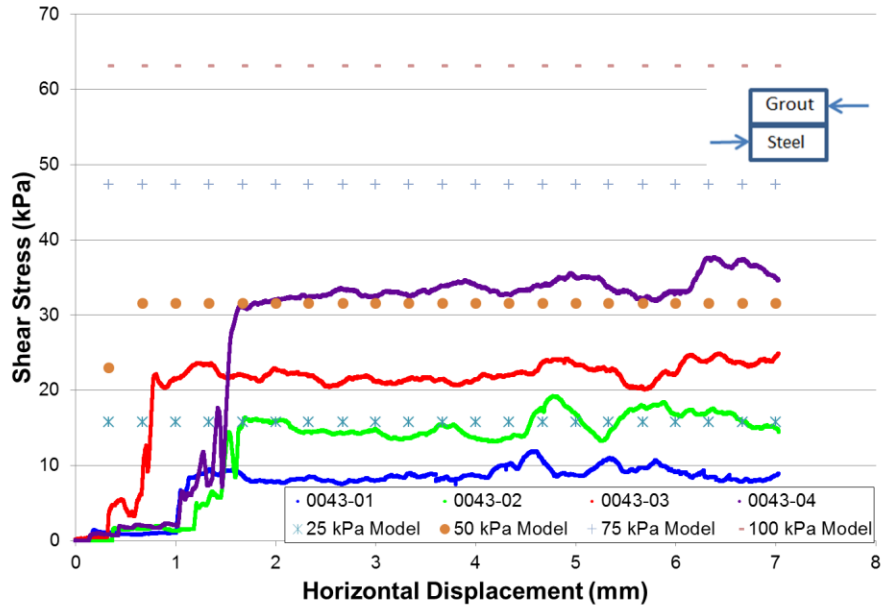


Figure C-31 Grout-steel sample, model versus test 0043

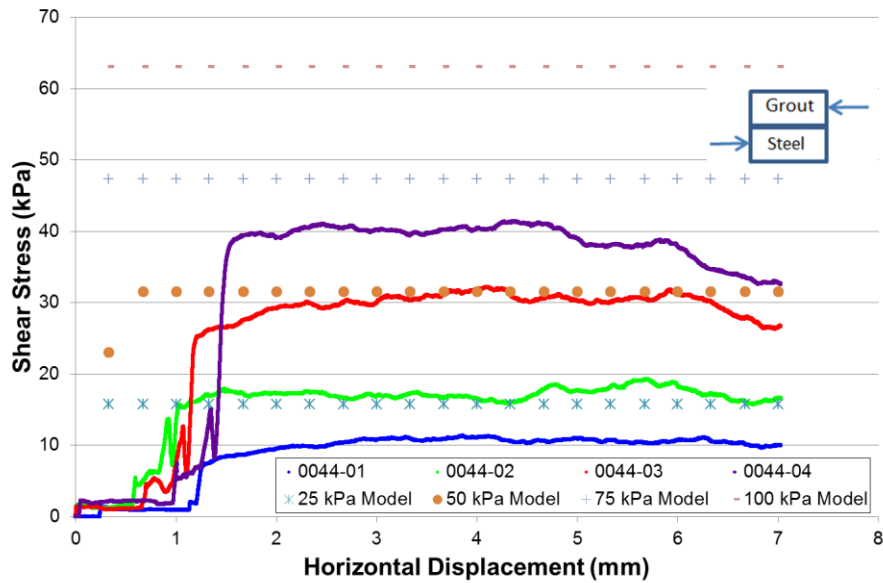


Figure C-32 Grout-steel sample, model versus test 0044

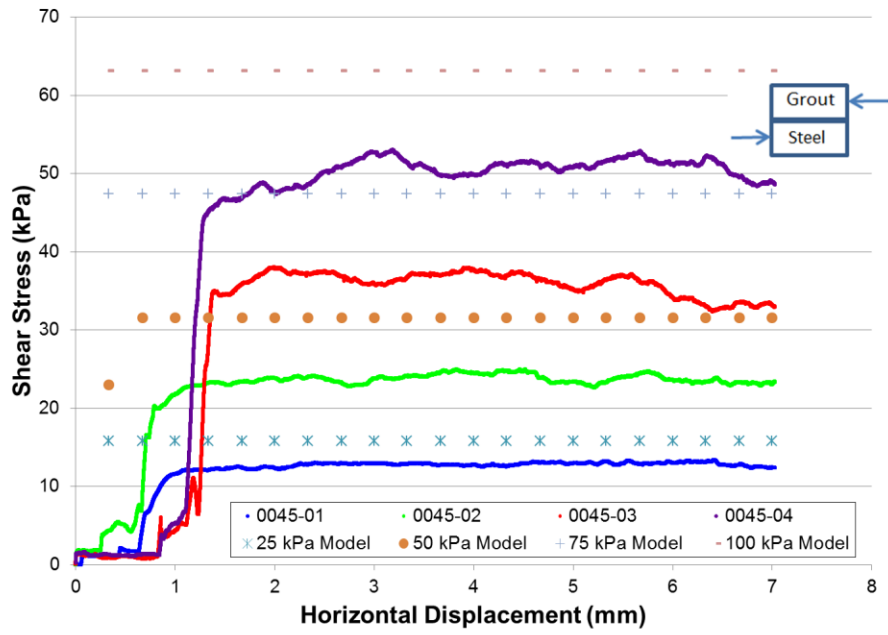


Figure C-33 Grout-steel sample, model versus test 0045

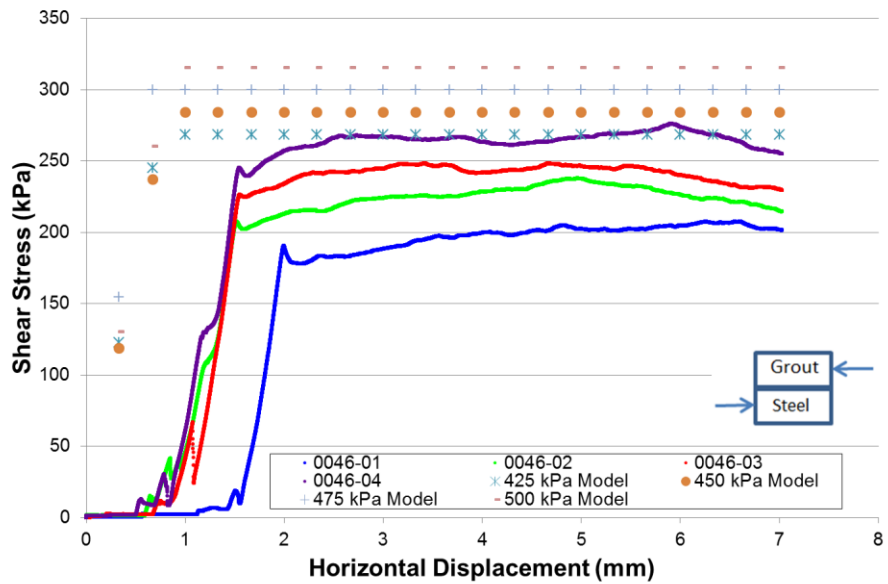


Figure C-34 Grout-steel sample, model versus test 0046

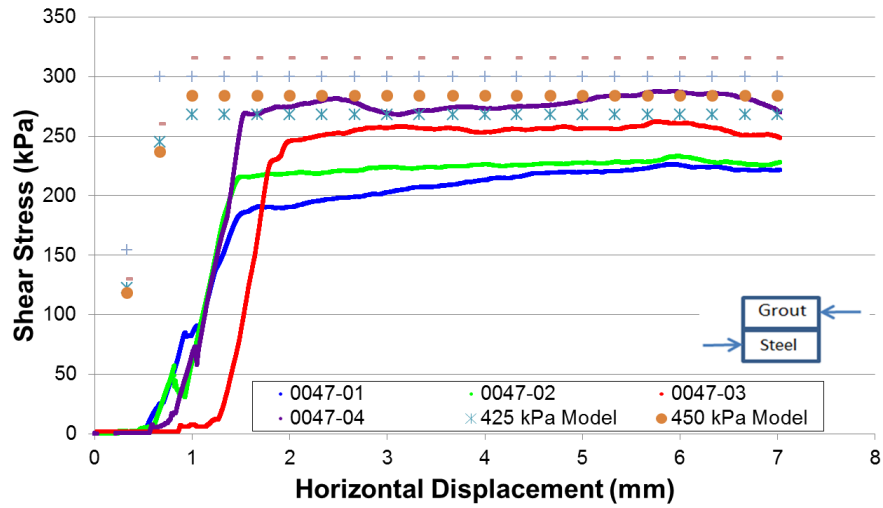


Figure C-35 Grout-steel sample, model versus test 0047

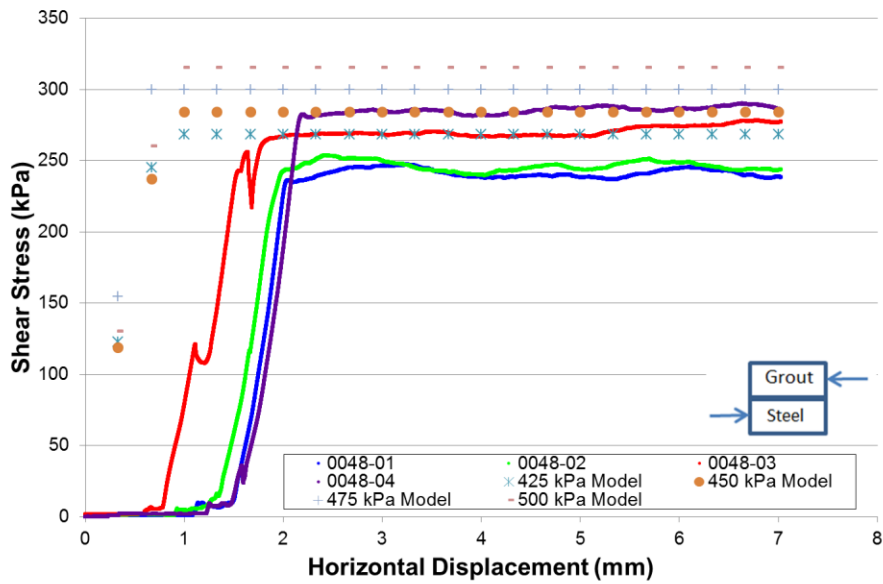


Figure C-36 Grout-steel sample, model versus test 0048

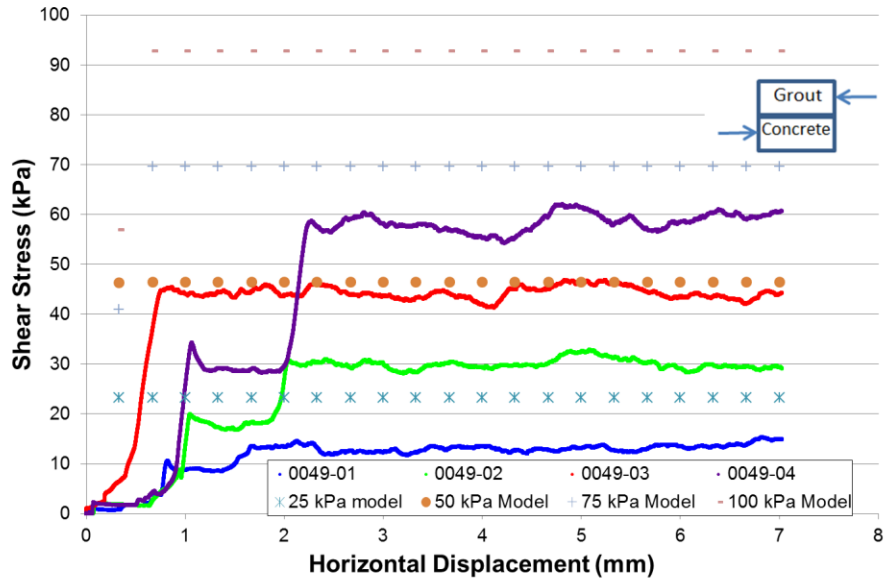


Figure C-37 Grout-concrete sample, model versus test 0049

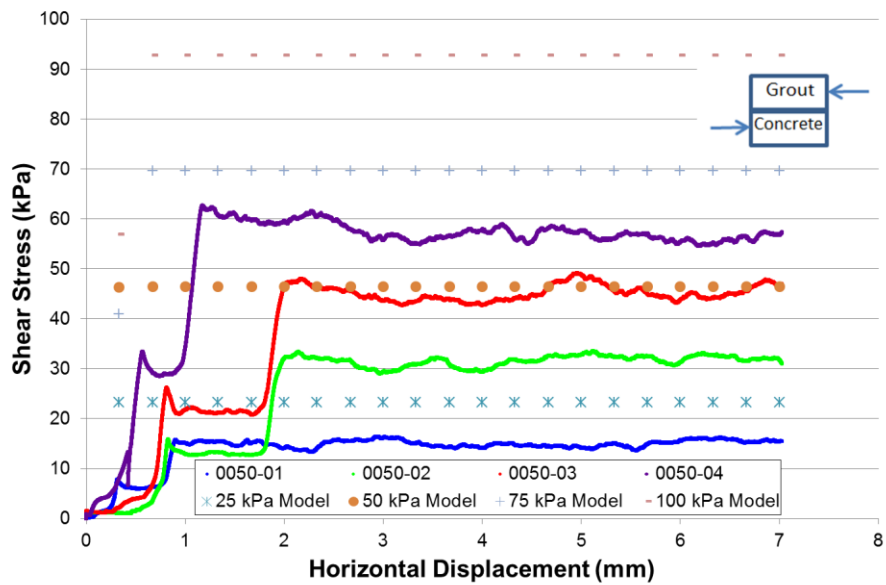


Figure C-38 Grout-concrete sample, model versus test 0050

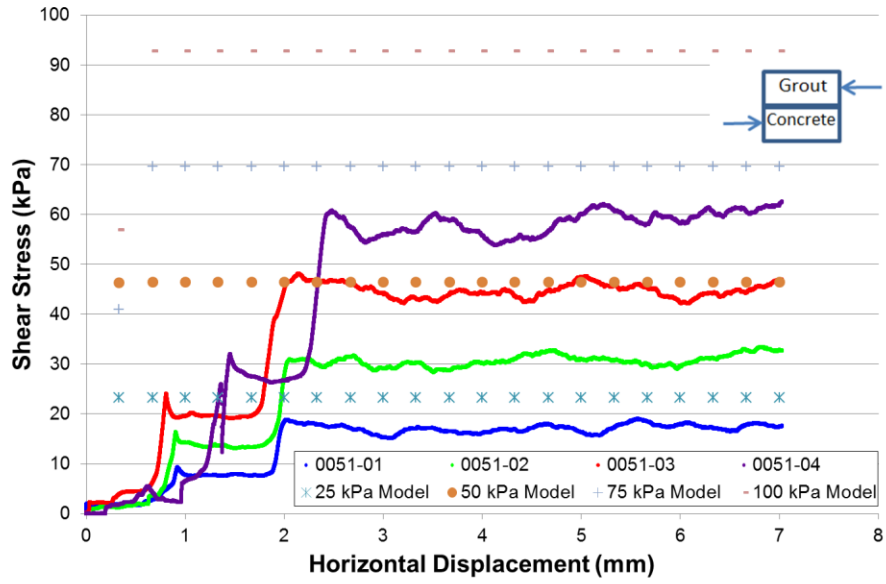


Figure C-39 Grout-concrete sample, model versus test 0051

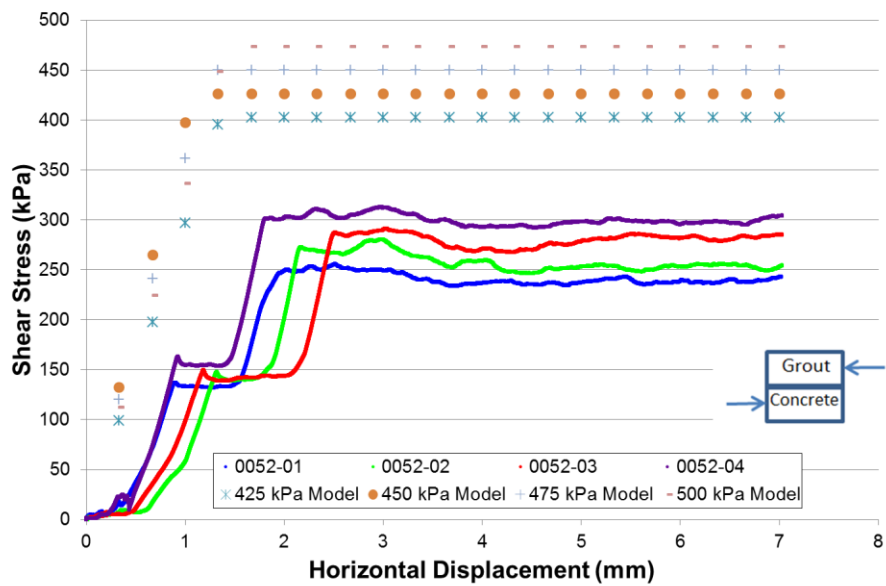


Figure C-40 Grout-concrete sample, model versus test 0052

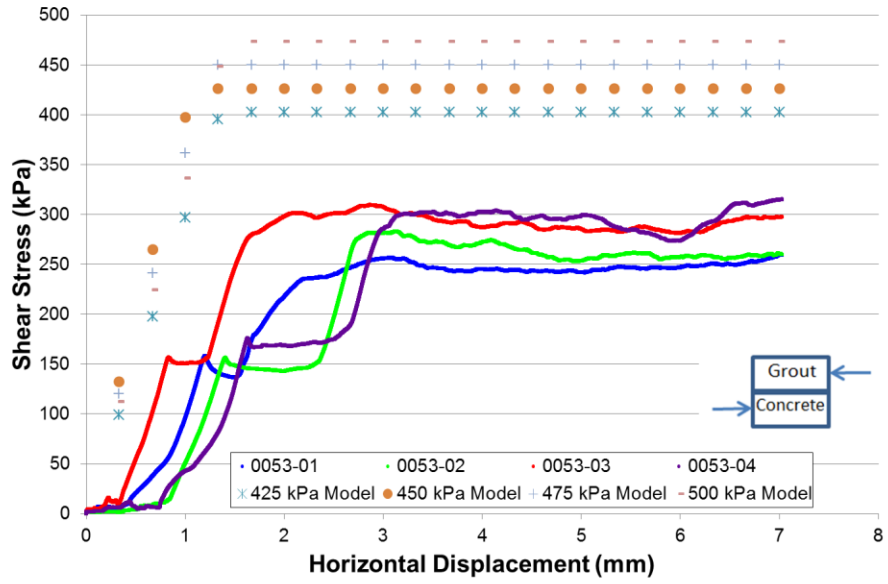


Figure C-41 Grout-concrete sample, model versus test 0053

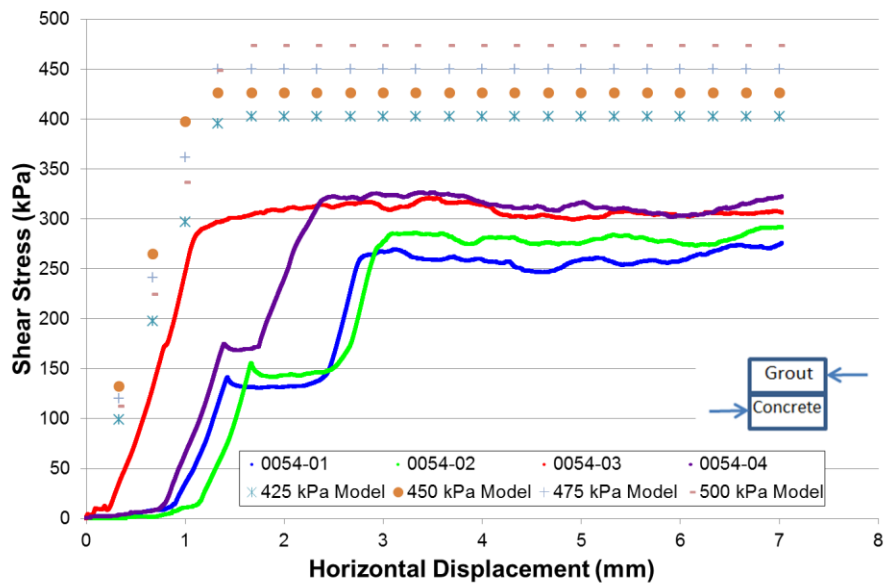


Figure C-42 Grout-concrete sample, model versus test 0054

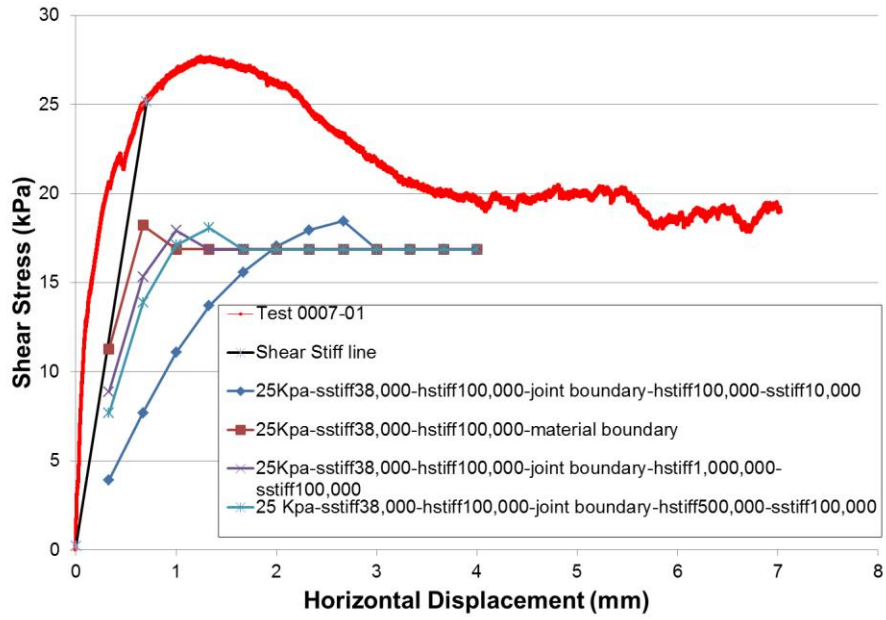


Figure C-43 Calibration of shearbox-sample boundary conditions at 25kPa normal stress with pure sand

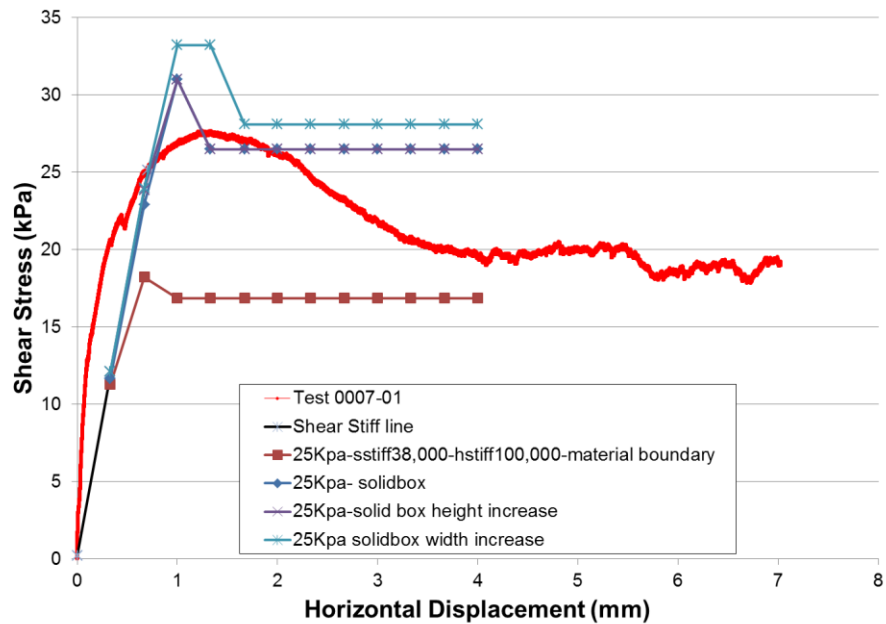
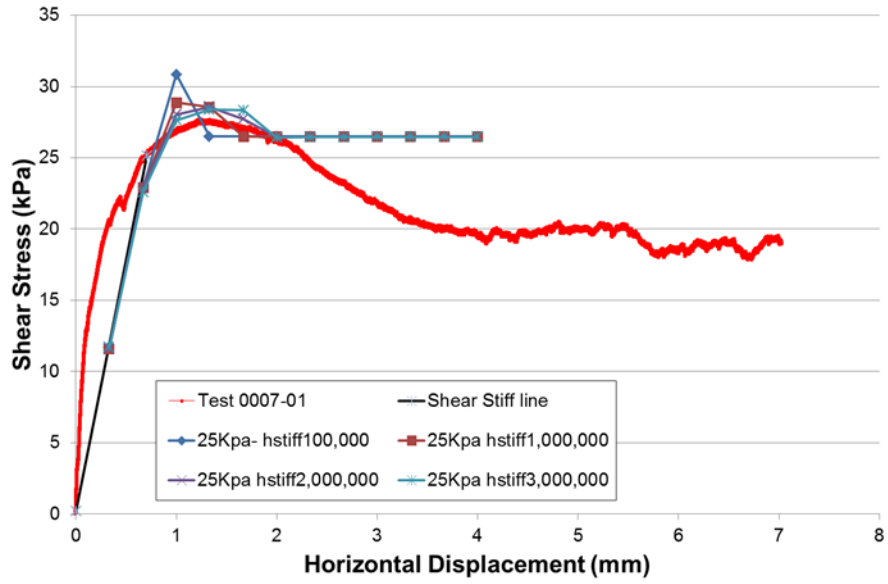


Figure C-44 Calibration of shearbox dimensions at 25 kPa normal stress with pure sand



**Figure C-45** Calibration of horizontal stiffness of shear joint at 25kPa normal stress with pure sand